ATMOSPHERIC CHEMISTRY OF HYDROCARBON FUELS

VOLUME I: EXPERIMENTS, RESULTS, AND DISCUSSION

WILLIAM P. L. CARTER, PAUL S. RIPLEY,
CECIL G. SMITH, AND JAMES N. PITTS, JR.

STATEWIDE AIR POLLUTION RESEARCH CENTER
UNIVERSITY OF CALIFORNIA
RIVERSIDE, CALIFORNIA 92521

NOVEMBER 1981

FINAL REPORT
MARCH 1980 - SEPTEMBER 1981

APPROVED FOR PUBLIC RELEASE: DISTRIBUTION UNLIMITED

AFESC

ENGINEERING & SERVICES LABORATORY
AIR FORCE ENGINEERING & SERVICES CENTER
TYNDALL AIR FORCE BASE, FLORIDA 32403

DISCLAIMER NOTICE

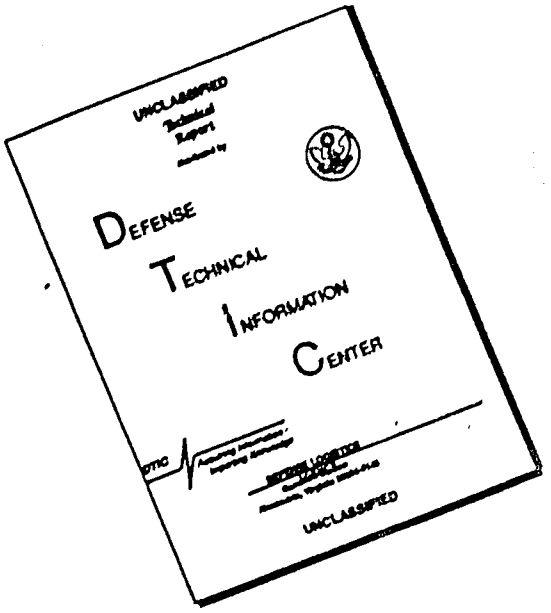

THIS DOCUMENT IS BEST QUALITY AVAILABLE. THE COPY FURNISHED TO DTIC CONTAINED A SIGNIFICANT NUMBER OF PAGES WHICH DO NOT REPRODUCE LEGIBLY.

NOTICE

Please do not request copies of this report from HQ AFESC/RD (Engineering and Services Laboratory). Additional copies may be purchased from:

National Technical Information Service
5285 Port Royal Road
Springfield, Virginia 22161

Federal Government agencies and their contractors registered with Defense Technical Information Center should direct requests for copies of this report to:

Defense Technical Information Center
Cameron Station
Alexandria, Virginia 22314

UNCLASSIFIED

SECURITY CLASSIFICATION OF THIS PAGE (When Data Entered)

REPORT DOCUMENTATION PAGE		READ INSTRUCTIONS BEFORE COMPLETING FORM
1. REPORT NUMBER ESL-TR-81-53	2. GOVT ACCESSION NO. A115536	3. RECIPIENT'S CATALOG NUMBER
4. TITLE (and Subtitle) ATMOSPHERIC CHEMISTRY OF HYDROCARBON FUELS Volume I: Experiments, Results and Discussion		5. TYPE OF REPORT & PERIOD COVERED Final Report March 1980 - September 1981 6. PERFORMING ORG. REPORT NUMBER
7. AUTHOR(s) William P. L. Carter, Paul S. Ripley, Cecil G. Smith and James N. Pitts, Jr.		8. CONTRACT OR GRANT NUMBER(s) F08635-80-C-0086
9. PERFORMING ORGANIZATION NAME AND ADDRESS Statewide Air Pollution Research Center University of California Riverside, California 92521		10. PROGRAM ELEMENT, PROJECT, TASK AREA & WORK UNIT NUMBERS PE 6260IF JON 19002020
11. CONTROLLING OFFICE NAME AND ADDRESS AIR FORCE ENGINEERING AND SERVICES CENTER Tyndall Air Force Base, Florida 32403		12. REPORT DATE November 1981 13. NUMBER OF PAGES 203
14. MONITORING AGENCY NAME & ADDRESS(if different from Controlling Office)		15. SECURITY CLASS. (of this report) UNCLASSIFIED 15a. DECLASSIFICATION/DOWNGRADING SCHEDULE

16. DISTRIBUTION STATEMENT (of this Report)

Approved for public release; distribution unlimited.

17. DISTRIBUTION STATEMENT (of the abstract entered in Block 20, if different from Report)

18. SUPPLEMENTARY NOTES

Availability of this report is specified on verso of front cover.

19. KEY WORDS (Continue on reverse side if necessary and identify by block number)

Hydrogen Fuels	Aerosol Formation
High-Energy Fuels	Environmental Simulation
Ozone Formation	Environmental Quality
Atmospheric Reactivity	Missile Fuels

20. ABSTRACT (Continue on reverse side if necessary and identify by block number)

Organic compounds in hydrocarbon fuels can, when released into the atmosphere in the presence of NO_x and sunlight, affect air quality both in the vacinity of their release and in downwind regions. Potentially adverse air quality impacts include the formation of ozone and a spectrum of other photochemical oxidants, the formation of secondary aerosols, and in certain cases the formation of toxic organic products. This program was designed to experimentally investigate the potential of selected Air Force and commercial

DD FORM 1 JAN 73 1473 EDITION OF 1 NOV 65 IS OBSOLETE

Unclassified

SECURITY CLASSIFICATION OF THIS PAGE (When Data Entered)

20. ABSTRACT (concluded)

fuels for producing some or all of these impacts.

A total 132 single- and multi-day outdoor environmental chamber experiments were carried out involving nine fuels. These included the petroleum-derived JP-4 and JP-8 military aviation fuels, their shale-oil-derived analogues, unleaded gasoline, diesel No. 2 fuel, and the experimental high-energy cruise-missile fuels JP-10, RJ-4, and RJ-5. In addition to NO_x-air irradiations of these fuels, an appropriate array of control experiments to characterize chamber effects was performed. Concentration-time data were obtained for ozone, NO-NO_2-NO_x, representative fuel components, selected aerosol parameters, and physical parameters such as temperature and ultraviolet (UV) light intensity. Rates of O_3 formation and NO oxidation, aerosol production, and maximum O_3 yields were taken as indices of the atmospheric reactivity of these fuels. Dual-chamber experiments were used to investigate the effects on reactivity of varying initial fuel or NO_x concentrations and of varying the type of fuel. For each fuel, four-day static and (in some cases) dynamic experiments were carried out to determine the reactivity of the fuels under multi-day conditions, including the effect of freshly injected NO_x on aged fuel mixtures.

The results of this study show that the Air Force fuels JP-4 and JP-8 (both petroleum- and shale-derived) are significantly less reactive with respect to rates of oxidant formation and NO to NO_2 conversion than unleaded gasoline. The cruise-missile fuels JP-10, RJ-4, and RJ-5 exhibit still lower reactivities. Under the meteorological conditions encountered during this study, the same general reactivity ranking was observed for multi-day irradiation conditions. However, under multi-day static irradiations with no further introduction of reactants, all of the military fuels studies (i.e., both kerosene-derived and high-energy) had similar maximum ozone-forming potentials. Additionally, there did not appear to be any substantial differences between the petroleum-derived or shale-oil-derived fuels. This study also showed that all of the fuels investigated formed significant amounts of aerosol materials, regardless of their reactivity with respect to rates of O_3 formation and NO oxidation.

The results obtained are interpreted in terms of our present understanding of the gas phase NO_x-photo-oxidation chemistry of organics, and recommendations for future research are presented. The latter include a suggestion that detailed experimental and modeling studies of representative individual components of Air Force fuels be conducted in order to develop a capacity for predicting the effects of changes in fuel composition on photochemical reactivity.

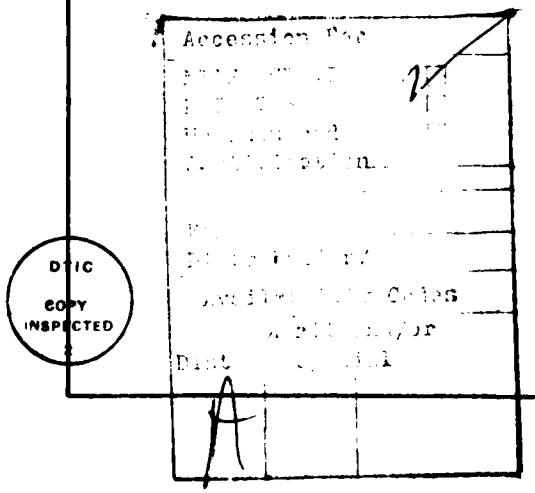

PREFACE

This report was prepared by the Statewide Air Pollution Research Center (SAPRC) of the University of California, Riverside, California 92521, under program element 1900, project 20, subtask 20, with the Air Force Engineering and Services Center, Tyndall Air Force Base, Florida 32403.

This report is presented in two volumes. Volume I contains a description of the experiments conducted under this program and a discussion of the results obtained. Volume II contains the detailed data sheets for the outdoor chamber runs. Volume II was not formally distributed, but is available through DTIC.

The work was performed during the period March 1980 through September 1981 under the direction of Dr. James N. Pitts, Jr., Director of SAPRC and Principal Investigator, and Dr. William P. L. Carter, Project Manager.

The principal research staff on this program were Mr. Paul S. Ripley and Ms. Cecil G. Smith. Drs. Roger Atkinson and Arthur M. Winer (Assistant Director of SAPRC) participated in supervision of this program, in technical discussions, and in the preparation of this report.

Assistance in conducting this program was provided by Mr. Dennis R. Fitz, Ms. Sara M. Aschmann, Mr. Frank R. Burleson, Ms. Margaret C. Dodd, Mr. Robert E. Burkey, Jr., Ms. JoMarie Faulkerson, and Mr. Glen C. Vogelaar. The gas chromatographic-mass spectrographic analyses were conducted by Mr. Thomas S. Fisher, and assistance in processing the data was provided by Mr. Jeffrey Everett, Mr. Joseph P. Lick, and Ms. Laurie A. Willis.

Appreciation is expressed to Ms. Christy J. Ranck, Ms. I. M. Minnich, Dr. Marian C. Carpelan, and Ms. Minn P. Poe for assistance in the preparation of this report.

The support and contribution to the conduct of this program by Dr. Daniel A. Stone, Project Officer, Maj. Ron Channell, and LtCol. Michael MacNaughton, Chief of the Environmental Sciences Division at the inception of this program are gratefully acknowledged.

This report has been reviewed by the Public Affairs Office (PA) and is releasable to the National Technical Information Service (NTIS). At NTIS it will be available to the general public, including foreign nationals.

This technical report has been reviewed and is approved for publication.

Daniel A. Stone
DANIEL A. STONE, GS-13
Project Officer

Ronald E. Channell
RONALD E. CHANNELL, Maj, USAF
Chief, Environmental Chemistry Branch

Michael J. Ryan
MICHAEL J. RYAN, LtCol, USAF,BSC
Chief, Environics Division

Francis B. Crowley III
FRANCIS B. CROWLEY III, Col, USAF
Dir, Engineering & Services Laboratory

TABLE OF CONTENTS

TABLE OF CONTENTS (CONTINUED)

TABLE OF CONTENTS (CONCLUDED)

LIST OF FIGURES

LIST OF FIGURES (CONTINUED)

LIST OF FIGURES (CONTINUED)

LIST OF FIGURES (CONTINUED)

LIST OF FIGURES (CONCLUDED)

LIST OF TABLES

LIST OF TABLES (CONTINUED)

LIST OF TABLES (CONCLUDED)

(The reverse of this page is blank.)

SECTION I

INTRODUCTION

Daily military operations involve large quantities of aircraft fuels. Release of a small portion of these fuels into the lower troposphere or at ground level is an inevitable consequence of their use, storage, and handling. In the presence of NO_x ($NO + NO_2$) and sunlight, the hydrocarbon components of such fuels can be photo-oxidized to yield ozone and other oxidants, as well as secondary aerosols. Although there has been much research carried out to date concerning many aspects of tropospheric chemistry, there have been no investigations of the photo-oxidations of complete aircraft fuels under realistically simulated atmospheric conditions in the presence of NO_x as a co-pollutant. Such simulations are required to provide a basis for comparing atmospheric impacts of military aircraft fuels to each other and other fuels currently used and to comply with Federal, state, and local air quality regulations.

Kerosene-based fuels are widely employed in present military aircraft. The most widely used military fuel for turbine powered aircraft in the United States is JP-4. However, the Navy favors the use of JP-5, since its narrower distillation cut gives it a higher flash point, making it safer to use at sea (References 1, 2). Recently, there has been a trend, particularly in United States Air Force operations in Europe, toward the use of JP-8; JP-8 is a higher distillation cut than JP-4 or JP-5 and is thus somewhat less volatile (Reference 2). Although the derivation of these fuels is similar, the distribution of their major hydrocarbon components, particularly the ratio of higher molecular weight to lower molecular weight compounds, is different for each of these fuels. These differences are expected to affect their atmospheric reactivity.

A further diversity in the jet aircraft fuels arises from the need to become independent of imported oil. This has lead to the development of shale-oil-derived fuels (and will likely, in the future, lead to coal-derived fuels). These shale-oil-derived fuels potentially include sulfur-, oxygen-, and, less likely (Reference 3) nitrogen-containing organics, together with a different distribution of molecular weight components

and different relative amounts of alkanes and aromatics than in the equivalent petroleum-derived fuels.

Although kerosene-based fuels are generally adequate for most present military aircraft, the new generation of strategic weapons such as cruise missiles require fuels which are much higher in energy content per unit volume. In order to satisfy this requirement, high energy fuels such as JP-10, RJ-4, and RJ-5 (and blends thereof) have been developed (Reference 1). These fuels are hydrogenated dimers of cyclopentadiene (JP-10), methylcyclopentadiene (RJ-4), and norbornadiene (RJ-5). The chemical structures of representative isomers are shown in Figure 1. Since usage of these and similar "high-energy" fuels is likely to increase significantly in the future, a knowledge of the atmospheric impact of their release is also necessary.

In order to obtain data from which the atmospheric impacts of releases of these fuels can be assessed and compared, the United States Air Force contracted the Statewide Air Pollution Research Center (SAPRC) to perform a series of single- and multi-day outdoor chamber experiments. In these, part-per-million (ppm) levels of various fuels were to be irradiated with natural sunlight in air in the presence of NO_x. The resulting chemical and physical transformations or reactivity were to be monitored by a variety of techniques. In this study emphasis was placed on the following reactivity indicies: the rate of formation and the maximum yield of ozone, the rate of NO oxidation, and the yields of secondary aerosol.

The specific military fuels specified for study were JP-4 and JP-8 derived from petroleum (as is currently used), JP-4 and JP-8 derived from shale-oil, and the high energy fuels JP-10, RJ-4, and RJ-5. In addition, in order that the atmospheric reactivity of the military fuels could be directly compared with those in common use in the private sector, similar experiments were conducted using unleaded gasoline and diesel No. 2 fuel. Thus, a total of nine different fuels were studied in this program.

The matrix of outdoor chamber experiments performed for the various fuels is given in Table 1. The nature and purpose of the different types of experiments are briefly indicated below:

JP-10

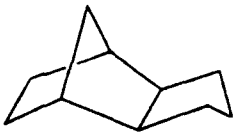

$C_{10}H_{16}$

RJ-4 ISOMERS

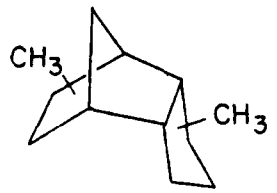

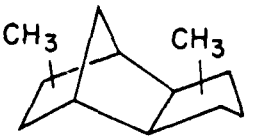

$C_{12}H_{20}$

REPRESENTATIVE RJ-5 ISOMERS

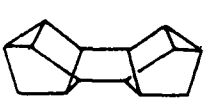

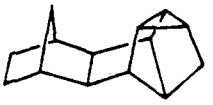

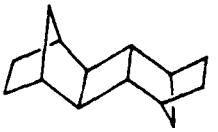

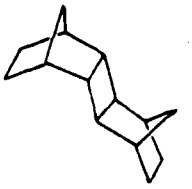

$C_{14}H_{16}$ $C_{14}H_{18}$ $C_{14}H_{20}$

Figure 1. Chemical Structures of the Major Components of the High Energy Missile Fuels JP-10, RJ-4 and RJ-5.

TABLE 1. MATRIX OF OUTDOOR ENVIRONMENTAL CHAMBER EXPERIMENTS.

Run Type	Run Days	Side 1	Fuel (ppmC)	NO_x (ppm)	Side 2	Fuel (ppmC)	NO_x (ppm)
Fuel A vs n-Butane	1	Fuel A	25	0.5	n-Butane	25	0.5
Fuel A vs Fuel B	2	Fuel A	25	0.5	Fuel B	25	0.5
Variable Initial NO_x	2	Fuel A	25	0.5	Fuel A	25	0.25
Variable Initial Fuel	2	Fuel A	25	0.5	Fuel A	12.5/50[a]	0.5
Four-Day Static	4	Fuel A	25	0.5	(Undivided)		
Dynamic[b]	2-3	Fuel A	25	0.5	(Undivided)		

[a]50 ppmC for less reactive fuels, 12.5 for more reactive fuels.

[b]Not done for all fuels.

(1) In order to determine the atmospheric reactivity of the fuels under multi-day conditions, the standard fuel-NO_x-air mixtures (~25 ppmC fuel, 0.5 ppm NO_x) were irradiated for four consecutive days. On the third or fourth day, depending on how long it took the initially-present NO_x to be consumed (thus rendering the mixture unreactive), additional NO_x was injected into the chamber to simulate the effects of NO_x emissions downwind of the fuel release.

(2) In order to determine the extent to which initial NO_x levels affect the reactivity of the fuel-NO_x-air mixtures, dual-chamber experiments were performed in which mixtures with two different initial NO_x levels were simultaneously irradiated for two days. Because of the dual-chamber design employed, initial fuel levels, temperature, humidity, and lighting conditions were exactly the same, and only NO_x was varied.

(3) In order to determine the extent to which initial fuel levels affect the reactivity of the system, dual-chamber irradiations were performed in which mixtures with two different initial concentrations of the same fuel were simultaneously irradiated for two days. The initial NO_x

levels, humidity, and temperature and lighting conditions were the same for both mixtures.

(4) In order to compare the atmospheric reactivity of the fuels with that of n-butane, one-day dual-chamber irradiations were performed in which n-butane-NO_x-air and fuel-NO_x-air mixtures (with approximately equal amounts of n-butane and fuel on a ppmC basis) were simultaneously irradiated. As with the variable fuel runs, the initial NO_x, temperature, and lighting conditions were the same for both mixtures. n-Butane was chosen as a reference organic, since its atmospheric photo-oxidation chemistry is among the best understood of all the reactive organics (References 4, 5) and its reactivity is known to be very sensitive to chamber effects and variations in temperature (References 4, 6). Thus n-butane-NO_x-air irradiations serve as useful control experiments under the same temperature, lighting, and initial NO_x conditions as the fuel-NO_x-air irradiations. n-Butane also serves as a standard for intercomparison of the reactivity of the less reactive fuels.

(5) To directly compare the atmospheric reactivities of different types of fuels, dual-chamber experiments were performed in which NO_x-air mixtures containing approximately equal levels of different fuels were simultaneously irradiated for one or two days. As with the variable fuel or the fuel versus n-butane runs, the initial NO_x levels and the temperature and lighting conditions were the same for both fuel mixtures. The following experiments were performed: (a) petroleum-derived JP-4 was compared with all other kerosene-type jet fuels (shale-derived JP-4, and shale- and petroleum-derived JP-8), unleaded gasoline, and diesel fuel; (b) petroleum-derived JP-8 was compared with shale-derived JP-8; (c) JP-10 was compared with RJ-4 and RJ-5. Two experiments were done for each fuel combination studied, with the chamber side interchanged in each case to factor out any possible effects of chamber side inequivalency.

(6) For shale- and petroleum-derived JP-4, unleaded gasoline and JP-10, two- and/or three-day "dynamic" irradiations were performed in which the fuel-NO_x mixture was diluted by ~10% each hour, seven times a day. These experiments were intended to determine the effect of continuous dilution on the reactivity of the fuel-NO_x mixture. These runs were not performed for the other fuels, since it was decided several months into this program that the direct fuel intercomparison runs would be more

useful for the purposes of this study. The statement of work was hence modified to replace the remaining scheduled dynamic runs with the fuel intercomparison runs.

In order that the outdoor chamber experiments be as useful as possible, an extensive developmental effort was required and a number of exploratory experiments were performed. The developmental effort primarily concerned optimizing the gas chromatographic techniques for the analyses of the heavier fuel components in the gas phase, the identification of the major fuel components, and the development of reliable and reproducible techniques for injecting the fuels into the gas phase. Exploratory experiments included the injection and irradiation of representative fuels in the SAPRC ~6000 ℓ indoor chamber. The latter were performed in order to identify any problems that might arise in the outdoor irradiations of the fuels and to obtain a preliminary indication of their reactivity. In addition, experiments were carried out to determine the kinetics of the reaction of hydroxyl radicals with JP-10 in order that the atmospheric half-life of this relatively unreactive cruise-missile fuel could be predicted.

In the following sections, the experimental facilities and analytical techniques employed in the outdoor chamber experiments and in the exploratory and developmental work are described and the results are presented. The implications of the results obtained concerning the atmospheric reactivities of the fuels studied are discussed and recommendations concerning future work relevant to the problems of assessing impacts of atmospheric releases of present and future hydrocarbon fuels are given.

Detailed data sheets are compiled as Volume II of this report.

SECTION II

DEVELOPMENTAL AND EXPLORATORY EXPERIMENTS

2.1 DEVELOPMENT OF GAS CHROMATOGRAPHIC ANALYSIS TECHNIQUES

The analyses of the fuel components in the gas phase were performed using capillary column gas chromatographic (GC) techniques. Although a technique for such analyses was already available from previous research, it was found to be unsuitable for the analyses of the heavier ($> C_{10}$) fuel components present in JP-8 and in diesel fuel. To reliably and reproducibly analyze these heavier compounds, modifications of the original technique were required. In this section, the techniques employed for the analyses of the fuel components in the gas phase and the associated developmental work are described.

Three capillary column gas chromatographs with flame-ionization detection (FID) were employed at various times in this program. Two of these were HP-5710A instruments with sub-ambient temperature capabilities and fitted with Carle micro-volume gas sampling valves. Fused silica capillary columns (30 m x 0.25 mm) coated with a 0.25 μ thick SE-52 film were employed for these two gas chromatographs. The other gas chromatograph employed was a Varian 3700 instrument with sub-ambient temperature capability, also equipped with a Carle micro-volume gas sampling valve. In this case the capillary column employed was a 30 m x 0.25 mm fused silica column coated with an 0.25 μ thick SE-54 film. Nitrogen was the carrier gas for the HP-5710A gas chromatograph used for developmental purposes; the others used helium as the carrier gas at a flow rate of ~1.4 ml min^{-1}. The HP-5710A instruments were each interfaced to a Spectra-Physics model 23000-011 Minigrator , while the Varian 3700 was interfaced to a Varian CDS-111 data system. Thus, in all cases the gas chromatographic response was reported as peak areas. Since the Varian instrument was not acquired until several months into the program, the majority of the developmental work was carried out on one of the HP-5710A instruments.

Most of the developmental work concerned the sampling technique, as described below. However, regardless of the sampling technique employed, the sample was injected onto the column by flushing a loop or trap containing the mixture to be analyzed with the carrier gas, while the column

was held at -50°C or -90°C. In most cases, although -50°C was satisfactory for the C_{6+} hydrocarbons, the column was held at -90°C, since that resulted in more satisfactory peak shapes for the butanes and pentanes. Once the sampling loop was completely flushed, the column was heated via a temperature programmed sequence to a maximum of 200°C. The exact temperature program varied, depending on the instrument and the time constraints of the analyses (the total analysis time in the experimental runs had to be less than one hour). A typical program was a temperature increase from -90°C to 20°C at 16°C min^{-1}, with the temperature then being increased at 4°C min^{-1} up to 200°C, which was the end of the program. This resulted in satisfactory peak separation and shape for most of the fuel analyses, as shown in the sample gas chromatograms given in Section 2.2.

The initial sampling method consisted of withdrawing 100 ml of the gas being sampled with a gas-tight, all-glass hypodermic syringe, passing its contents through an ~2 ml stainless steel loop filled with uncoated glass beads, and cooled with liquid argon (Figure 2). Cooling with liquid N_2 was found to result in condensation of O_2 when air samples were taken, which usually caused the flame on the FID to blow out when the sample was injected onto the column. The trap, which was connected to the gas sampling valve on the GC instrument, was then heated with boiling water. Simultaneously the gas sampling valve was turned so that the contents of the trap were flushed onto the head of the column, which (as mentioned above) was cooled to -50°C or -90°C.

Although this initial sampling technique resulted in satisfactory separation and peak shapes in the fuel analyses, there were several problems associated with it. The first problem experienced was that the flame continued to blow out during analyses of humidified air samples. To correct this problem, the auxillary makeup gas was changed from helium to nitrogen and the exit end of the capillary was withdrawn from within the base of the flame. The final conclusion was that the flame-outs were caused by H_2O concentrated from the sample; reducing the sample size from 100 ml to 50 ml corrected this problem.

The most intractable problem with the cryogenic trapping technique was that it was found not to be satisfactory for the analyses of heavier (C_{10+}) fuel components. This is illustrated in Table 2, which gives the

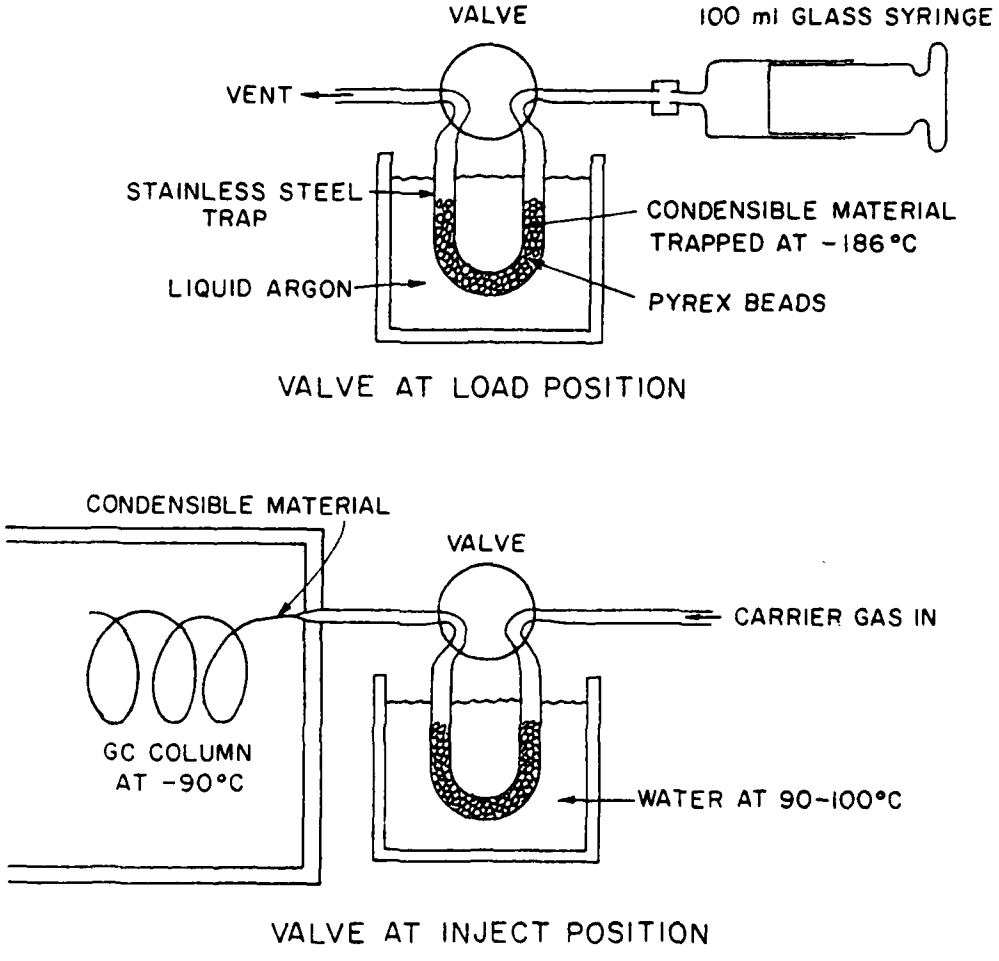

Figure 2. Trap Injection Technique for Capillary Column Gas Chromatographic Analyses of Gas-Phase Samples.

TABLE 2. DEPENDENCE OF THE CHROMATOGRAPHIC RESPONSE ON SAMPLING CONDITIONS.

	NORMALIZED RESPONSE (per ppbC)[a]			
		STAINLESS STEEL	GLASS LOOP	
ORGANIC	TRAP	LOOP	UNHEATED	HEATED
$n-C_7$	100	100	100	100
$n-C_8$	90	130	100	105
$n-C_9$	90	194	101	110
$n-C_{10}$	73	155	104	--
$n-C_{11}$	42	10	104	100
$n-C_{12}$	0	--	134	105
$n-C_{13}$	0	--	93	110
$n-C_{14}$	0	--	17[b]	119
$n-C_{15}$	0	--	0	78[b]
Benzene	--	--	105	90
Toluene	--	--	112	100

[a]Normalized to response for n-heptane = 100

[b]Highly scattered.

-- No data

FID GC area response per ppmC for the C_7 to C_{15} n-alkanes and for benzene and toluene for several of the sampling techniques examined. It can be seen that with this sampling technique the response per ppmC decreased as the size of the molecule increased. This is contrary to what one would expect for flame ionization detectors, where the response per carbon is normally constant. In addition, no response was observed for $n-C_{12}$ or heavier compounds, which indicated that these compounds (concentrated by a factor of ~25 when sampling) were being "hung up" in the loop or the valve during injection.

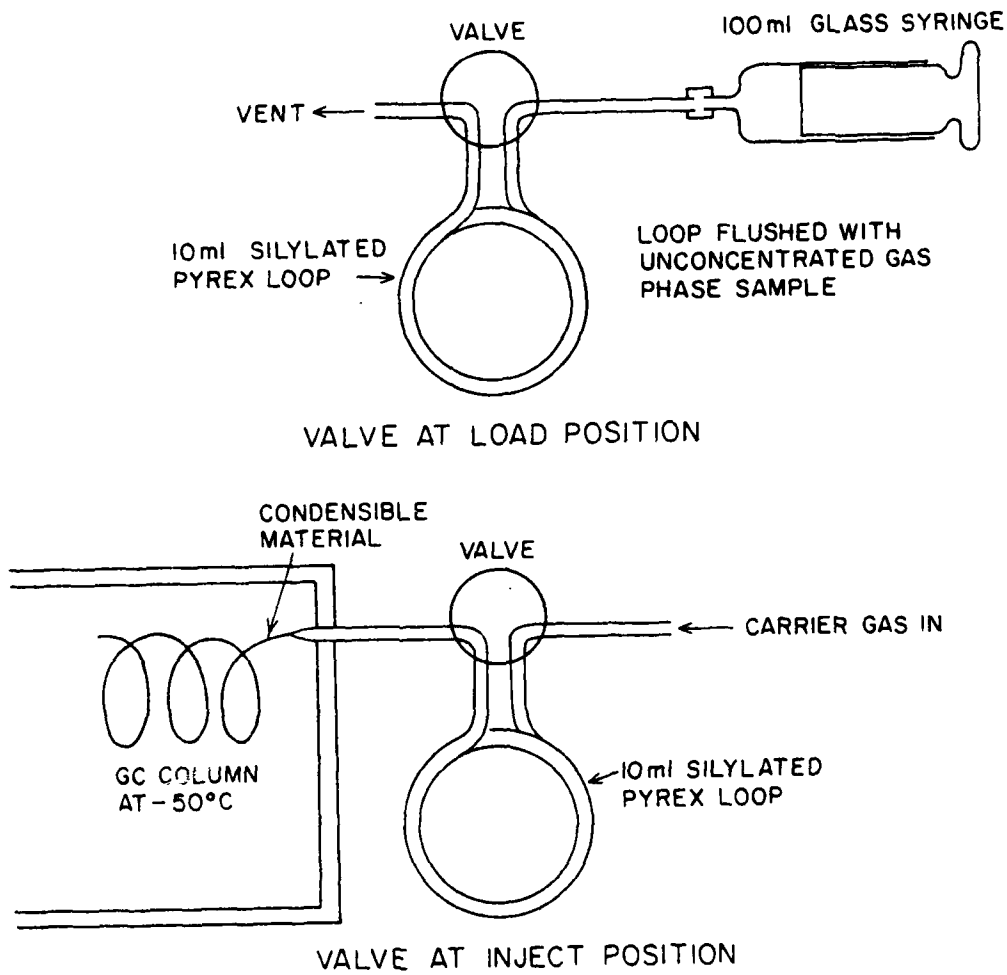

Figure 3. Loop Injection Technique for Capillary Column Gas Chromatographic Analyses of Gas-Phase Samples.

An alternate technique for sampling was the "loop" method, in which a loop attached to the GC inlet valve was flushed with the gas sample and its contents then injected onto the cooled column without pre-concentration (Figure 3). This method should in principle have given better results, since lower concentrations of the heavy compounds were exposed to the valve. However, it was found that, although satisfactory analyses of the n-C_5 through n-C_{11} alkanes were obtained when a well-conditioned 2 ml stainless steel loop was used, anomalous results were observed when attempts were made to use a new 10 ml loop made of the same material. A larger loop was required to obtain the sensitivity required for use in the experimental runs.

The problem observed when the new 10 ml loop was used was an apparent conversion of n-C_{11} and (to a lesser extent) n-C_{10} peaks to the n-C_9 peak; i.e., the n-C_9 peak was anomalously large and the n-C_{10} and n-C_{11} peaks were anomalously small. The n-C_5 to n-C_8 peaks were not affected and the peak shapes for all compounds were normal. Extensive tests were carried out to elucidate the cause of this problem. It was concluded that it was due to surface effects on the unconditioned trap, since similar results occurred when the old 2 ml loop was replaced by a new loop of the same volume. Furthermore, when the new 10 ml loop was conditioned by washing it with liquid JP-8, this effect decreased markedly. The magnitude of this effect also was significantly reduced when Teflon® or glass loops were used instead of stainless steel.

The best results were obtained when the 10 ml loop was made of ~2 mm i.d. Pyrex tubing, which was "silylated" by treatment with 10% dichlorodimethylsilane in toluene. The area response for the n-alkanes and the representative aromatics obtained when using this loop is shown in Table 2, and it can be seen that, unlike the "trap" technique, the response per ppmC is reasonably constant for the n-C_5 through n-C_{11} alkanes and the two aromatics studied. Furthermore, good reproducibility in the analyses of those compounds was attained. However, for n-C_{12+}, the variability of the analyses becomes significantly greater; in Table 2 the response is anomalous for n-C_{12}, and falls off for n-C_{13+}. Unfortunately, compounds in the n-C_{11} through n-C_{14} range appear to be the major constituents of JP-8 and compounds lighter than n-C_{11} are relatively minor in diesel fuel (Section 2.2). It should also be noted that the room temperature vapor pressure of

$n\text{-}C_{15}$ is estimated to be greater than 200 ppm and, hence, significant concentrations of C_{11} through C_{15} compounds should exist in the gas phase.

To ascertain whether the range of this "glass loop" analysis could be extended, the effect of heating the loop and/or valve during the injection process was examined. Optimum results were obtained when both the loop and the trap were heated to ~75°C with a heat gun during the sample injection procedure. The response per ppmC for representative compounds using this technique are shown in Table 2, from which it can be seen that heating allows the analyses to be extended by ~1-2 carbon numbers. This is probably the best that can be reasonably expected using the loop analysis technique.

Since manual heating of the valve and the loop during routine analyses is impractical, an insulated and heated oven for the loop and valve was constructed for the Varian 3700 GC used in this program. The oven for the injection system for the Varian 3700 GC was generally maintained at 150°C for most of the routine analyses during the outdoor experiments. Using this technique, reasonably satisfactory quantitative analyses were obtained for $n\text{-}C_{13}$, and qualitative analyses for $n\text{-}C_{14}$ and $n\text{-}C_{15}$ were possible.

The Varian 3700 GC with the heated glass loop injection system was used for the routine analyses in the outdoor chamber runs employing JP-8, diesel fuel, RJ-4, and RJ-5. In addition, most runs employing JP-10 together with some runs using petroleum-derived JP-4 were analyzed using this system. Most of the JP-4 runs and the unleaded gasoline runs were conducted relatively early in the program, before the optimum sampling technique was developed, and the analyses were carried out using the cryogenic trapping technique. Fortunately for those fuels, the C_{12+} hydrocarbons are of lesser importance (Section 2.2), so this did not represent a serious problem. The only runs where the capillary column GC analyses of the fuel components were unsatisfactory were some of the earlier JP-10 runs. These were carried out using the Varian 3700 GC soon after it was first set up. An improperly designed capillary column insert on the detector end caused greater sampling variability ($\pm$ 10-15%) than in later analyses. This problem was corrected before the JP-8 runs. The analysis systems used for specific runs are given in Section 3.4 and in the data sheets in Volume II.

Finally, the response per ppmC for n-C_{11} and lighter compounds analyzed using the heated loop injection technique was relatively constant and appeared not to depend significantly on whether the compound was an alkane, cycloalkane, or aromatic. Concentrations of unknown compounds expressed as ppmC could be estimated without the necessity for carrying out calibrations using authentic samples. This was useful for estimating the concentrations of unknowns in the kerosene-type fuels and for reporting the results of analyses of the major components of RJ-4 and RJ-5, since in the latter case the exact identities of the components were uncertain and authentic samples of the pure compounds were not available for this program.

2.2 IDENTIFICATION OF FUEL COMPONENTS

In order to obtain an indication of the major components of the fuels studied in this program and to confirm the gas chromatographic peak assignments made on the basis of retention times, gas chromatographic-mass spectrometric (GC-MS) analyses of the liquid fuels were carried out. The GC-MS techniques used and the results obtained are discussed in this section.

The GC-MS analyses were performed using a Hewlett-Packard 5710A capillary gas chromatograph interfaced to Finnigan Model 3200 mass spectrometer. This GC used a 30 m x 0.25 mm i.d. fused silica capillary column internally coated with a 0.25 μ film of SE-52. The injection port and transfer line were maintained at 300°C. The oven was initially held at -50°C for 30 seconds after the liquid injection, followed by a temperature rise of 16°C min^{-1} for four minutes, then of 4°C min^{-1} to the final temperature of 250°C. The mass spectrometer was scanned at one second intervals over the mass range of m/e 35 to m/e 350. Electron impact ionization was used at a potential of 70 volts.

Background subtracted mass spectra were generated using the Finnigan Model 6100 data system. Interpretation was performed by comparison with library spectra from the EPA/NBS mass spectral data base (Reference 7) or by analogy with known fragmentation pathways.

2.2.1 JP-4, JP-8, and Commercial Fuels

The major organic compounds identified by GC-MS for the kerosene-type military fuels, unleaded gasoline, and diesel No. 2 are listed

in Tables 3-8, along with the relative peak areas measured by GC-FID analyses of the fuels in the gas phase. As discussed in the previous section, the FID area response can be approximated as proportional to the ppmC gas phase concentration of the fuel components. Figures 4-9 show typical chromatograms of each of these fuels, with selected identified peaks labeled.

All these fuels consisted of alkane and aromatic mixtures and in no case were detectable amounts of alkenes or heteroatom-containing organics identified. In terms of the types and distribution of the fuel components, the kerosene-type military fuels are generally similar (regardless of whether they be shale oil- or petroleum-derived), except that JP-8 has much less of the lighter components and much more of the heavy components than JP-4. The gas chromatograms for these fuels are characterized by the regular n-alkane peaks, which is their most conspicuous feature. Unleaded gasoline is markedly different, with the n-alkanes being relatively less important and the dominant peaks being those of the various aromatic compounds. Diesel No. 2 consists primarily of heavier components; probably for this reason its gas chromatographic analyses were somewhat less reproducible.

The relative amounts of the various fuel components (Tables 3-8 and Figures 4-9) reflect the amounts of these species after the fuel has been injected into the gas phase (Section 2.3) and are not necessarily the same as the relative amounts of these species in the neat liquid fuel. To determine if there was a significant difference in this regard, one of the HP-5710A gas chromatographs was temporarily modified to allow direct injection of the liquid fuels. The injection system used was based on the standard sample splitting technique for GC analyses with capillary column systems and is shown schematically in Figure 10. The injection port was heated to 300°C and fuel analyses were initiated by injecting ~1 μℓ of the liquid fuels through this system using a microsyringe.

Three to five duplicate injections were carried out for each fuel, in some tests using the temperature program employed in the routine gas phase analyses and in other tests using the temperature program routinely employed on the GC-MS system. Although, as expected, the retention times varied with the temperature program used, there was no problem in determining the peak identifications from the different temperature programs.

TABLE 3. ORGANIC COMPOUNDS IDENTIFIED BY GC-MS IN PETROLEUM-DERIVED JP-4 AND RELATIVE AMOUNTS AS DETERMINED BY GC-FID PEAK AREAS.

Organic Compound	Compound Identification	G.C. Area (Relative)
C_5H_{12}	2-methylbutane	--
C_5H_{12}	n-pentane[a]	0.25
C_6H_{14}	2,2-dimethylbutane (tentative)	0.05
C_6H_{14}	branched alkane	0.08
C_6H_{14}	2-methylpentane	0.28
C_6H_{14}	3-methylpentane	0.19
C_6H_{14}	n-hexane	0.48
C_7H_{16}	2,4-dimethylpentane	0.03
C_6H_{12}	methylcyclopentane (tentative)	0.27
C_6H_{12}	cyclohexane	0.24
C_6H_6	benzene	0.10
C_7H_{16}	branched alkane	0.44
C_7H_{16}	branched alkane	0.41
C_7H_{14}	cycloalkane	0.11
C_7H_{16}	n-heptane	0.75
C_7H_{14}	methylcyclohexane	0.54
C_8H_{18}	branched alkane[a]	0.23
C_8H_{16}	cycloalkane	0.09
C_8H_{16}	trimethylcylopentane	0.05
C_8H_{18}	branched alkane	0.14
C_7H_8; C_8H_{18}	toluene + branched alkane[b]	1.00
C_8H_{16}	dimethylcyclohexane	0.07
C_8H_{18}	n-octane	0.80
C_9H_{20}	branched alkane	0.06
C_9H_{20}	dimethylheptane	0.10
C_9H_{18}	cycloalkane	0.12
C_9H_{18}	trimethylcyclohexane[a]	0.25
C_8H_{10}	ethylbenzene	0.10
C_8H_{10}	dimethylbenzene	0.28
C_9H_{20}	branched alkane	0.22
C_9H_{18}	cycloalkane	0.05

TABLE 3. ORGANIC COMPOUNDS IDENTIFIED BY GC-MS IN PETROLEUM-DERIVED JP-4 AND RELATIVE AMOUNTS AS DETERMINED BY GC-FID PEAK AREAS (concluded).

Organic Compound	Compound Identification	G.C. Area (Relative)
C_8H_{10}	dimethylbenzene or o-xylene	0.10
C_9H_{20}	n-nonane	0.47
C_9H_{18}	cycloalkane	0.04
C_9H_{12}	1,2,4,-trimethylbenzene	0.23
$C_{10}H_{22}$	n-decane	0.38
$C_{11}H_{24}$	n-undecane	0.43
$C_{12}H_{26}$	n-dodecane	0.42

[a]Not separated from other, unidentified fuel component(s).

[b]Not separated.

Calibration mixtures containing known amounts of n-alkanes and selected aromatics were also injected periodically to aid in peak identification.

The relative peak areas obtained were more variable for some fuels than others; as expected, they were unaffected by the temperature program employed. For diesel No. 2 and unleaded gasoline, good reproducibility in relative peak areas was observed in duplicate injections; but, for some components of petroleum-derived JP-4 (JP-4[pet]), variability by almost a factor of two in some ratios of peak areas was observed. The reason for this variability is unknown. However, for most fuels, much less variability was observed.

The relative peak areas for toluene and the n-alkanes observed in the analyses of the liquid fuels are summarized in Table 9 and compared with the relative areas for the gas phase analyses. For n-C_{11} and lighter components, there was a reasonably good correspondence between the gas- and liquid-phase analyses, but the amounts of gas-phase species heavier than n-C_{11} fell off rapidly relative to the amounts of these compounds in the neat liquid fuel. This is particularly dramatic for diesel No. 2, whose major components in the liquid fuel were too heavy to be seen

TABLE 4. ORGANIC COMPOUNDS IDENTIFIED BY GC-MS IN SHALE-DERIVED JP-4, AND RELATIVE AMOUNTS AS DETERMINED BY GC-FID PEAK AREAS.

Organic Compound	Compound Identification	G.C. Area (Relative)
C_5H_{12}	2-methylbutane[a]	0.12
C_5H_{12}	n-pentane[a]	0.21
C_6H_{14}	branched alkane	0.04
C_6H_{14}	2-methylpentane	0.21
C_6H_{14}	3-methylpentane	0.11
C_6H_{14}	n-hexane	0.26
C_6H_{12}	methylcylopentane (tentative)	0.11
C_6H_{12}; C_6H_6	cycloalkane + benzene[b]	0.14
C_7H_{16}	branched alkane[a]	0.14
C_7H_{16}	3-methylhexane	0.22
C_7H_{14}	cycloalkane	0.05
C_7H_{16}	n-heptane	0.35
C_7H_{14}	2-methylcyclohexane	0.42
C_8H_{18}	branched alkane	0.11
C_8H_{16}	trimethylcyclopentane (tentative)	0.03
C_8H_{18}	branched alkane[a]	0.03
C_7H_8; C_8H_{18}	toluene + branched alkane[b]	0.65
C_8H_{16}	dimethylcylohexane[c] (tentative)	0.29
C_8H_{16}	dimethylcyclohexane (tentative)	0.12
C_8H_{18}	n-octane	0.39
C_8H_{16}	cycloalkane	0.16
C_8H_{16}	cycloalkane	0.07
C_9H_{20}	2,6-dimethylheptane	0.16
C_9H_{18}	cycloalkane	0.18
C_9H_{18}	C_3 alkylcyclohexane (tentative)	0.25
C_9H_{18}	1,2,4-trimethylcyclohexane	0.10
C_8H_{10}	dimethylbenzene + m- and p-xylene (tentative)	0.29
C_9H_{20}	branched alkane	0.21
C_9H_{18}	cycloalkane	0.16
C_8H_{10}	dimethylbenzene	0.11

TABLE 4. ORGANIC COMPOUNDS IDENTIFIED BY GC-MS IN SHALE-DERIVED JP-4, AND RELATIVE AMOUNTS AS DETERMINED BY GC-FID PEAK AREAS (concluded).

Organic Compound	Compound Identification	G.C. Area (Relative)
C_9H_{20}	n-octane	0.57
C_9H_{18}	cycloalkane	0.10
$C_{10}H_{22}$	2,6-dimethyloctane	0.24
C_9H_{12}	1,2,4-trimethylbenzene	0.20
$C_{10}H_{22}$	n-decane	0.78
$C_{11}H_{24}$	4-methyldecane	0.36
$C_{10}H_{18}$	trans-decahydronapthalene	0.69
$C_{11}H_{24}$	n-undecane	1.00
$C_{12}H_{26}$	n-duodecane	0.29
$C_{13}H_{28}$	dimethylundecane	

[a]Not separated from other, unidentified fuel component(s).

[b]Not separated.

[c]More than one isomer.

in the gas phase. The problems involved in introducing diesel No. 2 and the other heavy fuels are discussed in more detail in Section 2.3.

2.2.2 High Energy Fuels

Representative chromatograms from the GC-FID analyses of RJ-4 and RJ-5 in the gas phase are shown in Figures 11 and 12, respectively. A chromatogram for JP-10, the other high-energy fuel studied in this program, is not shown since it was found to consist of a single peak corresponding to the sole significant component of that fuel, namely exotetrahydrodicyclopentadiene (Figure 1). The major peaks of RJ-4 and RJ-5, whose observed concentrations in the outdoor chamber runs are reported on the data sheets in Volume II, are also indicated in Figures 11 and 12 (A-G for RJ-4 and A-C for RJ-5).

In an attempt to identify the seven major components of RJ-4 and the three major components of RJ-5, GC-MS analyses were carried out on these fuels. Unfortunately, mass spectroscopy is not the best technique for

TABLE 5. ORGANIC COMPOUNDS IDENTIFIED BY GC-MS IN PETROLEUM-DERIVED JP-8 AND RELATIVE AMOUNTS AS DETERMINED BY GC-FID PEAK AREAS.

Organic Compound	Compound Identification	G.C. Area (Relative)
C_8H_{18}	n-octane	0.03
C_8H_{10}	m-xylene	0.06
C_8H_{10}	o-xylene	0.03
C_9H_{20}	n-nonane	0.12
C_9H_{12}	1,2,4-trimethylbenzene	0.09
C_9H_{12}	C_3-alkylbenzene	0.06
$C_{10}H_{22}$	n-decane	0.34
$C_{11}H_{24}$	4-methyldecane	0.15
$C_{11}H_{24}$	n-undecane	1.09
$C_{11}H_{20}$	methyldecahydronaphthalene	0.24
$C_{11}H_{16}$	mixture, mainly C_5-alkylbenzene	0.20
$C_{12}H_{24}$	cycloalkane	0.25
$C_{12}H_{26}$	n-dodecane	1.00
$C_{13}H_{28}$	dimethylundecane	0.31
$C_{14}H_{30}$	branched alkane	-
$C_{14}H_{28}$	cycloalkane	0.19
$C_{13}H_{28}$	n-tridecane	0.53
a	(not aromatic)	0.08

[a]Formula not determined

unambiguously identifying the compounds present in these fuels and the primary information obtained using this technique was their molecular weights.

For RJ-4, all eleven of the peaks larger than 10% of the height of the largest GC peak had a parent MS peak at an m/e of 164. This mass is consistent with the tetrahydrodi(methylcyclopentadiene) isomers in this fuel (Reference 1). Since all eleven mass spectra were very similar,

TABLE 6. ORGANIC COMPOUNDS IDENTIFIED BY GC-MS IN SHALE-DERIVED JP-8 AND RELATIVE AMOUNTS AS DETERMINED BY GC-FID PEAK AREAS.

Organic Compound	Compound Identification	G.C. Area (Relative)
C_7H_8	toluene	0.02
C_8H_{18}	n-octane	< 0.01
C_8H_{10}	m-xylene	0.05
C_8H_{10}	o-xylene	0.03
C_9H_{20}	n-nonane	0.09
C_9H_{18}	propylcyclohexane	0.04
$C_{10}H_{22}$	2,6-dimethyloctane	0.08
$C_{10}H_{22}$	branched alkane	0.09
$C_{10}H_{20}$	cycloalkane	0.10
$C_{10}H_{22}$	branched alkane + alkylbenzene[a]	0.23
$C_{10}H_{20}$	cycloalkane	0.13
C_9H_{12}	C_3 alkylbenzene	0.17
$C_{10}H_{22}$	n-decane	0.82
	alkylbenzene[a]	0.26
$C_{11}H_{24}$	4-methyldecane[a]	0.23
$C_{11}H_{24}$	methyldecane[a]	0.17
$C_{11}H_{24}$	n-undecane	1.00
$C_{12}H_{26}$	n-dodecane	0.56
$C_{13}H_{28}$	branched alkane[a]	0.83
$C_{14}H_{30}$	branched alkane[a]	0.10
$C_{13}H_{28}$	n-tridecane	0.19
$C_{15}H_{32}$	branched alkane	0.03
$C_{11}H_{30}$	n-tetradecane	0.05
$C_{15}H_{32}$	n-pentadecane	0.08

[a]More than one compound.

TABLE 7. ORGANIC COMPOUNDS IDENTIFIED BY GC-MS IN UNLEADED GASOLINE AND RELATIVE AMOUNTS AS DETERMINED BY GC-FID PEAK AREAS.

Organic Compound	Compound Identification	G.C. Area (Relative)
C_5H_{12}	n-pentane	0.37
C_5H_{10}	cyclopentane	0.16
C_6H_{14}	branched alkane	0.08
C_6H_{14}	branched alkane	0.26
C_6H_{14}	branched alkane	0.17
C_6H_{14}	n-hexane	0.14
C_6H_{12}	methylcyclopentane	0.16
C_6H_{12}	cycloalkane	
C_6H_6	benzene[a]	0.21
C_7H_{16}	branched alkane	0.22
C_7H_{16}	3-methylhexane (tentative)	0.17
C_7H_{16}	n-heptane	0.13
C_7H_{14}	methylcyclohexane	0.05
C_8H_{16}	cycloalkane	0.03
C_7H_8	toluene	1.00
C_8H_{18}	branched alkane	0.11
C_9H_{20}	branched alkane	0.07
C_8H_{10}	dimethylbenzene	0.18
C_8H_{10}	dimethylbenzene	0.69
C_8H_{10}	dimethylbenzene (possibly o-xylene)	0.25
C_9H_{20}	n-nonane	0.02
C_9H_{12}	C_3-alkylbenzene	0.02
C_9H_{12}	n-propylbenzene	0.05
C_9H_{12}	methylethylbenzene[a]	0.22
C_9H_{12}	trimethylbenzene	0.07
C_9H_{12}	methylethylbenzene	0.05
C_9H_{12}	1,2,4-trimethylbenzene	0.23
$C_{10}H_{22}$	n-decane	0.01
$C_{10}H_{14}$	C_4-alkylbenzene	0.05
C_9H_{12}	C_3-alkylbenzene	0.02
$C_{10}H_{14}$	methylpropylbenzene[b]	0.03

[a]Not separated from some other, non-aromatic compound.
[b]Probably more than one compound.

TABLE 8. ORGANIC COMPOUNDS IDENTIFIED BY GC-MS IN DIESEL NO. 2 AND RELATIVE AMOUNTS AS DETERMINED BY GC-FID PEAK AREAS.

Organic Compound	Compound Identification	G.C. Area (Relative)
C_5H_{12}	2-methylbutane	0.04
C_5H_{12}	n-pentane	0.04
C_6H_{14}	branched alkane	0.04
C_6H_{14}	branched alkane	0.10
C_6H_{14}	n-hexane	0.04
C_6H_{12}	methylcyclopentane	0.05
C_6H_{12}	cyclohexane (tentative)	0.05
C_6H_6	benzene	0.05
C_7H_{16}	3-methylhexane (tentative)	0.02
C_7H_{16}	n-heptane	0.02
C_7H_{14}	methylcyclohexane	0.13
C_7H_8	toluene	0.14
C_8H_{16}	cycloalkane	0.10
C_8H_{18}	n-octane	0.07
C_8H_{16}	cyclohexane (tentative)	0.05
C_8H_{10}	dialkyl benzene	0.05
C_8H_{10}	m-xylene	0.15
C_8H_{10}	o-xylene	0.08
C_9H_{20}	n-nonane	0.13
C_9H_{12}	C_3-alkylbenzene	0.12
$C_{10}H_{22}$	n-decane	0.23
$C_{11}H_{24}$	n-undecane	0.40
$C_{12}H_{26}$	n-dodecane	0.66
$C_{11}H_{10}$	methylnaphthalene	0.37
$C_{13}H_{28}$	n-tridecane	1.00
$C_{16}H_{30}$	n-tetradecane	0.40
$C_{15}H_{32}$	n-pentadecane	0.87

TABLE 9. RELATIVE AMOUNTS OF SELECTED COMPONENTS OF SHALE- AND PETROLEUM-DERIVED JP-4 AND JP-8, UNLEADED GASOLINE AND OF DIESEL No. 2, AND COMPARISON OF DIRECT LIQUID AND GAS PHASE ANALYSES.

FUEL COMPONENT	RELATIVE PEAK AREAS[a]											
	JP4-(PET)		JP-4(SHALE)		JP-8(PET)		JP-8(SHALE)		UNLEADED GASOLINE		DIESEL #2	
	LIQ.	GAS	LIQ.	GAS	LIQ.	GAS	LIQ.	GAS	LIQ.	GAS	LIQ.	GAS
Toluene	1.00	(1.00)[b]	0.45	~0.65	--	--	--	~0.02	1.00	(1.00)[b]	0.08	0.05
n-C_5	0.21	~0.25	0.11	~0.21	--	--	--	--	0.19	0.37	--	0.02
n-C_6	0.42	0.48	0.46	0.26	--	--	--	--	0.15	0.14	0.02	0.02
n-C_7	0.75	0.75	0.38	0.35	--	--	--	--	0.14	0.13	0.03	0.02
n-C_8	0.86	0.80	0.49	0.39	--	~0.02	--	--	0.08	--	0.05	0.03
n-C_9	0.47	0.47	0.62	0.57	0.07	0.09	0.06	0.09	0.02	0.02	0.06	0.04
n-C_{10}	0.34	0.38	0.89	0.78	0.24	0.25	0.80	0.82	--	--	0.08	0.08
n-C_{11}	0.38	0.43	1.00	(1.00)[b]	0.81	(0.81)[b]	1.00	(1.00)[b]	--	--	0.14	0.14
n-C_{12}	0.34	0.42	0.78	0.29	1.00	0.74	0.76	0.56	--	--	0.23	(0.23)[b]
n-C_{13}	0.22	--	0.39	--	0.72	0.39	0.36	0.19	--	--	0.40	0.35
n-C_{14}	0.12	--	0.15	--	0.47	--	0.11	~0.05	--	--	0.60	0.14
n-C_{15}	0.03	--	0.06	--	0.25	--	0.03	--	--	--	0.82	--
n-C_{16}[c]	--	--	--	--	--	--	--	--	--	--	1.00	--
n-C_{17}[c]	--	--	--	--	--	--	--	--	--	--	0.80	--
n-C_{18}[c]	--	--	--	--	--	--	--	--	--	--	0.67	--
n-C_{19}[c]	--	--	--	--	--	--	--	--	--	--	0.39	--
n-C_{20}[c]	--	--	--	--	--	--	--	--	--	--	0.16	--

[a]Areas given relative to the component which gave largest peak in liquid injection.

[b]Set to be the same as the relative amount in the liquid analysis. Other gas phase results relative to this.

[c]Assignment assumed; not verified by authentic samples.

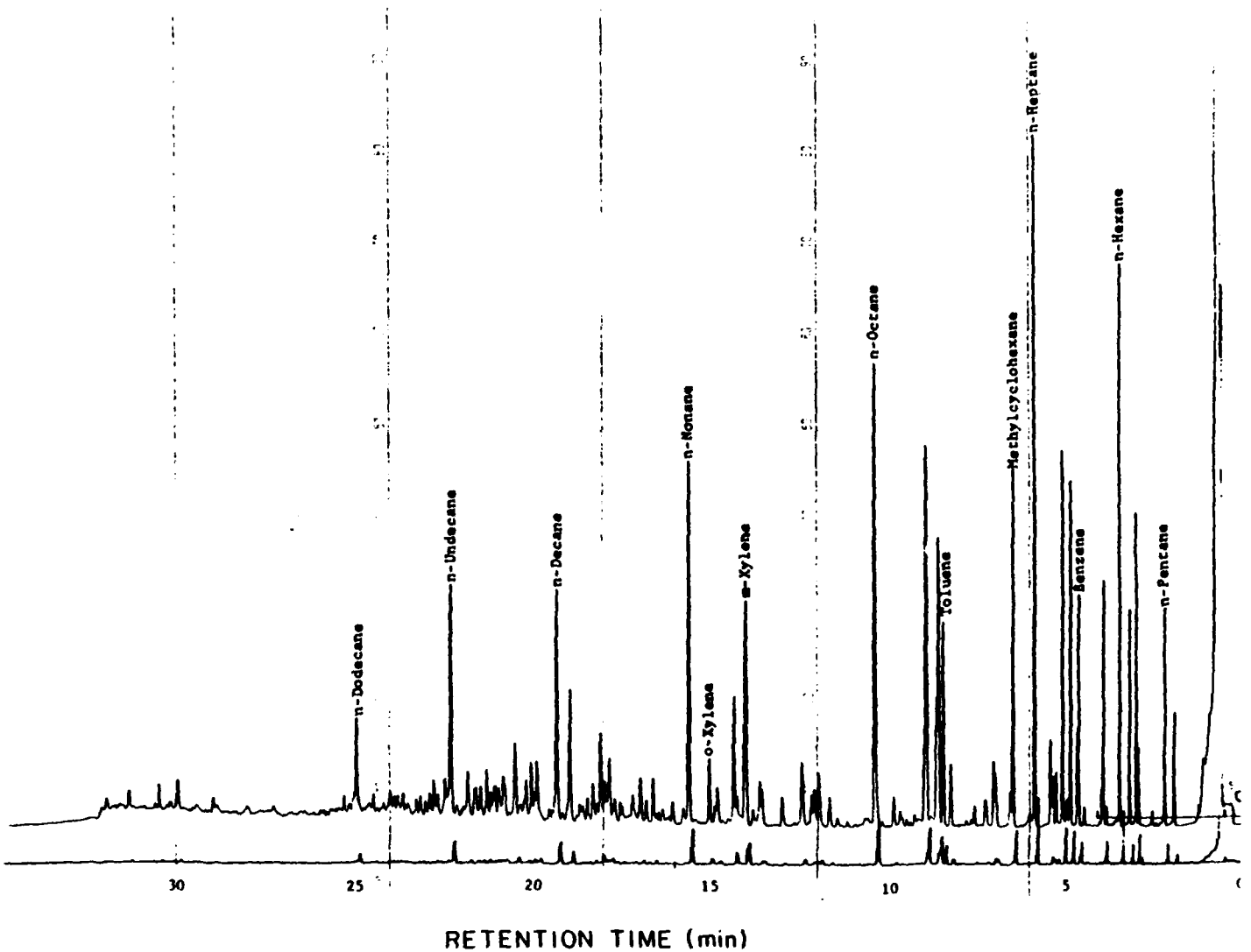

Figure 4. Representative Gas Chromatogram of Petroleum-Derived JP-4 in Air.

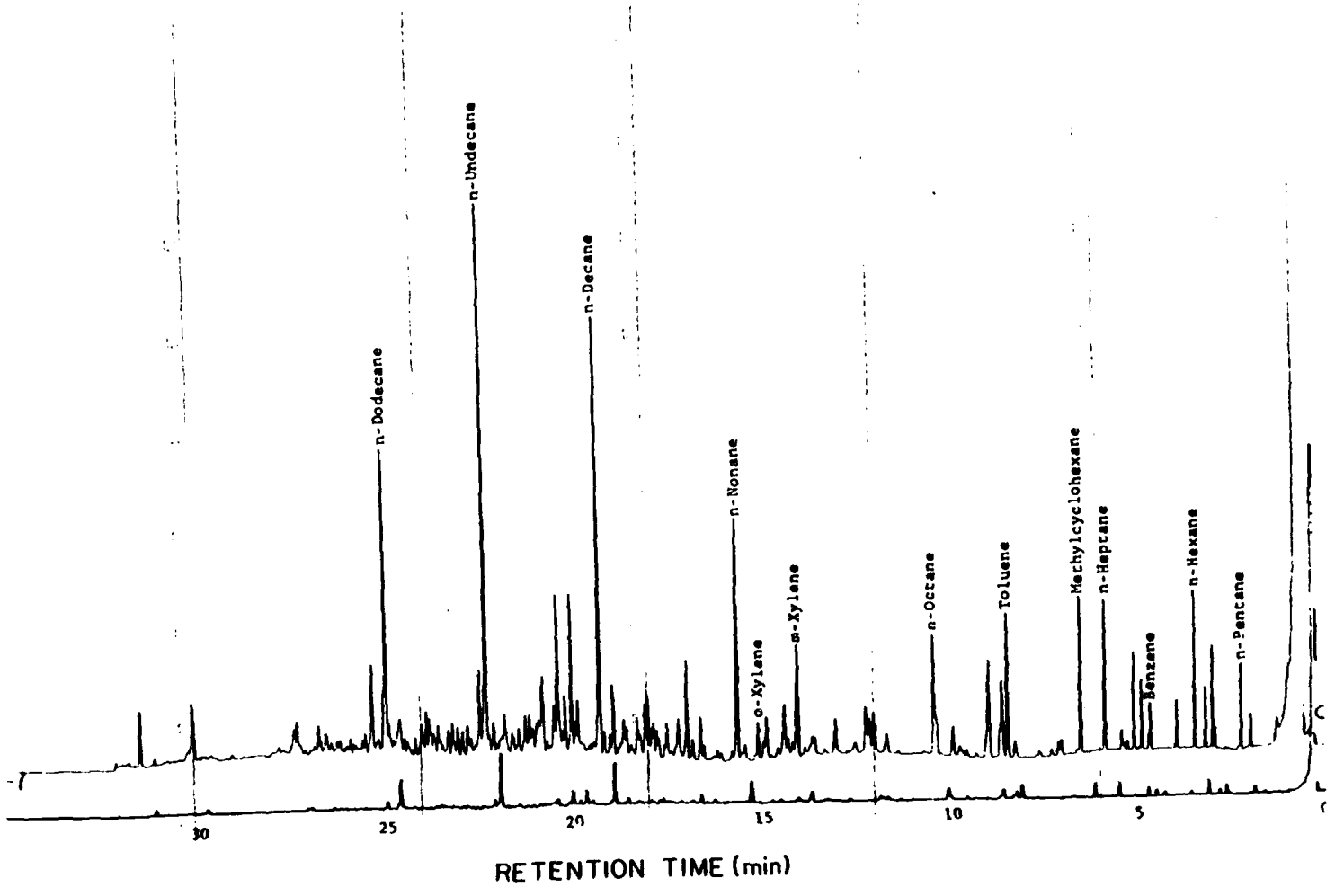

Figure 5. Representative Gas Chromatogram of Shale-Derived JP-4 in Air.

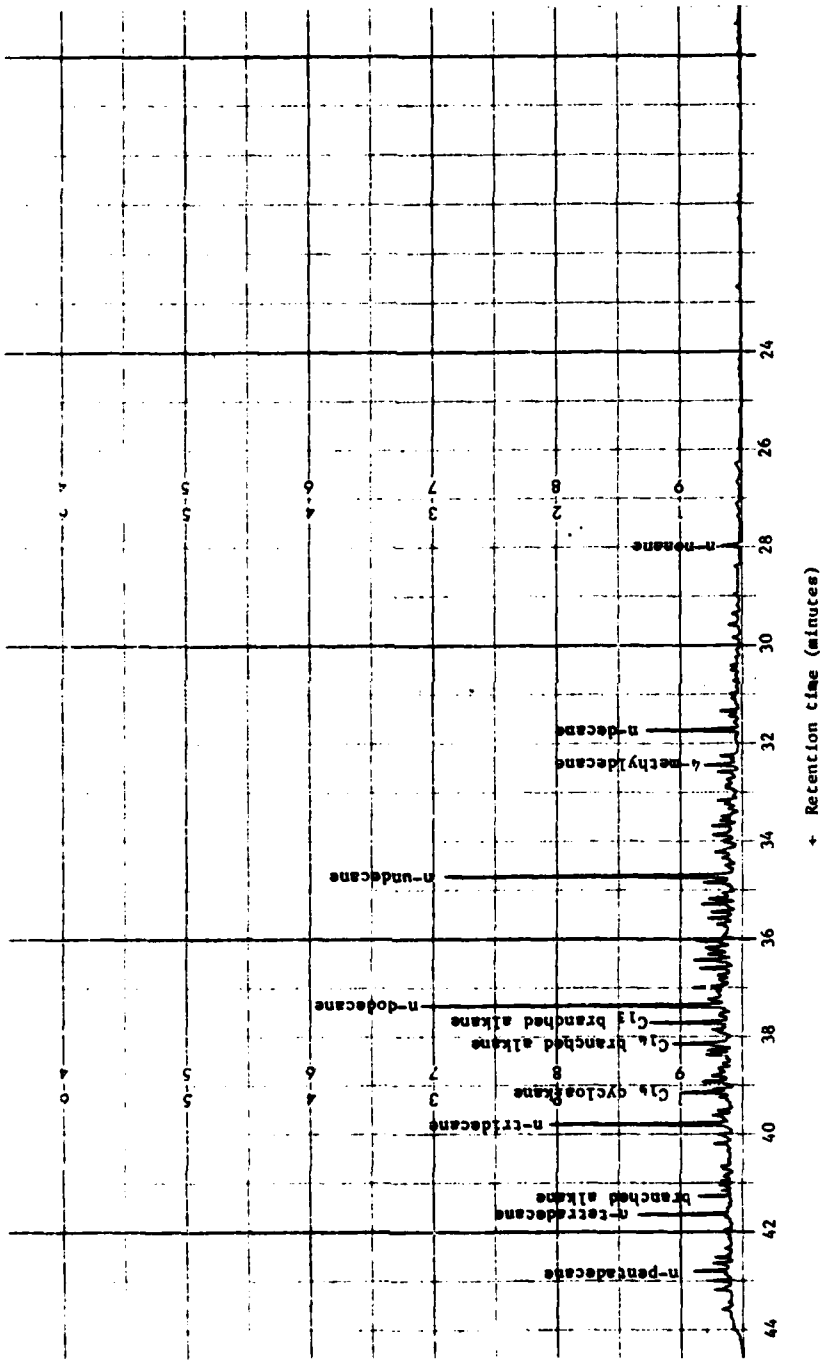

Figure 6. Representative Chromatogram of Petroleum-Derived JP-8 in Air.

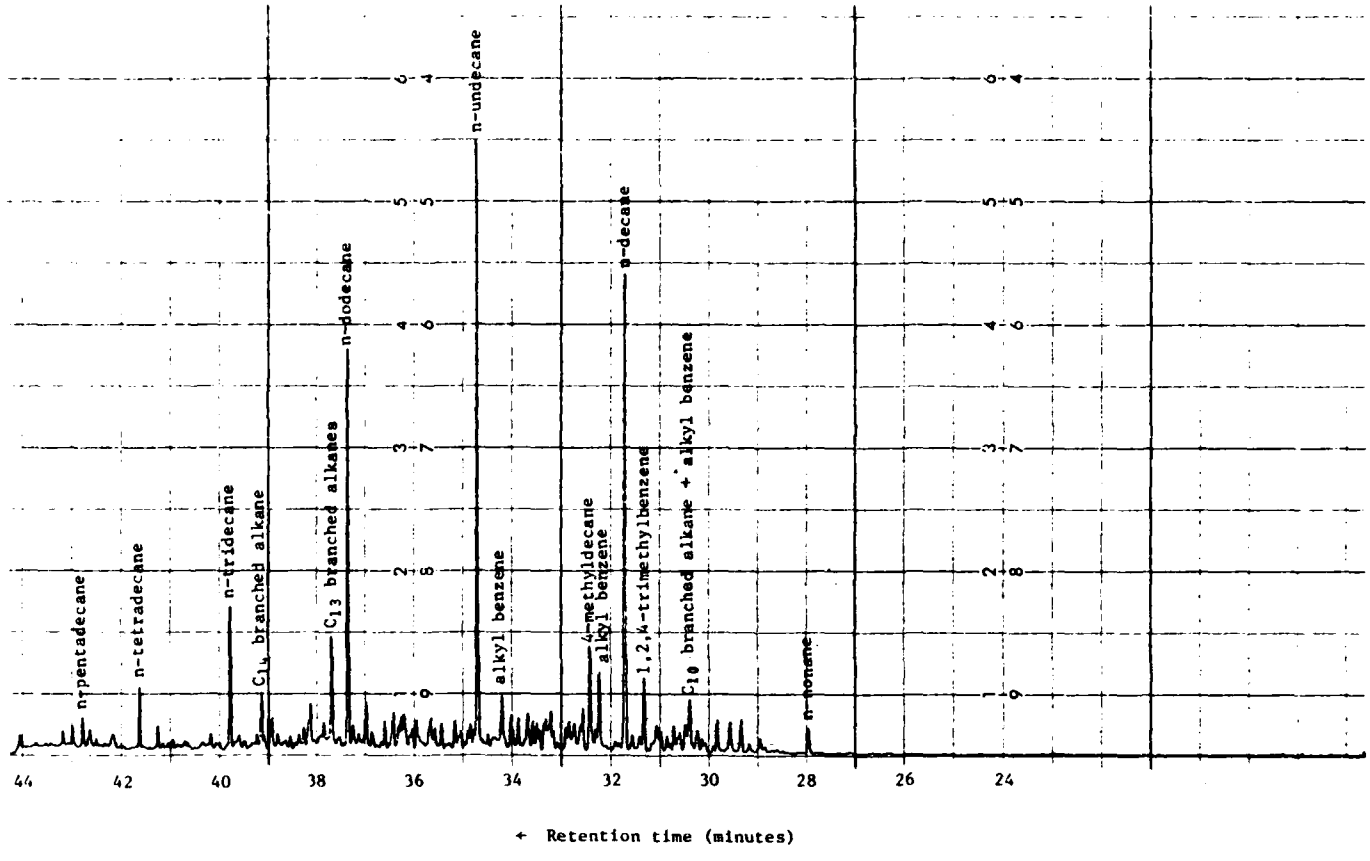

Figure 7. Representative Chromatogram of Shale-Derived JP-8 in Air.

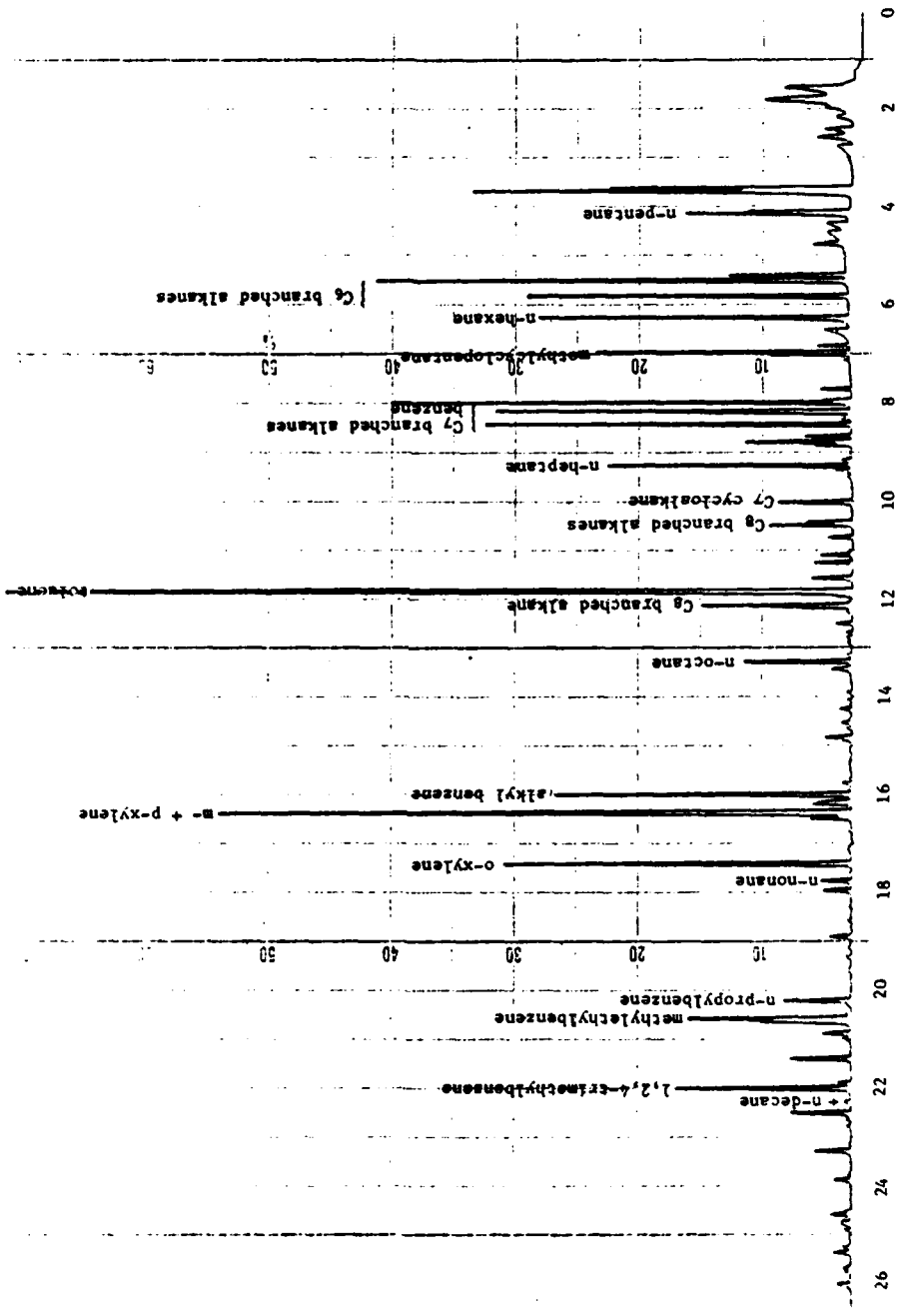

Figure 8. Representative Chromatogram of Unleaded Gasoline in Air.

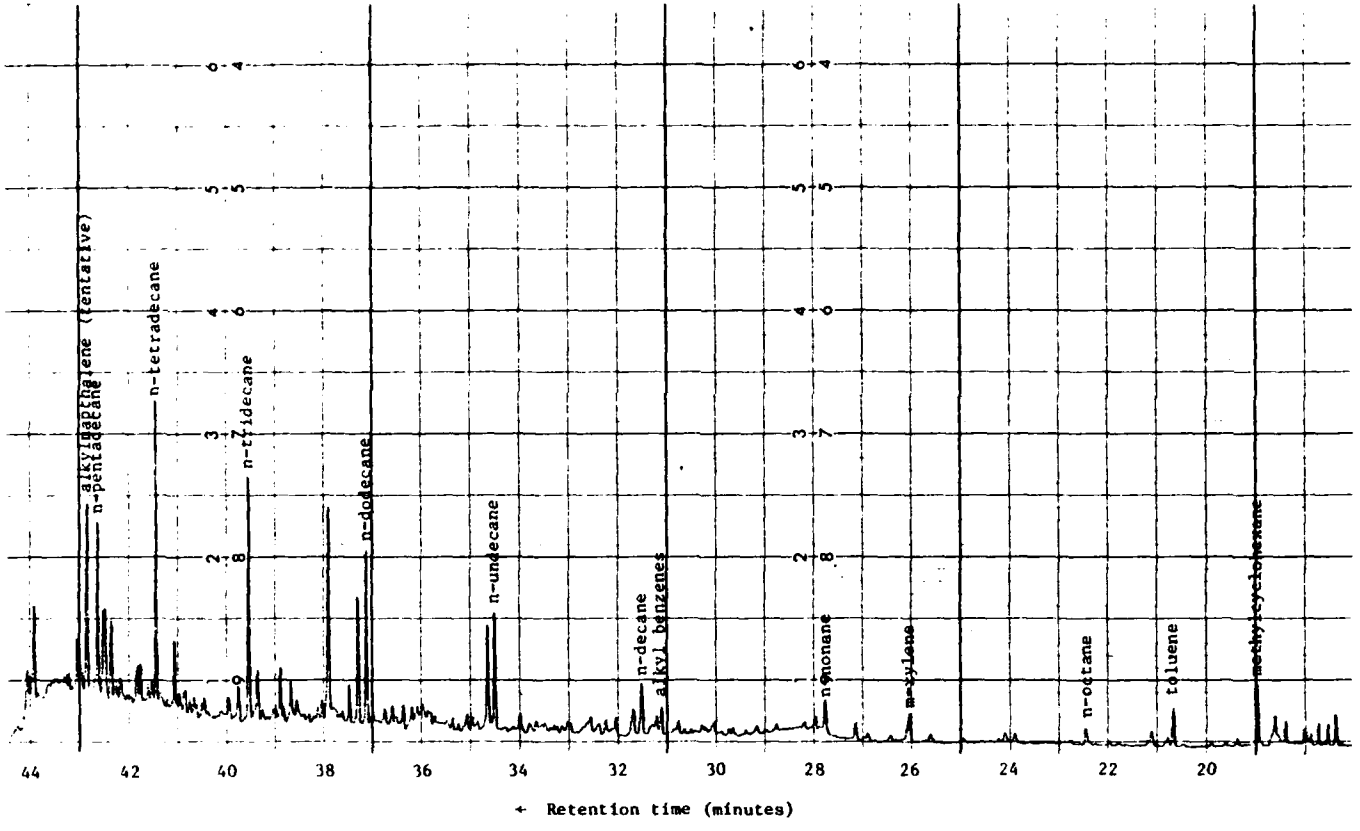

Figure 9. Representative Chromatogram of Diesel No. 2 in Air.

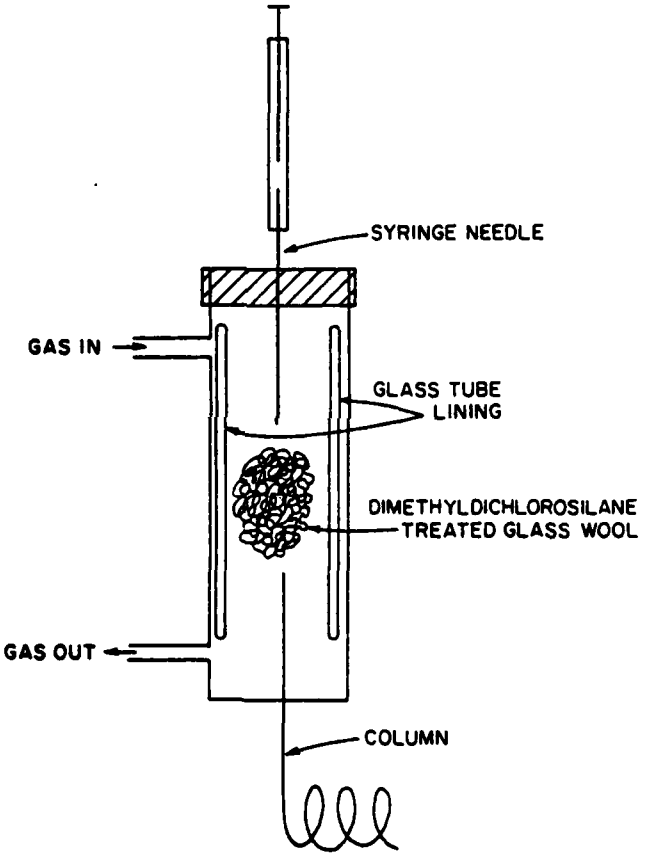

Figure 10. Injection System Used for Capillary Column Gas Chromatographic Analyses of the Neat Liquid Fuels.

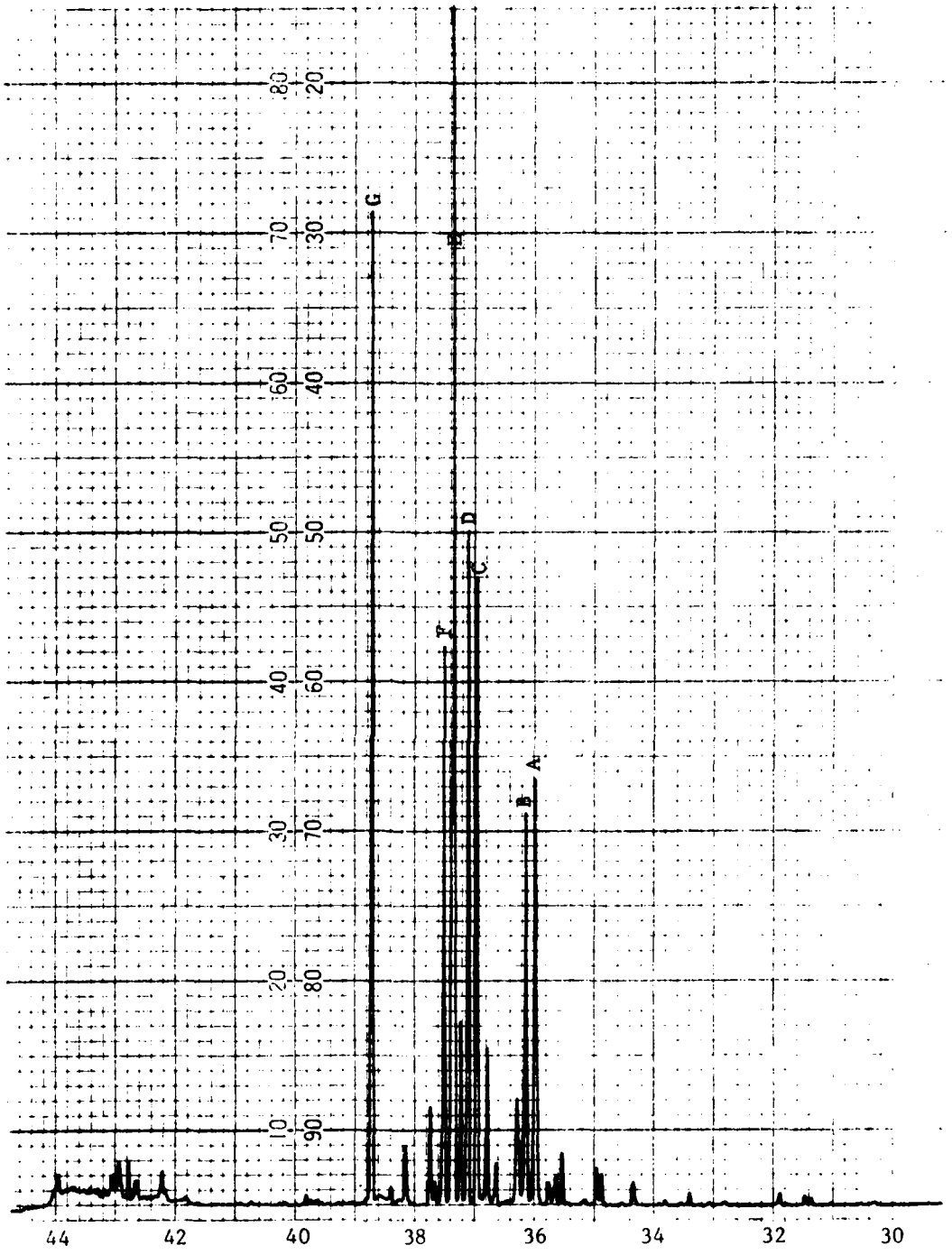

Figure 11. Representative Gas Chromatogram of RJ-4 in Air

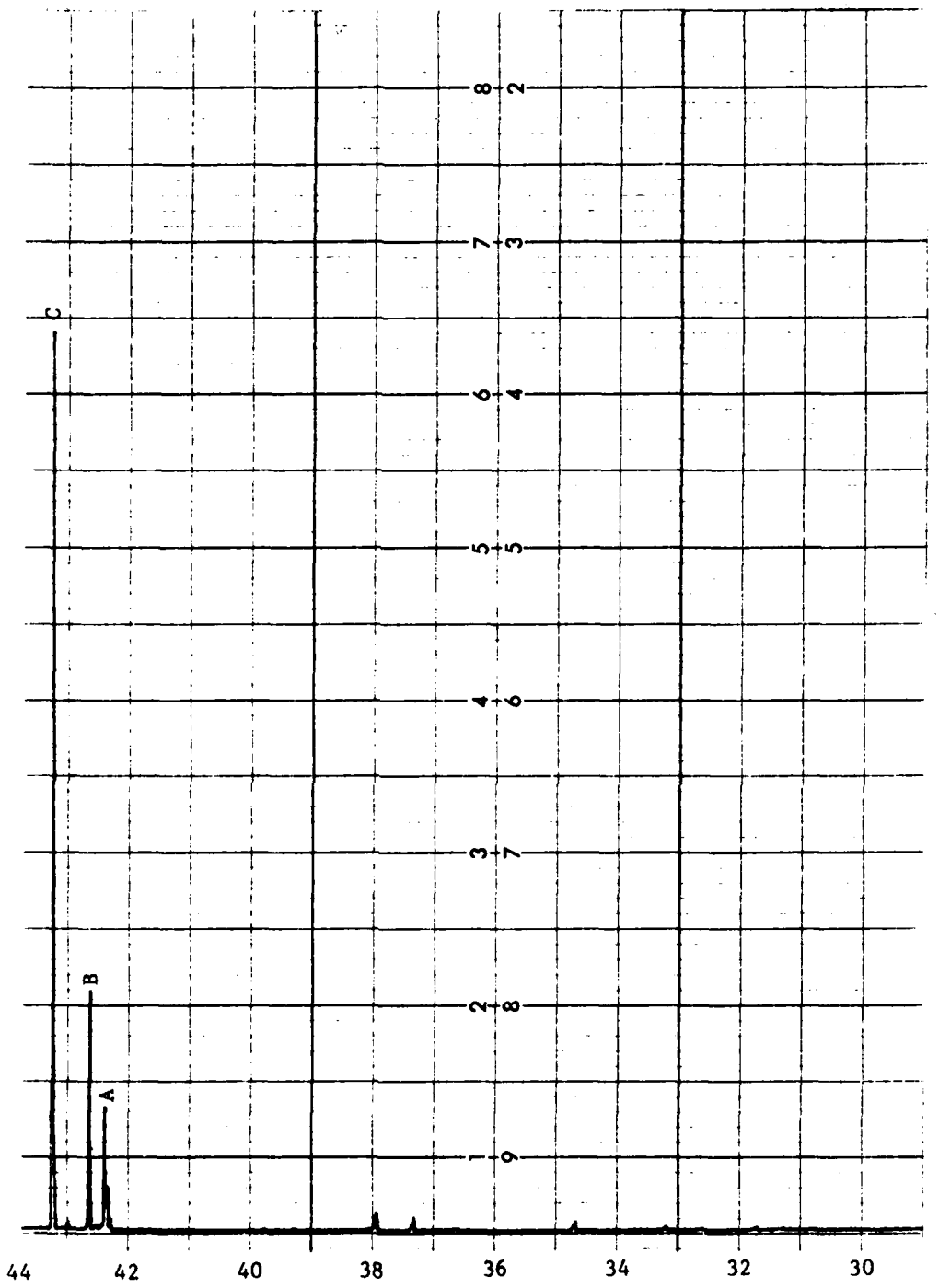

Figure 12. Representative Gas Chromatogram of FJ-5 in Air

exact identification of the isomers would require either obtaining authentic samples, or separating the components of RJ-4 and performing NMR and IR spectroscopic analyses (which was beyond the scope of this program).

For RJ-5 the two largest peaks in the gas chromatograms (components B and C in Figure 12) had a parent m/e of 186. This is consistent with these being among the possible $C_{14}H_{18}$ isomers of the hydrogenated norbornadiene dimers shown in Figure 1. Although we were unable to further elucidate which of the possible isomers these peaks corresponded to, the work of Ashland Oil, Inc. (Reference 8) indicates that the dominant $C_{14}H_{18}$ species are probably those shown in Figure 1.

The third largest GC peak in RJ-5 (A in Figure 12) was found to be a mixture of at least two compounds, with molecular weights of 184 and 188. This is consistent with the $C_{14}H_{16}$ and the $C_{14}H_{20}$ isomers of the hydrogenated norbornadiene compounds (Figure 1). As with RJ-4, the unambiguous elucidation of the structures of the major components of this fuel was beyond the scope of this project.

2.3 DEVELOPMENT OF FUEL INJECTION TECHNIQUES

For chamber irradiations of these fuels to be useful for comparative purposes, it was essential that the fuels be introduced into the gas phase in a reproducible manner. All of the fuels studied, except JP-10, were complex mixtures of different compounds of varying volatility, each of which may have a significantly different atmospheric reactivity. Thus, it was clearly not satisfactory to have varying amounts of the relatively heavier components introduced into the gas phase in different experiments, even if the amount of gas phase carbon was the same. For the fuels which consist primarily of volatile components, this was less of a problem, since the optimum technique was to assure that the fuel was completely vaporized and that none of the light components were lost during handling prior to injection. However, complete vaporization of the heavier fuels at room temperature was extremely difficult, if not impossible.

It is clearly impossible to introduce all of a fuel into the vapor phase, if the fuel contains components whose vapor pressure is lower than their gas phase concentration would be for complete vaporization. Based on our analyses of the liquid fuels (Section 2.2), the heaviest components present appear to be: for unleaded gasoline, n-C_9; JP-4, n-C_{15}; JP-8, n-C_{16}; and diesel fuel, probably n-C_{22} or n-C_{23}. Since the vapor pressure

of n-C_{16} is estimated to be ~88 ppmC (based on extrapolation of the data given in the CRC handbooks [Reference 9]), it should theoretically be possible to introduce essentially all of unleaded gasoline, JP-4, and JP-8 into the gas phase in experiments employing 50 ppmC of fuel (the highest concentration used in this study). However, it is probably not possible to introduce all of diesel fuel into the gas phase, no matter how efficient the injection techniques employed can be made.

In order to assess the problems which might be encountered regarding fuel volatility (or lack thereof) the following test was conducted for each of the fuels studied in this program: (1) An 0.25 in o.d. x 3 in silylated Pyrex® tube, packed with silylated Pyrex® wool previously flushed with N_2, was accurately weighed; (2) This tube was dosed with the desired volume of the fuel, using a microsyringe or micropipette, and weighed again; (3) The tube was allowed to sit for five minutes at room temperature and then re-weighed; (4) Finally, the tube was flushed with N_2 at 1 ℓ min^{-1} for three five-minute intervals and re-weighed after each interval. After 10 minutes of flushing, < 3% of unleaded gasoline, JP-4, JP-10, RJ-4, and JP-8 (shale) remained, but after 15 minutes of flushing ~5% of JP-8 (pet), ~68% of diesel fuel, and ~83% of RJ-5 still remained. JP-4 was the only fuel that evaporated to a significant extent at the five-minute period before the nitrogen flush; for example, in one test ~7% of JP-4 (pet) evaporated upon standing for five minutes. These results indicated that care had been taken to avoid evaporation of JP-4 while handling, and that JP-8, diesel fuel, and RJ-5 could probably not be injected in a reasonable amount of time without heating.

The technique employed for the injection of the more volatile fuels (unleaded gasoline, JP-4, and JP-10) is illustrated in Figure 13. The desired quantity of the liquid fuel (normally ~300 µl to 1000 µl for outdoor chamber runs and ~100 µl for indoor chamber runs) was placed in an ~1 ℓ bulb and the bulb was then flushed for 15 minutes with N_2 at 5 ℓ min^{-1}, while being heated with a heat gun. After this time period, all of the liquid fuel had disappeared, and tests showed that reasonably complete and reproducible injections could be obtained for these fuels using this technique.

These tests indicated that the technique illustrated in Figure 13 was not satisfactory for the less volatile fuels (JP-8, RJ-4, RJ-5, and diesel

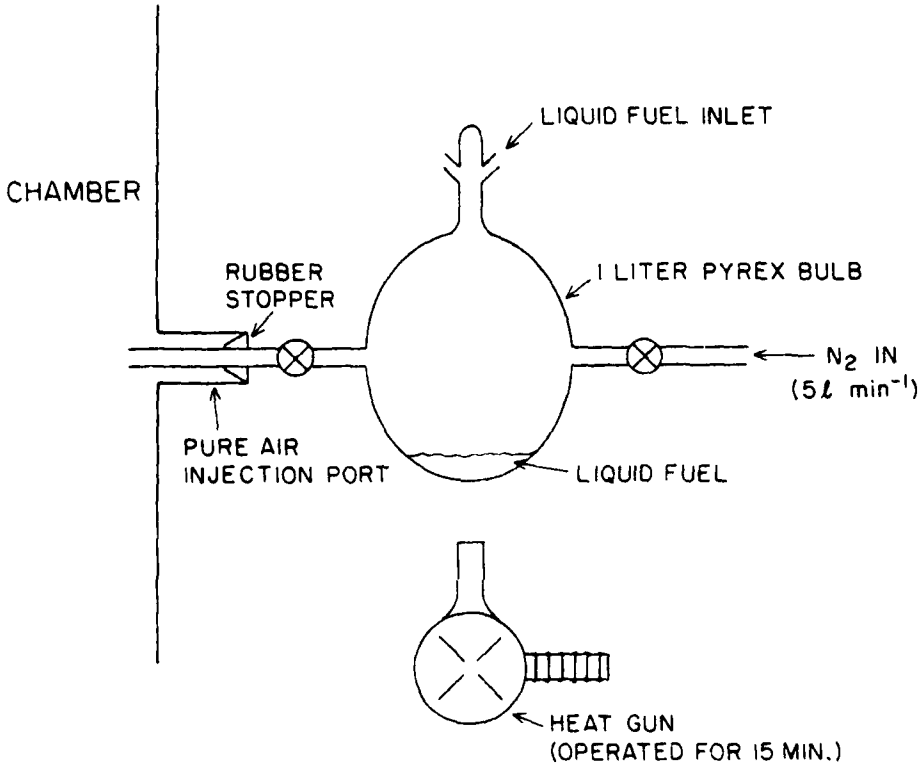

Figure 13. Technique for Injection of the Lighter Fuels into the Gas Phase.

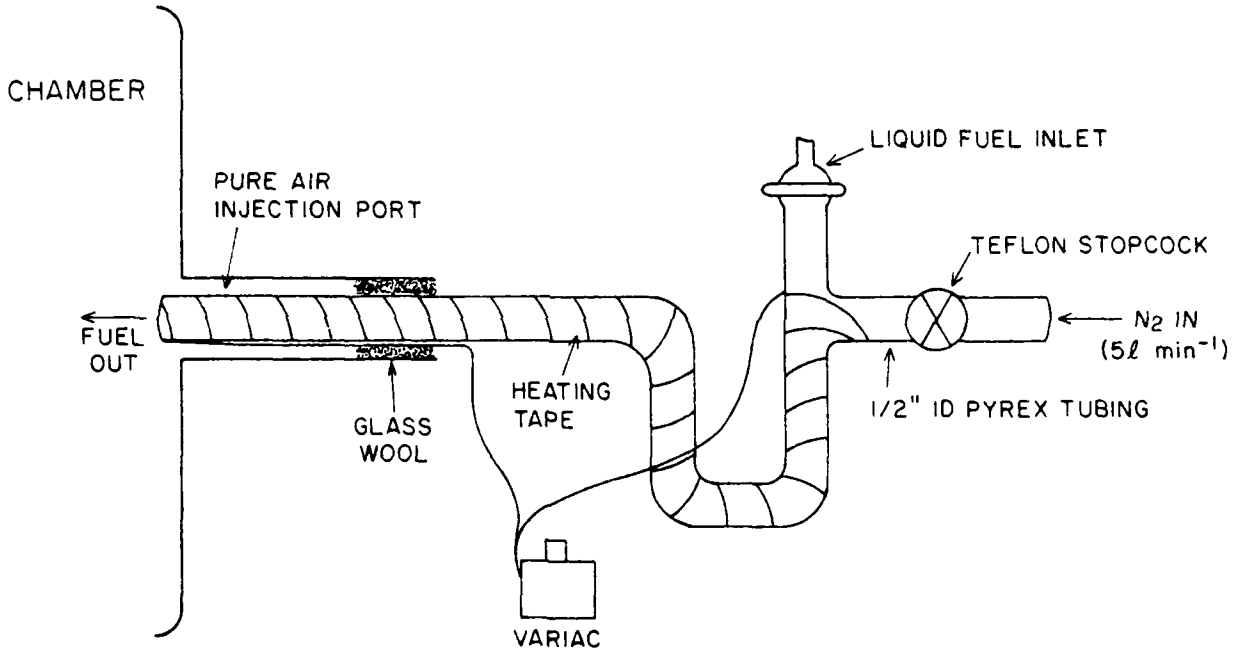

Figure 14. Apparatus for Introduction of the Less Volatile Fuels into the Gas Phase.

fuel), since these fuels tended to condense on the inlet tube where it could not easily be reached with the heat gun. To circumvent this problem, the injection system illustrated in Figure 14 was developed. As shown in the figure, this consisted of a 0.5 in i.d. Pyrex® tube wrapped with heating tape and clamped to the pure air injection port. The appropriate volume of the liquid fuel was placed in the unheated tube, which was then flushed with N_2 at 5 ℓ min^{-1} for two minutes without heat, and then for another ~30 minutes with heat. The Variac power for the heating tape was set to give an equilibrium temperature of 250°C and it took ~5 minutes to attain this temperature. No visible liquid fuel remained in the tube after this procedure.

This procedure was tested by injecting JP-8 or diesel fuel into the indoor Teflon® chamber (ITC). The results of these preliminary experiments indicated unsatisfactory reproducibility in these injections. (See Section 2.4 for more discussion on the indoor chamber experiments). This reproducibility problem was probably due to insufficient mixing occurring during the injection process, thus allowing the less volatile fuel components to condense out of the vapor phase when present in locally high concentrations. Since rapid mixing of the reactants was easier in large Teflon® bags (such as those employed in the outdoor runs) than in the ITC (because the sides of the outdoor bag could be agitated to a far greater extent), it was decided to discontinue the ITC tests and concentrate on obtaining reproducible fuel injections in the large outdoor bags.

Experiments were conducted using the outdoor chamber facility (Section 3.1), where JP-4 and JP-8 were injected using the heated tube with varying temperatures and N_2 flow rates. The total nonmethane hydrocarbon (NMHC) levels were measured by the Byron hydrocarbon analyzer and the individual fuel components were analyzed by gas chromatography (Section 2.1). The experimental conditions and selected results are summarized in Table 10. As expected, reasonably reproducible injections could be attained with JP-4 at 100°C, but at least 250°C was required to inject the heavier components of JP-8. There appear to be no significant differences between injections carried out with 4 ℓ min^{-1} flow rates and those at 2 ℓ min^{-1}. Thus, it can be concluded on the basis of the results of runs 5-7

(Table 10) that satisfactorily complete and reproducible injections of JP-8 could be obtained, providing that the injection temperature was at least 250°C.

Since this technique worked satisfactorily for JP-8, it was employed for the RJ-4, RJ-5, and diesel fuels for the injection technique to be consistent for all the heavy fuels employed in this study. An indication of how well this worked for the kerosene-type military fuels and the civilian fuels can be obtained from Table 9 in Section 2.2.1, where analyses of the fuels injected into the gas phase are compared with analyses of the neat liquid fuels. As noted there, the gas-liquid correspondence was reasonably good for the $n\text{-}C_{11}$ and lighter compounds, but the results suggest incomplete injection of $n\text{-}C_{12}$ and heavier species. However, it is not clear to what extent the failure to observe all of the heavier compounds in the gas phase was due to deficiencies in the fuel injection technique or deficiencies in the gas chromatographic analyses of these compounds (see Section 2.1).

An alternate way to assess how well the fuel injection technique worked is to compare the observed total hydrocarbon measurements in the outdoor chamber runs with the values calculated, using the mass of liquid fuel injected together with the percent of carbon in the whole fuel and the volume of the chamber. The ratios of observed to calculated total hydrocarbon for all of the outdoor chamber runs in which the standard concentration of fuel was employed (~25 ppmC, nominal) are summarized in Table 11. These data suggest that most of JP-4, unleaded gasoline, JP-10, and RJ-4 were injected into the gas phase. However, only ~75% of JP-8 (by comparing ratios for JP-8 with JP-4), 40-50% of RJ-5 (by comparing ratios for RJ-5 with RJ-4), and ~20-30% of diesel fuel could be injected into the gas phase with this technique. These figures are somewhat uncertain, since it is possible that some of the heavier components are lost in the sample lines before they reach the total carbon analyzer detector (Section 3.2.3). However, it is reasonably clear that much of diesel No. 2 was not being introduced into the gas phase, and it is probable that a non-negligible fraction of RJ-5 and the JP-8 fuels were also lost. These facts should be taken into account when comparing the atmospheric reactivities observed in this fuel study.

TABLE 10. CONDITIONS AND SELECTED RESULTS OF TRIAL FUEL INJECTIONS INTO THE OUTDOOR CHAMBER.

Run No.	Fuel	Injection Temp (°C)	Injection N_2 Flow (ℓ min^{-1})	NMHC[a] (ppmC)	Selected Fuel Compounds (ppb) $n\text{-}C_8$	$n\text{-}C_9$	$n\text{-}C_{10}$	$n\text{-}C_{11}$	$n\text{-}C_{12}$	$n\text{-}C_{13}$	Ratios $\frac{n\text{-}C_{11}}{n\text{-}C_8}$	$\frac{n\text{-}C_{13}}{n\text{-}C_9}$
1	JP-4(pet)	100	2	21.6	5.4	2.9	2.3	3.3	-	-	0.61	-
2	"	100	2	19.3	4.9	2.6	2.0	2.6	-	-	0.53	-
3	JP-8(pet)	100	2	13.5	4.3	9.5	26.2	83.0	63.8	38.7	19.3	4.1
4	"	200	2	16.7	4.0	11.7	25.3	84.9	80.2	65.9	21.2	5.6
5	"	250	2	17.2	3.3	9.0	25.0	86.3	83.8	72.4	26.2	8.1
6	"	250	4	17.0	3.7	8.9	24.5	82.8	80.5	66.9	22.4	7.5
7	"	250	4	17.1	3.3	9.6	26.0	87.8	86.4	77.3	26.6	8.1

[a]Measured by Byron hydrocarbon analyzer. Background levels subtracted.

TABLE 11. RATIOS OF OBSERVED-TO-CALCULATED TOTAL CARBON MEASUREMENTS IN THE OUTDOOR FUEL-NO_x CHAMBER RUNS.

Fuel	Observed THC / Calculated THC
JP-4(pet)	1.18 ± 0.13
JP-4(shale)	1.25 ± 0.30
JP-8(pet)	0.82 ± 0.08
JP-8(shale)	0.97 ± 0.06
Unleaded Gasoline	1.28 ± 0.14
Diesel No. 2	0.27 ± 0.07
JP-10	1.29 ± 0.30
RJ-4	1.53 ± 0.08
RJ-5	0.60 ± 0.09

2.4 INDOOR CHAMBER RUNS

To determine if any experimental or analytical problems had to be overcome before the outdoor fuel irradiations were conducted, and to obtain a preliminary indication of the reactivity of representative fuels to be studied in this program, several trial injections and irradiations using the SAPRC indoor all-Teflon® chamber (ITC) were carried out. The facility, procedure, experiments performed, and results are discussed briefly below.

2.4.1 Facility and Procedure

The SAPRC ~6,000 ℓ indoor all-Teflon® chamber is shown schematically in Figure 15. Like the outdoor chamber (Section 3.1), it consists of a replaceable 2 mil thick FEP Teflon® bag which can collapse as samples are withdrawn, thus avoiding contamination with laboratory air. The bag is attached to a semi-rigid framework, and can be collapsed to about 10% of its maximum volume. Irradiation is provided by two diametrically opposed banks of 40 Sylvania 40-W BL blacklights, backed by arrays of Alzak®-coated reflectors. The light intensity was determined in separate experiments (Reference 10) by measuring the rate of photolysis of NO_2 in N_2 using the quartz tube, continuous flow technique of Zafonte, et al.

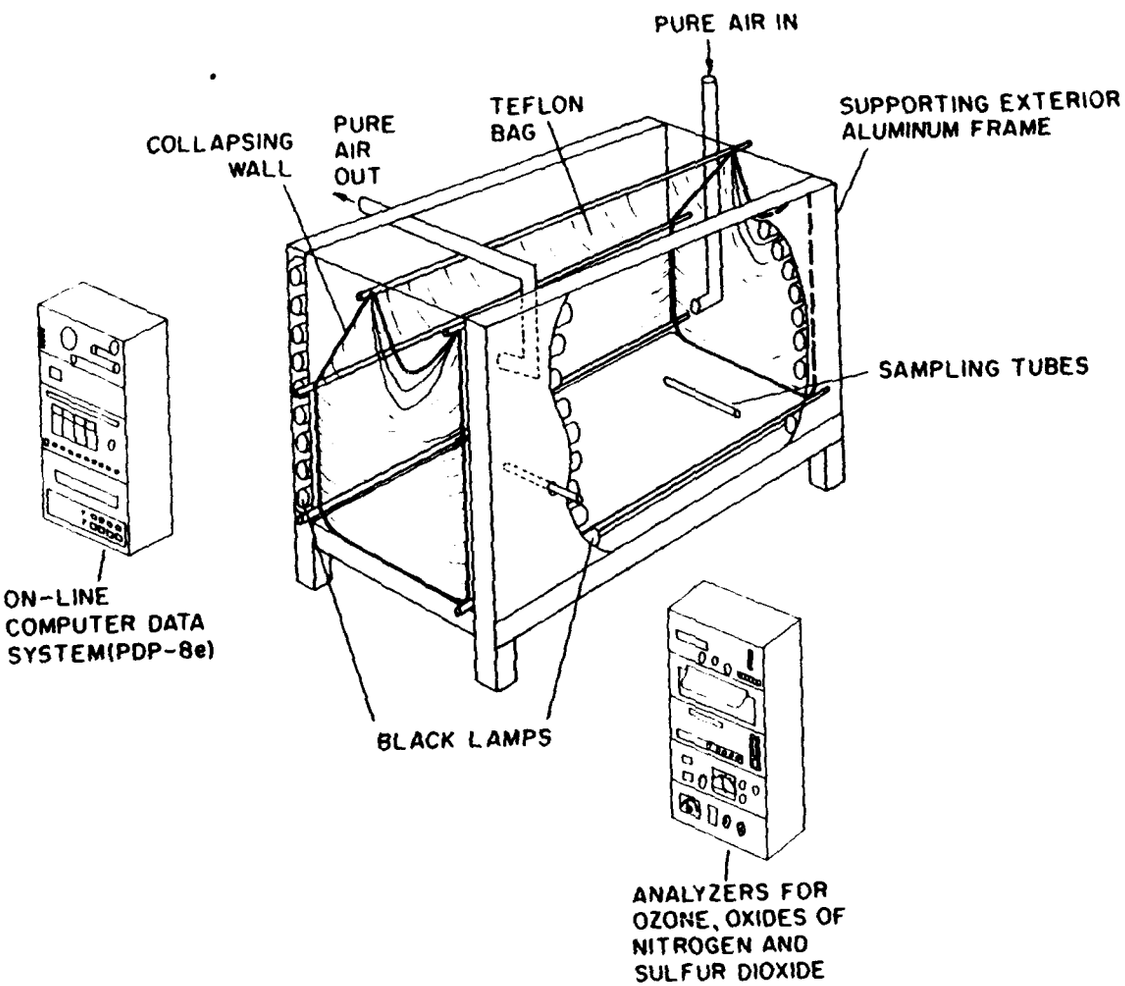

Figure 15. SAPRC ~6000 ℓ All-Teflon® Indoor Chamber and Associated Analytical Data-Acquisition Systems.

(Reference 11, Section 3.2.6). This intensity corresponded to an NO_2 photolysis rate of 0.45 min^{-1} at maximum light intensity.

Before each experiment, the chamber was flushed with purified air (Reference 12) by emptying and filling the bag three times. Unless noted otherwise below, each fuel was injected using the same technique as employed for that fuel in the outdoor runs (Section 23), except that JP-8 and diesel were injected with the injector heat set at 200°C instead of 250°C. The NO and NO_2 were injected using gas-tight all-glass syringes and flushed into the chamber using dry ultra-high purity N_2. Commercially available NO (Matheson, CP grade, 99.0% purity) was used without further purification and NO_2 was prepared by diluting this NO with dry, pure O_2 in a syringe. After the injections, the contents of the chamber were mixed by agitating the sides of the bag, but it took at least 30 minutes for the NO_x readings to stabilize. After the readings stabilized, gas chromatographic samples were taken and irradiation was begun and continued for five to six hours. Ozone, NO, NO_x, fuel components, and other organics were monitored using the techniques described in Section 3.2.

2.4.2 Reproducibility Tests and Dark Decay of Fuel Components

In order to check the reproducibility in the chromatographic analyses of the fuel components in the gas phase and determine if there was any significant wall loss for these compounds over an extended period of time, 200 µl of JP-4 (pet) was injected into the indoor Teflon® chamber using the technique developed for the lighter fuels (Section 2.3). The JP-4 components were analyzed with the HP-5710A GC system using the cryogenic trapping technique (Section 2.1) over a period of three days in the dark.

The reproducibility of the chromatographic analyses obtained following the JP-4 injection is shown in Table 12. It can be seen that, for samples taken on the same day, reproducibility of better than ±10% for the individual peak heights was attained; but, on subsequent days the relative amounts of the heavier compounds decreased. This was probably due to slow adsorption of the less volatile components on the chamber walls.

A slightly different technique was used in the analysis carried out on the second day. The sample in the trap was completely warmed (with the trap closed off) prior to the gas sample valve being switched to the inject position. It was hoped that this technique might give rise to more

reproducible retention times than obtained when the sample was heated and flushed onto the column at the same time. However, as seen in Table 12, it appears that the lighter compounds might have been lost when this technique was used; hence, this procedure was abandoned.

2.4.3 Fuel-NO_x Irradiations

Fuel-NO_x irradiations were carried out in the indoor Teflon® chamber using shale- and petroleum-derived JP-4 and JP-8, unleaded gasoline, diesel No. 2, and JP-10. In each case ~100 µl of the fuel was injected, corresponding to ~25 ppmC of the fuel in the gas phase in this chamber. In the initial experiment, JP-4 (shale) was irradiated with ~1 ppm NO_x (25% NO_2); but, the mixture was observed to be extremely unreactive, with only 16 ppb of O_3 being formed after 3.5 hours of irradiation. As a result of this run, it was decided to decrease the initial NO_x concentrations in the subsequent indoor and outdoor chamber runs, so that more reactive (and hence more informative) mixtures could be studied.

The results of the subsequent experiments, in which ~0.5 ppm of NO_x was employed, are shown on Table 13. It can be seen that the fuels varied significantly in terms of rates of NO oxidation and O_3 formation, with unleaded gasoline being far more reactive and JP-10 being far less reactive than the other fuels studied, in agreement with the subsequent results from the outdoor runs (Section 3.4). As mentioned in Section 2.3, a successful technique for reproducibly injecting the heavier JP-8 and diesel No. 2 fuels into the indoor chamber was not developed (probably because of mixing problems), so the results of runs ITC-385 through 388 should be considered as only qualitative in nature. Indeed, a comparison of the two JP-8 (pet) runs (ITC-385 and ITC-387), in which the fuel injection in the former run was accidentally carried out with the injector heat set at 80°C (instead of 200°C as used in ITC runs 386-388), shows the importance of the fuel injection temperature in affecting the gas phase fuel levels and the resulting reactivity in NO_x-air irradiations. However, other than this injection problem for the heavier fuels which was solved by improved mixing and higher injector temperatures in the outdoor runs (Section 2.3), the results of these preliminary irradiations indicated no significant unexpected problems to be overcome before the outdoor irradiations of those fuels could begin. Thus, these experiments successfully fulfilled their primary objective.

TABLE 12. REPRODUCIBILITY OF GAS CHROMATOGRAPHIC ANALYSES OF SELECTED COMPONENTS OF PETROLEUM-DERIVED JP-4 INJECTED INTO THE INDOOR TEFLON® CHAMBER.

Compound	Relative Height[a]	Relative Change[b]				
		Day 1			Day 2[c]	Day 3
		1	2	3	1	1
n-Hexane	0.74	--	1.0	0.98	0.58	1.05
n-Heptane	1.00	--	1.0	1.04	0.90	0.97
n-Nonane	0.45	0.92	1.0	1.03	0.91	0.84
n-Decane	0.42	1.03	1.0	1.03	0.95	0.68
n-Undecane	0.35	1.02	1.0	1.09	0.88	0.65
n-Dodecane	0.19	1.04	1.0	1.07	0.77	0.55

[a]Peak height relative to n-heptane for sample two, day one.

[b]Peak height ratioed to height of corresponding peak of sample two, day one.

[c]Sample on trap warmed completely prior to flushing onto column.

2.5 DETERMINATION OF THE RATE CONSTANT FOR THE REACTION OF OH RADICALS WITH JP-10

The only homogeneous gas phase process believed to be of any significance in removing saturated and non-olefinic aromatic hydrocarbons from the lower atmosphere is via reaction with the hydroxyl (OH) radical (Reference 13). Hence, a knowledge of the rate constant for the reaction of OH radicals with the major components of the cruise missile fuels allows their atmospheric lifetimes to be estimated. Since JP-10 is comprised of essentially a single component (exo-tetrahydrodicyclopentadiene, Reference 1), its OH radical reaction rate constant was determined using an environmental chamber relative rate technique.

This technique has been described in detail (References 13, 14) and is based on the assumption that the test compound (JP-10) and a reference compound, whose OH radical rate constant is accurately known (m-xylene), are both consumed in NO_x-hydrocarbon-air irradiations only by reaction with the OH radical. For saturated hydrocarbons and the simple aromatics,

TABLE 13. INITIAL CONDITIONS AND SELECTED RESULTS FOR INDOOR TEFLON® CHAMBER NO_x-AIR IRRADIATIONS OF SELECTED FUELS.

Fuel	JP-4 (Pet)	JP-4 (Shale)	JP-8 (Pet)	JP-8 (Pet)	JP-8 (Shale)	Unleaded Gasoline	Diesel #2	JP-10
ITC Run Number	372	371	385[a]	387	386	373	388	374
Initial Concentration (ppm)								
NO	0.278	0.27	0.365	0.329	0.362	0.237	0.335	0.447
NO_2	0.151	0.136	0.144	0.139	0.135	0.151	0.147	0.137
$n\text{-}C_9$	0.05	0.06	--	0.08	b	--	--	--
$n\text{-}C_{10}$	b	b	0.02	0.10	0.13	b	0.02[c]	--
$n\text{-}C_{11}$	b	b	0.09	0.15	0.18	b	0.02	--
$n\text{-}C_{12}$	b	b	0.09	0.20	0.12	b	0.05	--
$n\text{-}C_{13}$	b	b	0.09	0.11	0.06	b	0.05	--
-d[NO]/dt (0-60 min) (ppb min^{-1})	3.7	1.3	1.0	2.1	3.0	~15[d]	2.3	4.8
$[O_3]$ (ppm)								
t = 1 hr	0.008	~0.0	~0.0	0.002	0.005	0.567	~0.0	~0.0
t = 3 hr	0.164	0.032	~0.0	0.020	0.186	0.520	0.037	~0.0
t = 5 hr	~0.34	0.098	0.030	0.215	0.476	0.486	0.164	~0.0
t = 6 hr	--	--	--	0.131	0.588	--	0.232	~0.0

[a]Fuel injected at a maximum temperature of 80°C instead of 200°C.

[b]No data available.

[c]t = 0 GC data not available. Data is given for t = 4 hours.

[d]Given for first 15 minutes only.

this assumption is believed to be valid (Reference 13). The rate constant for the compound of interest is then obtained from the relative rates of consumption of the reference and the test compounds as described below.

If two hydrocarbons, HC_1 and HC_2, react solely with the OH radical, and dilution is avoided by use of a non-rigid Teflon® bag, as is the case here, then (Reference 14):

$$d[HC_1]/dt = k_1[HC_1][OH] \qquad (I)$$

$$d[HC_2]/dt = k_2[HC_2][OH] \qquad (II)$$

where k_1 and k_2 are the rate constants for the reactions of the OH radical with HC_1 and HC_2, respectively. These equations can be integrated and rearranged to obtain:

$$\ln \frac{[HC_2]_o}{[HC_2]_t} = \frac{k_2}{k_1} \ln \frac{[HC_1]_o}{[HC_1]_t} \qquad (III)$$

where $[HC_1]_o$ and $[HC_2]_o$ are the concentrations of HC_1 and HC_2 at time t_o, and $[HC_1]_t$ and $[HC_2]_t$ are the corresponding concentrations at time t during the irradiation. Thus, a plot of $\ln ([HC_2]_o/[HC_2]_t)$ vs $\ln ([HC_1]_o/[HC_1]_t)$ should give a straight line with the rate constant ratio k_1/k_2 being the slope. Therefore, if k_1 is known, k_2 can be determined.

Two experiments were carried out in the indoor 6000 ℓ all-Teflon® chamber using blacklamp irradiations (i.e., the same experimental conditions as used in the other indoor exploratory runs described in Section 2.5). In the first run (ITC-375), ~0.5 ppm NO, ~0.2 ppm NO_2, ~0.4 ppm JP-10, ~0.2 ppm toluene, and ~0.4 ppm m-xylene were injected into the chamber. In the second run (ITC-376), the conditions were similar, except ~0.3 ppm m-xylene was used and ~0.3 ppm o-xylene was also included. Both runs were carried out at ~50% relative humidity. The average temperatures for runs ITC-375 and ITC-376 were 32.5 ± 1°C and 33 ± 5°C, respectively.

Plots of $\ln ([HC_o]/[HC]_t)$ for JP-10 and toluene against m-xylene in run ITC-375 and for JP-10, toluene, and o-xylene against m-xylene for run ITC-376 are shown in Figures 16 and 17, respectively. It can be seen that

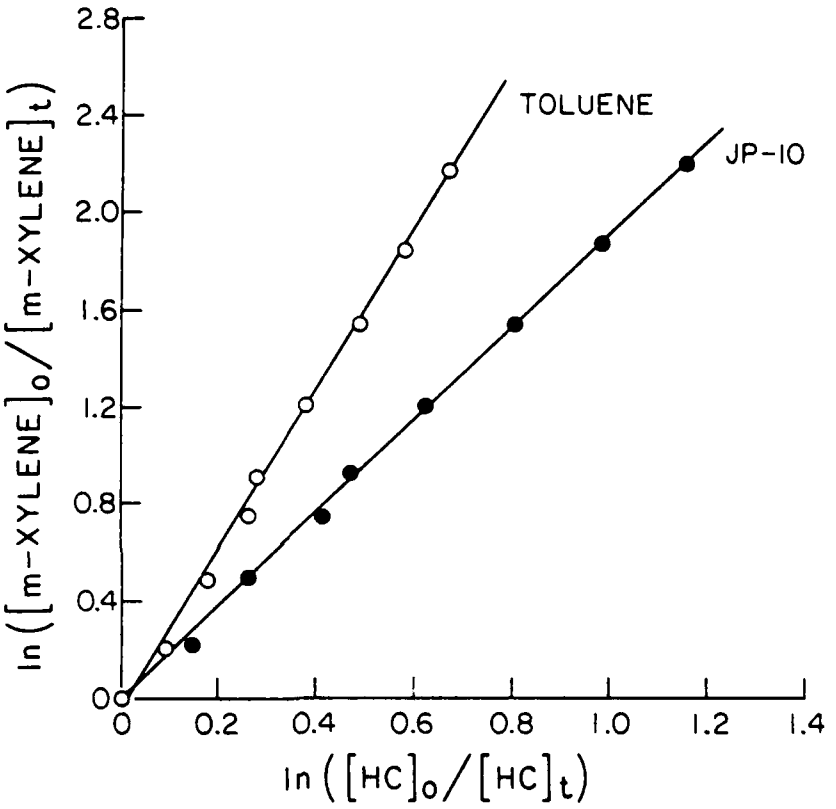

Figure 16. Plots of $\ln([HC]_o/[HC]_t)$ for Toluene and JP-10 vs m-Xylene for Run ITC-375.

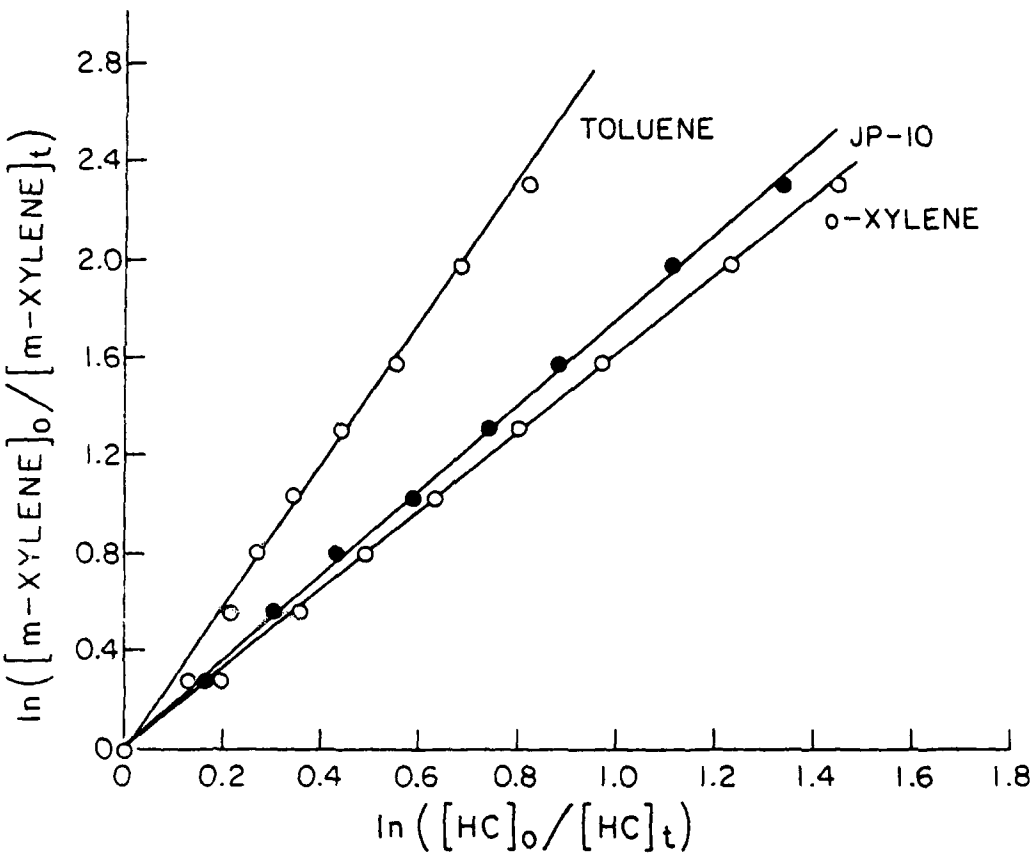

Figure 17. Plots of $\ln[HC]_o/[HC]_t$) for Toluene, JP-10 and o-Xylene vs m-Xylene for Run ITC-376.

in all cases excellent linear plots are obtained. m-Xylene was chosen as the reference compound, since its OH radical reaction rate constant is accurately known (References 15-17). The rate constant ratios k_1/k_2 (Table 14) for JP-10, toluene, and o-xylene, along with the values of k_1 placed on an absolute basis using a rate constant for the reaction of OH radicals with m-xylene of $k_2 = 2.43 \times 10^{-11}$ cm^3 molecule^{-1} sec^{-1}. This rate constant k_2 is the mean of the absolute rate constant data of: Hansen, et al. (Reference 15) [$k_2 = (2.36 \pm 0.24) \times 10^{-11}$ cm^3 molecule^{-1} sec^{-1}]; Perry, et al. (Reference 16) [$k_2 = (2.40 \pm 0.25) \times 10^{-11}$ cm^3 molecule^{-1} sec^{-1}]; and Nicovich, et al. (Reference 17) [$k_2 = (2.54 \pm 0.35) \times 10^{-11}$ cm^3 molecule^{-1} sec^{-1}]. The data of Ravishankara, et al. (Reference 18) has been neglected, due to possible wall adsorption problems in their static flash photolysis-resonance fluorescence system (Reference 17). While the rate constant obtained from ITC-376 for o-xylene is in excellent agreement with the absolute literative rate constants (Table 14), the present data for toluene are ~10-40% higher than the literature data. The data in Table 14 yield an OH + JP-10 rate constant of $(1.3 \pm 0.2) \times 10^{-11}$ cm^3 molecule^{-1} sec^{-1}, with the uncertainty reflecting both a 10% uncertainty in the value of k_2 for m-xylene and the discrepancy between the results of the two runs.

Rate constants for the reaction of OH radicals with unstrained alkanes at ~30°C can be estimated from the number of primary, secondary, and tertiary C-H bonds in the molecule using the following equation derived from published OH + alkane rate constant measurements (References 13, 19):

$$10^{12} \times k_1(30^{\circ}C) = 0.067\ n_1 + 0.588\ n_2 + 2.10\ n_3 \text{ cm}^3 \text{ molecule}^{-1} \text{ sec}^{-1} \quad \text{(IV)}$$

where n_1, n_2, and n_3 are the number of primary, secondary, and tertiary C-H bonds in the molecule, respectively, with which OH radicals can react. Using this formula, and the fact that JP-10 has 12 secondary and four tertiary C-H bonds, the calculated OH + JP-10 rate constant is 15.5×10^{-12} cm^3 molecule^{-1} sec^{-1}, which is ~20% higher than the measured value. This can be considered good agreement, especially in view of the fact that JP-10 has several moderately strained rings and strained ring compounds are known to react with OH radicals somewhat slower than calculated from equation (IV) (References 13, 19).

TABLE 14. RATE CONSTANT RATIOS k_1/k_2 AND RATE CONSTANTS k_1 FOR THE REACTION OF OH RADICALS WITH TOLUENE, JP-10, AND o-XYLENE.

Hydrocarbon	k_1/k_2[a] ITC-375	k_1/k_2[a] ITC-376	$10^{12} \times k_1$ (cm^3 $molecule^{-1}$ sec^{-1})[b] ITC-375	$10^{12} \times k_1$ (cm^3 $molecule^{-1}$ sec^{-1})[b] ITC-375	Absolute Literature Values
Toluene	0.300 ± 0.015	0.342 ± 0.016	7.3 ± 0.4	8.3 ± 0.4	6.11 ± 0.40 (Reference 20); 5.78 ± 0.58 (Reference 15); 6.40 ± 0.64 (Reference 16); 6.36 ± 0.69 (Reference 21)
JP-10	0.523 ± 0.020	0.570 ± 0.016	12.7 ± 0.5	13.9 ± 0.4	
o-Xylene	-	0.618 ± 0.011	-	15.0 ± 0.3	15.3 ± 1.5 (Reference 15); 14.3 ± 1.5 (Reference 16); 12.4 ± 1.2 (Reference 18); 14.2 ± 1.7 (Reference 17)

[a]Using $k_2 = 2.43 \times 10^{-11}$ cm^3 $molecule^{-1}$ sec^{-1}, the mean of the absolute rate constant data of References 15 through 17 (see text).

[b]Error limits are two standard deviations of the slopes of plot of equation (III).

SECTION III
OUTDOOR CHAMBER IRRADIATIONS

The major effort in this program was in conducting the outdoor chamber irradiations. A total of 132 experiments were performed, consisting of irradiations of the nine fuels studied and the associated characterization and conditioning runs. The facility, experimental techniques, and results obtained are discussed in the following sections.

3.1 OUTDOOR CHAMBER FACILITY

All outdoor chamber experiments were performed in the SAPRC Teflon® bag chamber operated in either single or dual mode, which is shown schematically in Figure 18. The reaction chamber consists of a replaceable 45,000-60,000 ℓ bag, which is constructed of 2 mil thick FEP Teflon® sheets heat-sealed together using a double lap seam and externally reinforced with Mylar® tape. Each bag uses nine 27 ft x 58 in Teflon® panels. As shown in Figure 18, the bags had two Teflon® flanges on the bottom, which were used for sampling from each side.

For the first bag used in this program, the fill, injection, and venting of the bag contents were carried out through an open flap in the middle of one side of the bag (not shown on the figure), which was tied closed during the run with flexible tubing. When this bag was used, problems were experienced with excessive rates of bag deflation, which made multi-day runs difficult. These problems were attributed to leakage through this flap. For all subsequent bags, the open flap was not included on the bag; the injections and the air fills were done through Teflon® flanges sealed to the bags with a design similar to that for the sampling ports. The two opposite corners were not heat sealed to empty the bag; but during the runs, these corners were clamped tightly shut with specially designed metal clamps. In addition to reducing leakage around the inlet and exhaust ports, these modifications had an additional advantage; eliminating the open flap made the bags easier to construct.

A total of 11 bags were used in this program, numbered consecutively from 14 through 24. In general, the bag was changed for each fuel studied, though in a few cases the same bag was used for studies of similar fuels. The bags were changed not only to minimize contamination problems, but also because they developed small leaks caused by creasing

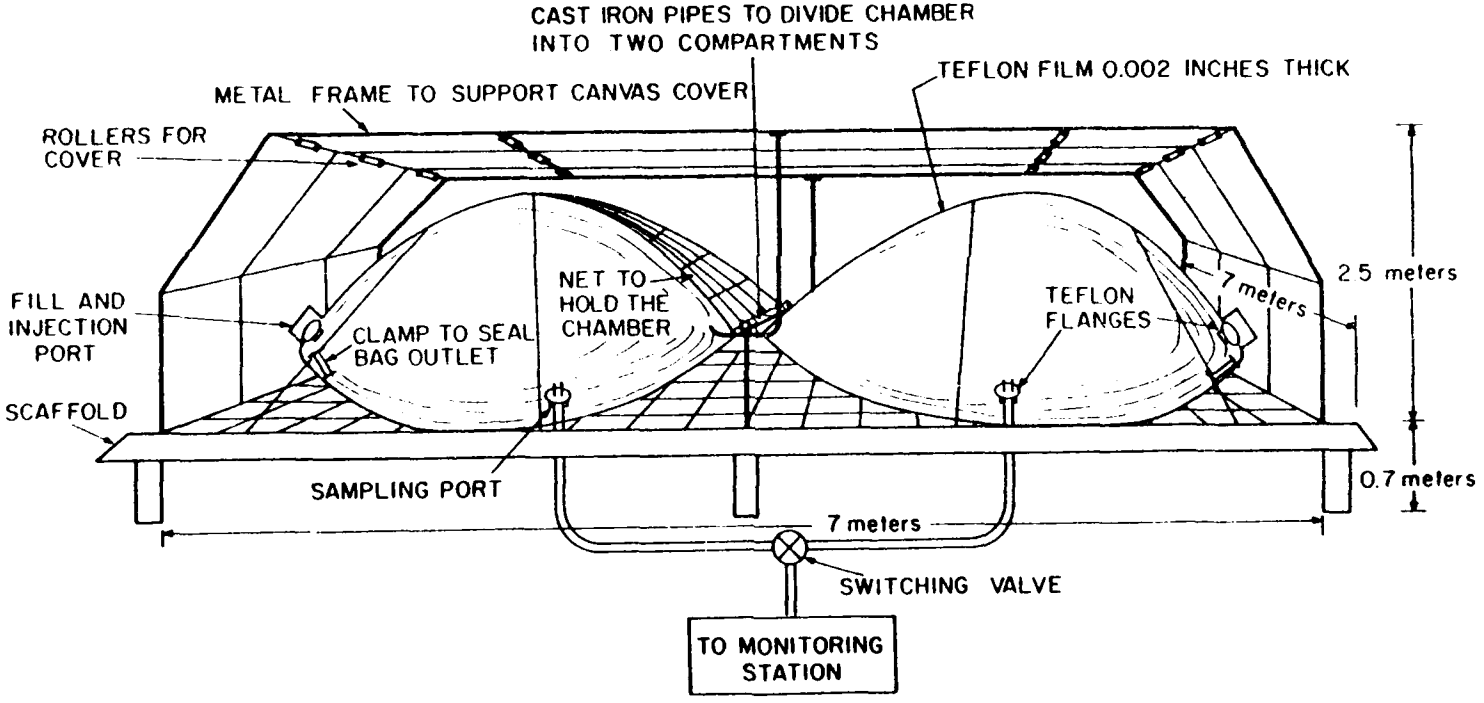

Figure 18. SAPRC Outdoor Teflon® Chamber Shown in Dual-Mode Configuration.

during use. This creasing was exacerbated by wind buffeting, which was minimized when necessary by placing a transparent Teflon® cover on the framework over the bag to serve as a windbreak. Construction of these bags so that they did not leak excessively required a certain amount of skill and experience, and it was found that bags Nos. 18 through 24 underwent significantly less deflation in multi-day runs than did earlier bags.

The Teflon® bags were supported by ropes running across a 25 ft x 20 ft cast iron, pipe tubing frame held three feet off the ground to allow air circulation under the chamber. No mechanical stirring device was used in our experiments since Wilson, et al. (Reference 22) showed that mechanical stirring dramatically inhibits aerosol formation in smog chambers. Wind action on the flexible chamber and temperature gradients within the chamber were sufficient to ensure adequate mixing during an experiment. The chamber was held on the frame with a net connected to the frame by a system of ropes. Between irradiations and during dark decay experiments, the framework above the bag was covered by an opaque, white L-16 tarp cover, which was pulled on or off the framework with a system of rollers designed to facilitate the process. The upper framework was also used to support the windbreak of Teflon® film, when necessary.

Most of the monitoring instruments employed in these runs were housed in an air conditioned 15 ft x 10 ft portable building approximately 10 feet from the chamber. The sample lines were constructed of 0.5 in o.d. FEP Teflon® tubing and connected to the sample ports on the bottom of each side of the bag (Figure 18). The Teflon® tubing from each side was attached to an all-Teflon® solenoid valve with an 0.5 in orifice. Following the valves, the lines were brought together with a Teflon® "T" and led into the glass sampling manifold within the monitoring station. The continuous monitoring instruments in the station withdrew air from that manifold and the samples for chromatographic analyses were also taken through a valve attached to this manifold. Most of the air flow through the manifold went out through a 1.5 in hose leading to the analysis chamber of the integrating nephelometer and then outside to a vacuum pump. The transit time from the Teflon® bag to the instruments was about two seconds.

A timer was built for the sampling systems so that it could operate unattended. This timer controlled the two solenoid valves, the pump, and

a relief port to ambient air. This device minimized the amount of sample drawn from the chamber. The following typical sequence was used:

Time	Operation
0000	Relief valve closed, solenoid valve No. 1 open, pump on
0010	Solenoid valve No. 1 off, solenoid valve No. 2 on
0020	Solenoid valve No. 2 off, pump off, relief valve open

This timer worked on either a 30- or 60-minute cycle.

As shown in Figure 18, the bag could also be operated in a dual mode configuration for the purpose of conducting parallel experiments under the same lighting and temperature conditions. This was done by means of three 1.5 in diameter cast iron pipes, two of which ran across the supports above the bag and the third which lay below. Initially, the bag was divided by raising the lower pipe and placing it tightly between the upper pipes. This was thought to effectively separate the two sides. However, in AFF-8, a JP-4 vs n-butane irradiation, significant leakage of n-butane into the JP-4 side was observed, thus invalidating the run. The bag division procedure was modified by taking the outer and middle two pipes as they were after the initial division procedure and rotating the pair 180 degrees. This change doubled the number of seals between the two sides of the bag. Using this bag-division procedure, tests were carried out by injecting Freon® 12 on one side of the divided bag, and monitoring it on the other side by gas chromatography. The exchange rate between the two sides was found to be < 0.1% per hour; thus, this bag-division procedure was used for all subsequent divided bag runs.

The bag was filled and flushed with purified matrix air, which was provided at a flow rate of 12-15 scfm by an air purification system detailed in Reference 12. In this system, ambient air is drawn through Purafil beds (to remove NO_x), compressed by a liquid (water) ring compressor to 100 psig, and passed successively through a heatless dryer, a Hopcalite tower (to remove CO), and a second heatless dryer packed with activated coconut charcoal. The latter acted as a pressure-swing adsorption unit and routinely reduced the hydrocarbon levels (as measured in the chamber) to ~800 ppb methane, < 5 ppb of C_2 hydrocarbons and propane, and

< 1 ppb of all higher hydrocarbons. After filtering this very dry, purified air stream to remove any charcoal dust, it was heated and then divided into two metered streams, one of which passed through a spray tower supplied with heated distilled water. The streams were recombined in the appropriate relative amounts to give the desired humidity.

3.2 ANALYTICAL TECHNIQUES EMPLOYED

Inorganic species, physical parameters, aerosol parameters, CO and total hydrocarbons, peroxyacetyl nitrate (PAN), formaldehyde, and individual organic reactants and products were monitored by the appropriate techniques, which are summarized below. Except as noted to the contrary, all instruments withdrew the gas to be sampled from the sampling manifold in the portable building next to the chamber.

3.2.1 Ozone

Ozone was monitored by a Dasibi model 1003AH UV absorption ozone monitor. It was calibrated in November 1979 and again in December 1980 by the California Air Resources Board using longpath UV absorption.

It should be noted that the UV absorption technique suffers from interferences from certain types of organic compounds which also absorb in the 254 nm region, such as cresols (Reference 23). This interference appears to be significant in mixtures containing JP-8 (both shale- and petroleum-derived) and diesel fuel, since ozone readings of up to 77 ppb were observed prior to the irradiation in runs using these fuels, even when sufficient NO was present to suppress O_3 far below detectable levels (due to their rapid mutual reaction). In runs using these fuels, the reported ozone values in the tables and figures showing reactivity comparisons in Section 3.4 were corrected by subtracting these initial ozone readings. These readings varied from run to run even when the same fuel was used. No such correction was made, however, in the data sheets given in Volume II or in any ozone time-concentration plots given in this report. This interference by fuel components did not appear to be a problem with the other fuels studied; but the possibility that products were formed, which gave a positive response on the ozone monitor, cannot be ruled out, particularly for JP-4 and unleaded gasoline. JP-4 and unleaded gasoline contain aromatics which can react to form cresols (Reference 23). This is less likely to be a problem with the alkane fuels such as JP-10, RJ-4, and RJ-5 and with n-butane.

3.2.2 Oxides of Nitrogen

Nitric oxide and total NO_x were monitored by a Bendix Model 8101 BX chemiluminescence NO-NO_x analyzer. In this instrument, NO is monitored directly, but total NO_x is measured by converting it to NO with two catalyst tubes filled with ultra-pure carbon heated to 285°C. NO_2 is assumed to be the difference between the two readings. This instrument was calibrated approximately every three to five weeks using an NBS calibration gas of known NO concentration. The gas was diluted to appropriate concentrations and the analyzer was then adjusted to give the correct reading. The instrument normally did not deviate more than 5% between calibration checks. The converter efficiency was checked using NO_2 generated by reacting the calibration NO with excess O_3, and was always found to be 100 $\pm$ 5%.

The analysis of NO_2 and NO_x is complicated by the fact that the converter has been shown (Reference 24) to convert PAN, organic nitrates, and HNO_3 to NO and thus such species give a positive interference in the NO_2 analysis (the NO data are unaffected). Conversion of PAN and organic nitrates has been shown to be essentially quantitative (Reference 24); so in principle, NO_2 can be corrected by subtracting the measured PAN and organic nitrate concentrations. Unfortunately, although PAN was monitored in most of our experiments, we were unable to monitor organic nitrates with the techniques employed. Organic nitrates are known to be formed in significant yields in NO_x-air irradiations of the larger alkanes (Reference 25), which are present in all of the fuels studied in this program, and thus significant interferences by them are expected. For this reason, no attempt was made to correct the NO_2 data for these interferences. Thus, the NO_2-UNC data given in Volume II must be considered upper limits to the true NO_2 values.

As mentioned above, HNO_3, which is believed to be a major sink for NO_x in NO_x-air photo-oxidations, also interferes with NO_2 readings, though this interference is in general not quantitative (Reference 24). In our system it is probable that HNO_3 was absorbed on the sample lines prior to entering the converter and thus did not interfere. This was tested by placing a nylon filter, which is known to efficiently remove gas phase HNO_3 (Reference 26), in the sampling line in the later stages of a typical

fuel NO_x run. No significant changes in the NO_2 readings were observed (see data sheets for run AFF-8 in Volume II).

3.2.3 Total Hydrocarbons and CO

Total hydrocarbons and CO were monitored either by a Beckman Model 6700 or a Byron Model 401 chromatographic hydrocarbon analyzer. The Byron was not acquired and functioning properly until relatively late in the program, while the Beckman was used throughout. For consistency in inter-run comparisons, only the Beckman data are used.

The Beckman was not located in the building adjacent to the chamber, but in a monitoring facility ~50 feet away, so a somewhat different sampling procedure was used for this instrument. A clean, 50 ft, 0.25 in line was installed from the sampling manifold to the Beckman. The Beckman has a sample time of 10 minutes for a complete cycle and the injection loops are continuously purged with sample air, except during injections. In order to allow the air from the chamber to reach the Beckman, the sample cycle was set to start at seven minutes and 17 minutes after the hour for Sides A and B, respectively. This starting time enabled the instrument to purge for seven minutes before a sample was injected and this compensated for the distance from the sampling manifold.

The Beckman was calibrated using specially prepared calibration gases which contained methane, CO, and n-hexane. Peak heights and/or peak areas were determined for each component. From these and the known concentrations of the components, factors were calculated for total hydrocarbons (THC), CH_4, and CO.

The FID response of the Beckman to the heavier fuels, such as diesel No. 2 and RJ-5, was quite low. This could be due in part to the heavier fuels tending to adhere to the walls of the sample loop and associated tubing, resulting in chromatographing of the fuels. In an attempt to correct for this, peak areas rather than peak heights were used in the total hydrocarbon measurements for diesel No. 2 fuel. However, the response was still lower than expected based on the amount of fuel injected (Section 2.3).

3.2.4 Temperature

Temperature was monitored by a Doric thermocouple temperature indicator. Two thermocouples were used, one in each of the sampling

lines, located just beneath the Teflon® sample parts. The thermocouples were calibrated by using a distilled ice bath or boiling distilled water.

3.2.5 Humidity

Humidity was measured during the pure air fill using either the wet bulb/dry bulb technique or an EG&G model 880 Dew Point Hygrometer. The wet bulb/dry bulb measurements were made using an Environmental Tectonics Corporation model CP-197 automatic psychrometer. The psychrometer is a self-contained unit with a wet-bulb thermometer, a dry-bulb thermometer, and a battery-operated fan to pull the sample air across the bulbs. The entire unit was placed inside the bag and allowed to operate for at least five minutes before the reading was taken.

The EG&G model 880 Dew Point Hygrometer is an automatic, optically sensed, thermoelectrically cooled, condensation dew-point hygrometer. It measures the dew point by presenting a cooled metal surface to the gas sample. Part of this metal surface is a gold plated mirror on which condensate will form at the dew point. This condensate is monitored by an optical system which varies the temperature until the exact dew point is found. The temperature is then read off the meter of the instrument. The instrument employs an internal calibration, which was used before every reading. When in use, it was connected directly to the sample manifold.

3.2.6 Light Intensity

Light intensity was monitored by an Eppley model 14290 Ultraviolet Radiometer located on the asphalt underneath the bag in the middle of Side A. The radiometer was cleaned for each run to ensure correct readings. The factor used to convert the radiometer output to cal cm^{-2} min^{-1} was that given by the factory in 1977. Comparison with another calibrated radiometer showed reasonable agreement.

A more fundamental measurement of light intensity, in terms of affects on atmospheric chemistry and O_3 production, is k_1, the NO_2 photolysis rate. Although it could not be monitored routinely for all experiments, a comparison test was performed in which simultaneous experimental k_1 and radiometer measurements were made. The technique for the k_1 measurements is described by Zafonte, et al. (Reference 11) and is only briefly described here. A mixture of ~1.6 ppm NO_2 in N_2 was passed through a 2 cm i.d. by 76.3 cm long quartz tube at ~1 ℓ min^{-1}. NO and NO_2 concentrations were measured when the tube was covered. The tube was then

uncovered and the changes in NO and NO_2 noted. The inlet and exit lines of the tube were wrapped in opaque tape so that the NO_2 photolysis occured only after the NO_2 was fully mixed. For some measurements, a darkened four-foot length of Pyrex tubing was placed ahead of the quartz tube in order to assure more uniform flow characteristics. The tube was located on top of the roof of the outdoor laboratory building, with the UV radiometer located next to it. The k_1 values were calculated from the changes in NO and NO_2 using the formula given by Zafonte, et al. (Reference 11). Table 15 gives the results of this experiment, which was performed under conditions of extremely clear and sunny weather.

Table 15 also gives the calculated theoretical maximum values for k_1 along with the radiometer readings. The theoretical maximum value of k_1 can be calculated for a clear day using the best estimate solar actinic irradiations as a function of zenith angle of Peterson (Reference 27) and currently accepted NO_2 absorption coefficients and quantum yields (Reference [illegible]), providing the solar zenith angle (determined by the time of day and the date) is specified (Reference 28). From this calculated maximum k_1, an expected radiometer reading can be calculated using the following empirical k_1-UV relations derived by Zafonte, et al. (Reference 11):

For $0^\circ < z < 40^\circ$

$$k_1(min^{-1}) = [0.079(1/\cos z)+0.022] \times \text{radiometric UV } (mW\ cm^{-2})$$

For $40^\circ < z < 90^\circ$

$$k_1(min^{-1}) = [0.16(1-\cos z)+ 0.088] \times \text{radiometric UV } (mW\ cm^{-2})$$

where z is the solar zenith angle. It can be seen from Table 15 that, with the exception of the readings obtained under cloudy conditions or at large zenith angles, the agreement for the k_1 values was generally within $\pm$ 10%. This suggests that our k_1 measurement technique was reasonably reliable. On the other hand, again with the exception of the readings obtained under cloudy conditions or at high zenith angles, the experimental radiometer readings were ~50% higher than the predicted values. This could be due to the placement of the radiometer during this study, since

TABLE 15. EXPERIMENTAL AND CALCULATED k_1 AND RADIOMETER READINGS MADE ON 18-20 FEBRUARY 1981.

		k_1 (min^{-1})			UV ($mW\ cm^{-2}$)			
Date	PST	Obs.	Calc.[a]	Obs./Calc.	Obs.	Calc.[b]	Obs./Calc.	Notes[c]
2/18	1154	0.394	0.390	1.01	3.95	2.86	1.38	
	1326	0.343	0.367	0.93	-	2.53	-	
	1355	0.352	0.347	1.01	-	2.28	-	A
2/19	1122	0.237	0.388	0.68	2.82	2.82	1.00	B
	1321	0.360	0.372	0.97	3.68	2.59	1.42	
	1324	0.366	0.370	0.99	3.83	2.57	1.49	
	1327	0.384	0.369	1.04	3.42	2.54	1.54	
	1556	0.060	0.175	0.34	0.79	0.88	0.90	C
2/20	0828	0.221	0.227	0.97	1.85	1.21	1.53	C
	0855	0.273	0.273	1.00	2.31	1.56	1.48	C
	0914	0.324	0.300	1.08	2.77	1.79	1.55	C
	0948	0.379	0.337	1.12	3.30	2.16	1.53	C
	1118	0.382	0.389	0.98	4.09	2.83	1.45	C
	1140	0.406	0.393	1.03	4.27	2.90	1.47	B,C
	1157	0.440	0.394	1.12	4.33	2.92	1.48	C,D
	1218	0.440	0.393	1.12	4.33	2.90	1.49	C

[a]Calculated from the actinic irradiations given by Peterson (Reference 27) and the NO_2 absorption coefficients and quantum yields recommended by Atkinson and Lloyd (Reference 5).

[b]Calculated from the theoretical k_1 values (Note a) using the empirical relationship of Zafonte, et al. (Reference 11).

[c]Notes for special conditions are as follows:
- A - Flow rate was 2 $\ell\ min^{-1}$
- B - Cloudy during this reading
- C - Four-foot Pyrex tube in series with quartz tube
- D - Flow rate was 3 $\ell\ min^{-1}$

it was located on the roof of the monitoring station instead of under the bag as it was for the chamber runs.

A comparison between experimental and calculated maximum radiometer readings under the actual conditions of the chamber experiments (Table 16) lists the maximum UV radiometer reading observed for each outdoor chamber irradiation, along with the calculated maximum radiometer reading appropriate for the date and time of day the reading was observed. It can be seen that in most cases, in contrast with the results of the experiment described above, the agreement between the observed and calculated radiometer readings are surprisingly good, considering the potential uncertainties in applying empirical relationships such as that used here. For most runs, the observed radiometer readings were 10% lower than the calculated values, which is expected due to the reduction in light intensity caused by passing through two layers of Teflon® film. The few cases where the observed radiometer reading is significantly lower than calculated value can be attributed to the run being performed on overcast days. These results indicate that the empirical k_1-UV radiometer relationship derived by Zafonte, et al. (Reference 11), should be useful for obtaining estimates for k_1 values applicable to the runs performed in this program.

3.2.7 Aerosol Parameters

Parameters relating to aerosol formation were measured by four different instruments, which are briefly described below. Because of equipment breakdowns and occasional temporary requirements for these instruments for other programs, there were a number of chamber runs in which not all four were used; though, in no case was a fuel-NO_x irradiation conducted without some aerosol measurement instrumentation on line. It should be noted that accurate and quantitative measurement of aerosol parameters is extremely difficult (in part because of deposition of the particles on the chamber walls and in the sampling line); the aerosol data should probably be considered qualitative in nature, though it should be useful for comparative purposes.

The Model Rich 100 Condensation Nuclei Monitor responds to atmospheric particles with diameters of 0.0025 μ and larger and covers a concentration range of 300 to 10^7 particles cm^{-3}. The instrument operates on the principle of a cloud chamber in which water is condensed upon submicroscopic particles to produce micron-sized droplets. The cloud which is produced

attenuates a light beam that is then electronically monitored and displayed on a panel indicator. The cloud chamber is then pressurized and flushed. The total measurement cycle time is approximately once per second.

The Climet Instrument Model 208A Particle Analyzer measures particles cm^{-3} in the range of 0.3 μ to 1.0 μ. Functionally, the components of the particle analyzer may be divided into three major sections: air sampling, optical, and electronic. Air is drawn into the analyzer sensor chamber by a high-speed pump. As the air sample passes through the sensor chamber, the optical system of the analyzer detects individual particles and produces electrical impulses. These impulses are converted to a signal, which is displayed on the face of the instrument. Incorporated into the analyzer is the calibrator circuit, which provides a complete check of optical system operation and permits simple, accurate calibration. At high particle concentrations such as those encountered with diesel fuel, there can be a problem with coincidence, i.e., two or more particles being counted as one. In general, coincidence was not a problem in our measurements.

The TSI Model 3030 Electrical Size Analyzer is designed to measure the size distribution of particles in the 0.0032 μ to 1 μ diameter range. The instrument is based on the "diffusion charging-mobility analysis" principle first described by Whitby and Clark (Reference 29). The aerosol is sampled into an aerosol charger to expose the particles to unipolar positive ions produced by a corona discharge. The charged aerosol then enters the mobility analyzer, which is comprised of a precipitator and an electrometer sensor. The mobility distribution is then measured and from these data the number of particles in various size ranges can be calculated. From this distribution, the total number of aerosol particles ("AER. N" on the data sheets in Volume II), the total volume of aerosol materials ("AER. V") and the total aerosol surface area ("AER. S") are calculated. It should be noted that throughout this program a number of problems occurred with the Model 3030 and, although they were corrected, the data should be looked upon as qualitative only.

The Meteorology Research, Inc., Model 1550B Integrating Nephelometer is designed to measure the atmospheric extinction coefficient due to light

TABLE 16. MAXIMUM RADIOMETER READINGS OBSERVED IN THE OUTDOOR CHAMBER RUNS AND COMPARISON WITH CALCULATED RADIOMETER AND k_1 VALUES.

Run	Date	Time[a] (PST)	Radiometer ($mW\ cm^{-2}$)			Calculated k_1 (min^{-1})	
			Observed	Calculated[b]	Observed / Calculated	From Radiometer[c]	Maximum[d]
2	6/4	1200	4.03	4.68	0.86	0.413	0.479
4	6/17	1200	4.53	4.70	0.96	0.463	0.481
7	6/19	1130	4.05	4.66	0.87	0.416	0.479
8	5/20	1200	4.05	4.70	0.86	0.414	0.481
9	6/26	1300	3.83	4.53	0.85	0.400	0.474
10	7/3	1130	4.29	4.65	0.92	0.442	0.478
11	7/11	1145	4.64	4.66	1.00	0.477	0.479
13	7/15	1230	3.97	4.61	0.86	0.411	0.477
14	7/16	1100	4.37	4.49	0.97	0.460	0.472
15	7/17	1300	3.82	4.48	0.85	0.402	0.472
17	7/21	1130	3.83	4.58	0.84	0.398	0.476
18	7/23	1400	4.09	3.96	1.03	0.463	0.448
19	7/30	1205	3.69	4.57	0.81	0.384	0.457
20	8/1	1200	3.60	4.55	0.79	0.375	0.475
21	8/5	1230	4.05	4.28	0.95	0.426	0.463
22	8/6	1200	4.26	4.51	0.94	0.447	0.473
23	8/7	1215	4.03	4.29	0.94	0.424	0.463
24	8/8	1255	3.74	4.35	0.36	0.401	0.466
25	8/15	1205	4.17	4.41	0.95	0.443	0.469
26	8/20	1105	4.08	4.20	0.97	0.446	0.459
27	8/21	1340	3.99	3.85	1.04	0.459	0.443
31	8/26	1305	~4.2	4.04	1.04	0.469	0.452
32	8/28	1115	3.62	4.12	0.88	0.401	0.456
33	9/4	1205	2.95	4.08	0.72	0.328	0.454
34	9/10	1045	2.84	3.68	0.77	0.335	0.435
35	9/11	1150	3.26	3.93	0.83	0.371	0.447
39	9/15	1310	5.09	3.60	0.41	0.608	0.431
40	9/18	1105	3.02	3.62	0.83	0.360	0.432
41	10/1	1130	3.13	3.39	0.98	0.387	0.419

TABLE 16. MAXIMUM RADIOMETER READINGS OBSERVED IN THE OUTDOOR CHAMBER RUNS AND COMPARISON WITH CALCULATED RADIOMETER AND k_1 VALUES (continued).

			Radiometer (mW cm^{-2})			Calculated k_1 (min^{-1})	
Run	Date	Time[a] (PST)	Observed	Calculated[b]	Observed / Calculated	From Radiometer[c]	Maximum[d]
42	10/3	1205	2.95	3.38	0.87	0.366	0.419
43	10/7	1205	2.50	3.25	0.77	0.317	0.413
44	10/14	1105	2.98	2.90	1.03	0.404	0.393
45	10/16	1105	2.68	2.84	0.94	0.367	0.381
46	10/20	1200	2.94	2.88	1.02	0.400	0.391
47	10/23	1145	2.86	2.79	1.03	0.396	0.386
48	10/24	1200	2.61	2.77	0.94	0.362	0.385
51	10/30	1200	2.52	2.62	0.96	0.360	0.374
52	11/7	1115	2.20	2.36	0.93	0.331	0.354
53	11/18	1215	2.20	2.23	0.99	0.344	0.343
54	12/2	1110	0.89	1.97	0.45	0.114	0.319
55	12/10	1205	1.86	2.00	0.93	0.299	0.322
56	12/16	1200	1.80	1.98	0.91	0.291	0.320
57	12/18	1200	1.18	1.98	0.60	0.191	0.320
58	1/2	1230	1.80	2.20	0.82	0.279	0.340
60	1/22	1245	1.49	2.18	0.68	0.232	0.339
61	2/3	1200	2.80	2.50	1.12	0.410	0.365
62	2/5	1215	2.63	2.53	1.04	0.382	0.368
63	3/10	1105	3.86	3.29	1.17	0.487	0.414
64	3/17	1205	3.06	3.63	0.84	0.364	0.432
65	3/24	1230	3.36	3.76	0.89	0.392	0.439
66	3/25	1130	2.79	3.79	0.74	0.324	0.440
68[e]	3/27	1530	1.17	1.92	0.61	0.191	0.314
69	4/6	1200	3.95	4.10	0.96	0.438	0.455
70	4/7	1205	3.73	4.11	0.91	0.413	0.455
71	4/9	1115	3.36	4.05	0.83	0.375	0.453
72	4/15	1205	3.47	4.26	0.81	0.377	0.462
73	4/21	1105	3.92	4.20	0.93	0.429	0.460
74	4/30	1115	3.87	4.37	0.89	0.414	0.467

TABLE 16. MAXIMUM RADIOMETER READINGS OBSERVED IN THE OUTDOOR CHAMBER RUNS AND COMPARISON WITH CALCULATED RADIOMETER AND k_1 VALUES (continued).

			Radiometer (mW cm^{-2})			Calculated k_1 (min^{-1})	
Run	Date	Time[a] (PST)	Observed	Calculated[b]	Observed / Calculated	From Radiometer[c]	Maximum[d]
75	5/6	1115	3.64	4.43	0.82	0.386	0.469
76	5/7	1015	3.73	4.02	0.93	0.419	0.451
77	5/12	1105	4.14	4.43	0.93	0.439	0.469
78	5/15	1115	4.15	4.50	0.92	0.436	0.472
79	5/19	1305	3.91	4.42	0.88	0.415	0.469
80	5/21	1105	4.32	4.49	0.96	0.454	0.472
81	5/27	1115	4.00	4.56	0.88	0.416	0.475
83	6/1	1225	4.27	4.64	0.92	0.440	0.478
84	6/2	1305	3.46	4.48	0.77	0.364	0.472
86	6/4	1115	4.68	4.59	1.02	0.486	0.476
88	6/8	1110	4.27	4.57	0.93	0.444	0.476
89	6/9	1130	4.36	4.65	0.94	0.449	0.479
90	6/11	1215	3.91	4.68	0.84	0.401	0.480
91	6/12	1100	4.18	4.53	0.92	0.437	0.474
92	6/16	1105	4.45	4.56	0.98	0.463	0.475
93	6/25	1105	4.00	4.56	0.88	0.417	0.475
94	6/30	1015	3.82	4.20	0.91	0.418	0.459
95	7/2	1115	4.41	4.60	0.96	0.457	0.476
97	7/8	1105	3.69	4.54	0.81	0.385	0.474
98	7/10	1115	3.82	4.58	0.83	0.397	0.476
100	7/15	1405	3.19	3.95	0.81	0.362	0.448
101	7/17	1105	3.91	4.51	0.87	0.410	0.473
103	7/21	1415	3.37	3.80	0.89	0.391	0.441
104	7/22	1100	3.87	4.45	0.87	0.409	0.470
105	7/23	1130	3.82	4.57	0.84	0.397	0.475
107	7/27	1245	3.46	4.50	0.77	0.36[illegible]	0.472
108	7/30	1205	4.45	4.57	0.97	0.463	0.475
109[f]	8/3	1405	2.86	3.81	0.75	0.331	0.441
110	8/4	1215	4.14	4.52	0.92	0.434	0.473

TABLE 16. MAXIMUM RADIOMETER READINGS OBSERVED IN THE OUTDOOR CHAMBER RUNS AND COMPARISON WITH CALCULATED RADIOMETER AND k_1 VALUES (concluded).

			Radiometer ($mW\ cm^{-2}$)			Calculated k_1 (min^{-1})	
Run	Date	Time[a] (PST)	Observed	Calculated[b]	Observed / Calculated	From Radiometer[c]	Maximum[d]
111	8/6	1115	3.55	4.41	0.81	0.377	0.469
112	8/10	1105	3.37	4.32	0.78	0.362	0.465
113	8/11	1105	3.64	4.31	0.84	0.392	0.464
114	8/13	1115	3.55	4.34	0.82	0.381	0.465
116	8/18	1215	3.05	4.36	0.70	0.326	0.466
117	8/19	1100	3.64	4.18	0.87	0.399	0.459
118	8/20	1130	4.45	4.30	1.03	0.480	0.464
119	8/21	1100	4.09	4.15	0.99	0.450	0.457
121	8/24	1100	4.55	4.11	1.11	0.504	0.455
122	8/28	1105	3.55	4.07	0.87	0.396	0.453
123[f]	8/31	1405	2.73	3.41	0.80	0.337	0.420
124	9/2	1205	3.64	4.12	0.88	0.402	0.465
125	9/3	1205	3.64	4.10	0.89	0.404	0.455
127	9/9	1205	4.00	3.98	1.01	0.451	0.449
128	9/11	1115	3.64	3.84	0.95	0.420	0.442
129	9/15	1205	3.09	3.84	0.80	0.356	0.443
131	9/18	1105	2.91	3.62	0.80	0.347	0.432
132	9/21	1200	3.46	3.70	0.94	0.407	0.436

[a]Time at which maximum radiometer reading was observed.

[b]Maximum radiometer reading calculated using the Zafonte, et al. (Reference 11) equations and the calculated maximum k_1 value (see note d).

[c]Calculated from the observed radiometer readings using the formula of Zafonte, et al. (Reference 11).

[d]Calculated from the actinic radiations given by Peterson (Reference 27) and the NO_2 absorption coefficients and quantum yields recommended by Atkinson and Lloyd (Reference 5).

[e]Only one value available for run.

[f]Only two values available for run.

scattering by both gases and aerosols in the air. Sample air is continuously drawn into the optics chamber where a flash lamp is mounted. With each flash, a photomultiplier (PM) tube detects the light scattered from the particles in the defined sampling area. The output of the PM tube, as well as that of a reference phototube, are manipulated electronically to give a reading, which is displayed on the front of the instrument. The instrument has a range of 0.1×10^{-4} to 100×10^{-4} m^{-1}. The nephelometer was calibrated approximately once a month using Freon® 12 as a reference standard (as per factory instructions). The major problem encountered with this instrument was ambient air leaking into the sampling chamber; this was corrected using silicone rubber sealant.

3.2.8 Organic Reactants and Products

Fuel components, background trace organics present in the pure air, and a limited number of products were monitored by gas chromatography (GC). Except as noted below, flame ionization detection was used. Samples were taken (using 100 ml syringes from the sampling manifold in the portable building adjacent to the chamber) and injected manually into the various GC instruments. The syringes were flushed with the air being sampled at least two times prior to taking the sample for analysis. Brief descriptions of each of the GC systems, the compounds monitored, and (where applicable) special procedures associated with them are given below.

The C_{5+} hydrocarbon fuel components were monitored by capillary column gas chromatography employing 30 m SE-52 or 30 m SE-54 coated fused silica capillary columns. These systems, which are described in more detail in Section 2.2, were capable of monitoring most of the individual C_5-C_{13} components of the fuels studied in this program. However, because of the large number of individual components of the fuels (except for JP-10, which is essentially a pure compound, and RJ-5, in which only three components were found to be present in significant amounts), concentrations of only selected fuel components are reported. The fuel components, whose concentrations are reported on the data sheets, depended on the fuel being used and (for the heavier components) whether the Varian gas chromatograph with the heated loop was employed (Section 2.2).

Calibration factors for the various alkane and aromatic fuel components were obtained as follows. Stock calibration solutions were made by

syringing the desired compounds into a weighed vial. Exact concentrations were obtained by weighing the vial on an Ainsworth type 10 balance after the addition of each compound. In general, each stock solution was made up of six compounds. One microliter of each stock solution was added to a 46.75 ℓ glass carboy. The carboy was cleaned before each calibration by heating it with a heat gun for 20 minutes on hot and 15 minutes on cool, then flushing the carboy with nitrogen for one hour. The compounds were added to the carboy the evening before a calibration so that the compounds would be completely mixed for the next morning. Calibration samples were then taken directly from the calibration carboy with a 100 ml all-glass gas-tight syringe.

Capillary column GC analyses of the fuel components were performed prior to the irradiation in each run and once an hour during the irradiation. In divided bag runs, samples alternated from side to side; for each side, data are available at two-hour intervals.

Aromatic hydrocarbons and oxygenates were monitored using a 10 ft x 0.125 in stainless steel column packed with 10% Carbowax-600 on C-22 Firebrick (100/120 mesh) operated at 70°C-75°C, with an N_2 flow rate of 50.5 ml min^{-1}. Using this system, samples were taken prior to fuel injection and at the beginning, middle (in most cases), and end of each day of irradiation. Samples were taken using cryogenic trapping techniques similar to those described in Section 2.2 (Reference 30).

Although this system was capable of monitoring the simpler C_2-C_5 aldehydes and ketones, in practice it could not be used for this purpose in fuel runs, because of the interferences by larger hydrocarbon fuel components having similar retention times on this system. For that reason, oxygenate data from this system are not reported for fuel runs. The primary utility of this system, with regard to oxygenate analyses, was to assure that there was no significant oxygenate contamination in the pure air used in the runs in this study.

This system was capable of monitoring toluene and the xylenes without apparent interference (except that meta- and para-xylene have the same retention time, so that only the sum of the two can be determined). Where available, such data are reported. However, in many cases, a discrepancy is noted in the toluene data between the capillary system and the C-600 system; the concentrations obtained in the capillary system are as much as

a factor of five higher. This is probably due to toluene not separating from some other fuel component on the capillary system.

C_1 and C_2 hydrocarbons were monitored prior to the fuel injection and at the beginning and end of each day of irradiation. A 5 ft x 0.125 in stainless steel column packed with 100/120 mesh Porapak N, held at 60°C, and with an N_2 flow rate of 30 ml min^{-1} was employed. This system was useful primarily to determine that there was no significant contamination from ambient air; except for selected control and characterization runs, data are not reported. The sampling technique, calibration procedure, and discussions of the accuracy of this technique are given elsewhere (Reference 30).

C_3-C_6 hydrocarbons and the Freon® 12 tracer were monitored using a 34 ft x 0.125 in stainless steel column packed with 10% 2,4-dimethylsulfolane (DMS) on C-22 Firebrick held at 0°C, in series with 2 ft x 0.125 in stainless steel "soaker" columns containing 10% Carbowax 600 on C-22 Firebrick (30/60 mesh). The N_2 flow rate was 26 ml min^{-1}. The analysis technique and frequency of analyses depended on the type of run. For all runs, samples were taken prior to and following fuel injection and at the end of the run using the cryogenic trapping technique (Reference 30). For fuel-butane runs and for dynamic runs, the n-butane or the Freon® tracer were analyzed hourly using the loop analysis technique (Reference 30). In the loop technique, a 2-3 ml stainless steel loop was flushed with the sample to be analyzed and then flushed directly on the column.

Two different GC's containing DMS columns were used in this program. One was located in the portable building next to the chamber and set up for automatic loop analysis. This was used in some, though not all, of the fuel-butane and dynamic runs. Most DMS analyses were done manually using a separate instrument in one of the main GC laboratories.

In the static runs not containing n-butane, the primary utility of this system was to assure that no contamination problem existed. Thus, concentrations of trace species monitored with this system are in general not reported, except for selected characterization runs.

Peroxyacetyl nitrate (PAN) was monitored using electron capture detection and 18 in x 0.125 in Teflon® columns of 5% Carbowax 400 on Chromosorb G (80/100 mesh) operating at ambient temperature (References 30-32). Analyses were done by flushing a ~2 ml loop with the sample and

then injecting the contents of the loop onto the column. The calibration of this system and factors affecting its accuracy are described elsewhere (Reference 30). Two instruments were employed at various times in this program. One was located in the building adjacent to the chamber and sampled automatically; the other was in one of our other laboratories and sampled manually. For most runs, PAN data were reported on an hourly basis.

In many runs, other GC peaks were observed in the PAN chromatograms. These were probably alkyl nitrates, for which this system is also sensitive. However, because the exact identities of the compounds causing these peaks were not established, they are not reported on the data sheets.

3.2.9 Formaldehyde

Formaldehyde was monitored at the beginning, middle, and end of the irradiations using an improved chromatropic acid technique (References 30, 33). Samples were taken at the rate of 1 $\ell\ min^{-1}$ in a single bubbler containing 10 ml of distilled water. The developed solutions were read on a Beckman 35 spectrometer. A more detailed discussion of this technique, as it is employed in our laboratories, is given elsewhere (Reference 30).

3.3 MATERIALS

All reactants were obtained from commercially available samples with the exception of NO_2 and the military fuels. NO_2 was prepared by reaction of NO with excess oxygen in a syringe (Reference 30). The unleaded gasoline was obtained from the University of California, Riverside (UCR), gas station (Chevron brand) and the diesel No. 2 from the UCR agricultural operations gas station. The military fuels were supplied by the Fuels Branch, Fuels and Lubrication Division of the Aero-Propulsion Laboratory at Wright-Patterson Air Force Base in Ohio. The bulk of the Air Force fuels were shipped in one-gallon metal containers, but small samples of each of the fuels in sealed glass containers were also obtained from the same source to assure the intregrity of bulk samples. After arrival, the fuels were immediately transferred to glass bottles with Teflon®-lined caps. The headspace was kept flushed with nitrogen and the bottles were stored in a refrigerator at -8°C.

3.4 EXPERIMENTAL PROCEDURES

3.4.1 Fuel Runs

Pure Air Fill. Except as noted below the outdoor bag was filled with air prior to injection of the reactants. After filling the bag but before addition of the reactants, samples were taken for all analytical systems to determine background levels.

There were two types of experiments in which additional air was added after the initial fill. These were the dynamic runs which were done for some of the fuels and the four-day static runs. During the dynamic runs, air was added once every hour after the bag was uncovered until before the last sampling period. The amount added each time was calculated to make a 10-12% dilution, with the dilution being measured by changes in the concentration of the Freon® 12 tracer. During the four-day static runs, air was added (usually on day three or day four) if the bag needed additional air to make it through all four days. If additional NO_x was also being added, it was injected into the pure air stream flow going into the bag.

The bag was flushed with pure air after each run, before the next experiment. This was done by filling the bag completely, and then emptying it.

Reactant Injections. Any reactants whose initial concentrations were the same on both sides were injected prior to separating the sides. The reactants were thoroughly mixed by agitation of the sides of the Teflon® bag before dividing the bag and before sampling was begun.

Injections and dilutions of gas phase reactants were generally done using hypodermic glass syringes (Becton-Dickerson Yale 5, 10, 20, and 100 ml). The reactants were injected from the syringe into a 1 ℓ bulb attached to the bag through the injection port by Teflon® tubing. The bulb was flushed for two minutes with nitrogen at 5 ℓ min^{-1}. When additional NO_x was added during the four-day static runs, the nitrogen flow was 200 ml min^{-1} with a 10-minute flush.

The procedures for injection of the fuels are described in Section 2.3. Briefly, the more volatile fuels (JP-4 [pet], and JP-4 [shale], unleaded gasoline, and JP-10) were injected by placing the fuel in a 2 ℓ bulb (with a microsyringe) and flushing the bulb at 5 ℓ min^{-1} with nitrogen while heating the bulb with a heat gun for 15 minutes. The less volatile fuels (JP-8 [pet], JP-8 [shale], RJ-4, RJ-5, and diesel) were placed

in a Pyrex® tube, which was first flushed with nitrogen for two minutes at 5 $\ell\,min^{-1}$. The tube was then uniformly heated to 250°C, while continuing the N_2 flush for an additional 30 minutes.

Irradiation Protocol. Procedures for covering and uncovering the bag for all of the fuel-NO_x runs were standardized as follows: (1) All bag uncoverings occurred at 0900 PST or as close to that as possible. (2) The bag covering on the first day of the two-day dual bag runs was done at 1630 PST and on the second day at 1530 PST. (3) On the undivided bag runs (four-day or dynamic), the bag was not covered until the last day of the experiment, when it was covered at 1530 PST.

Sampling. Background samples were taken on all of the instruments after the pure air fill before any reactants were added. After the reactants had been added and thoroughly mixed, and before the bag was uncovered, another set of samples was taken on all of the instruments. After the bag was uncovered, samples were taken hourly on all of the inorganic instruments, the PAN analyzers, and the capillary GC system. Sampling periods were standardized as follows: (1) The first sampling period of the day started at 1000 PST. (2) The last sampling period started at 1600 PST on day one of dual runs and on day one, two, and three of four-day static runs. (3) On day two of dual runs and day four of static runs, the last sampling period started at 1500 PST. (4) On undivided bag runs, sampling occurred from on the hour to 10 minutes after the hour. On divided bag runs, sampling occurred on Side A from on the hour to 10 minutes after the hour and on Side B from 10 after the hour to 20 after the hour.

Formaldehyde samples were taken prior to irradiation, from 1150-1210 PST, and during the last sampling period of the day. GC sampling on the Poropak-N, DMS, and C-600 columns (Section 3.2.8) was done prior to irradiation and during the last sampling period.

3.4.2 Conditioning and Characterization Runs

After each new bag was installed, the following minimum set of conditioning and characterization runs were done.

NO_x-air irradiations were carried out for the purpose of characterizing excess rates of radical initiation and NO oxidation due to chamber effects (References 34-36). These runs were done after the bag was newly

conditioned (after the propene-NO_x irradiation and the O_3 decay experiment), after the bag had been extensively used for fuel-NO_x irradiations, and, for most bags, when it was newly installed and not yet conditioned. The runs consisted of injecting 0.125 ppm NO, 0.3[illegible] ppm NO_2, and ~8 ppb each of propene, and propane, and irradiating for 2-2.5 hours, beginning at 11:00-12:00 PST. In most cases the bag was undivided, though several divided bag NO_x-air irradiations were done to test side equivalency. NO, NO_2, propene and propane, UV intensity, and temperature were monitored every 15 minutes. In general, analyses were carried out for the other species and parameters specified above at the beginning and end of the irradiation.

Propene-NO_x conditioning runs were done when the bag was new and as necessary to condition the bag sides equally for subsequent divided bag runs. In the latter case, these conditionings were done primarily in association with fuel-butane runs, since the bag conditioning could possibly be different following an n-butane-NO_x irradiation than following a fuel-NO_x irradiation. The propene-NO_x conditioning was either the first or the second (following a NO_x-air irradiation) run done for each new bag. These conditioning runs were done by injecting ~0.25 ppm each of NO and NO_2 and 0.5 ppm of propene and irradiating the undivided bag for ~5 hours. Because these runs were primarily for conditioning, relatively little sampling was done, though in most cases initial and final reactant concentrations and final O_3 yields were determined.

Ozone decay determinations were done for each new bag following the propene-NO_x conditioning to determine the O_3 dark decay rate in the conditioned bag. Ozone (3-4 ppm) was injected into the bag and kept in the covered, undivided bag for at least 24 hours. The ozone concentration was measured immediately after it was injected and at the end of the run; in general, other parameters were not monitored.

Pure air irradiations were done to characterize rates of ozone formation in the bags in the absence of added reactants. The irradiations were generally carried out for five hours. Ozone and NO_x were monitored at least hourly; other parameters were measured at the beginning and end of the irradiations. These runs were usually done following the ozone decay determinations in the newly conditioned bags, though in some cases they

were not carried out until several fuel runs in the bag had been completed.

An NO dark oxidation run was done around the beginning of the program as a test of the validity of our NO_x data. Approximately 1 ppm of NO was injected in the covered, undivided bag. NO and NO_2 data were taken at hourly intervals throughout the day as well as the following morning. Temperature and aerosol parameters were also monitored.

SECTION IV

RESULTS OF THE OUTDOOR CHAMBER IRRADIATIONS

A total of 132 single and multi-day outdoor chamber irradiations were performed during the 18 months of this program. These included 63 fuel-NO_x runs, 48 characterization experiments, 19 conditioning runs, and two runs which were aborted. Table 17 gives a chronological listing of the outdoor runs, showing for each the date the run started, the description of the run, the number of run-days, the bag number, the overall average temperature and UV intensity, any problems encountered, and an indication of which analytical systems were or were not used. Unless otherwise noted on this table, all of the analytical systems described in Section 3.2 were employed.

Detailed data tabulations for the runs listed in Table 17 are given in Volume II. In addition to tabulating the relevant experimental measurements made during each run, these data sheets indicate which instruments were used and give the daily and overall averages of the major physical parameters (temperature and UV intensity). Comments taken from the laboratory notebooks describing general weather conditions and any relevant problems or special situations which occurred during the run are also included on these data sheets. For the characterization runs, the relevant calculated results (e.g., decay rates, radical levels, etc.) are also briefly summarized along with the comments. A number of measurements were also carried out, which, because of relevancy considerations and space limitations, are not included in the tabulations. These include gas chromatographic measurements of the part-per-billion concentrations of trace compounds present in the pure matrix air used for the fuel runs, as well as measurements of methane (which is inert, and was always present at approximately its atmospheric background levels), and unidentified or minor fuel components. These data are kept on file at the Statewide Air Pollution Research Center (University of California, Riverside, CA 92521), and are available upon request.

The major results obtained in these experiments are summarized in the following sections.

4.1 RESULTS OF CHARACTERIZATION EXPERIMENTS

Four types of characterization experiments were performed in the outdoor chamber in this program. These included: (1) pure air irradiations to determine the rate of O_3 formation due to irradiation of background species or bag contaminants; (2) ozone decay determinations, to determine the ozone dark decay rate due to destruction at the bag surface; (3) NO_x-air irradiations, to determine the rates of radical input from chamber-dependent sources and of NO oxidation caused by contamination by reactive organics; and (4) an NO dark oxidation experiment, to assure that the NO_x analytical system was functioning correctly. The results of these experiments are summarized below.

4.1.1 Pure Air Irradiations

Table 18 gives the conditions, bag numbers, and selected results of the pure air irradiations done in this program. Most of the pure air irradiations were carried out immediately after a new bag was conditioned, but prior to any irradiations. The gradual formation of ozone was observed in all of these irradiations. As can be seen from Table 18, for unused bags the ozone formation rate was in the 2-9 ppb hr^{-1} range, corresponding to a maximum ozone production of ~60-70 ppb per day. Run AFF-14 was carried using bag No. 15, which was not used in any experimental fuel-NO_x run since it exhibited severe leakage problems. Furthermore, bag No. 15 also appeared to be highly contaminated, as indicated by the results of this and other characterization runs. Runs AFF-109 and AFF-123 were carried out after bags Nos. 23 and 24, respectively, had been used for fuel runs (RJ-5 and diesel fuel, respectively); their higher rate of O_3 formation reflects this fact. Since RJ-5 and diesel fuel were the heaviest fuels studied, contamination effects from the other, lighter fuels should have been much less.

4.1.2 Ozone Decay Determinations

Table 19 gives the ozone dark decay rates, which were observed in the bags employed in this program. With the exception of the ozone decay rates observed in bags Nos. 15 and 16, there was relatively little variation, with the average ozone decay rate being $0.42 \pm 0.08\%$ hr^{-1}. The variation observed could be attributed to variations in temperature, since

TABLE 17. CHRONOLOGICAL LISTING OF OUTDOOR RUNS PERFORMED TOGETHER WITH SELECTED CONDITIONS, PROBLEMS, AND PARAMETERS MONITORED.

Run No.	Run Started	Run Description	Run Days	Bag No.	Avg. T[a] (°C)	Avg. UV[b] (mW cm^{-2})	Problems or Notes	GC[c] Used	PAN[d] Data	HCHO[d] Data	Instruments not on Line[e] Inorg/ Physical	Aerosol	GC Backup
2	6/4/80	Pure air	2	14	29 ± 4	2.4 ± 1.5	1	-	-	-	W	CBP	PCD
3	6/13	O_3 decay	2	14	30 ± 1	-	2	-	-	-	WHL	P	PCD
4	6/16	NO dark oxidation	2	14	29 ± 6	-		-	-	-	WHL	P	PCD
5	6/17	Conditioning	1	14	28 ± 7	3.1 ± 0.9		-	Q	-			
6	6/18	O_3 decay	2	14	26 ± 5	-		-	-	-	WHL	P	PCD
7	6/19	Conditioning	1	14	28 ± 7	3.5 ± 0.6		-	X	-			
8	6/20	n-Butane vs. JP-4(S)	1	14	32 ± 6	2.8 ± 0.8	3	HT	X	X			
9	6/26	JP-4(S): var. fuel	2	14	34 ± 6	2.8 ± 0.6	4	HT	X	X		C	
10	7/2	JP-4(S): var. NO_x	2	14	32 ± 5	3.4 ± 0.8	5	HT	X	X		C	
11	7/11	NO_x-air	1	15	39 ± 3	3.9 ± 0.5		-	-	-	W	C	
12	7/12	O_3 decay	2	15	-	-	6	-	-	-	HTLW	CPBS	PCD
13	7/15	Conditioning	1	15	-	3.2 ±0.6	7	-	-	-	HTW	CPBS	C
14	7/16	Pure air	1	15	41 ± 5	3.4 ± 0.5	6	-	-	-	W	CPBS	PCD
15	7/17	Conditioning	1	16	32 ± 8	2.8 ± 0.6		-	-	-	HW	CPBS	D
16	7/18	O_3 decay	4	16	31 ± 7	-		-	-	-	HLW	CPBS	PCD
17	7/21	Pure air	1	16	35 ± 4	3.1 ± 0.4		-	-	-	W	C	PCD
18	7/22	JP-4(S): multi-day	4	16	37 ± 6	2.6 ± 0.6		HT	X	X		CS	
19	7/30	JP-4(S) vs. n-butane	1	16	38 ± 6	2.7 ± 0.5		HT	X	X		BS	
20	8/1	JP-4(P) vs. n-butane	1	16	37 ± 6	2.9 ± 0.5		HT	X	X		BS	
21	8/5	Conditioning	1	16	34 ± 4	3.4 ± 0.3	8	-	-	-	HW		P
22	8/6	JP-4(P) vs. JP_4(S)	1	16	34 ± 8	3.0 ± 0.6		HT	X	X			
23	8/7	JP-4(S) vs. JP-4(P)	1	16	36 ± 7	2.9 ± 0.6		HT	X	X			
24	8/8	NO_x-air	1	16	41 ± 3	3.2 ± 0.4	8	HT	-	X	W		
25	8/12	JP-4(P): multi-day	4	16	32 ± 6	2.8 ± 0.8		HT	X	X			
26	8/20	JP-4(S): dynamic	1	16	30 ± 8	3.0 ± 0.8	4	HT	X	X			

TABLE 17. CHRONOLOGICAL LISTING OF OUTDOOR RUNS PERFORMED TOGETHER WITH SELECTED CONDITIONS, PROBLEMS, AND PARAMETERS MONITORED (continued).

Run No.	Run Started	Run Description	Run Days	Bag No.	Avg. T[a] (°C)	Avg. UV[b] (mW cm^{-2})	Problems or Notes	GC[c] Used	PAN[d] Data	HCHO[d] Data	Instruments not on Line[e] Inorg/ Physical	Aerosol	GC Backup
27	8/21	NO_x-air	1	17	36 ± 1	2.7 ± 0.8		-	-	-	W	CPBS	
28	8/22	Conditioning	1	17	28 ± 6	-		-	-	-	HLW	CPBS	PCD
29	8/22	O_3 decay	4	17	-	-		-	-	-	NHTLW	CPBS	PCD
30	8/25	Pure air	1	17	-	-		-	-	-	NHTLW	CPBS	PCD
31	8/26	JP-4(S): dynamic	2	17	35 ± 7	3.0 ± 0.8	9	HT	X	X			
32	8/28	JP-4(P): var. NO_x	2	17	34 ± 7	2.8 ± 0.9		HT	-	X			
33	9/3	JP-4(P): dynamic	3	17	35 ± 6	2.2 ± 0.7	10	HT	X	X			
34	9/9	JP-4(P): var. fuel	2	17	28 ± 6	2.2 ± 0.6	11	HT	X	X			
35	9/11	NO_x-air	1	17	26 ± 3	3.1 ± 0.2		-	-	-	W	CPBS	
36	9/12	Conditioning	1	18	28 ± 5	-		-	-	-	WHL	CPBS	PCD
37	9/12	O_3 decay	4	18	-	-		-	-	-	NHTLW	CPBS	PCD
38	9/15	Pure air	1	18	-	-		-	-	-	NHTLW	CPBS	C
39	9/16	NO_x-air	1	18	36 ± 3	4.1 ± 0.7		-	-	-	W	CPBS	
40	9/18	U. gas: var. NO_x	2	18	33 ± 6	2.2 ± 0.5	12	HT	X	X		B	PC
41	10/1	NO_x-air	1	18	43 ± 1	2.7 ± 0.2		-	-	X		CPBS	C
42	10/2	U. gas: var. fuel	2	18	35 ± 7	2.2 ± 0.5		HT	X	X			
43	10/7	U. gas: multi-day	4	18	31 ± 6	1.5 ± 0.6		HT	X	X			
44	10/14	U. gas vs. n-butane	1	18	21 ± 3	1.6 ± 0.6		HT	X	X			
45	10/15	U. gas: dynamic	3	18	22 ± 4	1.6 ± 0.6		HT	X	X			
46	10/20	NO_x-air	1	18	32 ± 1	2.7 ± 0.2		-	-	X		CPBS	
47	10/23	NO_x-air	1	19	34 ± 1	2.3 ± 0.4		-	-	X	WO	CPBS	
48	10/24	Conditioning	1	19	31 ± 4	2.3 ± 0.3		-	-	-	WH	CPBS	
49	10/24	O_3 decay	4	19	-	-		-	-	-	NHTLW	CPBS	PCD
50	10/29	Pure air	1	19	28 ± 7	-		-	X	X	LW		
51	10/30	NO_x-air	1	19	32 ± 2	1.8 ± 0.4		-	-	X	W	CPBS	

TABLE 17. CHRONOLOGICAL LISTING OF OUTDOOR RUNS PERFORMED TOGETHER WITH SELECTED CONDITIONS, PROBLEMS, AND PARAMETERS MONITORED (continued).

Run No.	Run Started	Run Description	Run Days	Bag No.	Avg. T[a] (°C)	Avg. UV[b] (mW cm^{-2})	Problems or Notes	GC[c] Used	PAN[d] Data	HCHO[d] Data	Instruments not on Line[e] Inorg/ Physical	Aerosol	GC Backup
52	11/6	JP-10: var. NO_x	2	19	21 ± 5	1.3 ± 0.5	13	VTX	X	X			
53	11/18	JP-10 vs. n-butane	1	19	19 ± 5	1.6 ± 0.5	14	-	X	X	W		
54	12/2	JP-10: var. fuel	3	19	13 ± 2	0.6 ± 0.2	15	VTX	X	X			
55	12/10	JP-10: dynamic	3	19	22 ± 6	0.9 ± 0.4	16	VTX	X	X			
56	12/16	JP-4(S): dynamic	2	19	27 ± 7	0.8 ± 0.4	16	VTX	X	X			
57	12/18	JP-4(P): dynamic	2	19	17 ± 7	0.8 ± 0.3	16	VTX	X	X			
58	1/20/81	Conditioning	1	20	19 ± 3	1.2 ± 0.6		-	-	X	H	CPBS	
59	1/21	O_3 decay	2	20	19 ± 4	-		-	-	-	NHL	CPBS	PCD
60	1/22	Pure air	1	20	18 ± 8	0.9 ± 0.5	17	-	-	X		B	
61	2/3	NO_x-air	1	20	22 ± 1	2.5 ± 0.3		-	-	X		CPBS	
62	2/5	JP-4(P) vs. U. gas	2	20	18 ± 6	1.6 ± 0.6	16	VLX	X	X		B	
63	3/10	U. gas vs. JP-4(P)	2	20	23 ± 6	2.5 ± 0.9	18	HL	-	X		B	
64	3/17	Diesel: multi-day	3	20	23 ± 5	1.8 ± 0.8	19	VH	X	X		B	
65	3/24	NO_x-air	1	21	29 ± 1	2.7 ± 0.4		-	-	X		CPBS	
66	3/25	Conditioning	1	21	15 ± 2	2.4 ± 0.2		-	-	X		CPBS	
67	3/25	O_3 decay	2	21	-	-		-	-	-	NHTL	CPBS	PCD
68	3/27	Pure air	1	21	18 ± 2	1.2 ± 0.0		-	X	X			
69	4/6	NO_x-air	1	21	32 ± 1	3.6 ± 0.3		-	X	X		CPBS	
70	4/7	JP-8(P): var. NO_x	2	21	22 ± 4	2.6 ± 0.8		VH	X	X		B	
71	4/9	JP-8(P): var. fuel	2	21	22 ± 5	2.2 ± 0.7		VH	X	X		B	
72	4/14	JP-8(P): multi-day	4	21	25 ± 6	2.2 ± 0.9		VH	X	X		B	
73	4/21	JP-8(S): multi-day	4	21	26 ± 6	2.4 ± 1.0		VH	X	X		B	
74	4/30	JP-8(P) vs. JP-8(S)	2	21	30 ± 5	2.8 ± 0.8		VH	X	X		B	
75	5/5	JP-8(S) vs. JP-8(P)	2	21	25 ± 4	2.6 ± 0.8	20	VH	X	X			
76	5/7	JP-8(S) vs. JP-4(P)	2	21	29 ± 6	2.9 ± 0.8		VH	X	X		C	

TABLE 17. CHRONOLOGICAL LISTING OF OUTDOOR RUNS PERFORMED TOGETHER WITH SELECTED CONDITIONS, PROBLEMS, AND PARAMETERS MONITORED (continued).

Run No.	Run Started	Run Description	Run Days	Bag No.	Avg. T[a] (°C)	Avg. UV[b] (mW cm^{-2})	Problems or Notes	GC[c] Used	PAN[d] Data	HCHO[d] Data	Instruments not on Line[e] Inorg/ Physical	Aerosol	GC Backup
77	5/12	JP-4(P) vs. JP-8(S)	2	21	28 ± 5	3.2 ± 0.9		VH	X	X			C
78	5/14	JP-8(P) vs. JP-4(P)	2	21	22 ± 3	2.2 ± 0.9		VH	X	X			
79	5/19	JP-4(P) vs. JP-8(P)	2	21	23 ± 4	2.3 ± 0.8		VH	X	X			
80	5/21	JP-8(S): var. NO_x	2	21	27 ± 5	3.1 ± 0.9		VH	X	X			
81	5/27	JP-8(S): var. fuel	2	21	27 ± 5	2.7 ± 0.8		VH	X	X			
82	5/29	Conditioning	1	21	26 ± 9	-		-	-	-	HL	CPBS	PCD
83	6/1	NO_x-air	1	21	31 ± 1	3.9 ± 0.3		-	-	X		CPBS	
84	6/2	JP-8(P) vs. n-butane	1	21	25 ± 5	2.2 ± 0.9		VH	X	X			
85	6/3	Conditioning	1	21	31 ± 10	-		-	-	-	HL	CPBS	PCD
86	6/4	JP-8(S) vs. n-butane	1	21	40 ± 6	3.1 ± 1.1		VH	X	X			
87	6/5	O_3 decay	4	22	-	-		-	-	-	NHLWT	CPBS	PCD
88	6/8	Conditioning	1	22	38 ± 3	3.4 ± 0.9		-	X	X	H	CPBS	PCD
89	6/9	NO_x-air	1	22	34 ± 3	4.1 ± 0.2		-	X	X		CPBS	
90	6/10	RJ-4 vs. JP-10	2	22	30 ± 6	2.9 ± 0.8	21	VH	X	X			C
91	6/12	Pure air	1	22	30 ± 4	3.2 ± 0.9		-	X	X			
92	6/16	JP-10: multi-day	4	22	42 ± 5	2.6 ± 0.9		VH	X	X			
93	6/23	RJ-4: multi-day	4	22	39 ± 5	2.7 ± 0.7		VH	X	X			C
94	6/30	JP-10 vs. RJ-4	2	22	35 ± 6	3.0 ± 0.7		VH	X	X			
95	7/2	NO_x-air	1	22	39 ± 2	3.5 ± 0.6		-	X	X		CPBS	
97	7/8	RJ-4: var. NO_x	2	22	35 ± 5	2.7 ± 0.7		VH	X	X			
98	7/10	RJ-4 vs. n-butane	1	22	35 ± 6	2.9 ± 0.7		VH	X	X			
99	7/13	Conditioning	1	22	37 ± 7	-		-	-	-	HLW	CPBS	PCD
100	7/14	RJ-4: var. fuel	2	22	33 ± 6	1.7 ± 0.8		VH	X	X			C
101	7/16	JP-10: var. fuel	2	22	37 ± 6	2.7 ± 0.7		VH	X	X	H		C
102	7/20	Conditioning	1	22	38 ± 8	-		-	-	-	HLW	B only	PCD

TABLE 17. CHRONOLOGICAL LISTING OF OUTDOOR RUNS PERFORMED TOGETHER WITH SELECTED CONDITIONS, PROBLEMS, AND PARAMETERS MONITORED (continued).

Run No.	Run Started	Run Description	Run Days	Bag No.	Avg. T[a] (°C)	Avg. UV[b] (mW cm^{-2})	Problems or Notes	GC[c] Used	PAN[d] Data	HCHO[d] Data	Instruments not on Line[e] Inorg/ Physical	Aerosol	GC Backup
103	7/21	JP-10 vs. n-butane	1	22	37 ± 6	2.5 ± 0.8		VH	X	X	H		
104	7/22	NO_x-air	1	23	-	3.7 ± 0.2	22	-	X	X	HW	CPBS	
105	7/23	Conditioning	1	23	36 ± 6	3.3 ± 0.6		-	X	X	H	CPBS	C
106	7/24	O_3 decay	4	23	-	-		-	-	-	NHTLW	CPBS	PCD
107	7/27	NO_x-air	1	23	34 ± 3	3.1 ± 0.2		-	X	X	H	CPBS	
108	7/28	RJ-5: multi-day	4	23	32 ± 6	2.6 ± 0.9		VH	X	X			C
109	8/3	Pure air	1	23	31 ± 7	2.7 ± 0.3		VH	X	X	H		C
110	8/4	RJ-5: var. NO_x	2	23	35 ± 6	2.9 ± 0.9		VH	X	X			C
111	8/6	RJ-5: var. fuel	2	23	36 ± 6	2.6 ± 0.8		VH	X	X			C
112	8/10	Conditioning	1	23	36 ± 4	2.7 ± 0.5		VH	X	-			
113	8/11	RJ-5 *vs.* JP-10	2	23	34 ± 6	2.7 ± 0.7		VH	X	X			C
114	8/13	JP-10 vs. RJ-5	2	23	35 ± 6	2.5 ± 0.7		VH	X	X			C
115	8/17	Conditioning	1	23	34 ± 9	-		-	-	-	HL	CPBS	PCD
116	8/18	RJ-5 vs. n-butane	1	23	32 ± 6	2.4 ± 0.7		VH	X	X			C
117	8/19	NO_x-air	1	23	36 ± 2	3.4 ± 0.2		-	X	X		CPBS	C
118	8/20	NO_x-air	1	24	40 ± 2	4.2 ± 0.2		-	X	X		CPBS	
119	8/21	Conditioning	1	24	40 ± 5	3.4 ± 0.6		-	X	X	H	CPBS	
120	8/21	O_3 decay	3	24	-	-		-	-	-	NHTL	CPBS	PCD
121	8/24	NO_x-air	1	24	41 ± 2	4.0 ± 0.5		-	X	X		CPBS	
122	8/25	Diesel: multi-day	4	24	42 ± 5	2.4 ± 0.8		VH	X	X			C
123	8/31/81	Pure air	1	24	32 ± 7	2.4 ± 0.6		-	X	X	H		C
124	9/1	Diesel: var. NO_x	2	24	35 ± 5	2.8 ± 0.8		VH	X	X			C
125	9/3	Diesel: var. fuel	2	24	32 ± 5	2.6 ± 0.8		VH	X	X			C
126	9/8	Conditioning	1	24	-	-		-	-	-	HTL	CPBS	PCD
127	9/9	Diesel vs. JP-4(P)	2	24	35 ± 5	2.7 ± 1.0		VH	X	X			C

TABLE 17. CHRONOLOGICAL LISTING OF OUTDOOR RUNS PERFORMED TOGETHER WITH SELECTED CONDITIONS, PROBLEMS, AND PARAMETERS MONITORED (continued).

Run No.	Run Started	Run Description	Run Days	Bag No.	Avg. T[a] (°C)	Avg. UV[b] (mW cm^{-2})	Problems or Notes	GC[c] Used	PAN[d] Data	HCHO[d] Data	Instruments not on Line[e] Inorg/ Physical	Aerosol	GC Backup
128	9/11	NO_x-air	1	24	36 ± 3	3.1 ± 0.4		-	X	X		CPBS	C
129	9/15	JP-4(P) vs. diesel	2	24	35 ± 6	2.2 ± 0.7		VH	X	X			C
130	9/17	Conditioning	1	24	-	-		-	-	-	HTL	CPBS	PC
131	9/18	Diesel vs. n-butane	1	24	34 ± 6	2.0 ± 0.8		VH	X	X			C
132	9/21	NO_x-air	1	24	36 ± 2	3.2 ± 0.2		-	X	X		CPBS	C

[a]Average of all temperature measurements made during run, including (if applicable) measurements made when the bag was covered.

[b]Average of all UV measurements made when the bag was uncovered.

[c]Capillary GC codes:

- = No capillary GC data taken

HT = HP-5710, cryogenic trapping technique

HL = HP-5710, unheated Pyrex loop

VT = Varian 3700, cryogenic trapping

VL = Varian 3700, unheated Pyrex loop

VH = Varian 3700, heated Pyrex loop

VTX, VLX, VHX = Varian 3700, as above, but scattered data (~ ±15%) because of malfunction

[d]X = Data available; - = no data available; Q = Data available, but of questionable validity

[e]If the following codes appear, data of the indicated type is either not available, or of questionable validity (see data sheets for details in the latter case).

Inorganic/Physical Parameters

O = Ozone

N = NO-NO_2-NO_x

H = Total hydrocarbons and CO

T = Temperature

L = UV radiometric data

W = Humidity (i.e., RH or dew point not measured)

Aerosol Parameters

C = Condensation nuclei

P = Particle analyzer data (Climet)

B = Light scattering data (nephelometer)

S = Aerosol size data (TSF-3030)

Backup Chromatography

P = Poropak-N

C = Carbowax-600

D = DMS

TABLE 17. CHRONOLOGICAL LISTING OF OUTDOOR RUNS PERFORMED TOGETHER WITH SELECTED CONDITIONS, PROBLEMS, AND PARAMETERS MONITORED (concluded).

Problems or Notes

1. Bag divided, but no data taken from side B because of defective solenoid.
2. Some problems were discovered with the aerosol instruments and subsequently corrected.
3. N-butane observed to build up on JP-4(S) side of bag; run probably not valid.
4. Both sides of the bag were almost completely deflated at the beginning of the second day of the run, and the run was terminated early.
5. Side A lost volume far faster than side B; at end of second day side A was essently empty.
6. Significant bag deflation occurred.
7. Power lost in monitoring station, causing NO_x data to be lost four hours into run.
8. Bag divided to test side equality.
9. Starting with run number 31, UV radiometer data is from Eppley Radiometer 14290 which is under the bag.
10. Cooling line and integrator problems on the HP capillary system resulted in loss of data for the fuel components on the second and third days.
11. Side A leaked substantially, and only 5% of its volume remained overnight. After air was added, the THC on both sides was nearly equal.
12. Side B was leaking at a significant rate.
13. No JP-10 GC data is available for the first day of the run due to an instrument malfunction.
14. The JP-10 capillary GC data was highly scattered and was not used.
15. Rain on day two caused the run to be suspended and resulted in water in the bag. GC data still extremely variable.
16. Data on Capillary GC highly scattered.
17. Low solar intensity due to overcast conditions.
18. Side A leaked excessively and run was terminated early on day two.
19. The run was aborted on day three because of a large tear in the bag. Also, temperature used in the fuel injection was too low.
20. The aerosol size analyzer was not functioning correctly on day two.
21. NO and NO_x data appear to be anomolous.
22. Temperature measurements unreasonably high; probably wrong thermocouple used.

TABLE 18. EXPERIMENTAL CONDITIONS AND SELECTED RESULTS OF THE OUTDOOR PURE AIR IRRADIATIONS.

Bag No.	AFF Run No.	Average T (°C)	Average UV Rad. ($mW\ cm^{-2}$)	Average RH[a] (%)	Irradiation Time (min)	Final O_3 Conc. (ppb)	O_3 Formation Rate ($ppb\ hr^{-1}$)	Notes
14		230.5	3.10	15	300	8	1.6	b
15	14A	41.7	3.36	30	390	97	14.9	c
15	14B	42.6	3.36	30	400	160	24.0	c
16	17A	37.0	3.07	30	280	43	9.2	c
16	17B	37.6	3.07	30	290	37	7.7	c
17	30	--	--	30	300	32	6.4	
18	38	--	--	30	214	11	3.1	
19	50	27.5	--	30	300	21	4.2	
20	60	23.3	0.93	30	302	22	4.4	
21	68	17.7	1.17	48	300	11	2.2	
22	91	31.0	3.22	44	300	36	7.2	
23	109	32.8	2.66	25	305	64	12.6	d
24	123	34.8	2.34	32	305	88	17.3	e

[a]Approximate

[b]Run for two consecutive days. O_3 formation rate on day two = 1.0 $ppb\ hr^{-1}$.

[c]Divided bag run. A/B indicates side.

[d]Bag previously used for RJ-5-NO_x run.

[e]Bag previously used for diesel-NO_x run.

this is expected to affect the decay rates. The ozone decay rates in bags Nos. 15 and 16 were significantly higher than in the other bags.

4.1.3 NO_x-Air Irradiations

These experiments consisted of irradiating ~0.5 ppm of NO_x in air containing added trace levels of propene and propane in order to monitor the hydroxyl radical (OH) concentrations from their relative rates of decay (Reference 36). Under these experimental conditions, the only significant sink for propene and propane is via reaction with the OH radical.

TABLE 19. RESULTS OF OZONE DARK DECAY DETERMINATIONS IN THE OUTDOOR CHAMBERS.

Bag No.	AFF Run No.	Initial O_3 (ppm)	First Measurement Elapsed Time (hours)	First Measurement O_3 (ppm)	First Measurement Decay Rate (% hr^{-1})	Second Measurement Elapsed Time (hours)	Second Measurement O_3 (ppm)	Second Measurement Decay Rate (% hr^{-1})
14	3	3.398	25.72	4.150	0.29	--	--	--
14	6A[a]	0.274	6.92	0.266	0.43	13.80	0.249	0.48
14	6B[a]	0.277	6.83	0.263	0.76	13.90	0.240	0.66
15	12	1.960	23.40	1.345	1.6	--	--	--
16	16	2.991	3.53	2.879	1.1	63.42	1.334	1.2
17	29	4.591	48.15	3.498	0.56	15.02	3.277	0.43
18	37	4.361	63.67	3.373	0.40	--	--	--
19	49	3.597	18.50	3.247	0.55	44.92	2.808	0.32
20	59	2.552	6.50	2.505	0.29	15.50	2.342	0.43
21	67	2.168	14.50	1.992	0.58	6.17	1.959	0.27
22	87	2.282	67.50	1.738	0.40	--	--	--
23	106	3.896	20.30	3.685	0.27	44.33	3.278	0.26
24	120	3.010	42.30	2.498	0.44	--	--	--

[a]Divided bag run. A/B indicates side.

Hence, (References 34 and 36) the OH radical concentration is given by

$$[OH] = \frac{1}{(k_a - k_b)} \frac{d \ln ([propane]/[propene])}{dt}$$

where k_a and k_b are the rate constants for the reactions of the OH radical with propene and propane, respectively (Reference 13). Based on the known reactions occurring when NO_x is irradiated in air (References 4, 5, 23, 37, 38), radical sources in these systems should be negligible. However, significant radical levels are observed in NO_x-air irradiations (References 34-36), from which it has been concluded (References 35, 36) that radicals are produced from unknown, chamber-dependent sources. These NO_x-air irradiations were carried out to measure the rates of radical production from this source (or sources). Since radical initiation and

termination must balance and since, after the initial 30-60 minutes of the irradiation, the only significant radical sink is the reaction of OH radicals with NO_2 (References 34, 36), then

$$\text{radical initiation rate} \cong k_c\,[OH][NO_2]$$

where k_c is the known rate constant (References 5, 37, 38) for the reaction of OH radicals with NO_2.

Table 20 lists the experimental conditions, the calculated average hydroxyl radical levels, and radical input rates for the NO_x-air irradiations carried out during this program. These irradiations were conducted (a) when the bag was new, (b) after it had been conditioned but prior to any NO_x-fuel-air runs, and (c) after the bag had been extensively used for NO_x-fuel-air irradiations. For each bag, this latter NO_x-air irradiation was usually carried out immediately before the bag was finally removed. Except for bag No. 15, which appeared to be unusually contaminated and was not used for any fuel-NO_x runs, the radical input rate ranged from 0.02 to 0.13 ppb min^{-1} for new or newly-conditioned bags. The conditioning apparently had little effect on the observed radical levels. Following the fuel runs, the radical input rates when corrected for differences in light intensity (References 34-36), were approximately the same for bag No. 18 (used for unleaded gasoline). The rates were higher by factors of 1.5 to 3.5 for bags Nos. 21 and 24 (used for JP-8 and diesel No. 2, respectively), for bag No. 22 (used for JP-10 and RJ-4), and for bag No. 23 (used for RJ-5). It is not clear whether these differences were due to differences in the nature of the fuels or the intrinsic variability of the chamber-dependent radical sources. However, it is obvious from Table 18 that exposure of the bag to fuel-NO_x mixtures tended to increase the radical input rate in subsequent runs.

The consumption rate of NO observed in these runs served as a measure of the extent of contamination of the bag by reactive organics, since the oxidation rate of NO in NO_x-air irradiations is essentially totally due to the presence of RO_2 radicals formed from reactive organics (References 34, 36). In the presence of a reactive organic, the peroxy radicals (RO_2) formed during its atmospheric degradation react to convert NO to NO_2 and thus cause NO consumption:

TABLE 20. EXPERIMENTAL CONDITIONS AND SELECTED RESULTS OF NO_x-AIR IRRADIATIONS IN THE OUTDOOR CHAMBER.

Bag No.	AFF Run No.	T (°C)	UV Rad. ($mW\ cm^{-2}$)	RH[a] (%)	NO (ppm)	NO_2 (ppm)	[OH][b] (ppt)	Rad. Input[c] ($ppb\ min^{-1}$)	$\frac{-d[NO]}{dt}$ ($ppb\ min^{-1}$)
New Bag									
15	11	39	3.9	50	0.485	0.124	0.076	0.16	0.52
17	27	36	2.7	30	0.283	0.092	0.027	0.04	0.10
19	47	34	2.3	<10	0.394	0.144	0.026	0.06	~0
21	65	29	2.7	20	0.321	0.092	0.012	0.02	0.27
23	104	~35-40[d]	3.7	35	0.358	0.108	0.020	0.04	~0
24	118	40	4.2	20	0.391	0.119	0.033	0.06	0.13
Conditioned bag									
18	39	36	4.1	65	0.380	0.128	0.067	0.13	0.09
19	51	33	1.8	<10	0.404	0.133	~0.03[e]	~0.07	0.03
20	61	22	2.5	20	0.418	0.160	0.02	0.05	0.01
21	69	32	3.6	35	0.371	0.125	0.033	0.07	0.08
22	89	34	4.1	30	0.350	0.118	0.055	0.10	~0
23	107	34	3.1	30	0.307	0.081	0.032	0.04	0.06
24	121	41	4.0	25	0.360	0.125	0.032	0.06	0.07
Used bag									
16	24A[f]	41	3.2	50	0.461	0.138	0.093	0.23	0.86
16	24B	41	3.2	50	0.461	0.138	0.080	0.27	0.73
16	35	26	3.1	25	0.402	0.146	0.047	0.11	0.13
18	41	43	2.7	45	0.398	0.139	0.0o7	0.11	0.10
18	46	32	2.7	<10	0.370	0.147	0.037	0.08	~0
21	83	31	3.9	30	0.410	0.130	0.045	0.11	0.33
22	95	39	3.7	20	0.440	0.120	0.083	0.19	0.51
23	117	36	3.4	35	0.380	0.118	0.081	0.16	0.13
24	128A	37	3.1	25	0.339	0.100	0.032	0.08	0.68
24	128B	37	3.1	25	0.339	0.100	0.030	0.07	0.43
24	132A	36	3.2	25	0.356	0.111	0.040	0.09	0.59
24	132B	36	3.2	25	0.356	0.111	0.031	0.07	0.33

TABLE 20. EXPERIMENTAL CONDITIONS AND SELECTED RESULTS OF NO_x-AIR IRRADIATIONS IN THE OUTDOOR CHAMBER (concluded).

---

[a]Approximate RH at beginning of run.

[b]Calculated using: [OH](ppt) = 30.8 x d[ln (propane/propene)]/dt, based on published OH + propene and propane rate constants (Reference 13).

[c]Calculated using: radical input rate (ppb min^{-1}) = 16.0 x [OH](ppt) x [(60 + minute average NO_2 (ppm)], based on recommended 1 atm, 300 K OH + NO_2 rate constant (Reference 5).

[d]No temperature data available. Estimate based on weather conditions.

[e]Data highly scattered.

[f]Divided bag run. A or B indicates for which side data is given. Sides A and B have same average and initial conditions.

$$\text{Organic} + OH \xrightarrow{O_2} RO_2$$

$$RO_2 + NO \rightarrow RO + NO_2$$

$$RO + O_2 \rightarrow HO_2 + \text{Products}$$

$$HO_2 + NO \rightarrow OH + NO_2$$

While essentially no NO oxidation was observed during several of these NO_x-air irradiations, in most cases measurable NO consumption did occur, indicating some contamination by reactive organics. As expected (Table 20), the NO consumption rate was highest in the bags previously used for fuel-NO_x irradiations, except for bag 18, which had been used for unleaded gasoline (the most volatile of the fuels studied, but also the most reactive with respect to NO oxidation [Section 4.2]). It should be noted that the very high NO oxidation rate observed in run AFF-24 appeared to be anomalous, since a subsequent NO_x-air irradiation using the same bag (AFF-35) yielded a relatively low NO oxidation rate. It may be that some of the high NO oxidation rates observed were due to an incomplete flushing of the bag between experiments.

4.1.4 NO Dark Oxidation

At the beginning of this program, an NO dark oxidation experiment was carried out to test the validity of our NO_x analytical system. For this experiment, the initial NO and NO_2 concentrations were 0.86 and 0.06 ppm, respectively. After 20 hours the respective concentrations were 0.62 and 0.24 ppm. These data yielded an average NO loss rate of 2.0×10^{-4} ppm min^{-1} and an average NO_2 formation rate of 1.5×10^{-4} ppm min^{-1}. The discrepancy between the NO loss rate and the NO_2 formation rate amounted to a total NO_x loss rate of 0.1% per hour, which was not considered excessive. The theoretical NO oxidation rate at 300 K, calculated from the thermal NO oxidation rate data of Hampson and Garvin (Reference 37), is 1.6×10^{-4} ppm $mole^{-1}$ (in agreement with the result of this run).

4.2 RESULTS OF FUEL-NO_x EXPERIMENTS

A total of 62 useable fuel-NO_x-air outdoor chamber runs were performed in this program, including 45 which were carried out with the chamber in divided mode. Including the n-butane-NO_x-air experiments, this means that 107 different fuel-NO_x-air mixtures were irradiated during this program. Tables 21-30 summarize the relevant conditions and major results of the static irradiations for each fuel, including n-butane; Table 31 summarizes the conditions and results of the dynamic runs. As discussed in the Introduction, the outdoor fuel-NO_x-air runs can also be further categorized into four-day runs, dynamic runs, runs with variable initial NO_x, runs with variable initial fuel runs, and fuel versus fuel (or n-butane) runs. In the following sections, the results of these different types of runs are discussed.

4.2.1 Four-Day Irradiations

For each fuel, the conditions and selected results of the four-day runs are summarized in Tables 21-29. Concentration-time profiles for selected monitored species and parameters are plotted in Figures 19-27. As discussed in Section I, these runs consisted of irradiating the standard fuel-NO_x mixture (~25 ppmC fuel, 0.5 ppm NO_x) for four days, diluting at the beginning of the day if necessary to maintain the bag volume, and adding NO_x at the beginning of the third or fourth day, depending on how long it took for the mixture to become unreactive.

In terms of reactivity with respect to O_3 formation and NO_x consumption on the first two days, these runs can be classified into two groups: (a) those which exhibit greatest O_3 formation and NO_x consumption on the first day, have essentially all of the NO_x consumed by the beginning of the second day, and are consequently photochemically unreactive until additional NO_x is injected; and (b) those which exhibit relatively little O_3 formation and NO_x consumption on the first day, but rapid O_3 formation on the second day. The runs involving the JP-4 and JP-8 fuels (Figures 19-22), unleaded gasoline (Figure 23), diesel No. 2 (Figure 24), and RJ-4 (Figure 26) fall in the first category, while the JP-10 (Figure 25) and the RJ-5 (Figure 27) runs fall in the second group. In either case, the mixture was essentially unreactive with respect to O_3 formation on the day following that of most rapid O_3 formation. This behavior is expected, since NO_x is required for significant O_3 formation to occur, and the ozone formed on the previous day reacts with and consumes the remaining NO_x (if any) during the night. For the less reactive runs, the amount of O_3 formed on the first day is insufficient to consume all of the NO_x during that night (instead, it is the O_3 which is consumed). The next morning NO_x remains to allow O_3 formation to occur during the second day.

Following the consumption of the initially-present NO_x, by the beginning of the third day (at the latest), the mixtures appeared to be photochemically unreactive. In some runs (those employing unleaded gasoline, diesel No. 2, and RJ-5), the O_3 levels dropped slowly on these days at rates approximating those observed in the O_3 dark decay runs. In other runs employing JP-4 (pet), JP-8 (shale), and JP-10, the O_3 levels increased slowly at rates in the range observed in the pure air irradiations. In the JP-4 (shale), JP-8 (pet), and RJ-4 runs, the O_3 was essentially constant on the day following NO_x consumption. It is probable that the behavior of O_3 on the photochemically unreactive days was more a function of the conditions of the run (temperature, UV intensity, amount the mixture was diluted, bag conditions, etc.) and not the nature of the fuel, since there appears to be no obvious relation between the type of fuel and the behavior of O_3 on those days.

It was clear that relatively little additional information could be obtained by irradiating a photochemically unreactive mixture for more than one day. Hence, in order to simulate an aged fuel mixture passing a fresh

(The reverse of this page is blank)

TABLE 21. INITIAL CONDITIONS AND SELECTED RESULTS FOR STATIC JP-4 (PETROLEUM-DERIVED)-NO_x-

AFF Run No.		22	23	78	79	76	77	127	129	62	63	20	
Side		A	B	B	A	B	A	B	A	A	B	A	
Run Type		Std.	Std.	Std.	Std.	Std.	Std.	Std.	Std.	Std.	Std.	Std.	
vs		JP-4(s)	JP-4(s)	JP-8(p)	JP-8(p)	JP-8(s)	JP-8(s)	Diesel	Diesel	U. Gas	U. Gas	$n-C_4$	L
Day 1													
Avg. T	(^{o}C)	34±8	37±7	23±2	24±3	31±2	30±2	38±2	36±2	18±7	24±6	37±6	
UV. Int.	(mw cm^{-2})	3.0±0.6	2.9±0.6	1.7±0.6	2.2±0.7	2.8±1.0	3.0±1.0	2.6±1	2.1±0.8	1.8±0.6	2.5±0.9	2.9±0.5	2
Init. Fuel (calc)	(ppmC)	27.5	27.7	21.2	19.6	21.2	22.3	18.8	19.9	22.7	23.3	25.8	
Fuel (obs)	(ppmC)	35.2	31.8	24.5	21.7	24.5	23.3	21.1	27.5	24.1	22.7	33.0	
NO	(ppm)	0.461	0.455	0.291	0.278	0.292	0.309	0.323	0.350	0.344	0.357	0.416	
NO_2	(ppm)	0.157	0.152	0.102	0.091	0.101	0.102	0.103	0.119	0.131	0.140	0.154	
Final NO_2 (uncorr)	(ppm)	0.132	0.098	0.232	0.209	0.122	0.142	0.092	0.139	0.329	0.171	0.112	
$d([O_3]-[NO])/dt$	(ppb min^{-1})	4.26	4.67	1.63	1.12	2.68	2.78	3.11	2.60	1.43	2.58	4.69	
Time O_3 max	(PST)	1405	1315	Final	Final	1515	Final	1415	1505	1505	1515	1405	
Maximum: O_3	(ppm)	0.81	0.57	0.29	0.41	0.71	0.74	0.84	0.68	0.15	0.54	0.99	
PAN	(ppm)	0.023	0.021	0.054	0.045	0.145	0.148	0.083	0.080	0.014	--	0.024	
HCHO	(ppm)	0.061	0.138	0.038	0.036	0.061	0.068	0.115	0.050	0.024	0.052	0.134	
Aerosol Vol.	(μm^3 cm^{-3})	148	119	8	10	21	21	45	62	34	107	--	
B_{scat}	($10^{-4} m^{-1}$)	18.8	15.2	1.2	3.8	4.1	8.0	20.0	16.4	--	--	--	
Condens. Nuc.	(10^3counts)	100	88	42	40	42	51	47	49	50	83	78	
Aerosol No.	(10^3 cm^{-3})	110	140	120	110	180	190	88	75	88	110	--	
No. Particles >0.3 μ	(cm^{-3})	354	31	6	33	214	215	317	303	1	338	347	
No. Particles >1 μ	(cm^{-3})	37	0	0	0	0	0	0	0	0	0	0	
Days 2-4:	Day	--	--	(2)	(2)	(2)	(2)	(2)	(2)	(2)	--	--	
Dilution	(final/initial)	--	--	--	--	--	--	--	--	--	--	--	
Avg. T	(^{o}C)	--	--	24±1	24±2	32±2	30±2	37±2	38±3	18±5	--	--	
UV Int.	(mw cm^{-2})	--	--	2.7±0.9	2.5±0.8	3.2±0.6	3.3±0.7	2.7±0.8	2.3±0.6	1.5±0.6	--	--	3
Init. Fuel	(ppmC)	--	--	21.8	18.7	19.2	17.8	--	--	22.5	--	--	
O_3	(ppm)	--	--	0.109	0.205	0.509	0.530	0.581	0.437	~0	--	--	
NO	(ppm)	--	--	~0	~0	~0	~0	~0	~0	~0	--	--	
NO_2 (uncorr)	(ppm)	--	--	0.062	0.063	0.062	0.062	0.038	0.048	0.145	--	--	
Final NO_2 (uncorr)	(ppm)	--	--	0.082	0.090	0.074	0.083	0.052	0.052	0.102	--	--	
Time $[O_3]$ max	(PST)	--	--	Final	Final	Init.	Init.	Init.	Init.	Final	--	--	
Maximum: O_3	(ppm)	--	--	0.27	0.30	(0.51)	(0.53)	(0.58)	(0.44)	0.30	--	--	
PAN	(ppm)	--	--	0.083	0.065	0.061	0.071	0.021	0.029	--	--	--	
HCHO	(ppm)	--	--	0.058	0.070	0.100	0.106	0.107	0.100	0.042	--	--	
Aerosol Vol.	(μm^3 cm^{-3})	--	--	5	7	5	5	9	7	7	--	--	
B_{scat}	(10^{-4} m^{-1})	--	--	1.1	1.7	2.0	2.2	3.6	4.1	--	--	--	
Condens. Nuc.	(10^3counts)	--	--	1	3	1	1	~0	~0	0	--	--	
Aerosol No.	(10^3 cm^{-3})	--	--	5.2	12	5.0	6.5	3.7	4.5	1.0	--	--	
No. Particles >0.3 μ	(cm^{-3})	--	--	179	105	223	162	198	282	159	--	--	
No. Particles >1 μ	(cm^{-3})	--	--	0	0	0	0	0	~0	~0	--	--	

ONDITIONS AND SELECTED RESULTS FOR STATIC JP-4 (PETROLEUM-DERIVED)-NO_x-AIR OUTDOOR CHAMBER RUNS.

79	76	77	127	129	62	63	20	32	34	25			32	34
A	B	A	B	A	A	B	A	A	A	-			B	B
Std.	Std.	Std.	Std.	Std.	Std.	Std.	Std.	Std.	Std.	Std.			Low NO_x	Low Fuel
-8(p)	JP-8(s)	JP-8(s)	Diesel	Diesel	U. Gas	U. Gas	n-C_4	Low NO_x	Low Fuel	--			Std.	Std.
24±3	31±2	30±2	38±2	36±2	18±7	24±6	37±6	37±3	30±4	39±3			37±3	30±4
.2±0.7	2.8±1.0	3.0±1.0	2.6±1	2.1±0.8	1.8±0.6	2.5±0.9	2.9±0.5	2.4±1.0	2.1±0.6	3.0±.5			2.4±1.0	2.1±0.6
19.6	21.2	22.3	18.8	19.9	22.7	23.3	25.8	25.0	25.3	23.7			25.0	12.6
21.7	24.5	23.3	21.1	27.5	24.1	22.7	33.0	29.3	36.0	25.4			29.0	20.6
0.278	0.292	0.309	0.323	0.350	0.344	0.357	0.416	0.342	0.372	0.342			0.161	0.367
0.091	0.101	0.102	0.103	0.119	0.131	0.140	0.154	0.135	0.149	0.135			0.107	0.150
0.209	0.122	0.142	0.092	0.139	0.329	0.171	0.112	0.110	0.168	0.088			0.063	0.243
1.12	2.68	2.78	3.11	2.60	1.43	2.58	4.69	3.58	2.95	3.36			3.29	2.11
Final	1515	Final	1415	1505	1505	1515	1405	1505	1505	1405			1415	1515
0.41	0.71	0.74	0.84	0.68	0.15	0.54	0.99	0.86	0.60	0.93			0.64	0.33
0.045	0.145	0.148	0.083	0.080	0.014	--	0.024	--	0.006	0.019			--	0.003
0.036	0.061	0.068	0.115	0.050	0.024	0.052	0.134	0.130	0.075	0.134			0.098	0.075
10	21	21	45	62	34	107	--	164	180	191			111	63
3.8	4.1	8.0	20.0	16.4	--	--	--	15.5	9.8	12.8			6.0	2.8
40	42	51	47	49	50	93	78	53	53	73			52	74
110	180	190	88	75	88	110	--	110	110	65			91	96
33	214	215	317	303	1	338	347	340	211	264			81	6
0	0	0	0	0	0	0	0	0	0	0			0	0
(2)	(2)	(2)	(2)	(2)	(2)	--	--	(2)	(2)	(2)	(3)	(4)	(2)	(2)
--	--	--	--	--	--	--	--	--	0.224	0.178	0.084	0.048	--	0.339
24±2	32±2	30±2	37±2	38±3	18±3	--	--	37±4	31±4	31±6	29±5	30±5	37±4	31±4
.5±0.8	3.2±0.6	3.3±0.7	2.7±0.8	2.3±0.6	1.5±0.6	--	--	3.2±0.6	2.3±0.5	2.6±0.9	2.5±1.0	3.1±0.8	3.2±0.6	2.3±0.5
18.7	19.2	17.8	--	--	22.5	--	--	22.6	7.2	4.35	2.49	1.73	24.0	6.6
0.205	0.509	0.533	0.581	0.437	<0	--	--	0.643	0.061	0.097	0.003	0.058	0.476	0.033
<0	<0	<0	<0	<0	0	--	--	<0	<0	<0	0.093	<0	<0	<0
0.063	0.062	0.062	0.038	0.048	0.145	--	--	0.039	0.024	0.008	0.120	0.024	0.032	0.033
0.090	0.074	0.083	0.052	0.052	0.132	--	--	0.050	0.061	0.020	0.161	0.032	0.048	0.038
Final	Init.	Init.	Init.	Init.	Final	--	--	Init.	Final	Final	Final	Final	Init.	Final
0.30	(0.51)	(0.53	(0.38)	(0.44)	0.30	--	--	(0.64)	0.186	0.200	0.136	0.262	(0.476)	0.199
0.065	0.061	0.071	0.021	0.024	--	--	--	--	0.001	0	0	0.002	--	0.001
0.070	0.100	0.109	0.097	0.100	0.062	--	--	0.167	0.042	0.148	--	--	0.121	0.067
7	5	5	9	7	7	--	--	7	25	12	2	7	7	23
1.7	2.0	2.2	3.6	4.1	--	--	--	1.8	1.8	1.1	<0	<0	1.0	1.4
3	1	1	<0	<0	0	--	--	<0	3	<0	<0	2	1	12
12	5.0	6.6	3.7	4.5	1.0	--	--	4.6	6.8	7.1	0.8	3.9	4.8	20
105	223	162	198	282	159	--	--	139	14	6	4	3	18	20
0	0	0	0	0	0	--	--	0	0	<0	0	0	0	0

(The reverse of this page is blank)

TABLE 22. INITIAL CONDITIONS AND SELECTED RESULTS FOR STATIC DARK (DIALK)-NO_x-AIR OUTDOOR CHAMBER RUNS.

AFF Run No.		22	23	19	10	9	18			10	9
Side		B	A	A	A	A	-			B	B
Run Type		Std.	Std.	Std.	Std.	Std.	Std.			Low NO_x	Low Fuel
vs		JP-4(p)	JP-4(p)	n-C_4	Low NO_x	Low Fuel	-			Std.	Std.
Day 1											
Avg. T	(°C)	34±8	36±6	38±6	34±1	38±3	42±4			34±1	38±3
UV Int.	(mw cm^{-2})	3.0±0.6	2.9±0.6	2.7±0.5	3.3±0.8	3.2±0.8	2.8±0.3			3.3±0.8	3.2±0.8
Init. Fuel (calc)	(ppmC)	28.5	28.7	30.0	22.9	19.5	25.2			22.9	9.76
Fuel (obs)	(ppmC)	33.0	32.4	33.1	26.5	33.7	24.9			26.5	21.0
NO	(ppm)	0.461	0.452	0.465	0.372	0.302	0.341			0.142	0.305
NO_2	(ppm)	0.152	0.153	0.168	0.125	0.100	0.133			0.075	0.103
Final NO_2 (uncorr)	(ppm)	0.150	0.100	0.117	0.288	0.280	0.078			0.080	0.262
$d([O_3]-[NO])/dt$	(ppb min^{-1})	2.65	2.79	3.00	2.10	1.22	2.31			1.54	1.40
Time O_3 max	(PST)	Final	1505	Final	Final	Final	1505			*Final*	*Final*
Maximum: O_3	(ppm)	0.62	0.58	0.90	0.360	0.342	0.78			0.337	0.297
PAN	(ppm)	0.022	0.013	0.005	0.015	0.007	0.018			0.021	0.008
HCHO	(ppm)	0.079	0.096	0.048	0.031	0.033	0.096			0.036	0.061
Aerosol Vol.	(μm^3 cm^{-3})	11	69	—	9	4	--			18	20
B_{scat}	(10^{-4} m^{-1})	7	26	--	6	2	24			10	2
Condens. Nuc.	(10^3 counts)	0	17	11	--	--	--			--	--
Aerosol No.	(10^3 cm^{-3})	1.6	35	--	6.1	1.7	--			8.4	18
No. Particles >0.3 μ	(cm^{-3})	372	430	450	255	190	441			342	5
No. Particles >1 μ	(cm^{-3})	37	40	70	0	0	35			4	0
Days 2-4:	Day	--	--	--	(2)	(2)	(2)	(3)	(4)	(2)	(2)
Dilution	(final/initial)	--	--	--	--	--	0.58	0.296	0.160	--	--
Avg. T	(°C)	--	--	--	30±5	32±5	34±5	35±5	38±7	30±5	32±5
UV Int.	(mw cm^{-2})	--	--	--	3.4±1.0	2.5±0.4	2.7±9	2.0±0.7	2.7±0.5	3.4±1.0	2.5±0.4
Init. Fuel	(ppmC)	--	--	—	22.9	21.9	13.5	7.0	3.2	22.9	18.2
O_3	(ppm)	--	--	--	0.059	0.102	0.26	0.008	0.126	0.056	0.015
NO	(ppm)	--	--	--	~0	~0	~0	0.167	~0	~0	~0
NO_2 (uncorr)	(ppm)	--	--	--	0.048	0.039	0.024	0.313	0.042	0.028	0.063
Final NO_2 (uncorr)	(ppm)	--	--	--	0.072	0.056	0.027	0.299	0.037	0.039	0.064
Time $[O_3]$ max	(PST)	--	--	--	Final	Final	1305	Final	Final	Final	Final
Maximum: O_3	(ppm)	--	--	--	0.280	0.191	0.280	0.387	0.375	0.273	0.250
PAN	(ppm)	--	--	--	0.010	0.011	0.002	0.009	0.009	0.006	0.015
HCHO	(ppm)	--	--	--	--	0.100	0.092	0.052	0.042	--	--
Aerosol Vol.	(μm^3 cm^{-3})	--	--	--	3	3	--	--	--	9	17
B_{scat}	(10^{-4} m^{-1})	--	--	--	1	1	1	~0	1	1	1
Condens. Nuc.	(10^3 counts)	--	--	--	--	--	--	--	--	--	--
Aerosol No.	(10^3 cm^{-3})	--	--	--	5.4	2.7	--	--	--	18	24
No. Particles >0.1 μ	(cm^{-3})	--	--	--	63	65	132	21	97	68	10
No. Particles >1 μ	(cm^{-3})	--	--	--	0	0	1	0	0	0	0

(The reverse of this page is blank)

TABLE 23. INITIAL CONDITIONS AND SELECTED RESULTS FOR STATIC JP-8 (PETROLEUM-DERIVED-NO_x-AIR OUTDOOR CHAMBER RUNS.

AFF Run No.		78	79	74	75	84	70	71	72			70	71
Side		A	B	A	B	A	A	B	-			B	A
Run Type		Std.	Std.	Std.	Std.	Std.	Std.	Std.	Std.			Low NO_x Std.	High Fuel Std.
vs		JP-4(p)	JP-4(p)	JP-8(s)	JP-8(s)	n-C_4	Low NO_x	High Fuel	-				
Day 1													
Avg. T	(°C)	23±2	24±3	32±4	26±2	25±5	24±2	26±2	28±3			24±2	26±2
UV Int.	(mw cm^{-2})	1.7±0.6	2.2±0.7	2.8±1.0	2.2±0.8	2.2±0.9	2.4±0.8	2.3±0.9	2.5±1.0			2.4±0.8	2.3±0.9
Init. Fuel (calc)	(ppmC)	23.8	21.9	24.5	24.5	24.0	34.7	31.8	36.8			34.7	63.6
Fuel (obs)	(ppmC)	17.5	19.3	17.4	19.2	19.3	27.7	30.2	32.7			28.4	53.0
NO	(ppm)	0.292	0.279	0.269	0.293	0.369	0.329	0.250	0.297			0.156	0.249
NO_2	(ppm)	0.106	0.091	0.102	0.101	0.125	0.143	0.111	0.130			0.080	0.107
Final NO_2 (uncorr)	(ppm)	0.306	0.222	0.093	0.130	0.040	0.325	0.142	0.120			0.108	0.078
$d([O_3]-[NO])/dt$	(ppb min^{-1})	0.88	0.78	2.00	2.04	0.80	1.26	1.27	1.50			0.97	1.64
Time O_3 max	(PST)	1505	Final	1505	Final	Final	Final	Final	Final			1515	1505
Maximum: O_3	(ppm)	0.066	0.236	0.597	0.428	0.217	0.122	0.338	0.468			0.187	0.405
PAN	(ppm)	0.019	0.035	0.045	0.055	0.029	0.032	0.045	0.028			0.041	0.068
HCHO	(ppm)	0.021	0.025	0.061	0.039	0.031	0.027	0.038	0.054			0.039	0.066
Aerosol Vol.	(μm^3 cm^{-3})	10	11	28	31	15	104	119	125			127	219
B_{scat}	(10^{-4} m^{-1})	4.3	5.5	--	--	11.0	--	--	--			--	--
Condens. Nuc.	(10^3 counts)	33	28	31	74	19	54	27	45			49	59
Aerosol No.	(10^3 cm^{-3})	120	100	100	340	52	73	41	78			99	120
No. Particles >0.3 μ	(cm^{-3})	118	356	458	425	365	278	421	455			307	457
No. Particles >1 μ	(cm^{-3})	0	2	68	18	2	0	22	93			0.	84
Days 2-4:	Day	(2)	(2)	(2)	(2)	--	(2)	(2)	(2)	(3)	(4)	(2)	(2)
Dilution	(final/initial)	--	--	--	--	--	--	--	--	0.83	0.83	--	--
Avg. T	(°C)	24±1	24±2	31±2	28±2	--	23±3	22±2	25±7	23±4	22±5	23±3	22±2
UV Int.	(mw cm^{-2})	2.7±0.9	2.5±0.8	2.8±0.6	3.0±0.7	--	2.8±0.7	2.0±0.5	2.3±1.0	2.2±0.9	1.8±0.8	2.8±0.7	2.0±0.5
Init. Fuel	(ppmC)	15.8	16.5	12.9	15.1	--	23.3	25.9	--	23.9	17.9	25.3	43.1
O_3	(ppm)	~0	0.058	0.429	0.276	--	0.007	0.193	0.325	0.246	0.546	0.127	0.269
NO	(ppm)	~0	~0	~0	~0	--	~0	~0	~0	0.061	~0	~0	~0
NO_2 (uncorr)	(ppm)	0.161	0.039	0.041	0.051	--	0.127	0.042	0.052	0.377	0.069	0.030	0.042
Final NO_2 (uncorr)	(ppm)	0.082	0.071	0.056	0.052	--	0.069	0.059	0.052	0.110	0.085	0.036	0.059
$d([O_3]-[NO])/dt$	(ppb min^{-1})	--	--	--	--	--	--	--	--	2.61	--	--	--
Time $[O_3]$ max	(PST)	Final	1415	Init.	Final	--	1405	Final	1505	1505	Init.	Final	Init.
Maximum: O_3	(ppm)	0.380	0.204	(0.429)	0.330	--	0.326	0.203	0.349	0.747	(0.546)	0.172	(0.269)
PAN	(ppm)	0.085	0.058	0.019	0.034	--	0.092	0.042	0.026	0.034	0.022	0.041	0.042
HCHO	(ppm)	0.058	0.060	0.094	0.077	--	0.043	0.068	0.065	0.121	0.145	0.051	0.101
Aerosol Vol.	(μm^3 cm^{-3})	8	20	11	--	--	72	13	18	12	8	30	19
B_{scat}	(10^{-4} m^{-1})	12.0	4.0	--	1.2	--	--	--	--	--	--	--	--
Condens. Nuc.	(10^3 counts)	2	10	6	1	--	7	~0	~0	~0	~0	13	1
Aerosol No.	(10^3 cm^{-3})	15	49	27	--	--	15	1.4	17	1.6	1.1	26	3.1
No. Particles >0.3 μ	(cm^{-3})	413	320	345	340	--	380	326	361	374	281	134	298
No. Particles >1 μ	(cm^{-3})	17	1	4	13	--	9	8	25	87	12	0	5

TABLE 24. INITIAL CONDITIONS AND SELECTED RESULTS FOR STATIC JP-8 (SHALE-DERIVED)-NO_x-AIR OUTDOOR CHAMBER RUNS.

AFF Run No.		76	77	74	75	86	80	81	73			80	81
Side		A	B	B	A	A	A	B	-			B	A
Run Type		Std.	Std.	Std.	Std.	Std.	Std.	Std.	Std.			Low NO_x Std.	High Fuel Std.
vs		JP-4(p)	JP-4(p)	JP-8(p)	JP-8(p)	n-C_4	Low NO_x	High Fuel	-				
Day 1													
Avg. T	(^oC)	31±2	30±2	32±4	26±2	40±6	28±3	28±2	29±2			28±3	28±2
UV Int.	(mw cm^{-2})	2.8±1.0	3.0±1.0	2.8±1.0	2.2±0.8	3.3±1.1	3.2±1.1	2.4±0.8	2.7±0.9			3.2±1.1	2.4±0.8
Init. Fuel (calc)	(ppmC)	24.2	25.4	24.0	24.0	24.1	23.7	23.2	32.0			23.7	46.3
Fuel (obs)	(ppmC)	22.7	24.8	23.9	21.8	26.3	22.0	23.1	29.4			22.7	44.2
NO	(ppm)	0.292	0.309	0.263	0.297	0.362	0.360	0.362	0.330			0.178	0.362
NO_2	(ppm)	0.103	0.102	0.102	0.101	0.148	0.140	0.128	0.149			0.069	0.128
Final NO_2 (uncorr)	(ppm)	0.092	0.106	0.089	0.120	—	0.132	0.139	0.105			0.079	0.108
d([O_3]-[NO])/dt	(ppb min^{-1})	2.42	2.51	2.40	1.82	4.02	1.38	2.76	2.74			2.25	2.88
Time O_3 max	(PST)	1505	1415	1415	Final	>1305	Final	Final	1505			1415	1405
Maximum: O_3	(ppm)	0.615	0.653	0.650	0.498	>0.717	0.650	0.543	0.410			0.483	0.530
PAN	(ppm)	0.136	0.154	0.054	0.058	>0.104	0.130	0.108	0.053			0.104	0.098
HCHO	(ppm)	0.062	0.072	0.076	0.045	0.065	0.067	0.054	0.077			0.060	0.073
Aerosol Vol.	(μm^3 cm^{-3})	28	28	31	21	28	21	25	153			19	37
B_{scat}	(10^{-4} m^{-1})	22.0	12.8	--	--	25.0	24.0	10.0	--			7.0	36.0
Condens. Nuc.	(10^3 counts)	32	31	53	40	14	17	44	30			16	22
Aerosol No.	(10^3 cm^{-3})	120	110	160	130	81	77	210	40			74	77
No. Particles >0.3 μ	(cm^{-3})	429	428	425	408	>449	445	428	452			393	462
No. Particles >1 μ	(cm^{-3})	18	17	8	9	>54	58	24	62			4	108
Days 2-4:	Day	(2)	(2)	(2)	(2)	--	(2)	(2)	(2)	(3)	(4)	(2)	(2)
Dilution	(final/initial)	--	--	--	--	--	—	--	—	0.76	0.76	--	—
Avg. T	(^oC)	32±2	30±2	31±2	28±2	--	30±3	31±2	32±4	28±6	21±5	30±3	31±2
UV Int.	(mw cm^{-2})	3.0±0.6	3.3±0.7	2.8±0.6	3.0±0.7	—	3.0±0.6	3.1±0.5	2.6±0.9	2.4±1	1.7±1	3.0±0.6	3.1±0.5
Init. Fuel	(ppmC)	16.3	18.6	18.0	17.1	—	16.2	17.6	23.4	17.1	12.7	18.3	37.1
O_3	(ppm)	0.426	0.448	0.459	0.346	--	0.435	0.345	0.360	0.072	0.577	0.334	0.322
NO	(ppm)	<0	<0	<0	<0	--	<0	<0	<0	0.040	<0	<0	<0
NO_2 (uncorr)	(ppm)	0.047	0.048	0.039	0.050	--	0.063	0.057	0.068	0.411	0.070	0.042	0.046
Final NO_2 (uncorr)	(ppm)	0.067	0.070	0.054	0.070	--	0.087	0.089	0.051	0.130	0.091	0.064	0.071
d([O_3]-[NO])/dt	(ppb min^{-1})	--	--	--	--	--	—	--	—	2.00	--	--	—
Time [O_3] max	(PST)	Init.	Init.	Init.	Final	--	Final	1415	1405	1405	Init.	Init.	Final
Maximum: O_3	(ppm)	(0.426)	(0.448)	(0.459)	0.368	—	0.445	0.389	0.465	0.825	(0.577)	(0.334)	0.354
PAN	(ppm)	0.057	0.067	0.017	0.042	—	0.076	0.063	0.039	0.050	0.028	0.051	0.046
HCHO	(ppm)	0.130	0.105	0.113	0.096	--	0.115	0.117	0.130	0.162	0.196	0.090	0.122
Aerosol Vol.	(μm^3 cm^{-3})	5	5	4	--	--	4	12	8	6	4	13	5
B_{scat}	(10^{-4} m^{-1})	4.0	2.1	—	2.8	—	4.6	2.5	--	--	—	2.0	4.0
Condens. Nuc.	(10^3 counts)	2	<0	<0	1	--	1	<0	<0	<0	<0	3	<0
Aerosol No.	(10^3 cm^{-3})	8.8	3.2	3.2	--	--	7.9	4.3	1	1.2	1.1	14	2.9
No. Particles >0.3 μ	(cm^{-3})	316	245	232	305	—	361	315	256	384	157	281	301
No. Particles >1 μ	(cm^{-3})	2	4	5	3	—	6	7	12	65	3	1	12

TABLE 25. INITIAL CONDITIONS AND SELECTED RESULTS FOR STATIC JP-8 (SHALE-DERIVED)-NO_x-AIR OUTDOOR CHAMBER RUNS.

AFF Run No.		62	63	44	40	42	43			40	42
Side		B	A	A	A	A	-			B	B
Run Type		Std.	Std.	Std.	Std.	Std.	Std.			Low NO_x	Low Fuel
vs		JP-4(p)	JP-4(p)	n-C_4	Low NO_x	Low Fuel	-			Std.	Std.
Day 1											
Avg. T	(°C)	18±7	24±6	21±3	37±3	38±4	34±6			37±3	38±4
UV Int.	(mw cm^{-2})	1.8±0.6	2.5±0.9	1.6±0.7	2.3±0.6	2.0±0.6	1.7±0.6			2.3±0.6	2.0±0.6
Init. Fuel (calc)	(ppmC)	25.7	26.4	26.8	27.6	26.8	24.0			27.6	13.4
Fuel (obs)	(ppmC)	29.3	27.6	36.9	35.2	36.7	32.6			35.4	19.8
NO	(ppm)	0.333	0.338	0.367	0.321	0.332	0.293			0.119	0.329
NO_2	(ppm)	0.132	0.140	0.140	0.162	0.129	0.121			0.133	0.132
Final NO_2 (uncorr)	(ppm)	0.229	0.200	0.232	0.097	0.083	0.076			0.060	0.098
$d([O_3]-[NO])/dt$	(ppb min^{-1})	11.7	>11.3	15.7	13.5	20.8	16.7			6.2	12.9
Time O_3 max	(PST)	1115	1105	1105	1205	1305	1305			1215	1315
Maximum: O_3	(ppm)	0.475	0.542	0.528	0.658	0.650	0.600			0.433	0.758
PAN	(ppm)	0.195	--	0.177	0.041	0.079	0.041			0.019	0.086
HCHO	(ppm)	0.118	0.213	0.179	0.313	0.305	0.324			0.255	0.217
Aerosol Vol.	(μm^3 cm^{-3})	207	225	179	119	138	135			84	70
B_{scat}	(10^{-4} m^{-1})	--	--	6.7	--	4.7	4.1			--	2.8
Condens. Nuc.	(10^3 counts)	110	100	96	92	108	110			9.8	72
Aerosol No.	(10^3 cm^{-3})	140	190	180	280	250	240			220	160
No. Particles >0.3 μ	(cm^{-3})	150	125	72	62	34	27			3	15
No. Particles >1 μ	(cm^{-3})	0	0	0	0	0	0			0	0
Days 2-4:	Day	(2)	--	--	(2)	(2)	(2)	(3)	(4)	(2)	(2)
Dilution	(final/initial)	--	--	--	--	--	--	0.80	0.80	--	--
Avg. T	(°C)	18±5	--	--	34±2	36±5	34±5	32±5	28±5	34±2	36±5
UV Int.	(mw cm^{-2})	1.5±0.6	--	--	2.2±0.5	2.4±0.4	1.5±0.7	1.4±0.6	1.5±0.6	2.2±0.5	2.4±0.4
Init. Fuel	(ppmC)	24.7	--	--	26.7	26.9	24.6	16.4	14.0	27.6	13.6
O_3	(ppm)	0.333	--	--	0.436	0.419	0.390	0.071	0.451	0.255	0.506
NO	(ppm)	~0	--	--	~0	~0	~0	0.042	~0	~0	~0
NO_2 (uncorr)	(ppm)	0.199	--	--	0.052	0.047	0.058	0.381	0.103	0.038	0.048
Final NO_2 (uncorr)	(ppm)	0.192	--	--	0.051	0.050	0.043	0.170	0.096	0.053	0.049
$d([O_3]-[NO])/dt$	(ppb min^{-1})	--	--	--	--		--	4.34	--	--	--
Time $[O_3]$ max	(PST)	Init.	--	--	Init.	Init.	Init.	1405	Init.	Init.	Init.
Maximum: O_3	(ppm)	(0.333)	--	--	(0.436)	(0.419)	(0.390)	0.678	(0.451)	(0.253)	(0.506)
PAN	(ppm)	0.086	--	--	0.009	0.012	0.015	0.088	0.054	0.010	0.010
HCHO	(ppm)	0.156	--	--	0.370	0.369	0.355	0.341	0.304	0.266	0.258
Aerosol Vol.	(μm^3 cm^{-3})	8	--	--	3	6	14	24	10	2	6
B_{scat}	(10^{-4} m^{-1})	--	--	--	--	1.6	1.4	1.7	1.0	--	1.7
Condens. Nuc.	(10^3 counts)	~0	--	--	~0	2	~0	7	~1	~0	1
Aerosol No.	(10^3 cm^{-3})	1.8	--	--	1.4	1.6	14	13	6.1	1.3	0.9
No. Particles >0.3 μ	(cm^{-3})	139	--	--	67	48	89	15	27	2	22
No. Particles >1 μ	(cm^{-3})	0	--	--	0	0	0	0	0	0	0

TABLE 26. INITIAL CONDITIONS AND SELECTED RESULTS FOR STATIC DIESEL NO. 2-NO_x-AIR OUTDOOR CHAMBER RUNS.

AFF Run No.		127	129	131	124	125	64	122			124	125
Side		A	B	A	A	A	-	-			B	B
Run Type		Std.	Std.	Std.	Std.	Std.	Std.	Std.			Low NO_x	Low Fuel
vs		JP-4(p)	JP-4(p)	n-C_4	Low NO_x	Low Fuel	-	-			Std.	Std.
Day 1												
Avg. T	(°C)	38±2	36±2	36±3	37±2	34±3	24±3	44±2			37±2	34±3
UV Int.	(mw cm^{-2})	2.6±1.0	2.1±0.8	2.0±0.8	2.6±1.0	2.5±0.9	2.0±0.8	2.5±1.0			2.6±1.0	2.5±0.9
Init. Fuel (calc)	(ppmC)	29.5	31.2	31.7	34.8	32.8	43.3	38.6			34.8	16.4
Fuel (obs)	(ppmC)	~9	--	--	~10	~7	~8	~14			~10	~5
NO	(ppm)	0.329	0.349	0.341	0.377	0.359	0.308	0.348			0.132	0.362
NO_2	(ppm)	0.106	0.114	0.111	0.143	0.119	0.113	0.125			0.071	0.118
Final NO_2 (uncorr)	(ppm)	0.052	0.070	0.053	0.059	0.075	0.091	0.022			0.033	0.142
$d([O_3]-[NO])/dt$	(ppb min^{-1})	3.74	3.27	2.97	4.72	4.05	2.48	5.04			3.48	2.17
Time O_3 max	(PST)	1405	1415	1405	1405	1405	Final	1205			1315	Final
Maximum: O_3	(ppm)	0.494	0.415	0.428	0.470	0.493	0.345	0.451			0.344	0.413
PAN	(ppm)	0.053	0.060	0.048	0.061	0.064	0.000	0.036			0.041	0.061
HCHO	(ppm)	0.094	0.063	0.050	0.088	0.105	0.065	0.092			0.044	0.042
Aerosol Vol.	(μm^3 cm^{-3})	158	148	112	100	119	42	127			65	85
B_{scat}	(10^{-4} m^{-1})	>100	>100	77	>100	>100	--	>100			99	88
Condens. Nuc.	(10^3 counts)	15	18	6	8	10	2	30			8	21
Aerosol No.	(10^3 cm^{-3})	91	88	47	63	130	5.6	160			64	80
No. Particles >0.3 μ	(cm^{-3})	516	528	551	542	537	554	541			517	498
No. Particles >1 μ	(cm^{-3})	334	348	358	323	373	367	378			272	229
Days 2-4:	Day	(2)	(2)	--	(2)	(2)	(2)	(2)	(3)	(4)	(2)	(2)
Dilution	(final/initial)	--	--	--	--	--	--	--	0.84	0.84	--	--
Avg. T	(°C)	37±2	38±3	--	36±3	34±3	24±4	42±5	44±5	42±5	36±3	34±3
UV Int.	(mw cm^{-2})	2.7±0.8	2.3±0.6	--	2.9±0.7	2.6±0.6	1.6±0.8	2.3±0.9	2.4±0.9	24±0.7	2.9±0.7	2.6±0.6
Init. Fuel	(ppmC)	--	--	--	~9	--	~8	~10	~10	~9	~9	--
O_3	(ppm)	0.241	0.202	--	0.227	0.258	0.142	0.159	0.023	0.497	0.153	0.208
NO	(ppm)	~0	~0	--	~0	~0	~0	~0	0.151	~0	~0	~0
NO_2 (uncorr)	(ppm)	0.021	0.030	--	0.022	0.033	0.057	0.020	0.280	0.030	0.016	0.038
Final NO_2 (uncorr)	(ppm)	0.042	0.038	--	0.041	0.050	0.057	0.020	0.039	0.037	0.030	0.058
$d([O_3]-[NO])/dt$	(ppb min^{-1})			—								
Time $[O_3]$ max	(PST)	Init.	1315	--	Final	Init.	1405	Init.	1305	Init.	1315	1415
Maximum: O_3	(ppm)	(0.241)	0.215	--	0.229	(0.258)	0.206	(0.159)	0.815	(0.497)	0.167	0.282
PAN	(ppm)	0.020	0.025	—	0.027	0.034	0.000	0.007	0.043	0.009	0.018	0.040
HCHO	(ppm)	0.113	0.092	--	0.172	0.190	0.111	0.387	0.178	0.222	0.056	0.073
Aerosol Vol.	(μm^3 cm^{-3})	66	27	--	46	71	43	14	30	14	35	52
B_{scat}	(10^{-4} m^{-1})	40	26	--	48	46	--	17.0	50	12.2	33	37
Condens. Nuc.	(10^3 counts)	11	2	--	19	10	4	2	3	2	8	12
Aerosol No.	(10^3 cm^{-3})	37	17	--	77	53	8.2	11	24	7.7	30	48
No. Particles >0.3 μ	(cm^{-3})	438	468	--	452	451	494	175	516	439	436	444
No. Particles >1 μ	(cm^{-3})	79	110	--	80	89	64	186	212	49	55	67

TABLE 27. INITIAL CONDITIONS AND SELECTED RESULTS FOR STATIC JP-10-NO_x-AIR OUTDOOR CHAMBER RUNS.

AFF Run No.		90	94	113	114	53	103	52	54	101	92			52	54	101
Side		B	A	B	A	A	A	A	A	B	-			B	B	A
Run Type		Std.	Std.	Std.	Std.	Std.	Std.	Std.	Std.	Std.	Std.			Low NO_x	High Fuel	High Fuel
vs		RJ-4	RJ-4	RJ-5	RJ-5	n-C_4	n-C_4	Low NO_x	High Fuel	High Fuel	-			Std.	Std.	Std.
Day 1																
Avg. T	(°C)	34±5	39±2	37±3	36±3	19±5	39±3	19±3	16±2	38±2	44±2			19±3	16±2	38±2
UV Int.	(mw cm^{-2})	2.9±0.9	3.0±0.8	2.5±0.9	2.5±0.8	1.6±0.5	2.5±0.8	1.1±0.5	0.5±0.3	2.6±0.7	3.3±0.9			1.1±0.5	0.5±0.3	2.6±0.7
Init. Fuel (calc)	(ppmC)	22.1	22.6	21.6	20.9	24.1	23.0	30.6	26.2	22.6	21.0			30.6	52.4	45.1
Fuel (obs)	(ppmC)	40.2	36.8	30.8	30.8	23.5	22.7	32.5	25.1	24.8	31.2			33.2	45.2	45.9
NO	(ppm)	0.356	0.380	0.351	0.338	0.368	0.389	0.308	0.380	0.375	0.397			0.158	0.373	0.371
NO_2	(ppm)	0.115	0.120	0.111	0.109	0.142	0.125	0.160	0.150	0.115	0.136			0.097	0.145	0.119
Final NO	(ppm)	0.023	0.030	0.132	0.111	0.291	0.045	0.233	0.298	0.030	0.131			0.105	0.296	0.016
NO_2 (uncorr)	(ppm)	--	0.410	0.282	0.290	0.182	0.419	0.199	0.189	0.390	0.325			0.130	0.191	0.375
$d([O_3]-[NO])/dt$	(ppb min^{-1})	--	1.081	0.605	0.611	0.278	0.941	0.243	0.136	1.062	0.649			0.179	0.124	1.200
Final O_3	(ppm)	-0	0.070	-0	0.012	-0	0.038	-0	-0	0.061	0.012			-0	-0	0.156
PAN	(ppm)	0.011	0.003	0.001	0.002	0.000	0.001	0.000	0.000	0.002	-0			0.000	0.000	0.004
HCHO	(ppm)	0.002	0.027	0.013	0.013	0.008	0.036	0.067	0.008	0.008	0.008			0.047	0.013	0.017
Aerosol Vol.	(μm^3 cm^{-3})	5	-0	6	10	1	-6	7	8	16	5			12	9	10
B_{scat}	(10^{-4} m^{-1})	1.8	4.5	2.6	7.0	-0	1.2	1.7	0.8	17.0	-0			1.8	0.9	2.5
Condens. Nuc.	(10^3 counts)	1	-0	-0	1	-0	-0	-0	1	2	0			-0	1	-0
Aerosol No.	(10^3 cm^{-3})	7.1	5.7	1.6	5.4	12	1.0	0.9	6.1	8.7	1.5			1.3	6.9	1.8
No. Particles >0.3 μ	(cm^{-3})	240	390	172	357	18	54	142	12	465	70			135	20	102
No. Particles >1 μ	(cm^{-3})	0	34	4	3	0	13	0	0	17	7			0	0	18
Days 2-4:	Day	(2)	(2)	(2)	(2)	--	--	(2)	(2)	(2)	(2)	(3)	(4)	(2)	(2)	(2)
Dilution	(final/initial)	--	--	--	--	--	--	--	--	--	--	--	0.63	--	--	--
Avg. T	(°C)	32±4	37±5	34±3	39±2	--	--	25±4	15±1	39±3	44±4	41±5	40±4	25±4	15±1	39±3
UV Int.	(mw cm^{-2})	3.0±0.8	3.1±0.5	2.9±0.6	2.6±0.6	--	--	1.5±0.5	0.6±0.2	2.9±0.7	2.3±0.1	2.1±0.6	2.7±0.8	1.5±0.5	0.6±0.2	2.9±0.7
Init. Fuel	(ppmC)	39.9	34.0	29.9	29.0	--	--	32.8	25.2	23.5	29.4	25.2	15.3	32.6	45.0	44.6
O_3	(ppm)	-0	0.012	-0	-0	--	--	-0	-0	-0	0.023	0.206	0.015	0.000	-0	-0
NO	(ppm)	0.101	-0	0.112	0.090	--	--	0.219	0.210	-0	0.092	-0	0.133	0.101	0.216	-0
NO_2 (uncorr)	(ppm)	0.135	0.320	0.291	0.303	--	--	0.222	0.207	0.330	0.353	0.029	0.370	0.133	0.225	0.179
Final NO_2 (uncorr)	(ppm)	0.088	0.185	0.343	0.307	--	--	0.262	0.225	0.142	0.265	0.028	0.405	0.183	0.308	0.061
$d([O_3]-[NO])/dt$	(ppb min^{-1})	3.52	--	0.448	0.738	--	--	0.295	0.581	--	0.750	--	0.667	0.376	0.488	--
Time $[O_3]$ max	(PST)	--	Final	Final	Final	--	--	1205	1405	Final	Final	1505	Final	Final	1415	Final
Maximum: O_3	(ppm)	0.014	0.495	0.094	0.217	--	--	-0	-0	0.624	0.369	0.238	0.118	0.059	-0	0.553
PAN	(ppm)	0.014	0.013	0.002	0.002	--	--	0.000	--	0.022	0.005	0.008	0.002	0.001	--	0.015
HCHO	(ppm)	0.021	0.033	0.008	0.019	--	--	0.036	--	0.036	0.038	0.044	0.036	0.027	--	0.047
Aerosol Vol.	(μm^3 cm^{-3})	5	7	2	6	--	--	13	3	12	-0	-0	10	12	4	22
B_{scat}	(10^{-4} m^{-1})	1.6	2.5	-0	1.1	--	--	1.1	-0	12.5	0.8	1.8	2.5	2.1	-0	15.0
Condens. Nuc.	(10^3 counts)	-0	-0	0	0	--	--	-0	-0	-0	0	0	-0	-0	-0	1
Aerosol No.	(10^3 cm^{-3})	12	2.7	0.9	1.4	--	--	21	5.2	4.5	2.0	4.7	4.2	20	5.3	6.1
No. Particles >0.3 μ	(cm^{-3})	54	233	18	61	--	--	43	9	380	12	292	330	206	5	427
No. Particles >1 μ	(cm^{-3})	4	42	2	20	--	--	0	0	55	10	3	22	0	0	60

TABLE 28. INITIAL CONDITIONS AND SELECTED RESULTS FOR STATIC RJ-4-NO_x-AIR OUTDOOR CHAMBER RUNS.

AFP Run No.		90	94	98	97	100	93			97	100
Side		A	B	A	A	B	-			B	A
Run Type		Std.	Std.	Std.	Std.	Std.[a]	Std.			Low NO_x	High Fuel
vs		JP-10	JP-10	n-C_4	Low NO_x	High Fuel	-			Std.	Std.[a]
Day 1											
Avg. T	(°C)	34±5	39±2	35±6	37±2	38±2	40±2			37±2	38±2
UV Int.	(mw cm^{-2})	2.9±0.9	3.2±0.8	2.9±0.7	2.8±0.8	2.1±0.8	3.0±0.7			2.8±0.5	2.1±0.8
Init. Fuel (calc)	(ppmC)	21.6	22.1	22.5	22.9	22.2	20.5			22.9	44.4
Fuel (obs)	(ppmC)	31.1	35.6	34.3	33.9	36.2	30.3			34.7	63.3
NO	(ppm)	0.363	0.345	0.366	0.380	0.102	0.400			0.196	0.101
NO_2	(ppm)	0.118	0.150	0.121	0.121	0.372	0.110			0.065	0.372
Final NO	(ppm)	0.120	~0	~0	~0	~0	~0			~0	~0
NO_2(uncorr)	(ppm)	0.282	0.090	0.242	0.261	0.041	0.320			0.037	0.023
d([O_3]-[NO])/dt	(ppb min^{-1})	0.465	1.728	1.330	1.341	1.253	1.24			1.221	1.538
Time O_3 max	(PST)	Final	Final	Final	Final	1515	Final			Final	1405
Maximum: O_3	(ppm)	0.008	0.472	0.303	0.278	0.449	0.212			0.382	0.482
PAN	(ppm)	0.002	0.012	0.013	0.009	0.014	0.005			0.011	0.013
HCHO	(ppm)	0.004	0.042	0.040	0.029	0.027	0.025			0.019	0.042
Aerosol Vol.	(μm^3 cm^{-3})	16	35	33	26	48	28			30	52
B_{scat}	(10^{-4} m^{-1})	4.6	2.1	53.0	50.0	87.0	10.5			53.0	98.0
Condens. Nuc.	(10^3 counts)	13	15	24	12	20	16			11.3	13
Aersol No.	(10^3 cm^{-3})	51	67	76	47	81	84			49	75
No. Particles >0.3 μ	(cm^{-3})	308	495	465	465	483	452			465	494
No. Particles >1 μ	(cm^{-3})	0	149	84	81	161	62			86	192
Days 2-4:	Day	(2)	(2)	—	(2)	(2)	(2)	(3)	(4)	(2)	(2)
Dilution	(final/initial)	--	--	--	--	--	--	0.72	0.72	--	--
Avg. T	(°C)	32±4	37±5	—	37±2	32±4	40±4	40±5	39±4	37±2	32±4
UV Int.	(mw cm^{-2})	3.0±0.8	3.1±0.5	--	2.7±0.5	1.4±0.7	2.8±0.7	2.7±0.8	2.6±0.7	2.7±0.5	1.4±0.7
Init. Fuel	(ppmC)	30.1	27.1	--	25.9	27.8	23.6	15.4	8.9	28.8	54.8
O_3	(ppm)	~0	0.289	—	0.044	0.345	0.189	~0	0.475	0.278	0.326
NO	(ppm)	0.100	~0	--	~0	~0	~0	0.260	~0	~0	~0
NO_2 (uncorr)	(ppm)	0.294	0.015	—	0.018	0.019	0.010	0.220	0.020	0.011	0.015
Final NO_2 (uncorr)	(ppm)	0.265	0.040	—	0.028	0.030	0.010	0.095	0.030	0.027	0.029
d([O_3]-[NO])/dt	(ppb min^{-1})	0.457	--	--	--	--	--	1.81	--	--	--
Time [O_3] max	(PST)	Final	Initial	—	Final	Initial	1305	Final	Init.	Init.	Init.
Maximum: O_3	(ppm)	0.164	(0.289)	—	0.175	(0.345)	0.202	0.654	(0.475)	(0.278)	(0.326)
PAN	(ppm)	0.007	0.009	--	0.007	0.005	0.006	0.030	0.011	0.006	0.005
HCHO	(ppm)	0.029	0.038	—	0.059	0.031	0.050	0.073	0.077	0.031	0.059
Aerosol Vol.	(μm^3 cm^{-3})	4	13	—	13	7	10	18	11	6	7
B_{scat}	(10^{-4} m^{-1})	2.0	1.7	--	20.0	5.8	3.6	7.0	2.4	7.2	3.8
Condens. Nuc.	(10^3 counts)	~0	~0	--	6	~0	~0	1	~0	~0	~0
Aerosol No.	(10^3 cm^{-3})	10	4.6	--	28	3.7	3.5	19	4.7	5.3	3.6
No. Particles >0.3 μ	(cm^{-3})	220	362	—	400	337	334	451	324	338	273
No. Particles >1 μ	(cm^{-3})	92	14	--	14	6	23	149	16	8	2

[a]Error in NO_x injection resulted in initial NO and NO_2 being interchanged, relative to the standard amounts.

TABLE 29. INITIAL CONDITIONS AND SELECTED RESULTS FOR STATIC RJ-5-NO_x-AIR OUTDOOR CHAMBER RUNS.

AFF Run No.		113	114	116	110	111	108			110	111
Side		A	B	A	A	B	-			B	A
Run Type		Std.	Std.	Std.	Std.	Std.	Std.			Low NO_x	High Fuel
vs		JP-10	JP-10	n-C_4	Low NO_x	High Fuel	-			Std.	Std.
Day 1											
Avg. T	(°C)	37±3	36±3	34±3	37±2	39±3	36±4			37±2	39±3
UV Int.	(mw cm^{-2})	2.5±0.9	2.5±0.8	2.4±0.7	2.8±1.0	2.5±0.8	2.6±0.8			2.8±1.0	2.5±0.8
Init. Fuel (calc)	(ppmC)	22.2	21.4	22.3	22.8	22.8	34.5			22.8	46.0
Fuel (obs)	(ppmC)	~15	~15	~14	~10	~13	~20			~10	~20
NO	(ppm)	0.348	0.336	0.354	0.348	0.367	0.353			0.159	0.362
NO_2	(ppm)	0.110	0.107	0.109	0.152	0.111	0.121			0.055	0.108
Final NO	(ppm)	0.062	0.048	0.070	0.089	0.029	0.062			0.013	~0
NO_2(uncorr)	(ppm)	0.307	0.300	0.291	0.311	0.324	0.288			0.145	0.159
$d([O_3]-[NO])/dt$	(ppb min^{-1})	0.811	0.866	0.805	0.724	1.026	0.795			0.487	1.276
Time O_3 max	(PST)	Final	Final	Final	Final	Final	Final			Final	Final
Maximum: O_3	(ppm)	0.022	0.027	0.020	0.021	0.040	0.026			0.066	0.270
PAN	(ppm)	0.002	0.001	0.002	0.001	~0	0.004			~0	0.001
HCHO	(ppm)	0.017	0.004	0.017	0.006	0.025	0.048			0.006	0.038
Aerosol Vol.	(μm^3 cm^{-3})	41	35	28	42	62	30			34	100
B_{scat}	(10^{-4} m^{-1})	28	28	28	26	44	29			23.5	80
Condens. Nuc.	(10^3 counts)	17	17	13	11	22	21			12	13
Aersol No.	(10^3 cm^{-3})	43	38	45	50	53	60			39	78
No. Particles >0.3 μ	(cm^{-3})	429	429	435	415	455	419			395	516
No. Particles >1 μ	(cm^{-3})	28	28	36	18	68	22			8	219
Days 2-4:	Day	(2)	(2)	--	(2)	(2)	(2)	(3)	(4)	(2)	(2)
Dilution	(final/initial)	--	--	--	--	--	--	--	0.78	--	--
Avg. T	(°C)	34±3	39±2	--	38±4	39±2	33±5	32±7	32±7	38±4	39±2
UV Int.	(mw cm^{-2})	2.9±0.6	2.6±0.6	--	2.9±0.7	2.7±0.7	2.5±0.9	2.8±1.1	2.6±0.9	2.9±0.7	2.7±0.7
Init. Fuel	(ppmC)	~13	~13	--	--	~11	~20	~18	~12	--	~15
O_3	(ppm)	0.005	0.005	--	0.005	0.009	0.053	0.298	0.017	0.004	0.135
NO	(ppm)	0.023	0.015	--	0.049	0.009	0.038	~0	0.162	~0	0.008
NO_2 (uncorr)	(ppm)	0.330	0.327	--	0.342	0.280	0.272	0.011	0.278	0.079	0.012
Final NO_2 (uncorr)	(ppm)	0.131	0.031	--	0.172	0.020	0.019	0.011	0.325	0.016	0.015
$d([O_3]-[NO])/dt$	(ppb min^{-1})	--	--	--	0.514		0.408	--	0.483	--	
Time $[O_3]$ max	(PST)	Final	1415	--	Final	1415	1405	Initial	Final	Final	Initial
Maximum: O_3	(ppm)	0.357	0.431	--	0.317	0.409	0.407	(0.298)	0.086	0.205	(0.135)
PAN	(ppm)	0.004	0.002	--	0.002	0.002	0.005	0.003	0.003	~0	0.002
HCHO	(ppm)	0.015	0.008	--	0.015	0.013	0.067	0.050	0.006	0.008	0.017
Aerosol Vol.	(μm^3 cm^{-3})	23	60	--	18	47	43	14	28	26	96
B_{scat}	(10^{-4} m^{-1})	23	50	--	20	50	49	15	21	22	32
Condens. Nuc.	(10^3 counts)	4	5	--	3	10.5	6	5	3	4	50
Aerosol No.	(10^3 cm^{-3})	19	21	--	23	20	28	15	13	28	92
No. Particles >0.3 μ	(cm^{-3})	462	493	--	395	492	481	369	469	426	418
No. Particles >1 μ	(cm^{-3})	101	149	--	98	152	126	7	39	47	9

TABLE 30. INITIAL CONDITIONS AND SELECTED RESULTS FOR n-BUTANE-NO_x-AIR OUTDOOR CHAMBER RUNS.

AFF Run No.			20	19	84	86	44	131	53	103	98	116
Side			B	B	B	B	B	B	B	B	B	B
vs.			JP-4(p)	JP-4(s)	JP-8(p)	JP-8(s)	U.Gas	Diesel	JP-10	JP-10	RJ-4	RJ-5
Day 1												
Avg. T		(^oC)	37±6	39±6	25±5	40±5	22±3	34±6	19±5	37±6	35±6	32±6
UV Int.		(mW cm^{-2})	2.9±0.5	2.7±0.5	2.2±0.9	3.3±1.1	1.6±0.7	2.0±0.8	1.6±0.5	2.5±0.8	2.9±0.7	2.4±0.7
Init. $n-C_4$		(ppm)	8.93	8.65	5.19	5.83	7.17	5.66	7.31	6.51	5.54	6.36
	NO	(ppm)	0.414	0.465	0.372	0.370	0.373	0.348	0.376	0.390	0.369	0.354
	NO_2	(ppm)	0.155	0.162	0.127	0.153	0.133	0.113	0.141	0.131	0.128	0.109
Final NO		(ppm)	~0	~0	0.040	--	0.172	~0	0.202	~0	~0	~0
	NO_2	(ppm)	0.467	0.484	0.451	--	0.322	0.421	0.278	0.431	0.359	0.410
$d([O_3]-[NO])/dt$		(ppb min^{-1})	2.39	2.55	0.74	2.58	0.54	1.35	0.58	2.01	2.10	1.28
Maximum:	O_3	(ppm)	0.573	0.640	0.028	≥0.192	~0	0.121	~0	0.418	0.530	0.130
	PAN	(ppm)	0.014	0.033	0.021	≥0.047	0.006	0.029	0.000	0.035	0.094	0.028
	HCHO	(ppm)	0.044	0.063	0.008	0.059	0.018	0.002	0.015	0.029	0.038	0.015

TABLE 31. INITIAL CONDITIONS AND SELECTED RESULTS FOR DYNAMIC OUTDOOR FUEL RUNS.

Fuel		JP-4(PET)		JP-4(SHALE)			UNLEADED GASOLINE		JP-10	
AFF Run No.		33	57	26	31	56	45		55	
Day 1										
Avg. T	(°C)	35±5	15±4	30±8	38±4	31±6	22±3		23±5	
UV Int.	(mw cm^{-2})	2.3±0.9	0.8±0.3	3.0±0.8	2.9±0.8	0.9±0.5	1.5±0.7		1.1±0.5	
Init. Fuel (calc)	(ppmC)	21.3	24.2	20.	22.1	20.4	21.7		28.8	
Fuel (obs)	(ppmC)	26.2	31.8	21.3	24.3	37.1	30.1		36.0	
NO	(ppm)	0.319	0.375	0.288	0.317	0.330	0.272		0.337	
NO_2	(ppm)	0.119	0.158	0.105	0.123	0.100	0.113		0.122	
Max. $[O_3]$	(ppm)	0.530	0.036	0.411	0.408	0.024	0.410		0.006	
Time	(PST)	1405	1500	Final	1505	1500	1005		1005	
Max. $[O_3]$/Dilution	(ppm)	0.905	0.067	0.809	0.742	0.026	0.446		0.007	
Overall Dilution(fin./init.)		0.49	0.48	0.51	0.42	0.66	0.47		0.52	
Maximum:										
Aerosol Vol.	(μm^3 cm^{-3})	78	18	14	11	17	92		7	
B_{scat}	(10^{-4} m^{-1})	4.7	1.0	3.3	3.4	~0	2.3		~0	
Condens. Nuc.	(10^3 counts)	61	~0	1	~1	~0	72		~0	
Aerosol No.	(10^3 cm^{-3})	70	49	1.7	0.9	58	110		35	
No. Particles >0.3 μ	(cm^{-3})	46	0	247	268	1	~0		12	
No. Particles >1 μ	(cm^{-3})	0	0	~0	3	0	0		~0	
Days 2-3:	Day	(2)	(3)	--	--	(2)	(2)	(2)	(3)	(2)	(3)
Avg. T	(°C)	37±3	37±3	--	--	35±7	25±4	22±3	24±4	25±5	20±2
UV Int.	(mw cm^{-2})	2.1±0.7	2.2±0.5	--	--	3.2±0.9	0.8±0.3	1.7±0.7	1.6±0.5	1.0±0.5	0.7±0.2
Init. Fuel	(ppmC)	9.86	4.77	--	--	8.71	22.9	11.4	5.73	21.1	11.4
O_3	(ppm)	0.341	0.140	--	--	0.301	0.036	0.180	0.013	~0	0.016
NO	(ppm)	~0	~0	--	--	~0	0.063	~0	0.123	0.157	0.067
NO_2 (uncorr)	(ppm)	0.032	0.027	--	--	0.019	0.194	0.070	0.269	0.109	0.082
Max. $[O_3]$	(ppm)	(0.341)	0.176	--	--	(0.301)	0.195	0.181	0.226	0.033	0.023
Time	(PST)	Initial	1305	--	--	Initial	1300	1305	Final	1205	1205
Max. $[O_3]$/Dilution	(ppm)	0.702	1.13	--	--	0.711	0.448	0.547	1.77	0.088	0.141
Overall Dilution(fin./init.)		0.24	0.13	--	--	0.19	0.34	0.23	0.13	0.27	0.08
Maximum:											
Aerosol Vol.	(μm^3 cm^{-3})	6	8	--	--	4	24	4	2	5	15
B_{scat}	(10^{-4} m^{-1})	~1	~1	--	--	1.1	1.0	~0	~0	~0	0.4
Condens. Nuc.	(10^3 counts)	~0	4	--	--	~0	~0	2	1	~0	~0
Aerosol No.	(10^3 cm^{-3})	2.1	6.9	--	--	1.2	67	6.5	1.3	93	54
No. Particles >0.3 μ	(cm^{-3})	28	26	--	--	28	690	1	1	4	23
No. Particles >1 μ	(cm^{-3})	0	0	--	--	0	0	0	0	0	0

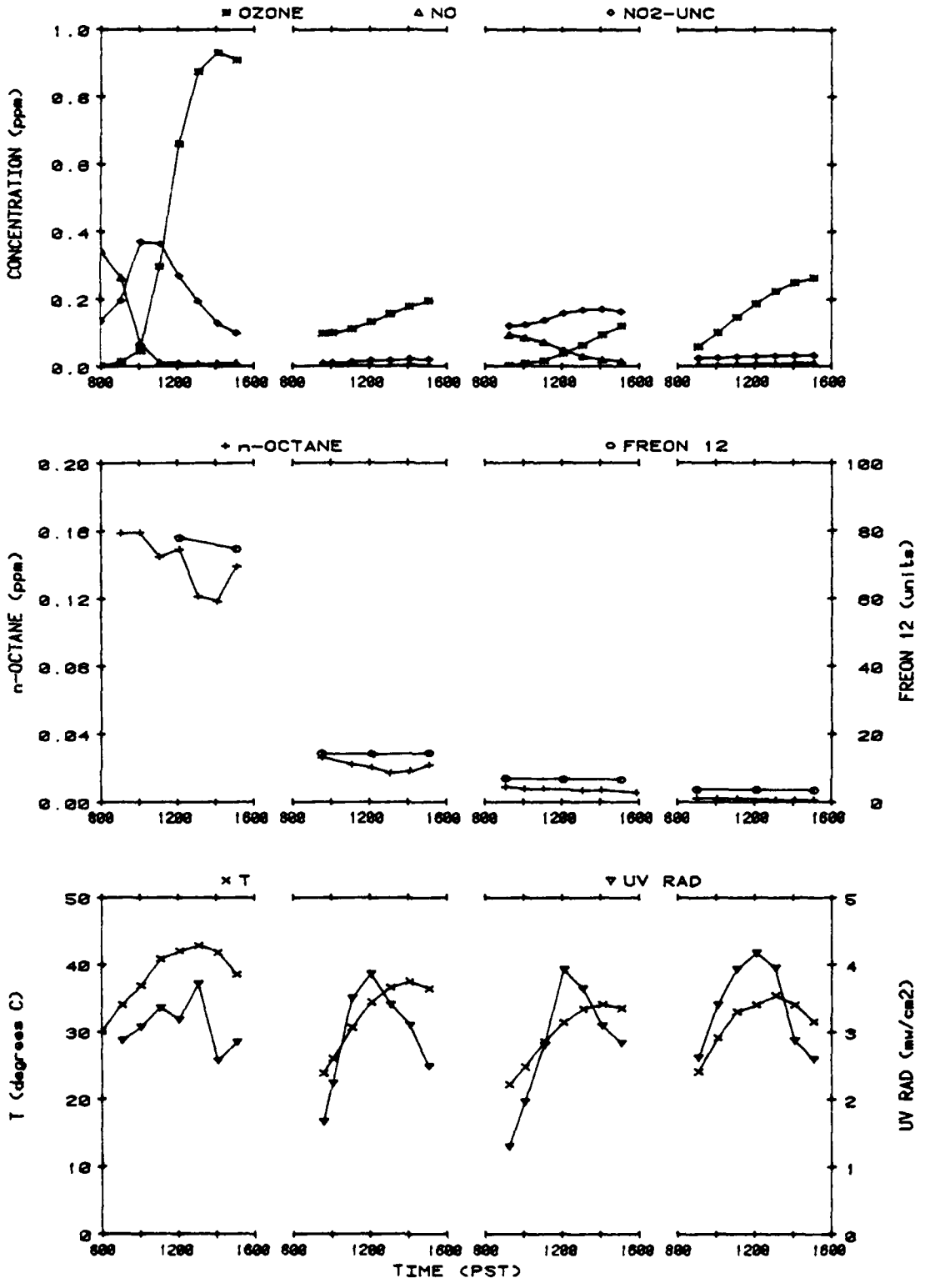

Figure 19. Concentration-Time Profiles for Selected Species, and Physical and Aerosol Measurements for the Four-Day, JP-4(Pet)-NO_x Outdoor Chamber Run AFF-25.

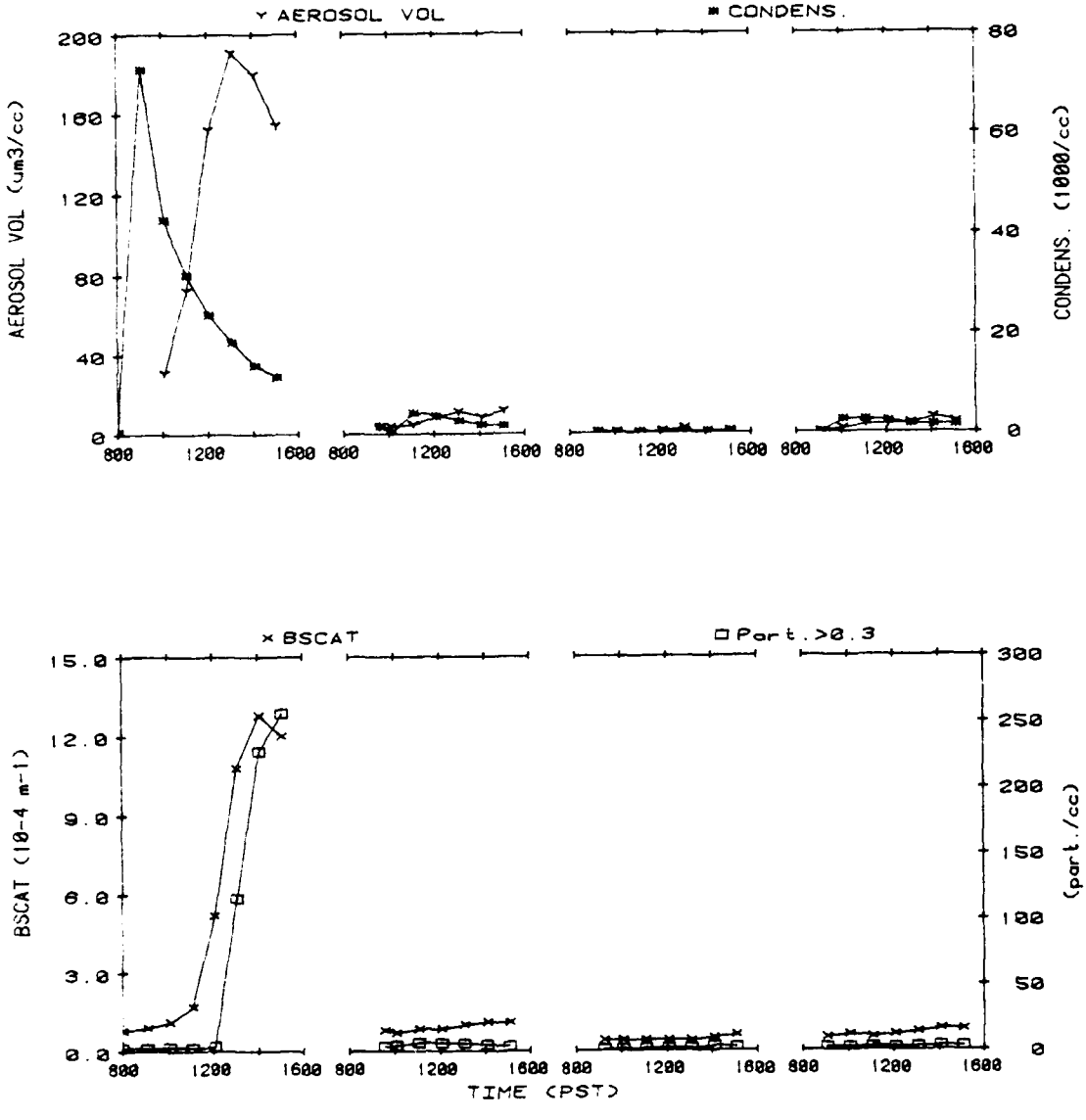

Figure 19. Concentration-Time Profiles for Selected Species, and Physical and Aerosol Measurements for the Four-Day, JP-4(Pet)-NO_x Outdoor Chamber Run AFF-25 (concluded).

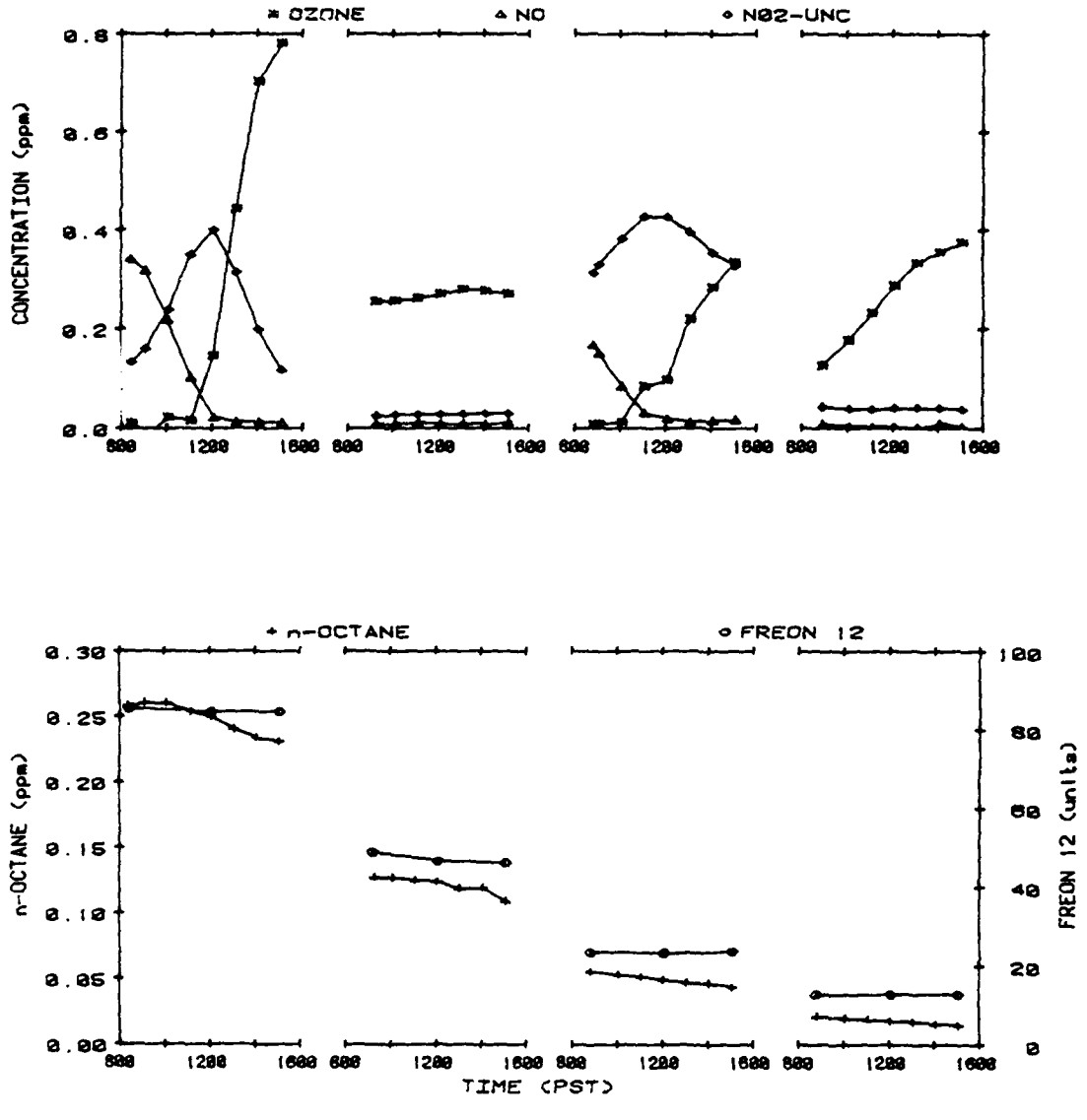

Figure 20. Concentration-Time Profiles for Selected Species, and Physical and Aerosol Measurements for the Four-Day, JP-4(Shale)-NO_x Outdoor Chamber Run AFF-18.

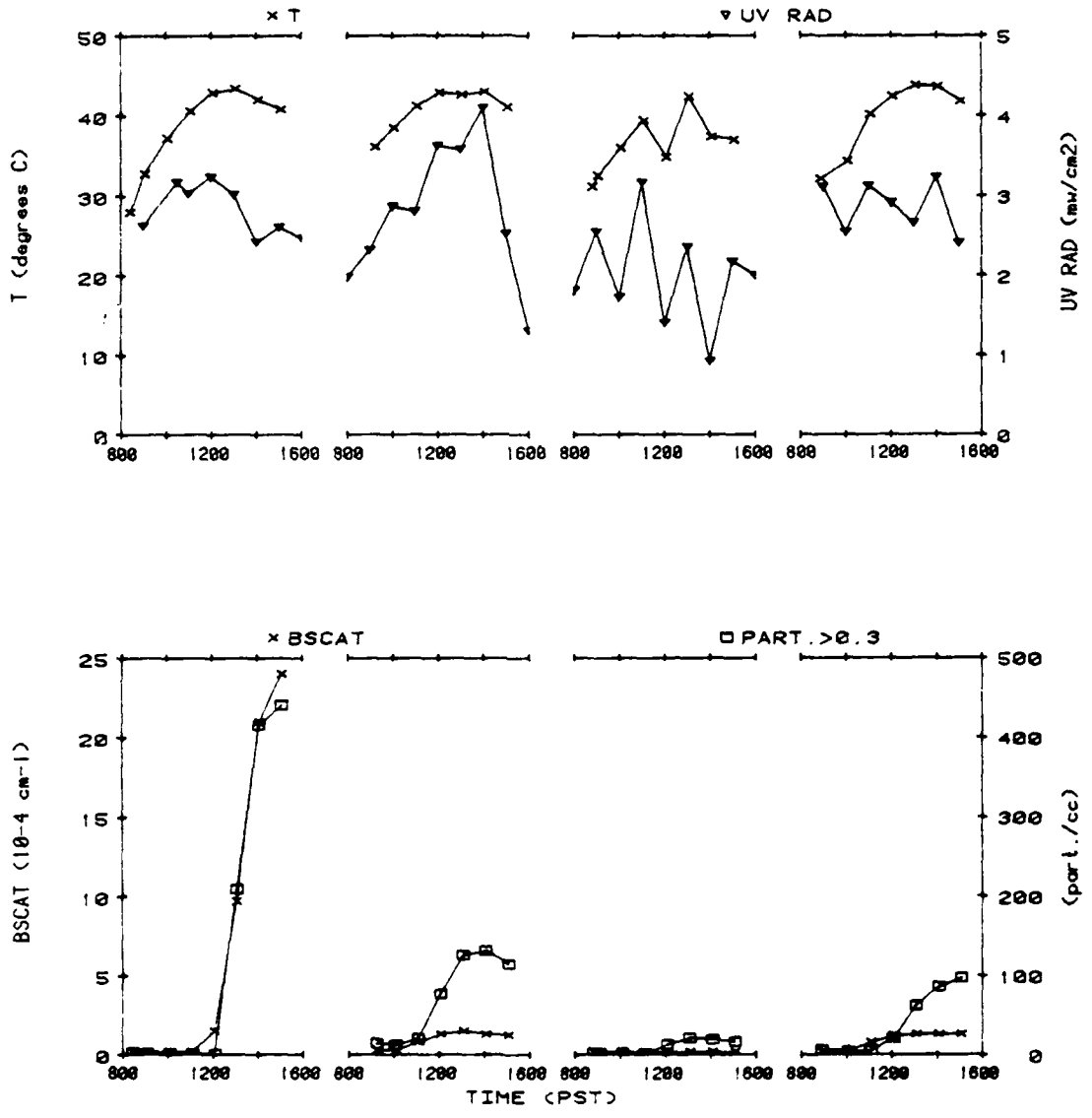

Figure 20. Concentration-Time Profiles for Selected Species, and Physical and Aerosol Measurements for the Four-Day, JP-4(Shale)-NO_x Outdoor Chamber Run AFF-18 (concluded).

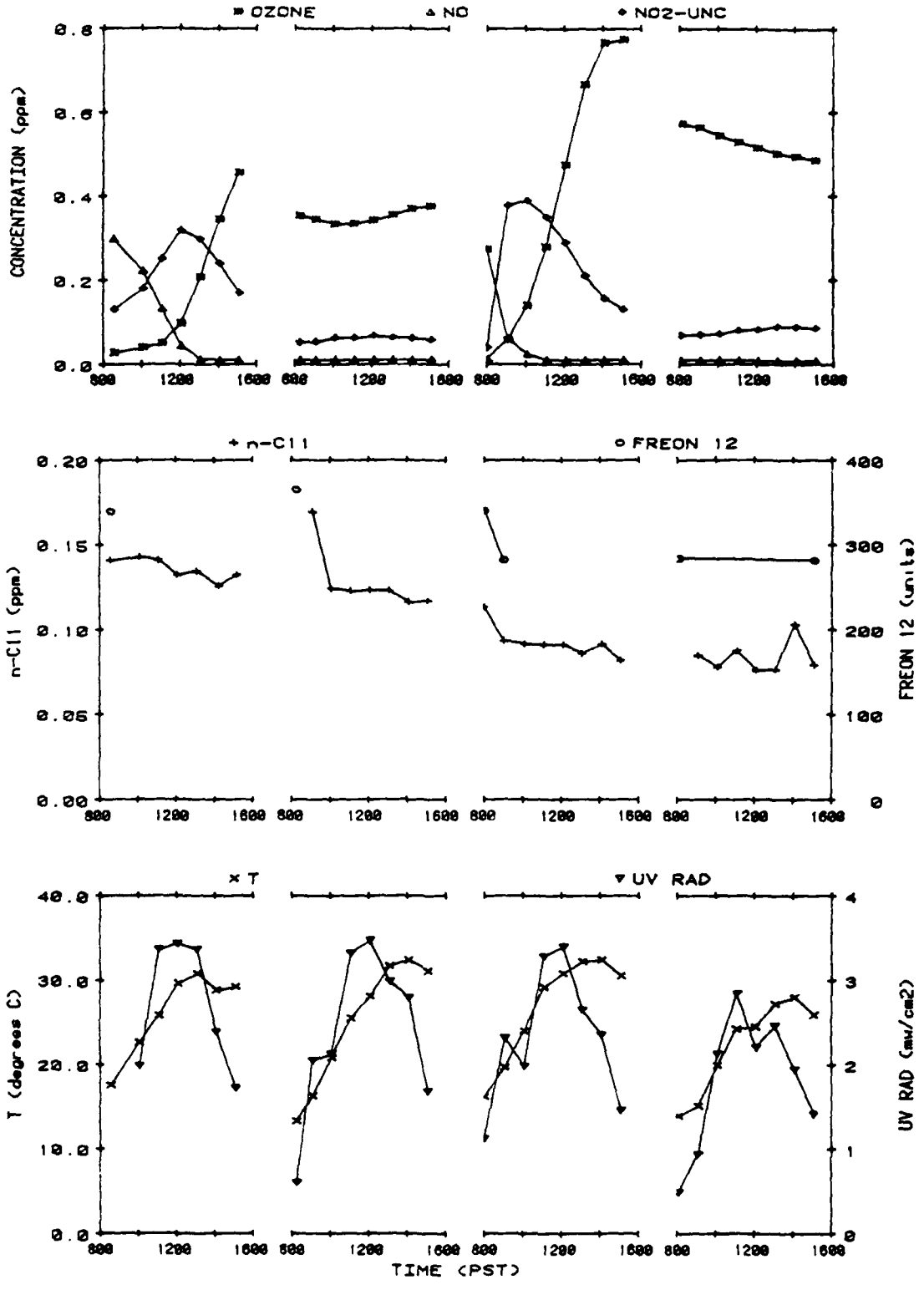

Figure 21. Concentration-Time Profiles for Selected Species, and Physical and Aerosol Measurements for the Four-Day, JP-8(Pet)-NO_x Outdoor Chamber Run AFF-72.

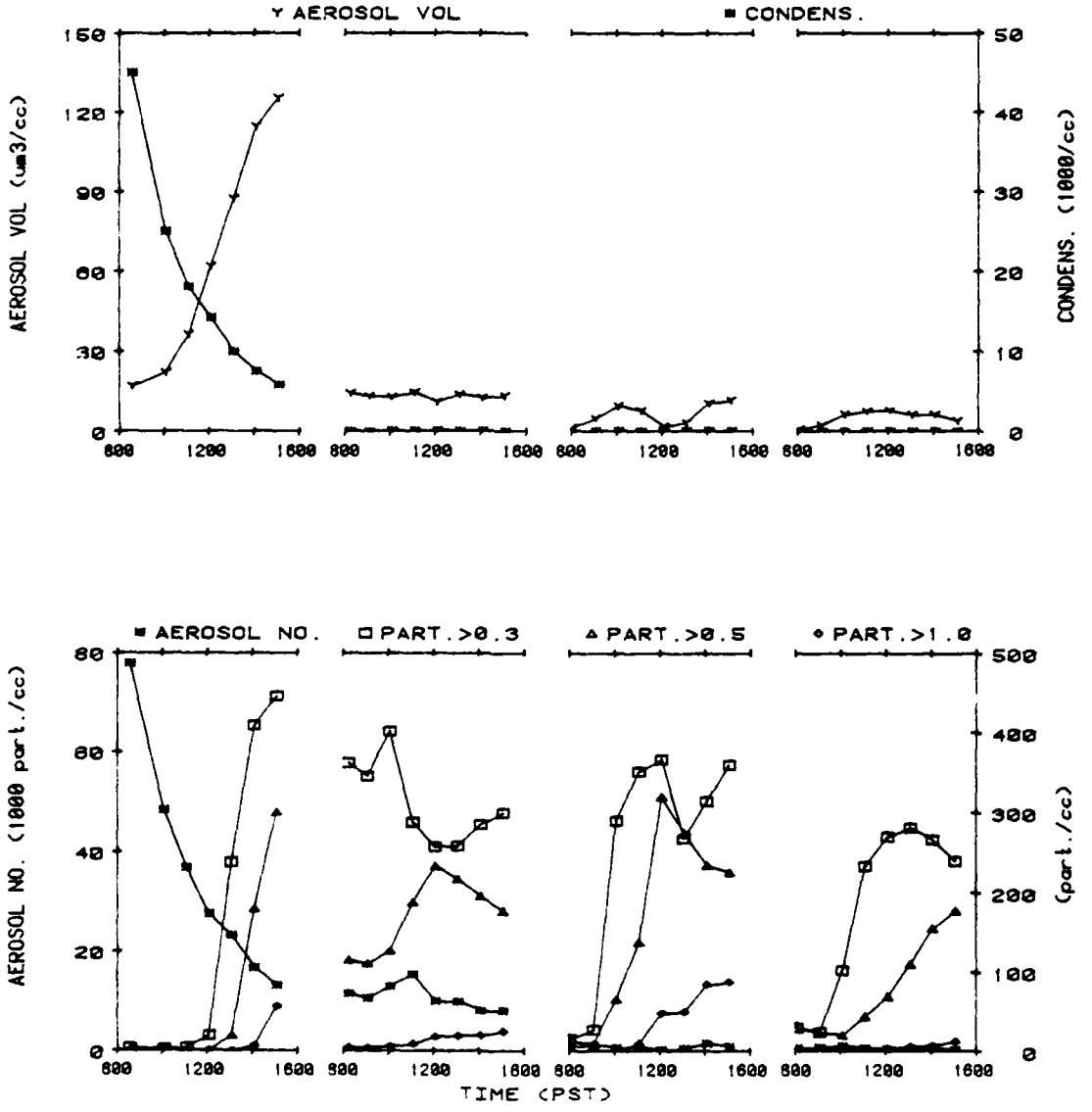

Figure 21. Concentration-Time Profiles for Selected Species, and Physical and Aerosol Measurements for the Four-Day, JP-8(Pet)-NO_x Outdoor Chamber Run AFF-72 (concluded).

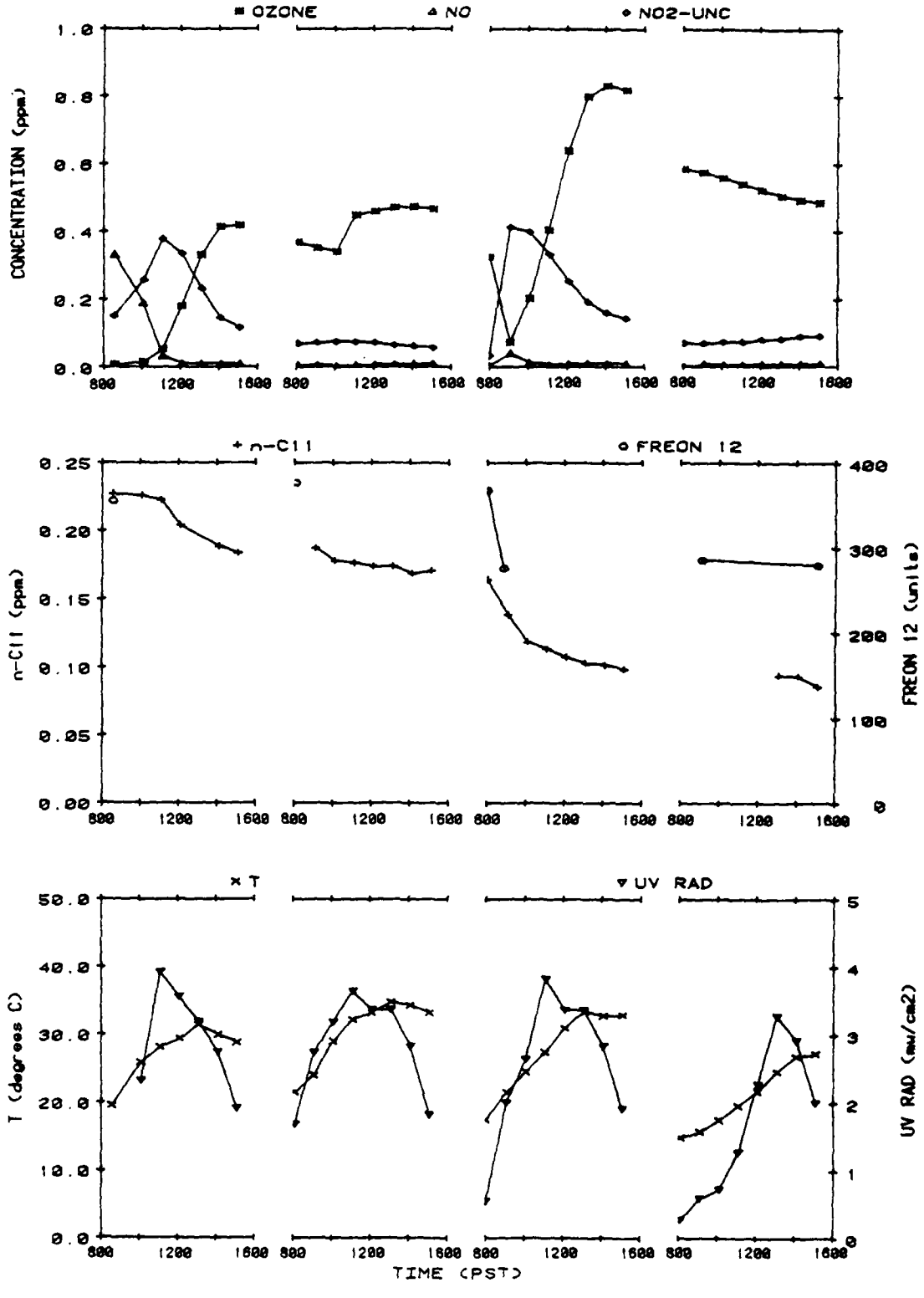

Figure 22. Concentration-Time Profiles for Selected Species, and Physical and Aerosol Measurements for the Four-Day, JP-8(Shale)-NO_x Outdoor Chamber Run AFF-73.

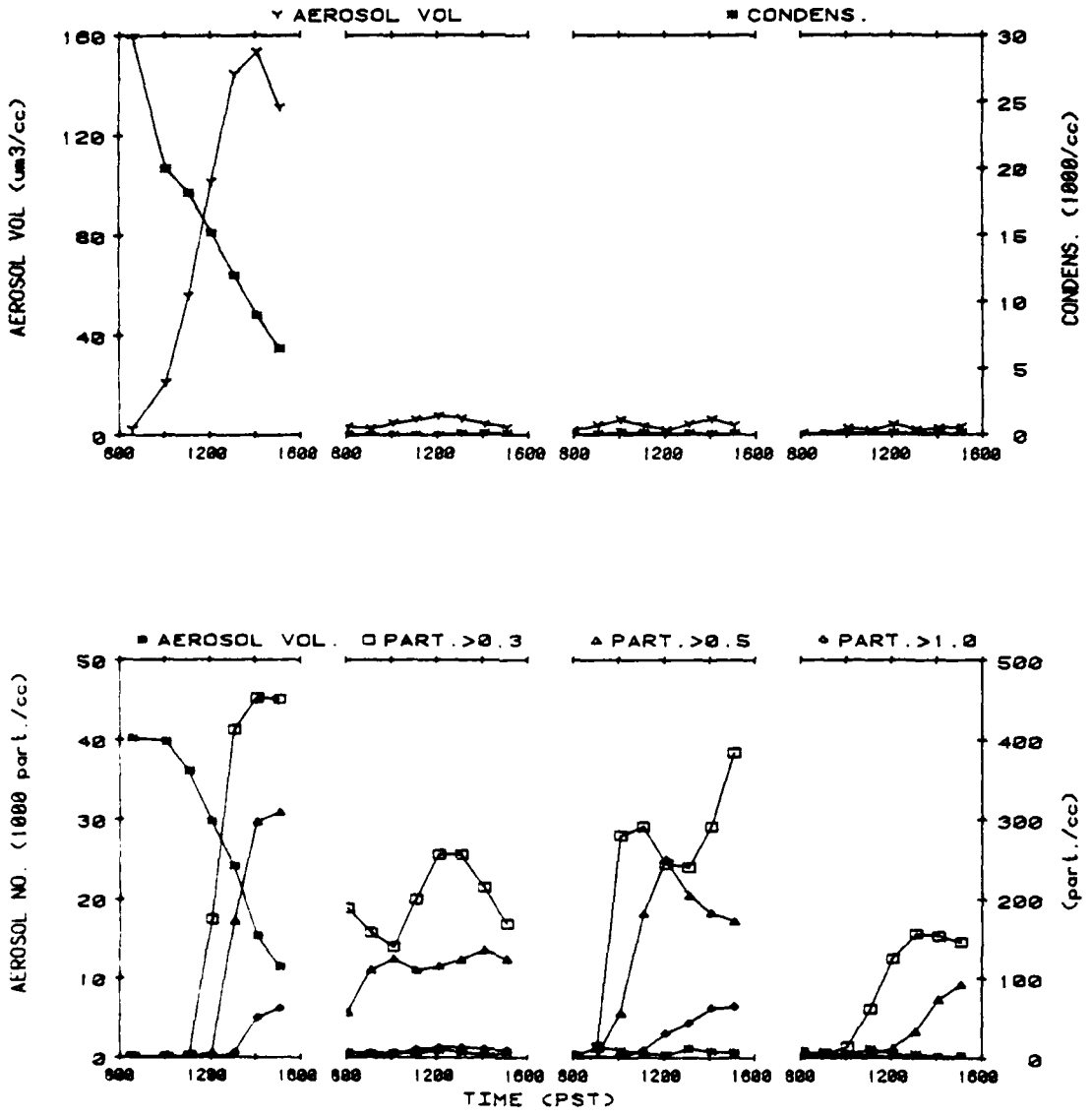

Figure 22. Concentration-Time Profiles for Selected Species, and Physical and Aerosol Measurements for the Four-Day, JP-8(Shale)-NO_x Outdoor Chamber Run AFF-73 (concluded).

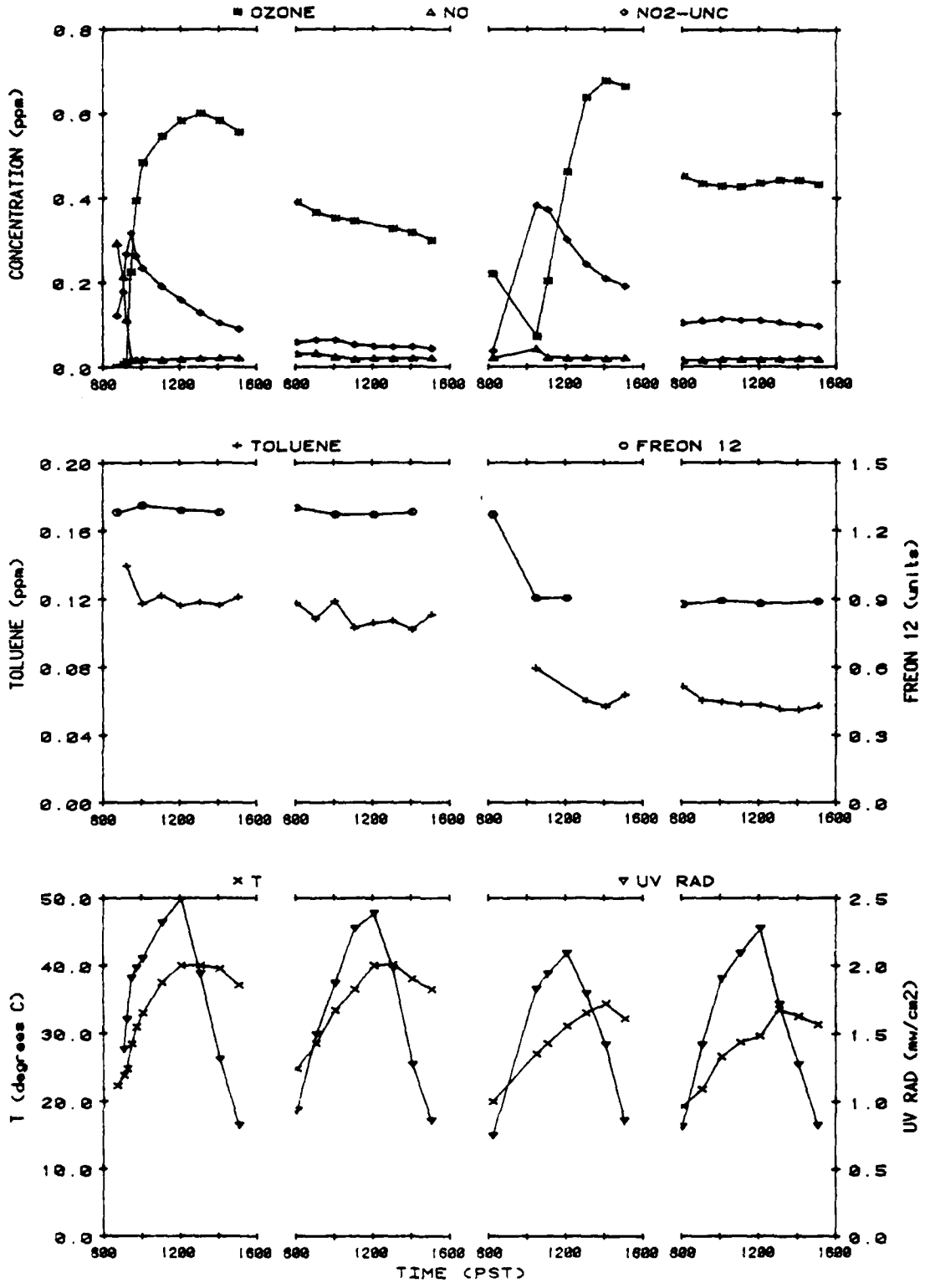

Figure 23. Concentration-Time Profiles for Selected Species, and Physical and Aerosol Measurements for the Four-Day, Unleaded Gasoline-NO_x Outdoor Chamber Run AFF-43.

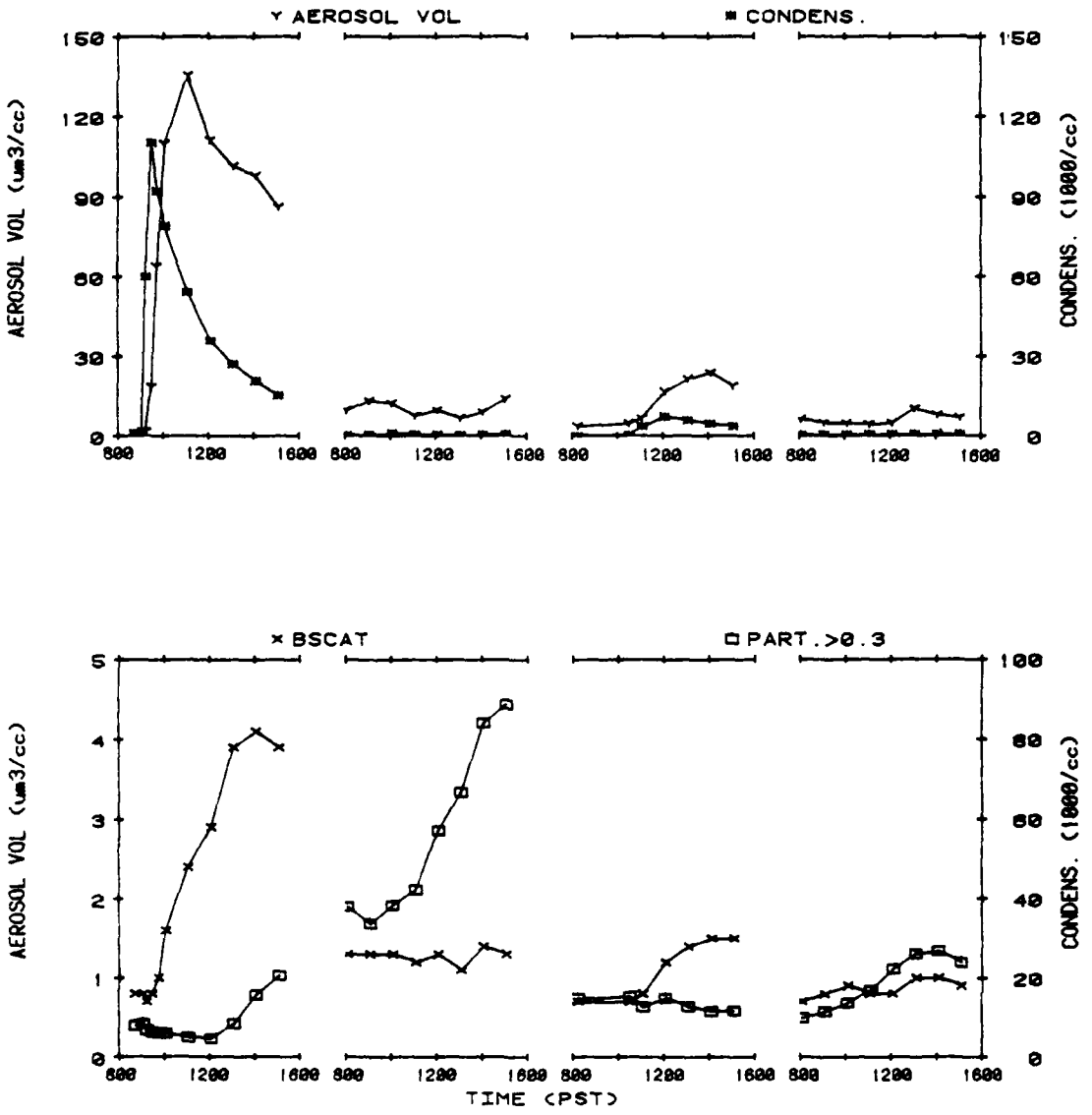

Figure 23. Concentration-Time Profiles for Selected Species, and Physical and Aerosol Measurements for the Four-Day, Unleaded Gasoline-NO_x Outdoor Chamber Run AFF-43 (concluded).

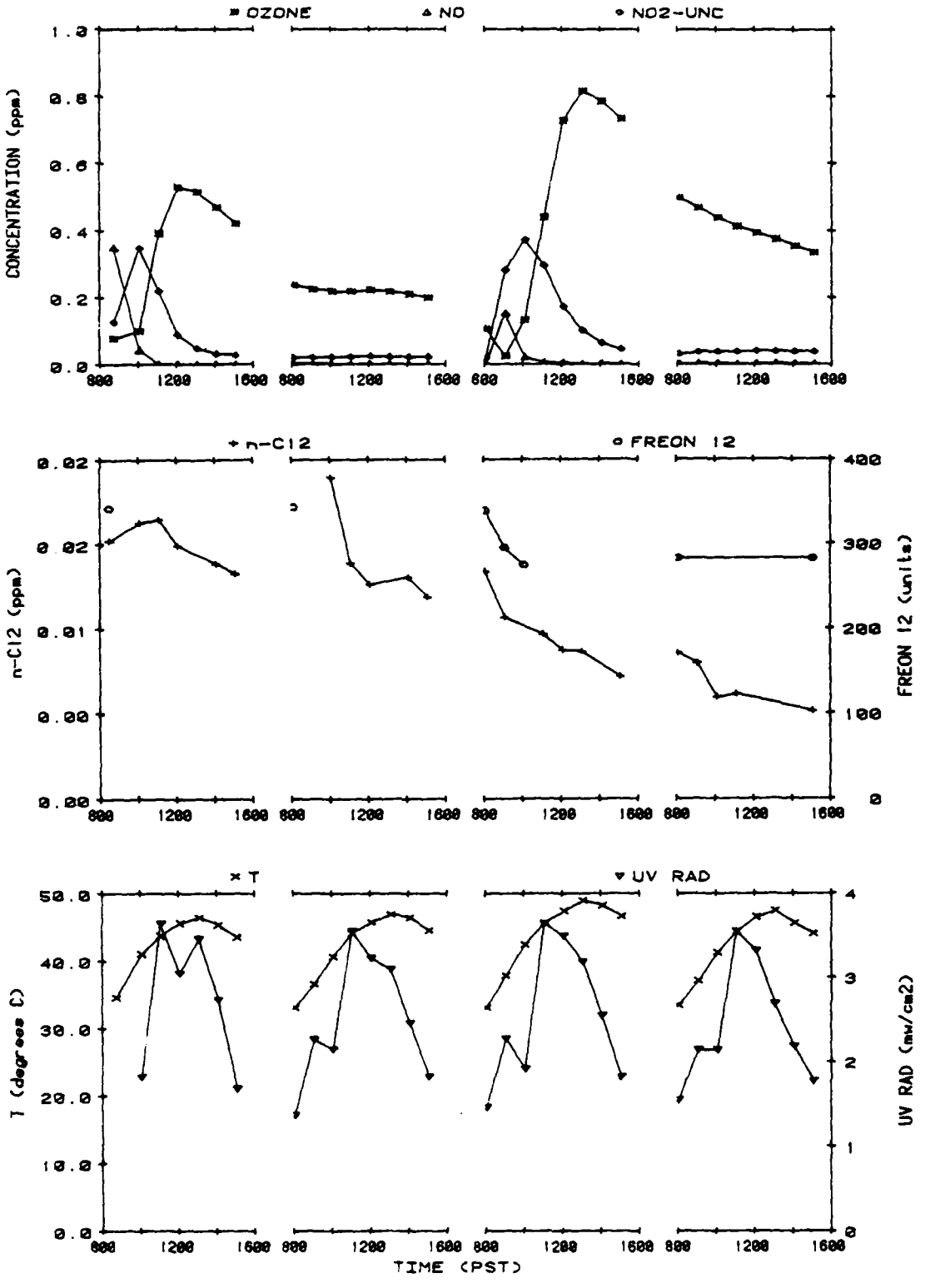

Figure 24. Concentration-Time Profiles for Selected Species, and Physical and Aerosol Measurements for the Four-Day, Diesel No. 2-NO_x Outdoor Chamber Run AFF-122.

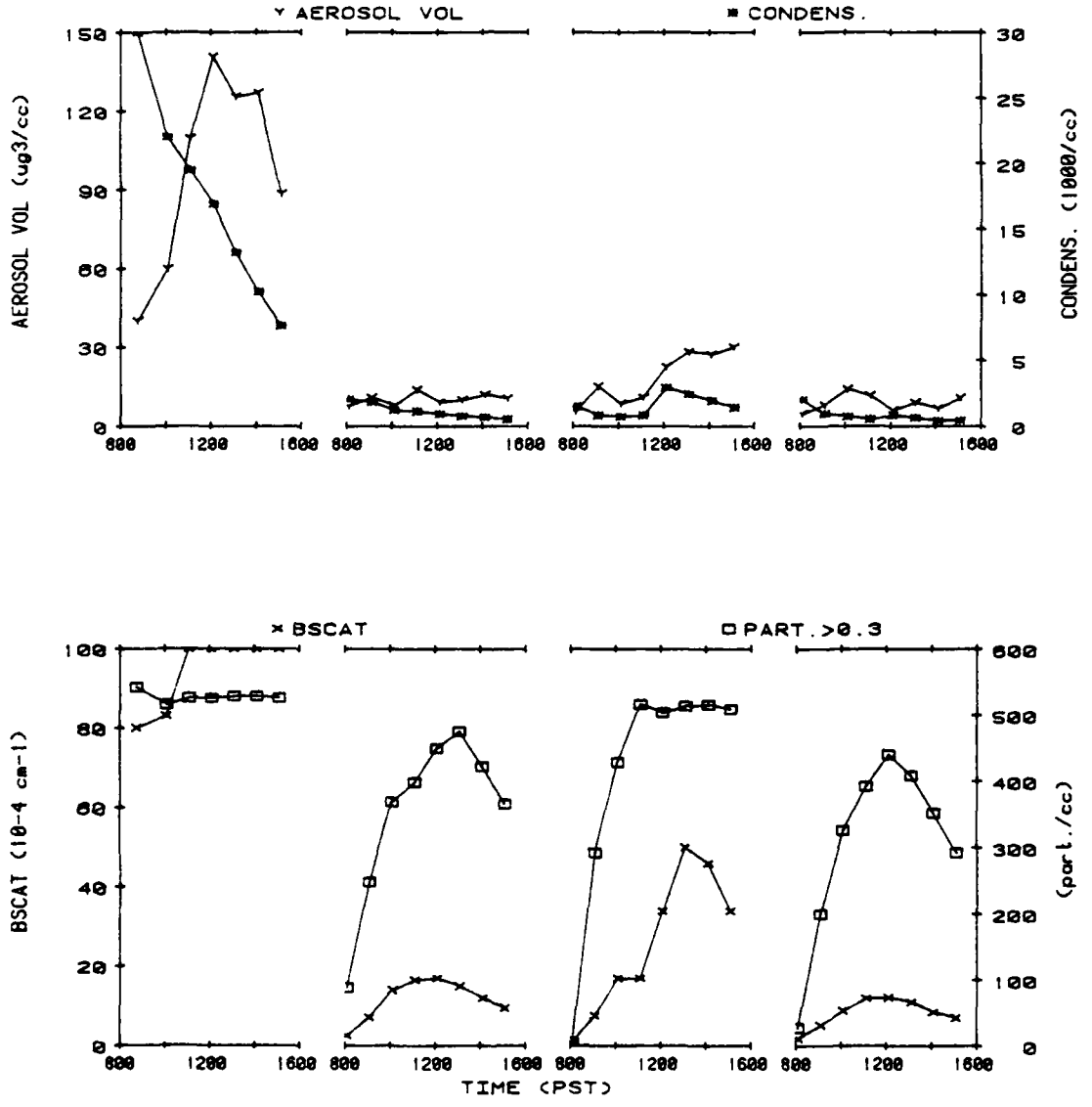

Figure 24. Concentration-Time Profiles for Selected Species, and Physical and Aerosol Measurements for the Four-Day, Diesel No. 2-NO_x Outdoor Chamber Run AFF-122 (concluded).

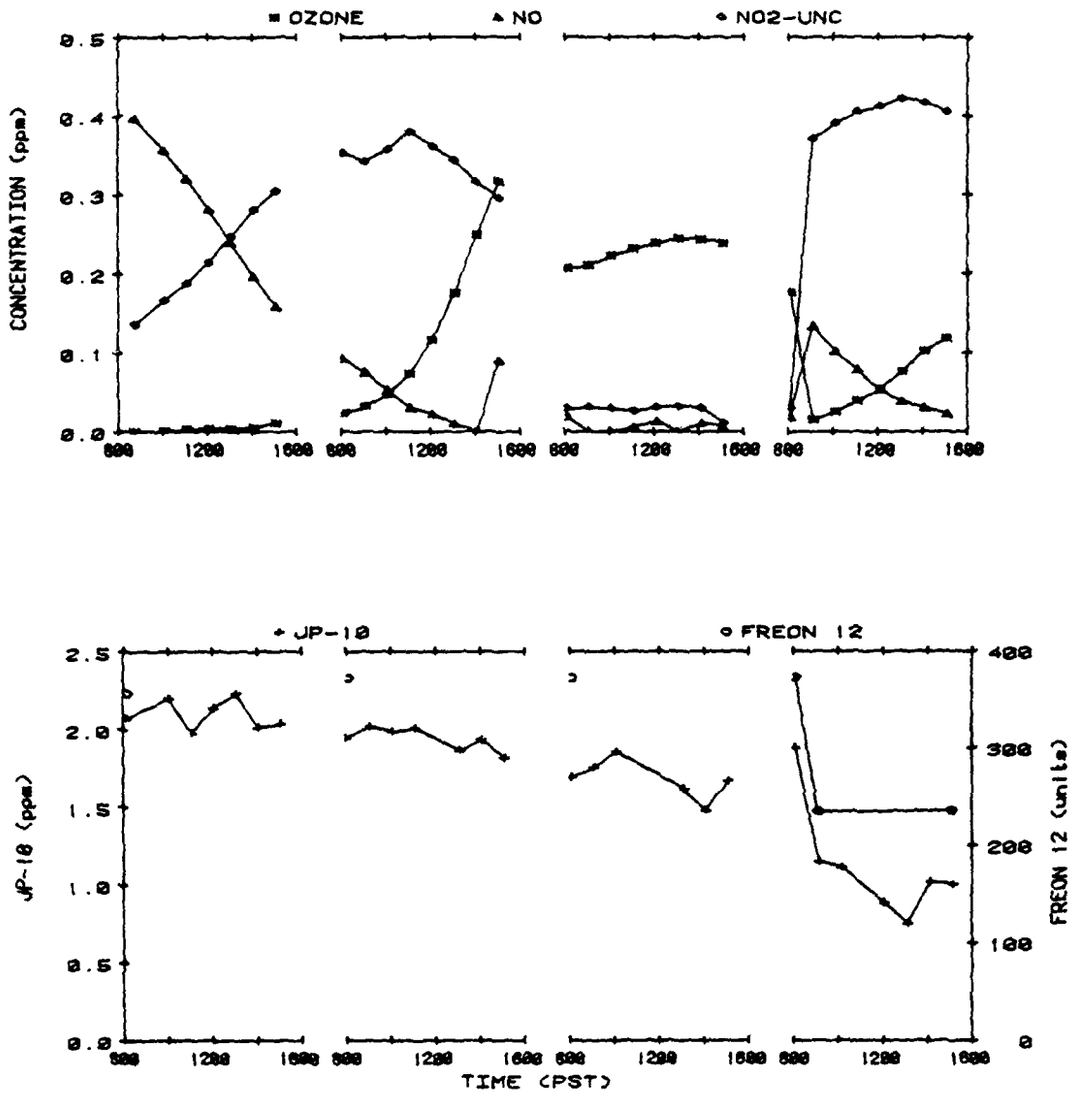

Figure 25. Concentration-Time Profiles for Selected Species, and Physical and Aerosol Measurements for the Four-Day, JP-10-NO_x Outdoor Chamber Run AFF-92.

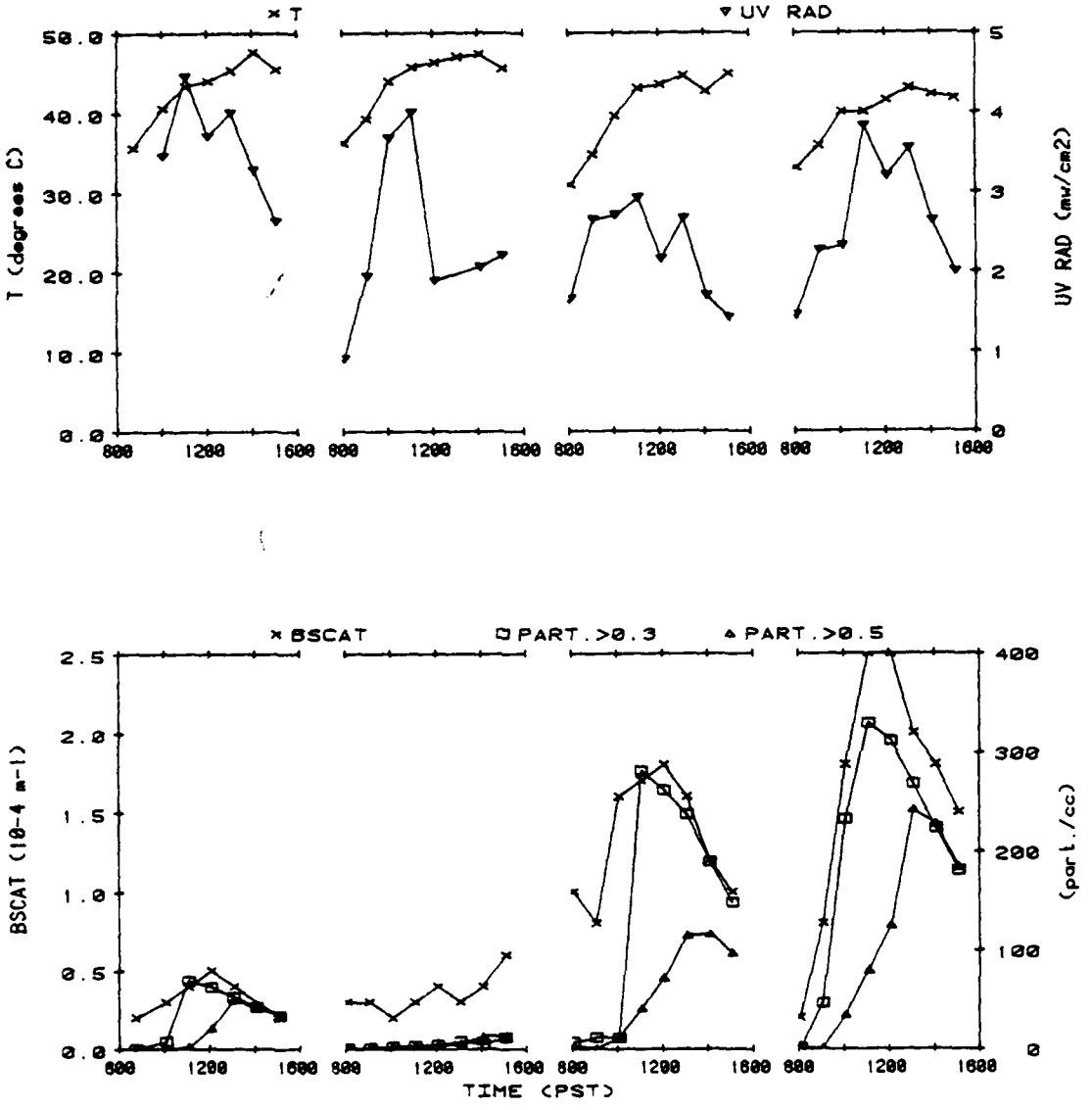

Figure 25. Concentration-Time Profiles for Selected Species, and Physical and Aerosol Measurements for the Four-Day, JP-10-NO_x Outdoor Chamber Run AFF-92 (concluded).

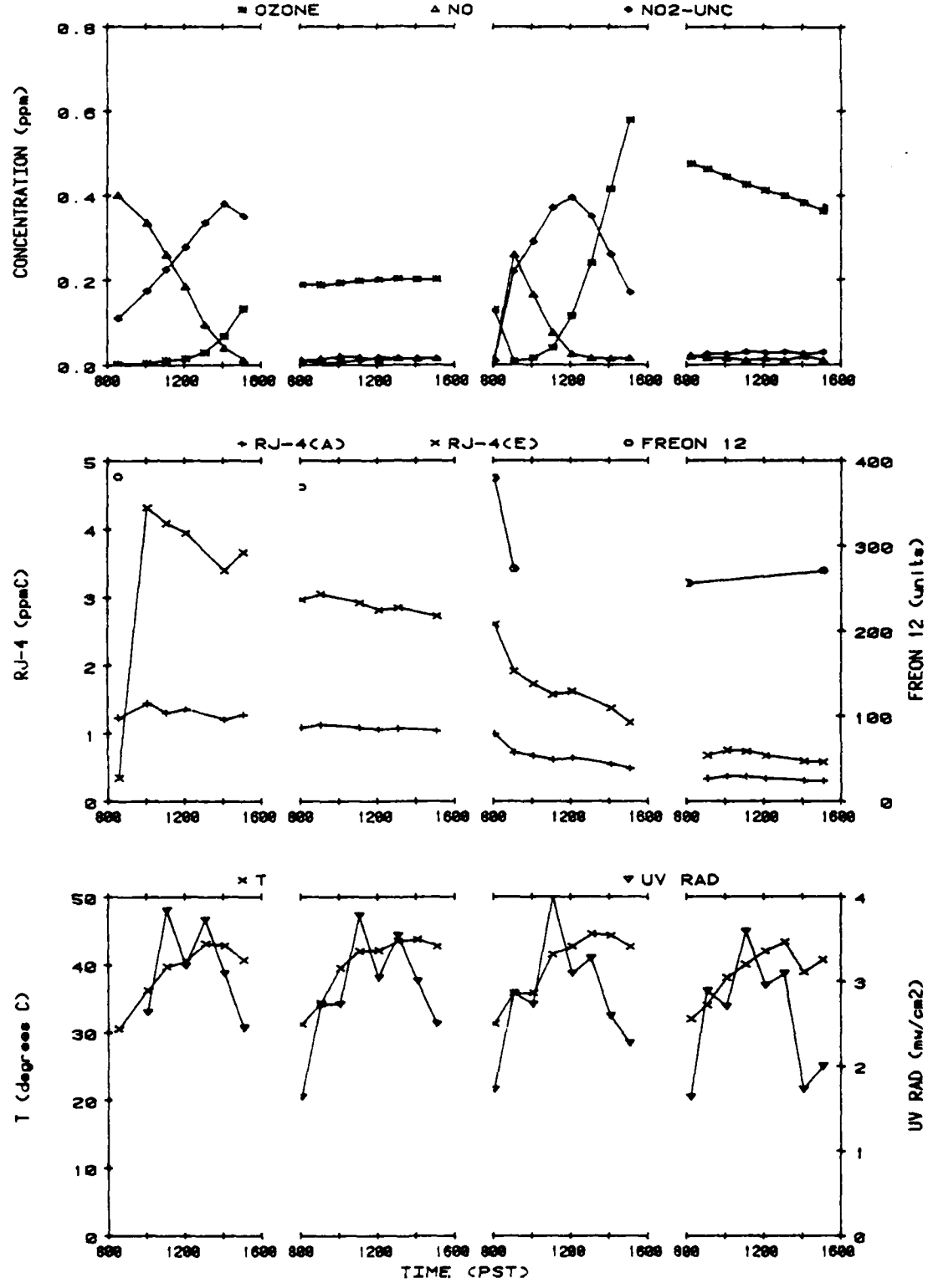

Figure 26. Concentration-Time Profiles for Selected Species, and Physical and Aerosol Measurements for the Four-Day, RJ-4-NO_x Outdoor Chamber Run AFF-93.

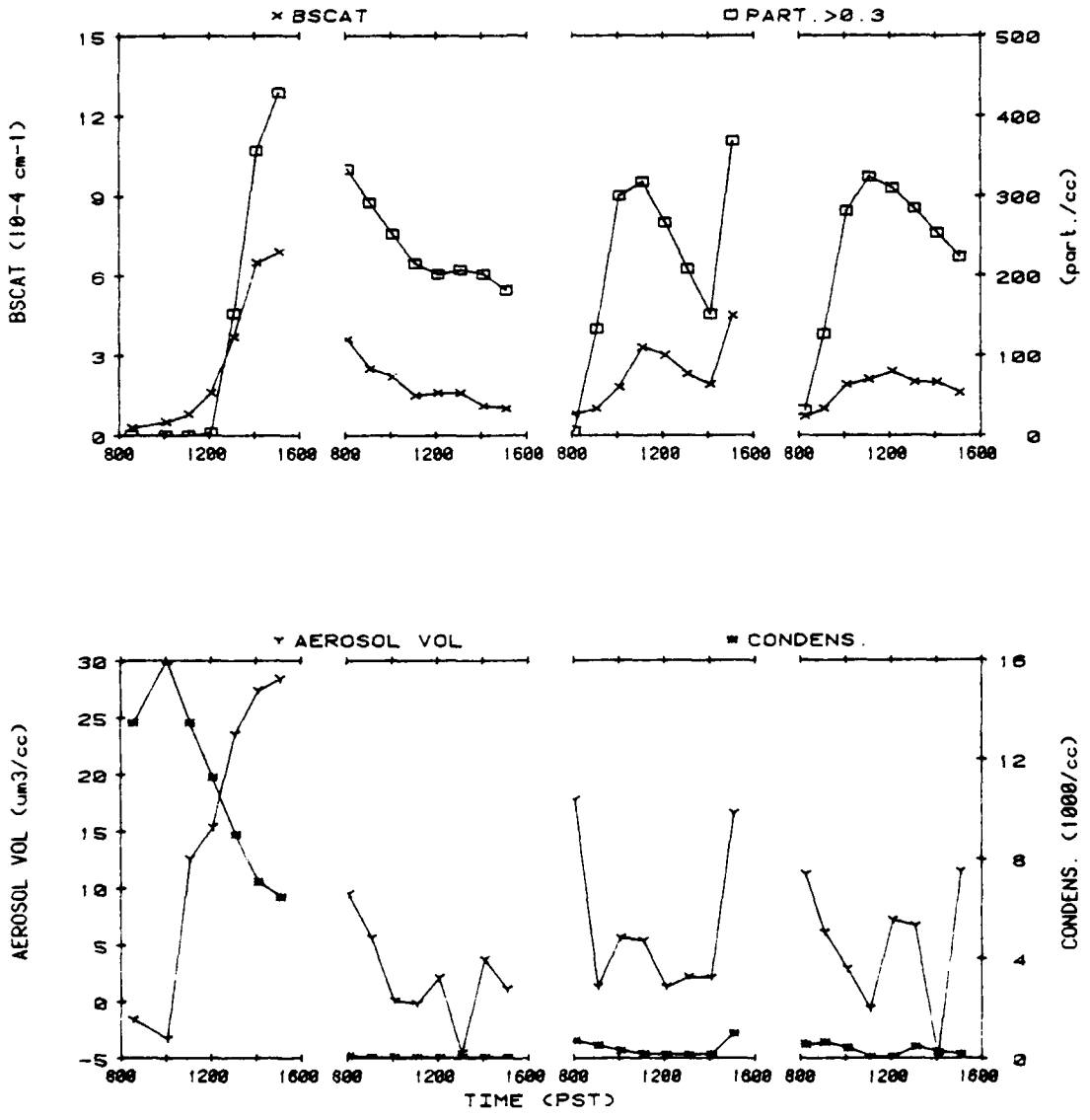

Figure 26. Concentration-Time Profiles for Selected Species, and Physical and Aerosol Measurements for the Four-Day, RJ-4-NO_x Outdoor Chamber Run AFF-93 (concluded).

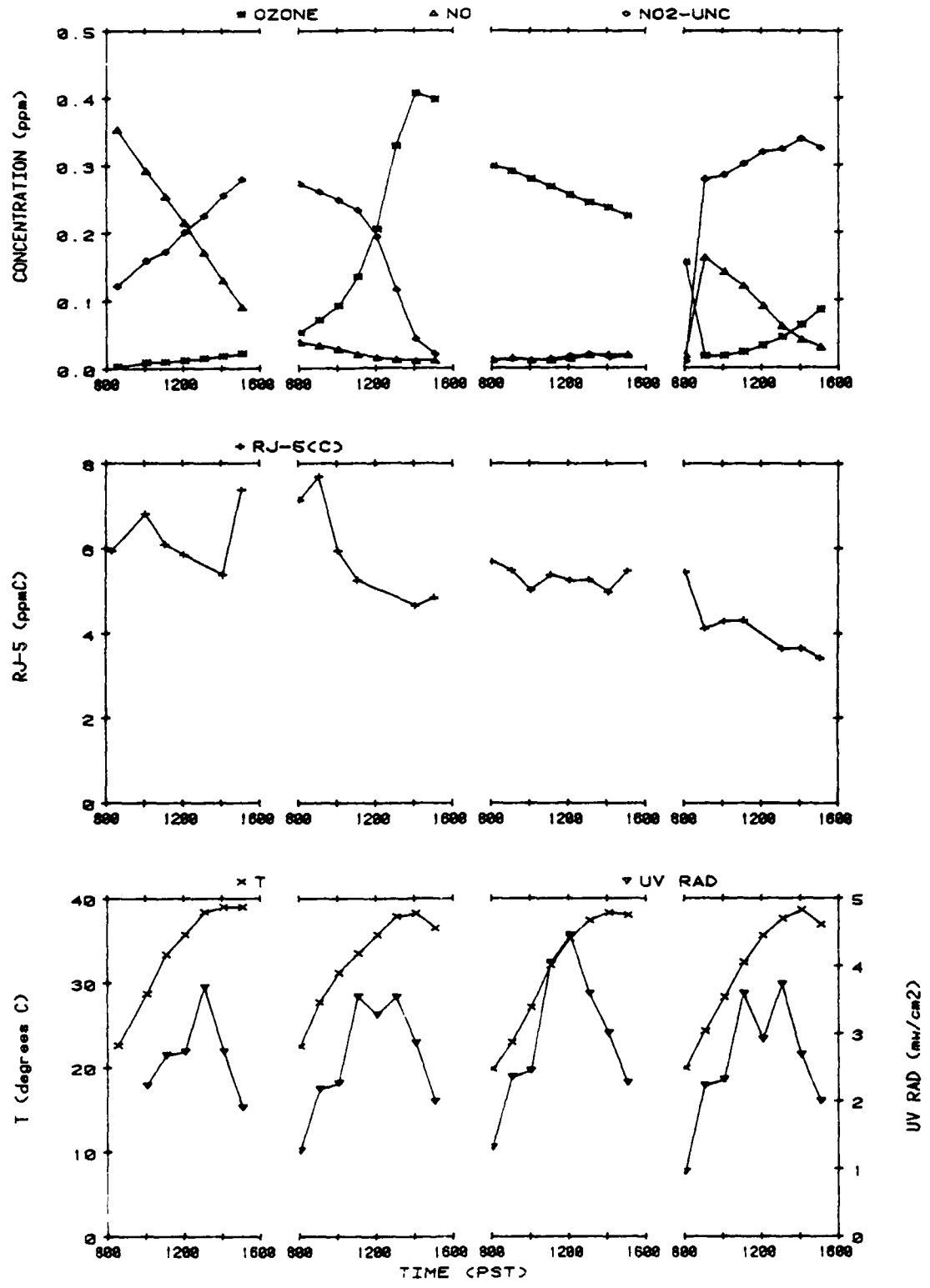

Figure 27. Concentration-Time Profiles for Selected Species, and Physical and Aerosol Measurements for the Four-Day, RJ-5-NO_x Outdoor Chamber Run AFF-108.

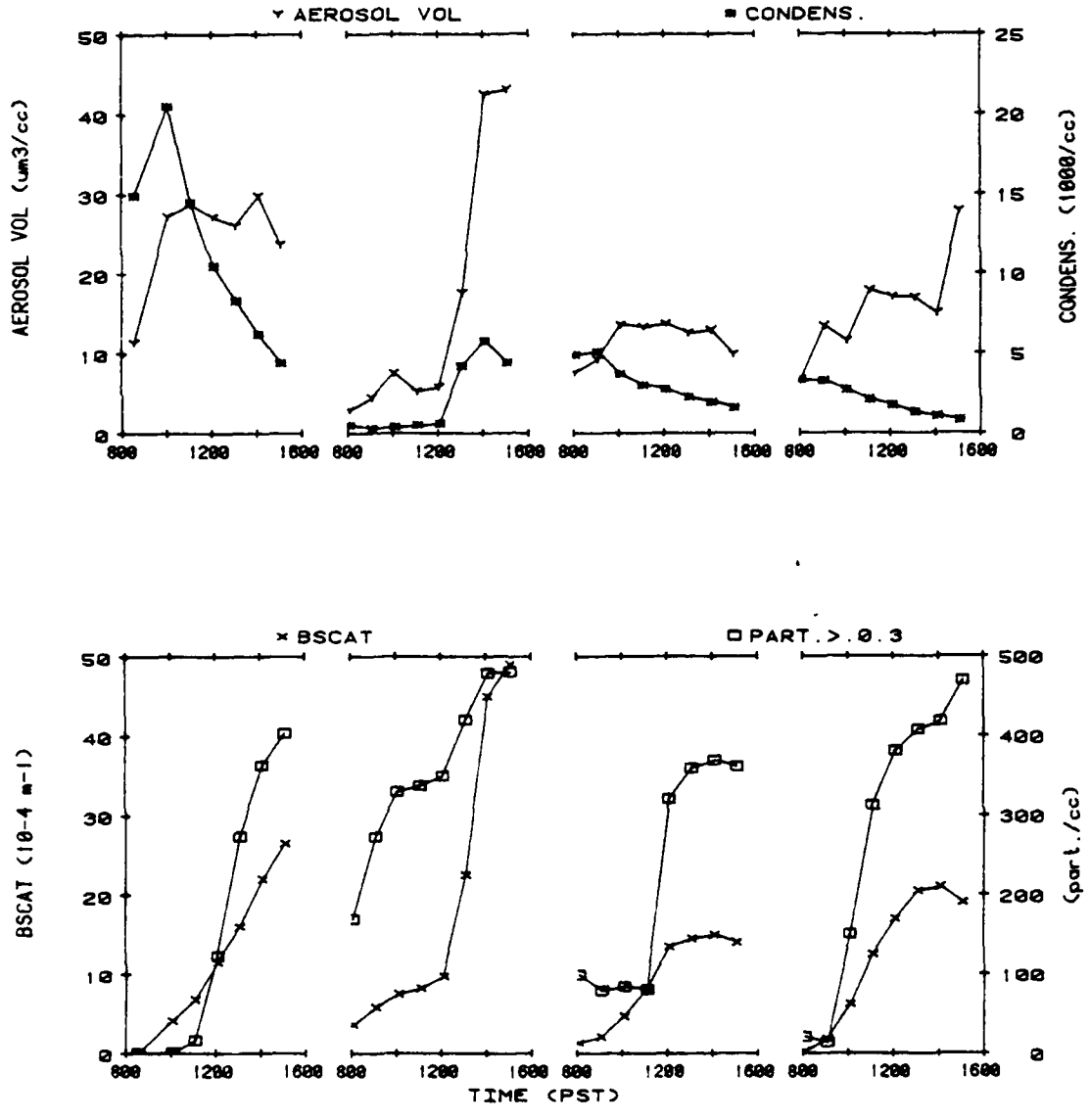

Figure 27. Concentration-Time Profiles for Selected Species, and Physical and Aerosol Measurements for the Four-Day, RJ-5-NO_x Outdoor Chamber Run AFF-108 (concluded).

NO_x source (e.g., downwind of the original fuel release), additional NO_x was injected into the mixture on the third or fourth day, depending on the time required for the initial NO_x to be consumed. In all cases, rapid formation of additional ozone occurred with the resulting maximum O_3 concentration generally being greater than that which had occurred on the first or second day. For the two JP-4 runs (particularly JP-4 [pet]), less O_3 was formed, since the mixtures were diluted to a far greater extent by the time the supplemental NO_x was injected than in the runs using the other fuels. The dilution factors, as measured by the ratio of the final-to-initial concentrations of the Freon® 12 tracer, were 0.084 and 0.30 for JP-4 (pet) and JP-4 (shale), respectively, compared with an average of 0.77 ± 0.07 for the other fuels. The O_3 maximum resulting after the second NO_x injection was also less than the first ozone maximum for JP-10 and RJ-5. However, both of these fuels were relatively unreactive and it generally took at least two days for the maximum O_3 to form.

Significant aerosol formation was observed to occur from all fuels in these runs, although the pattern observed using the various aerosol monitoring instruments was quite variable from run to run and for a given run from day to day. For the JP-4 and JP-8 runs, aerosol formation, as measured by aerosol volume, occurred essentially only on the first day of the run and its formation did not appear to be affected by the injection of NO_x on the third or fourth day (Figures 19-22). However, for JP-8, the particle numbers measured by the optical particle counter increased on all days of the runs.

For unleaded gasoline, the maximum light scattering occurred on the first day; but, it also increased somewhat on the third day after the second NO_x injection (Figure 23). In contrast, particle numbers in the unleaded gasoline run, as measured by the optical particle counter, increased most rapidly on the second day and went up significantly on the fourth day. Both of these days were those for which the mixture was unreactive with respect to O_3 formation.

For diesel fuel (Figure 24), the behavior of light scattering measurements was similar to that observed for unleaded gasoline (except that much higher light scattering values were observed). However, data from the optical particle counter showed the opposite behavior; the highest values were attained when the mixture was photochemically reactive. For JP-10

light scattering and optical particle counter readings increased each day of the irradiation (Figure 25), while for RJ-5, aerosol readings were generally the same on each day (except for condensation nuclei, which were always highest at the start of the first day for the heavier fuels). For these two fuels, there was no obvious correlation of the aerosol parameters with the O_3 forming reactivity of the mixtures. Finally, for RJ-4, slightly higher rates of aerosol formation were observed on days which were photochemically reactive.

It is difficult to generalize about the patterns of aerosol formation observed in these multi-day irradiations, except to point out that if there was any relationship between ozone formation and aerosol formation, it depended either on the fuel employed or the conditions (temperature, etc.) under which the runs were conducted. A discussion of how the various fuels differed in the amounts of aerosol they formed is given of the standard runs and the inter-fuel comparison runs.

4.2.2 Dynamic Runs

For JP-4 (pet), JP-4 (shale), unleaded gasoline, and JP-10, one- to three-day dynamic runs were performed in which the mixture was diluted by ~10% each hour during the day, with no dilutions being carried out at night. The conditions and results of these runs are summarized in Table 31. Figures 28-31 give the O_3 and NO_x concentration-time profiles observed in a selected dynamic run for each of these fuels. Also shown in those figures are the concentrations of the inert Freon® 12 tracer, which was added to the mixture to monitor the dilution rate.

The results of these runs generally followed the same patterns as the four-day runs discussed above except that (as expected) less O_3 and aerosol were formed, because of the dilution of the reaction mixture. Because of the non-linearity of the chemistry involved, it would not be expected a priori that the maximum O_3 yields would be reduced by exactly the amount the mixture was diluted. In fact, however, when the observed maximum ozone yields are divided by the dilution factor, they are generally within the range of the ozone yields observed in the static runs carried out under similar temperature and lighting conditions. However, because of the variability observed in the outdoor chamber runs (Section 4.2.3) and the relatively small number of dynamic runs conducted, the present data are inadequate to conclude that this is generally true. As with the

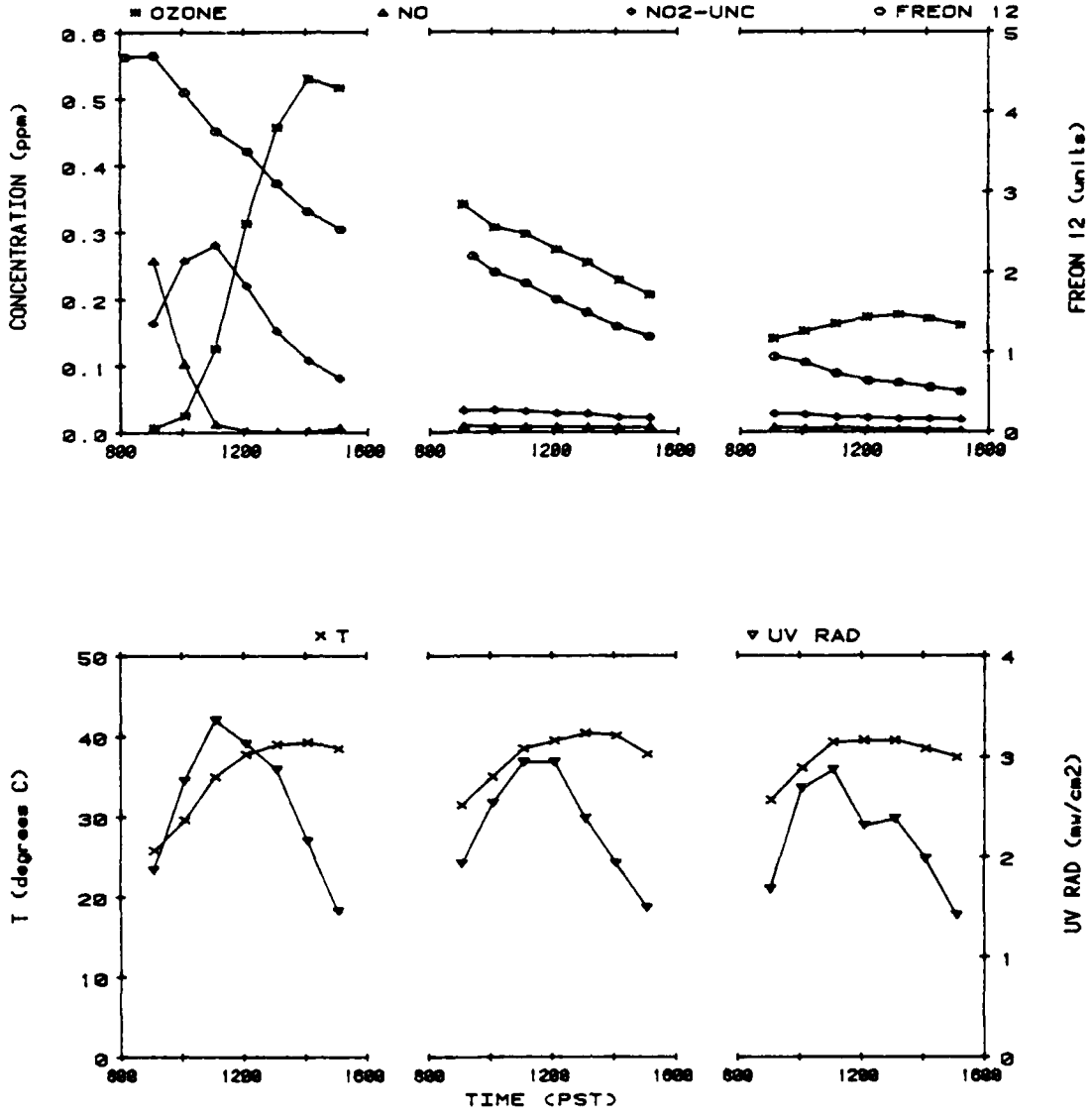

Figure 28. Concentration-Time Profiles for Selected Species, and Physical Measurements for the Dynamic, JP-4(Pet)-NO_x Outdoor Chamber Run AFF-33.

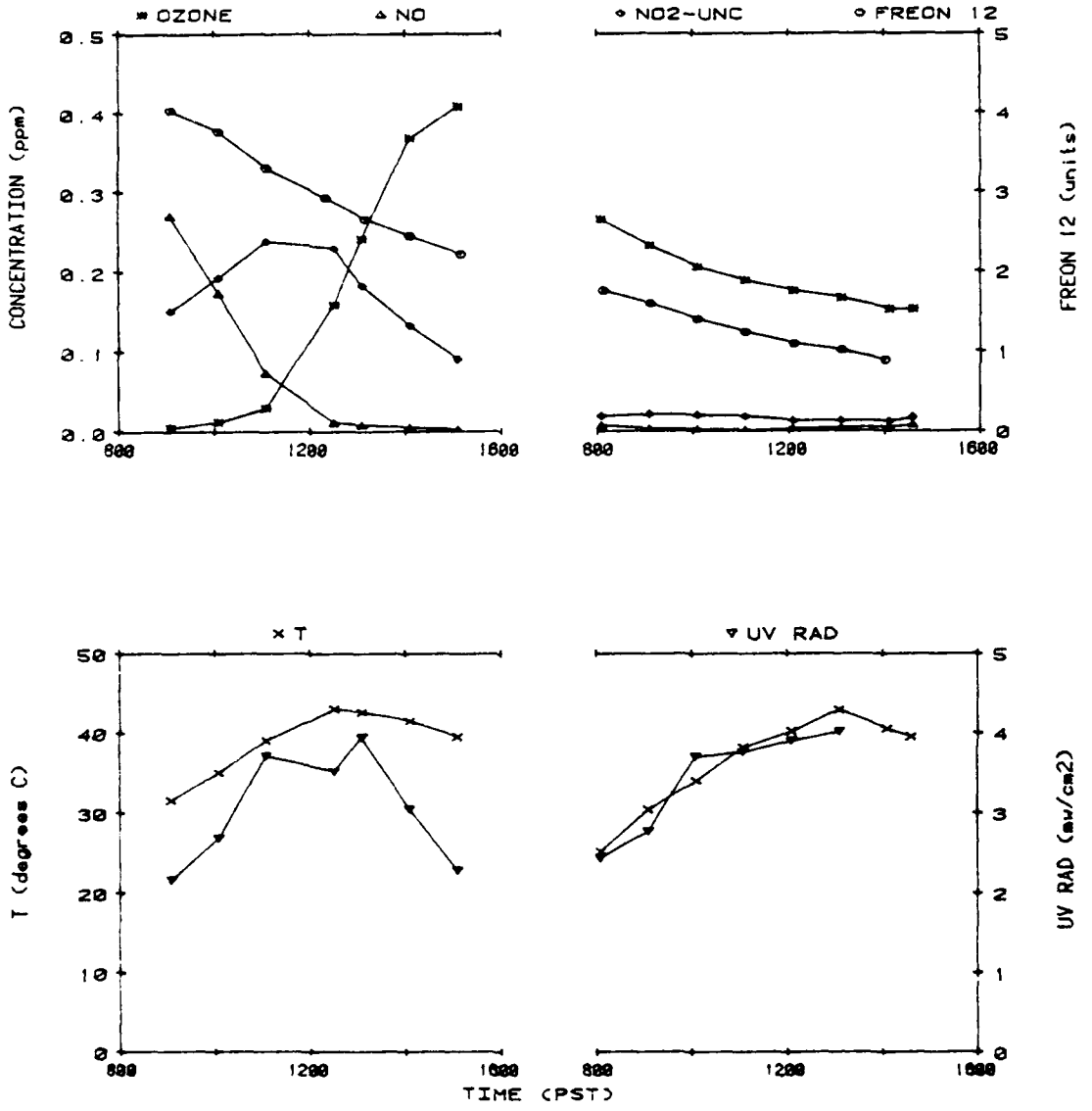

Figure 29. Concentration-Time Profiles for Selected Species, and Physical Measurements for the Dynamic, JP-4(Shale)-NO_x Outdoor Chamber Run AFF-31.

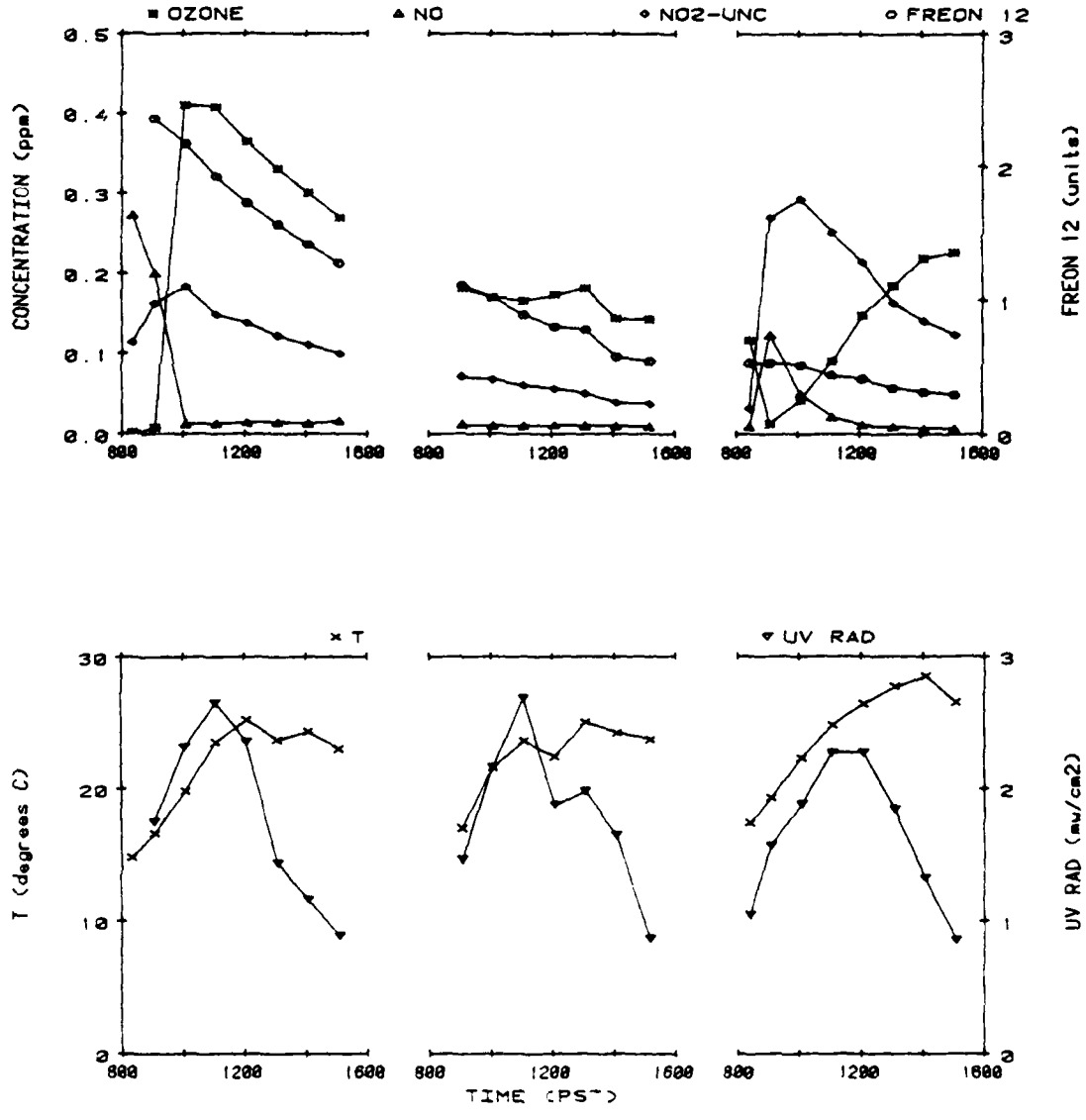

Figure 30. Concentration-Time Profiles for Selected Species, and Physical Measurements for the Dynamic, Unleaded Gasoline-NO_x Outdoor Chamber Run AFF-45.

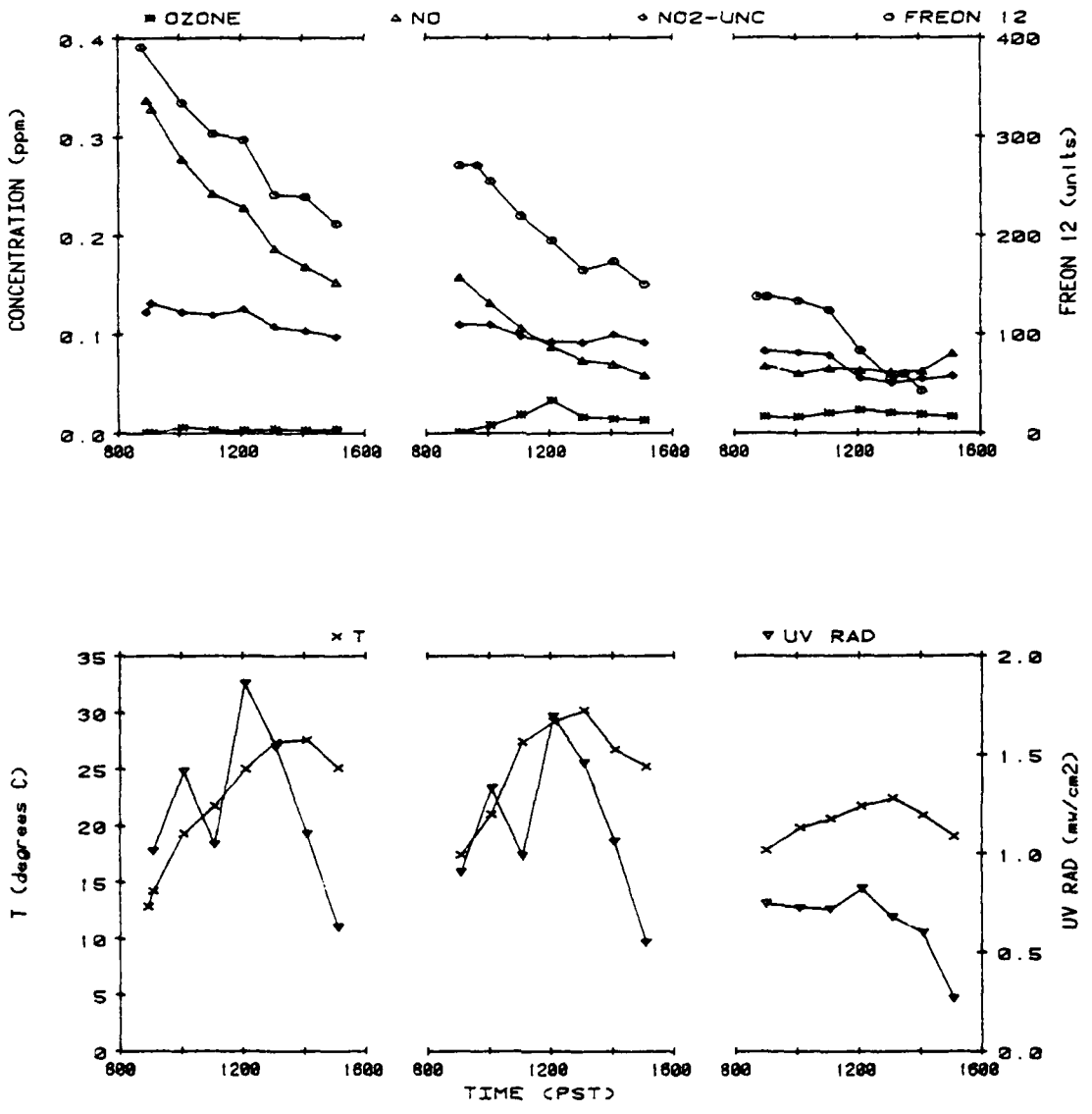

Figure 31. Concentration-Time Profiles for Selected Species, and Physical Measurements for the Dynamic, JP-10-NO_x Outdoor Chamber Run AFF-55.

static runs, the dynamic runs fell into two categories, depending on whether the maximum O_3 formation occurred on the first or the second day (with no significant O_3 formation occurring after that). The ozone maximum occurred on the first day in the JP-4 (pet) and the unleaded gasoline runs and on the first day in one of the two JP-4 (shale) two-day runs (Figures 28, 29). The maximum O_3 yield occurred on the second day of the JP-10 dynamic run (Figure 31) (as observed for most of the other JP-10 runs). This was also the case for the JP-4 (shale) run (AFF-56, Table 31), which was carried out under conditions of unusually low light intensity.

For the unleaded gasoline three-day dynamic run (Figure 30), NO_x was injected at the beginning of the third day (after the initially-present NO_x was consumed) and, as observed in the four-day runs, rapid O_3 formation then resulted. In general it can be concluded that, apart from lower yields of the products and a more rapid decrease in the concentrations of the reactants, dilution does not appear to have any qualitative effect on the pattern of results in these multi-day irradiations.

4.2.3 Standard Runs

The experimental protocol for the outdoor chamber runs in this program called for a minimum of six repeats of a standard run to be carried out for each fuel. These standard runs consisted of irradiations of a nominal 25 ppmC fuel and 0.5 ppm NO_x mixture, without dilution in air for at least one day. Most of these runs, except for the four-day, undivided bag run, were conducted with the bag in a divided mode, with the two sides of the bag having either different reactant concentrations or different fuels. These six repeats consisted of the four-day run, the variable NO_x, the variable fuel, the fuel versus n-butane, and the two fuel versus JP-4 (pet) or JP-10 runs. The largest number of repeats were for JP-4 (pet) and JP-10, since they were used as the standard fuels against which the other fuels of the kerosene or high energy type were compared. In addition, a number of replicate irradiations were conducted for n-butane, which was used as a model hydrocarbon fuel for comparison purposes (see Section I). Furthermore, the standard JP-4 (pet), JP-10, and n-butane runs were performed under a variety of weather conditions, thus showing the effects of meteorological variables on the reactivity of these three fuels.

In this section, some of the major results of these standard runs are summarized. This discussion will focus primarily on the following three important aspects of reactivity of these fuels under atmospheric conditions: (1) the rate of NO consumption, and the initial rate of O_3 formation, which is measured by the quantity $d([O_3]-[NO])/dt$, hereafter referred to as the "NO oxidation rate"; (2) the maximum amounts of O_3 formed on the first two days of the irradiation; and (3) aerosol formation, as measured by various experimental methods. The significance of these and other aspects of fuel reactivity in atmospheric systems, and their implications in terms of the effects of fuel reactivity on air quality impacts, will be discussed in Section V.

Table 32 gives the ranges of the experimental conditions employed, together with averages of selected results of the standard runs for the fuels (including n-butane) studied in this program. These results exhibit significant variability, particularly for the aerosol parameters measured, but also for the rates of NO oxidation and (for the less reactive fuels), for the maximum ozone yields. The variability of the initial reactant concentrations was ~ ± 20% (the reasonable expectation when a non-rigid chamber of varying volume is employed). The variability in temperature and UV intensity (as measured by the standard deviation of the averages) was ± 2-4°C and ± 0.2-0.4 mW cm^{-2}, respectively, for fuel runs performed around the same time of the year during stable weather conditions. The variability in temperature and UV intensity was ± 7°C-10°C and 0.5-0.9 mW cm^{-2}, respectively, for fuels used as comparison standards (JP-4 [pet], JP-10, and n-butane), or for a fuel studied at two different times of the year (diesel No. 2) or during a period of variable weather (unleaded gasoline).

In order to examine the effect of the variability in meteorological conditions on the reactivity data from these replicate irradiations, correlation coefficients between selected reactivity parameters and temperature and UV intensity were calculated for the three fuels used as comparison standards. These correlation coefficients are listed in Table 33. In general, except for the O_3 yields on the first day of the JP-10 runs (which were < 0.07 ppm, even under favorable conditions), the ozone yields and NO oxidation rates correlated reasonably well with temperature and UV

TABLE 32. AVERAGES OF SELECTED REACTION CONDITIONS AND RESULTS FOR STANDARD STATIC FUEL-NO_x-AIR OUTDOOR CHAMBER RUNS.

PARAMETER	DAY	FUEL									
		JP-4(Pet)	JP-4(Shale)	JP-8(Pet)	JP-8(Shale)	Unleaded Gasoline	Diesel No. 2	JP-10	RJ-4	RJ-5	n-Butane
NO. RUNS[a]		14/10	6/3	8/7	8/7	6/4	7/6	10/8	6/5	6/5	10/0
Avg. T (^oC)	1	32±7	37±2	26±3	31±4	29±9	36±6	32±10	37±2	37±2	32±7
UV Int. (w cm^{-2})	1	2.5±0.5	3.0±0.2	2.3±0.3	2.8±0.4	2.0±0.4	2.3±0.3	2.3±0.9	2.8±0.4	2.6±0.1	2.4±0.6
Initial NO_x (ppm)	1	0.48±0.08	0.54±0.09	0.41±0.05	0.44±0.06	0.47±0.03	0.46±0.03	0.49±0.03	0.49±0.02	0.47±0.02	0.52±0.05
Fuel (ppmC)	1	23±3	31±4	23±6	24±3	33±4	~10±3	30±6	34±3	~15±3	27±5
O_3 max (ppm)	1	0.7±0.2	0.6±0.2	0.07-0.60	0.59±0.10	0.58±0.07	0.44±0.05	~0±0.07	0.01-0.47	0.026±0.007	~0-0.64
	2	0.4±0.2	0.06-0.26	0.32±0.09	0.43±0.04	0.39±0.05	0.22±0.03	~0-0.62	0.24±0.08	0.38±0.05	-
$d([O_3]-[NO])/dt$ (ppb min^{-1})	1	3.0±1.1	2.3±0.6	1.3±0.5	2.5±0.8	15±4	3.8±0.9	0.1-1.1[b]	1.2±0.4	0.84±0.10	0.5-2.6
PAN max (ppm)	1	0.05±0.05	0.013±0.006	0.04±0.01	0.10±0.04	0.11±0.07	0.05±0.01	0.002±0.003	0.009±0.005	0.002±0.001	0.03±0.03
HCHO max (ppm)	1	0.08±0.04	0.06±0.03	0.04±0.01	0.07±0.01	0.24±0.08	0.08±0.02	0.02±0.02	0.03±0.01	0.02±0.02	0.03±0.02
Aerosol Volume (μm^3 cm^{-3})	1	8-191[b]	4-69[b]	10-125	21-153	170±40	115±40	0-16	30±10	40±12	~0
	2	5-25	3[b]	8-72[b]	4-12[b]	3-14	14-71	2-13	9±4	18-60	-
B_{scat} (10^{-4} m^{-1})	1	1.2-20	2-26	4.3-11[b]	19±7[b]	5.2±1.4[b]	77->100[b]	~0-17	2-87	31±7	~0
	2	1.1-4.1	1	1.2-12[b]	2.1-4.6[b]	1.5±0.1[b]	17-48[b]	~0-12.5	2-20	20-50	-
Condens. Nuc. (10^3 counts)	1	61±20	0-17[b]	40±20	14-53	103±8	2-30	0-2	17±5	17±4	~0
	2	0-3	-[b]	0-10	0-2	0-2	2-19	~0	0.6	4-11	-
Aerosol Number (10^3 cm^{-3})	1	115±37[b]	1.6-35[b]	41-340	40-210	210±50	6-160	1-12	70±15	48±8	~0
	2	1-12	2.7-6.4[b]	1.4-49[b]	1-8.8	1.4-14	8-77	1-21	4-28	22±4	-
No. Particles >0.3 μ (cm^{-3})	1	6-354	350±100	360±15	430±15	27-150	540±15	12-465	445±70	430±15	~0
	2	6-282	90±40	355±33	290±50	48-139	460±20	9-380	330±70	465±40	-
No. Particles >1 μ (cm^{-3})	1	~0[c]	0-70	0-93	8->54	0	355±20	0-34	0-149	18-68	~0
	2	0	0	1-25	2-12	0	64-386	0-55	6-92	125±25	-

[a]First number is total number of runs; second is number of runs for which day two data is available.

[b]Not all runs have data of this type.

[c]One run had an anomolously high value of 37 cm^{-3}, the rest were zero.

TABLE 33. CORRELATION COEFFICIENTS BETWEEN MEASURED REACTIVITY AND AEROSOL PARAMETERS AND TEMPERATURE AND LIGHT INTENSITY FOR THE JP-4 (PET), JP-10, AND n-BUTANE OUTDOOR CHAMBER RUNS.

PHYSICAL PARAMETER	TEMPERATURE			UV RADIOMETER		
FUEL	JP-4 (Pet)	JP-10	$n\text{-}C_4$	JP-4 (Pet)	JP-10	$n\text{-}C_4$
Correlation Coefficients:						
Maximum O_3, Day One	0.88	0.53	0.86	0.76	0.45	0.89
Maximum O_3, Day Two	0.59	0.67	--	0.60	0.58	--
NO Oxidation Rate	0.79	0.84	0.95	0.73	0.81	0.91
Aerosol Volume	0.53	0.10	--	0.33	-0.09	--
No. Particles > 0.3 μ	0.61	0.47	--	0.50	0.48	--
Aerosol Number	-0.12	-0.32	--	0.35	-0.13	--
B_{scat}	0.86	0.32	--	0.39	0.24	--
UV Radiometer	0.65	0.94	0.87			

intensity. The correlation with temperature was observed to be somewhat better. The correlation between aerosol parameters and meteorological conditions was not as good; there appears to be no significant correlation for the aerosol parameters in the JP-10 runs, or for the aerosol number measurements in the JP-4 (pet) runs. Because the influence of meteorological conditions on aerosol measurements appears to be substantially less than on the NO oxidation rates and ozone yields, these will be considered separately.

NO Oxidation and Maximum Ozone Formation. Plots of the NO oxidation rates and maximum ozone yields for days one and two against the average temperature for JP-4 (pet), JP-10, and n-butane are shown in Figures 32 and 33. The rates of NO oxidation and the first day ozone yields could be fit reasonably well to the following relations (which are shown as lines on the figures):

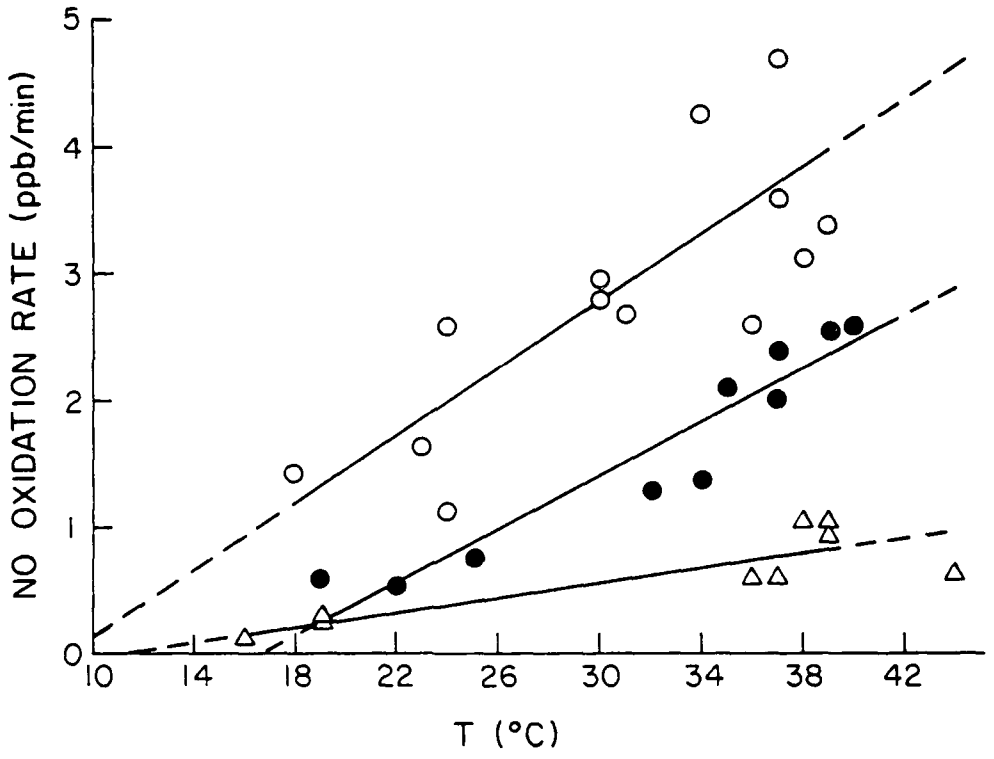

Figure 32. Plots of NO Oxidation Rates vs Average Temperature for the Standard Outdoor Chamber Runs Using JP-4 (Pet), n-Butane and JP-10.

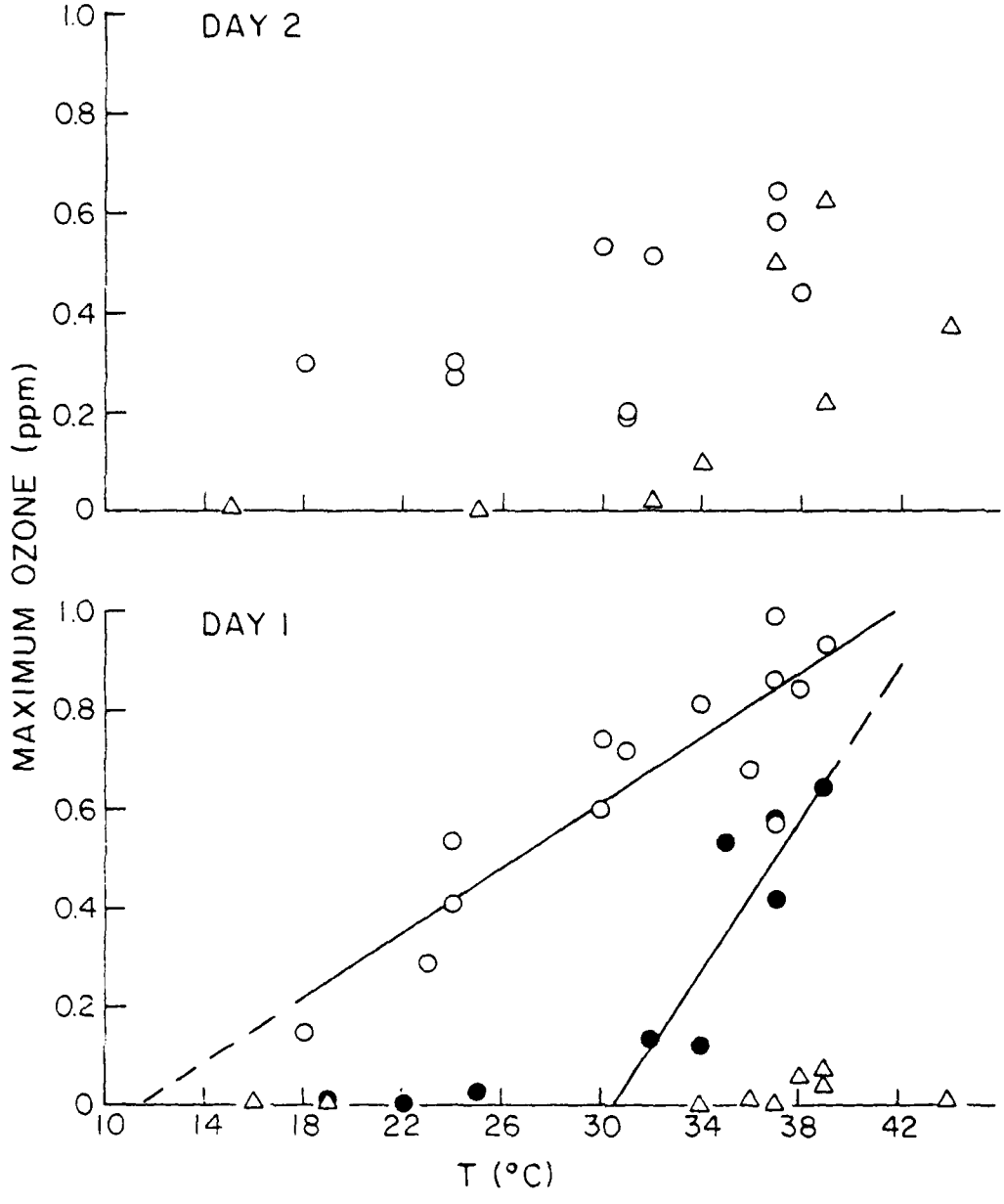

Figure 33. Plots of Day One and Day Two Maximum Ozone Yields vs Average Temperature for the Standard Outdoor Chamber Runs Using JP-4(Pet), n-Butane, and JP-10.

JP-4 (pet):

NO oxidation rate = 0.13 T - 1.14, $20 < T < 40$

Day one O_3 maximum = 0.032 T - 0.36, $20 < T < 40$

n-Butane:

NO oxidation rate = 0.104 T - 1.72, $20 < T < 40$

Day one O_3 maximum $\cong$ 0.0 $T < 30$

= 0.077 T - 2.36, $30 < T < 40$

JP-10:

NO oxidation rate = 0.028 T - 0.27, $20 < T < 40$

Day one O_3 maximum $\cong$ 0.0 $T < 40$

where T is the average temperature (^{o}C), the NO oxidation rate is in ppb min^{-1}, and the O_3 maximum is in ppm. From these relationships, the reactivities (in terms of the first day O_3 maxima or in terms of the NO oxidation rates) of the standard 25 ppmC fuel-0.5 ppm NO_x mixtures involving JP-4 (pet), JP-10, and n-butane can be estimated for any temperature over the range $20^{o}C$-$40^{o}C$ and used to compare these three fuels. From these relations (also Figures 32, 33), the obvious order of reactivity is JP-4 (pet) > n-butane > JP-10. However, the relationships suggest that the differences in maximum ozone yield, at least between JP-4 (pet) and n-butane, become significantly less as the temperature is increased.

For most of the other fuels studied in this program, the number of replicate irradiations are insufficient (given the variety of meteorological conditions under which the irradiations were performed) to derive similar relations between the reactivity parameters and the meteorological conditions. Thus, intercomparisons for these fuels are more difficult. Figures 34 and 35 give plots of the NO oxidation rates, and Figures 36 and 37 give plots of first and second day ozone maxima for all of the replicate standard runs. The data are plotted such that the average temperature and UV intensity is shown for the run from which each point was taken. Because of their significantly lower overall reactivity, the results for the high energy fuels (JP-10, RJ-4, and RJ-5) are shown on plots separate from those for JP-4, JP-8, and the commercial fuels.

The data shown in Figures 34 and 35 suggest that, in terms of NO oxidation rates in the standard fuel-NO_x mixtures, the approximate order of

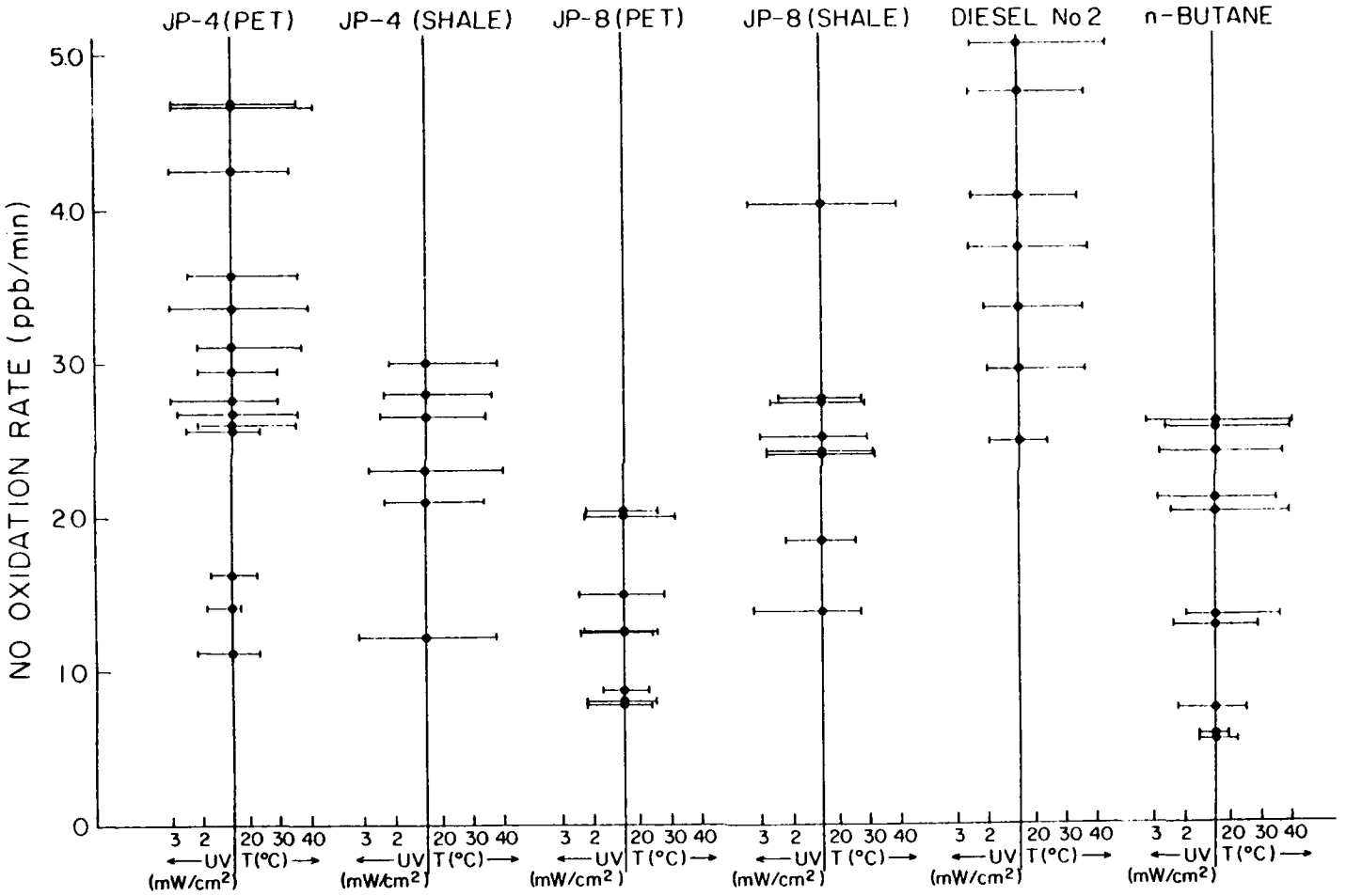

Figure 34. Plots of NO Oxidation Rates Showing Average Temperatures and UV Intensities for the Standard Outdoor Chamber Runs Using Petroleum and Shale-Derived JP-4 and JP-8, Diesel No. 2, and n-Butane.

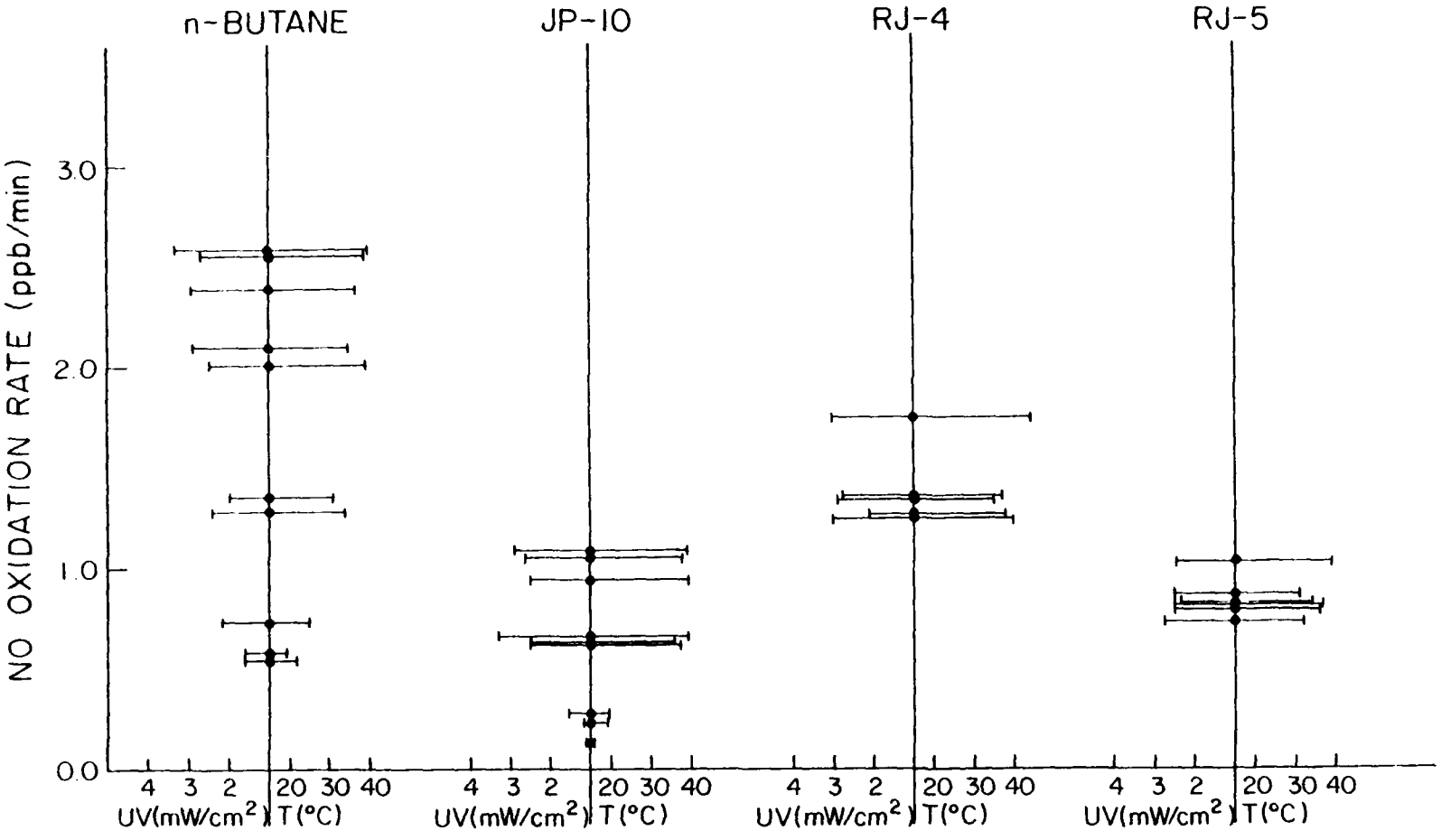

Figure 35. Plots of NO Oxidation Rates Showing Average Temperatures and UV Intensities for the Standard Outdoor Chamber Runs Using n-Butane, JP-10, RJ-4, and RJ-5.

reactivity is: unleaded gasoline >> diesel No. 2 > JP-4 (pet) > JP-8 (shale) > JP-4 (shale) > n-butane ≈ JP-8 (pet) > RJ-4 > RJ-5 ≡ JP-10. Unleaded gasoline is far more reactive in this respect than even diesel No. 2 and its NO oxidation rates are not shown in Figure 34, since they would be offscale.

From Figures 36 and 37, the order of reactivity in terms of O_3 yields is not necessarily the same as that derived from the NO oxidation rates. Figure 36 shows that, in terms of the first and second day O_3 yields, diesel No. 2 appears to form somewhat less O_3 than JP-4, JP-8, and unleaded gasoline. For these latter fuels, the data do not suggest any significant differences in the first day O_3 yields. The first day O_3 yields for JP-8 (pet) were the lowest on average. However, most of these latter runs were carried out under low temperature and light intensity conditions, relative to the other fuels, and the second day O_3 yields for JP-8 (pet) were more similar to those for the other fuels. For JP-4 (shale), the O_3-yield data are too scattered for useful comparisons.

The relative O_3 yields contrast with the reactivity ranking obtained from NO oxidation rates, since unleaded gasoline, by far the most reactive fuel in the latter regard, forms about the same amount of ozone as the JP-4 and JP-8 fuels. Moreover, diesel No. 2, the second most reactive fuel with respect to NO oxidation, forms less ozone, especially on the second day.

For n-butane and the less reactive, high energy fuels (Figure 37), the first day ozone yields correlate well with the rates of NO oxidation. This is as expected, since ozone yields in less reactive hydrocarbon-NO_x mixtures are determined by the rates of NO conversion rather than by the ozone-forming potential (since the O_3 maximum is generally not reached, Section 5.1). On the other hand, the second day ozone yields for the high energy fuels were not well correlated with the NO oxidation rates (in contrast to JP-4, JP-8, and the commercial fuels). Thus, RJ-5 formed more O_3 on day two than did RJ-4; and JP-10, probably the least reactive fuel in terms of NO oxidation rates, formed more O_3 on day two in some cases than did all of the fuels on the first or second day, except JP-4 (pet). In general, in terms of the O_3-forming potential on the second and subsequent days of irradiation, these data indicate that all of the fuels

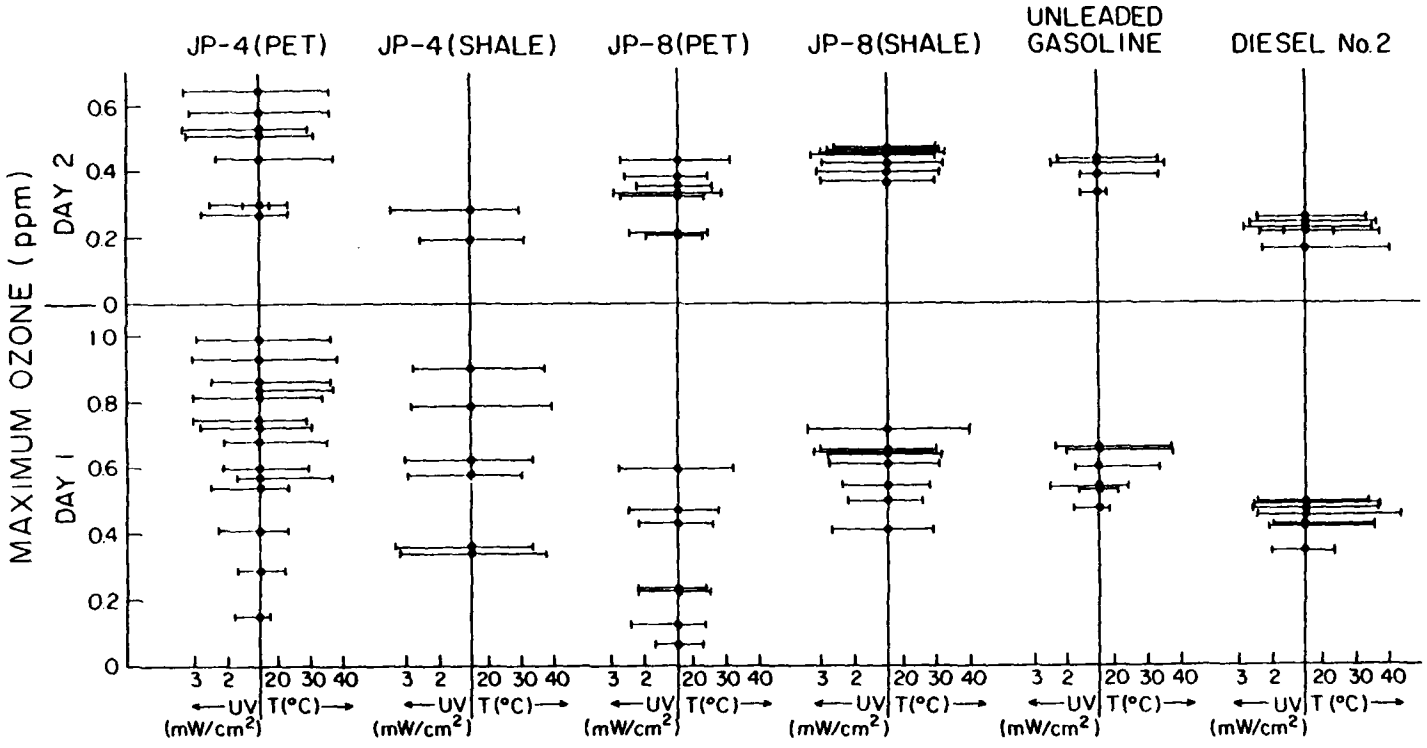

Figure 36. Plots of Day One and Day Two Maximum Ozone Yields Showing Average Temperatures and UV Intensities for the Standard Outdoor Chamber Runs Using Petroleum and Shale-Derived JP-4 and JP-8, Unleaded Gasoline, and Diesel No. 2.

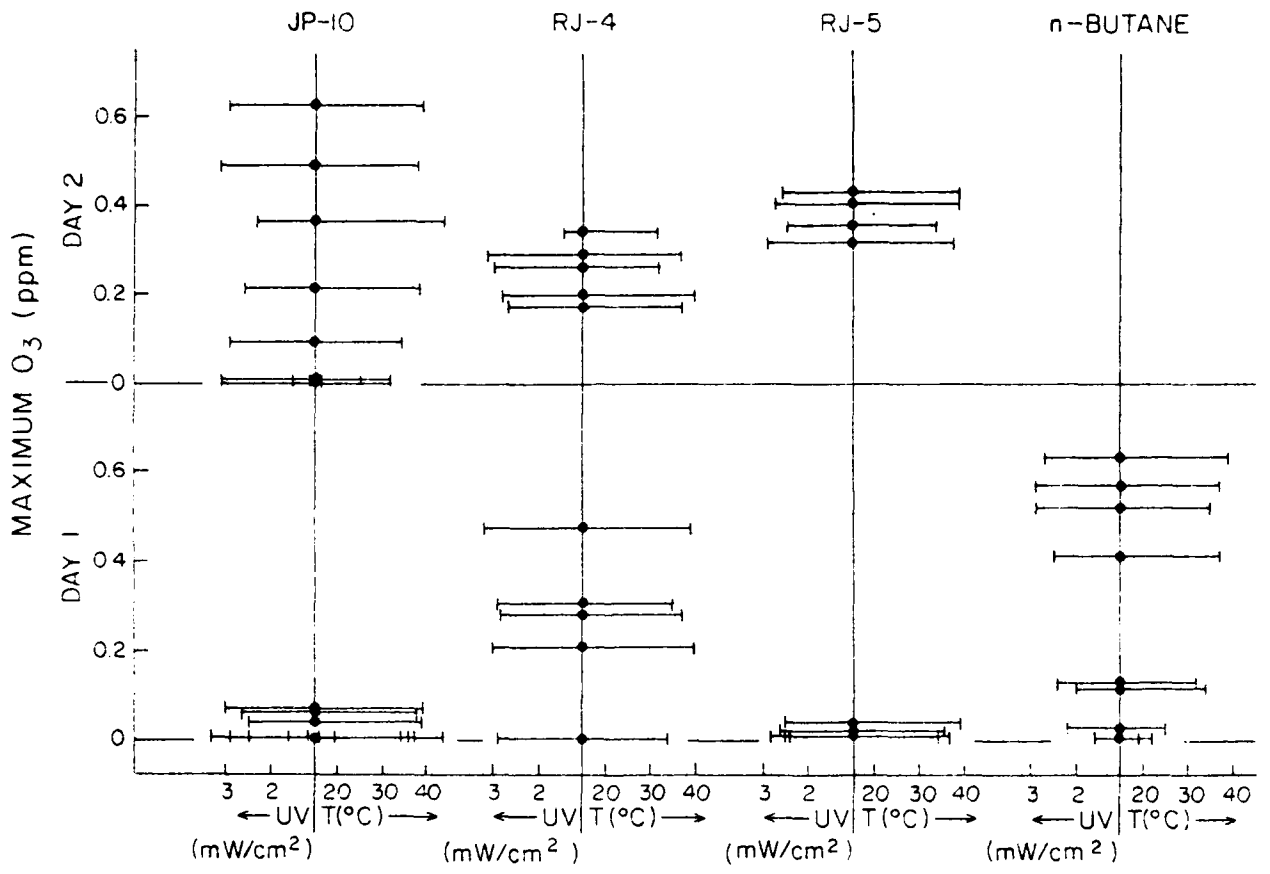

Figure 37. Plots of Day One and Day Two Maximum Ozone Yields Showing Average Temperatures and UV Intensities for the Standard Outdoor Chamber Runs Using JP-10, RJ-4, RJ-5, and Butane.

studied in this program are surprisingly similar, despite wide differences in their NO oxidation rates.

Aerosol Formation. The aerosol measurements obtained in these experiments varied widely and, unlike O_3 formation and NO oxidation rates, did not appear to be strongly correlated with meteorological conditions. While the cause of these variations is presently unknown, there are in some cases distinct differences in the distributions of these measurements, allowing some inter-fuel comparisons to be made. In Figure 38, the distributions are shown of four different types of aerosol measurements from the replicate runs for all of the military and commercial fuels studied in this program. Aerosol data for the n-butane runs are not shown in this figure, since the irradiation of n-butane-NO_x mixtures resulted in essentially no aerosol formation measured by any of the techniques employed. It should be noted that aerosol formation in the NO_x-air or pure air irradiations was also negligible. The lack of aerosol formation in the n-butane or control irradiations indicates that the aerosol formation observed from irradiation of NO_x-air mixtures containing the military and commercial fuels is real and not a chamber effect or other experimental artifact.

Figure 38 shows that fuels which formed more aerosol measured by one technique were not necessarily those which gave the highest aerosol readings as measured by another technique. The most dramatic examples of this were unleaded gasoline and diesel fuel. Generally, unleaded gasoline formed the highest aerosol volume (i.e., mass of aerosol) and condensation nuclei (i.e., number of particles), yet it was about average in light scattering (B_{scat}) capacity and appeared to form the smallest number of large particles (> 1 μ). On the other hand, diesel No. 2, which was also relatively high in the volume of aerosol formed, was by far the highest in terms of light scattering and in the formation of large (> 1 μ) particles, but was only average in terms of condensation nuclei formation. This suggests that while these two commercial fuels form similar amounts of aerosol material, unleaded gasoline produces a large numbers of small particles; diesel No. 2 produces a relatively small number of very large particles.

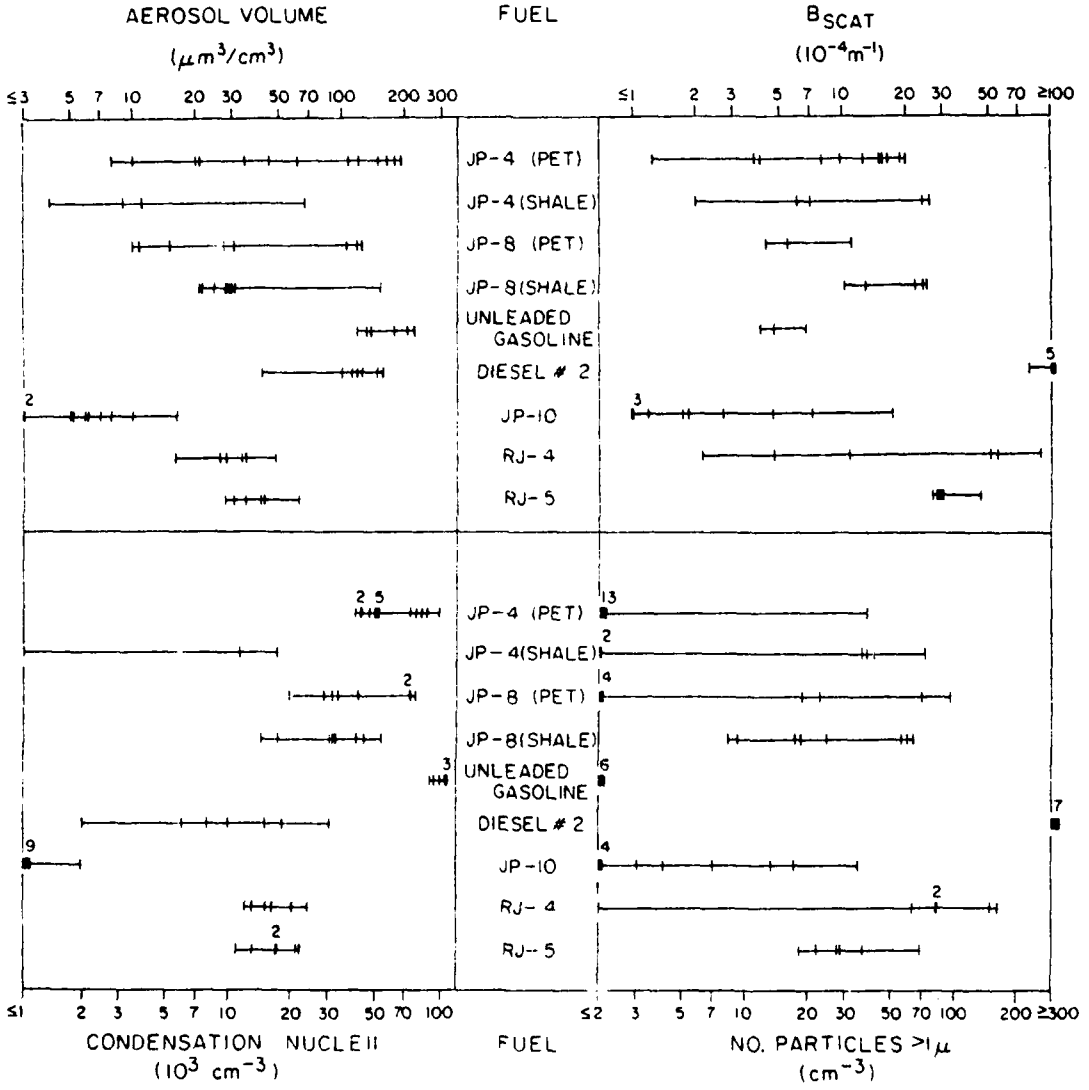

Figure 38. Plots of One-Day Maximum Values of Selected Aerosol Measurements Obtained in the Standard Outdoor Chamber Experiments.

In general, the military fuels formed a somewhat lesser volume of aerosol material than the commercial fuels and their size distribution appeared to be intermediate between the extremes defined by unleaded gasoline and diesel No. 2. In terms of aerosol volume, JP-4 (pet), both types of JP-8, RJ-4, and RJ-5 were similar; JP-4 (shale) appeared to form slightly less and JP-10 formed the least. The aerosol formed from JP-4 (pet) appeared to have more small particles, relative to the other military fuels. What little aerosol was formed from JP-10 appeared to have more large particles. When the variability of the aerosol results are taken into account, the particle size distributions for the remaining military fuels appear not to differ dramatically from each other and are probably in an intermediate range between those for JP-4 (pet) and JP-10.

4.2.4 Fuel Versus Fuel Runs

Because of the inherent variability of meteorological and physical parameters in outdoor chamber irradiations, experiments in which near-equal amounts of two different fuels are simultaneously irradiated in the chamber under dual-mode conditions are potentially the most useful. Dual chamber experiments compared all fuels to n-butane and compared JP-4 (shale), JP-8 (pet and shale), and commercial fuels with JP-4 (pet) (Section I). JP-10 was also compared with the other high energy fuels, RJ-4 and RJ-5. The major results of these direct intercomparison experiments are discussed in this section.

Since n-butane formed no observable aerosol and was sufficiently unreactive that n-butane-NO_x mixtures generally did not form their maximum ozone during the first day of irradiation, the results of the one-day fuel versus n-butane experiments were primarily useful for comparing NO oxidation rates. The observed NO oxidation rates, relative to that for n-butane, for all of the fuel-butane runs are shown in Figure 39. Since only one usable fuel-butane run was carried out for each fuel, the variability in these results cannot be assessed. However, these data indicate that the order of reactivity is: unleaded gasoline >> diesel No. 2 > JP-4 (pet) > JP-8 (shale) > JP-4 (shale) > JP-8 (pet) > n-butane > RJ-4 ≅ RJ-5 > JP-10. This order is consistent with the ranking obtained from comparing the NO oxidation rates observed in the full sets of standard runs (Section 4.2.3), except that the data from the standard runs could not be

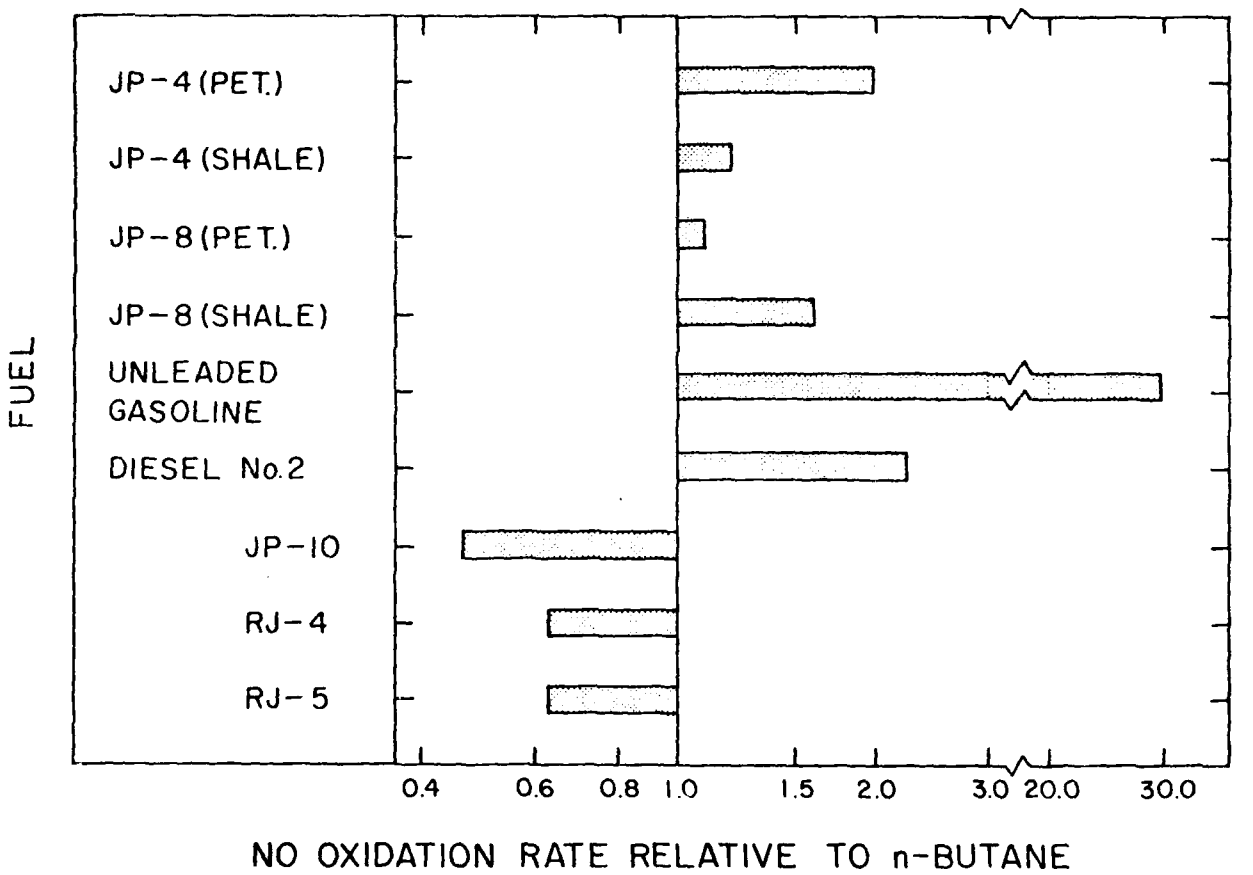

Figure 39. Plots of NO Oxidation Rates Observed in the Fuel-NO_x Sides, Relative to Those Observed in the n-Butane-NO_x Sides, in the Dual-Chamber Fuel vs n-Butane Runs.

used to determine if JP-8 (pet) was more reactive than n-butane or whether RJ-5 was any more reactive than JP-10. While the standard runs employing RJ-4 had, as a group, considerably higher NO oxidation rates than those employing RJ-5 (Figure 35), the data from the fuel-butane runs for RJ-4 and RJ-5 gave similar ratios of reactivity relative to n-butane (Figure 39). Because the replicate runs for RJ-4 and RJ-5 were generally done under similar meteorological conditions (Figure 35, Tables 28, 29), it can be concluded that RJ-4 produced somewhat higher NO oxidation rates than RJ-5.

Figures 40 and 41 show the ratio of the NO oxidation rates to the maximum O_3 yields observed in the fuel versus JP-4 (pet) and in the fuel versus JP-10 runs, respectively. Since two runs of each type were carried out, some indication of the variability of the data can be obtained, though it should be noted that in most cases the two runs comparing a given set of fuels were conducted at approximately the same time under similar meteorological conditions. It can be seen that reasonably good agreement between relative NO oxidation rates were obtained in the replicate runs and the order of reactivity is consistent with that derived by comparing either the replicate standard runs or the fuel versus n-butane runs. The maximum O_3 yield data were more variable, and it is probably more useful to use the results of the replicate standard runs for comparing the maximum O_3-forming potential of the fuels. This is because, depending on the relative NO oxidation rates of the two fuels being compared and the meteorological conditions of the particular fuel versus fuel runs, the observed ratios of the O_3 yields could reflect two things: (a) the relative NO oxidation rates, if the run was done under conditions of low temperature and light intensity and/or if both fuels have relatively low NO oxidation rates; or (b) the NO oxidation rate for one fuel and the O_3-forming potential for the other (i.e., if one fuel reaches maximum O_3 while the other does not). Thus, only under certain conditions would the ratio of ozone yields reflect the O_3-forming potentials for both fuels. Since the replicate standard runs were generally carried out under a wider variety of conditions, it is likely that at least one run for any fuel would be done under conditions favorable for maximum O_3 formation.

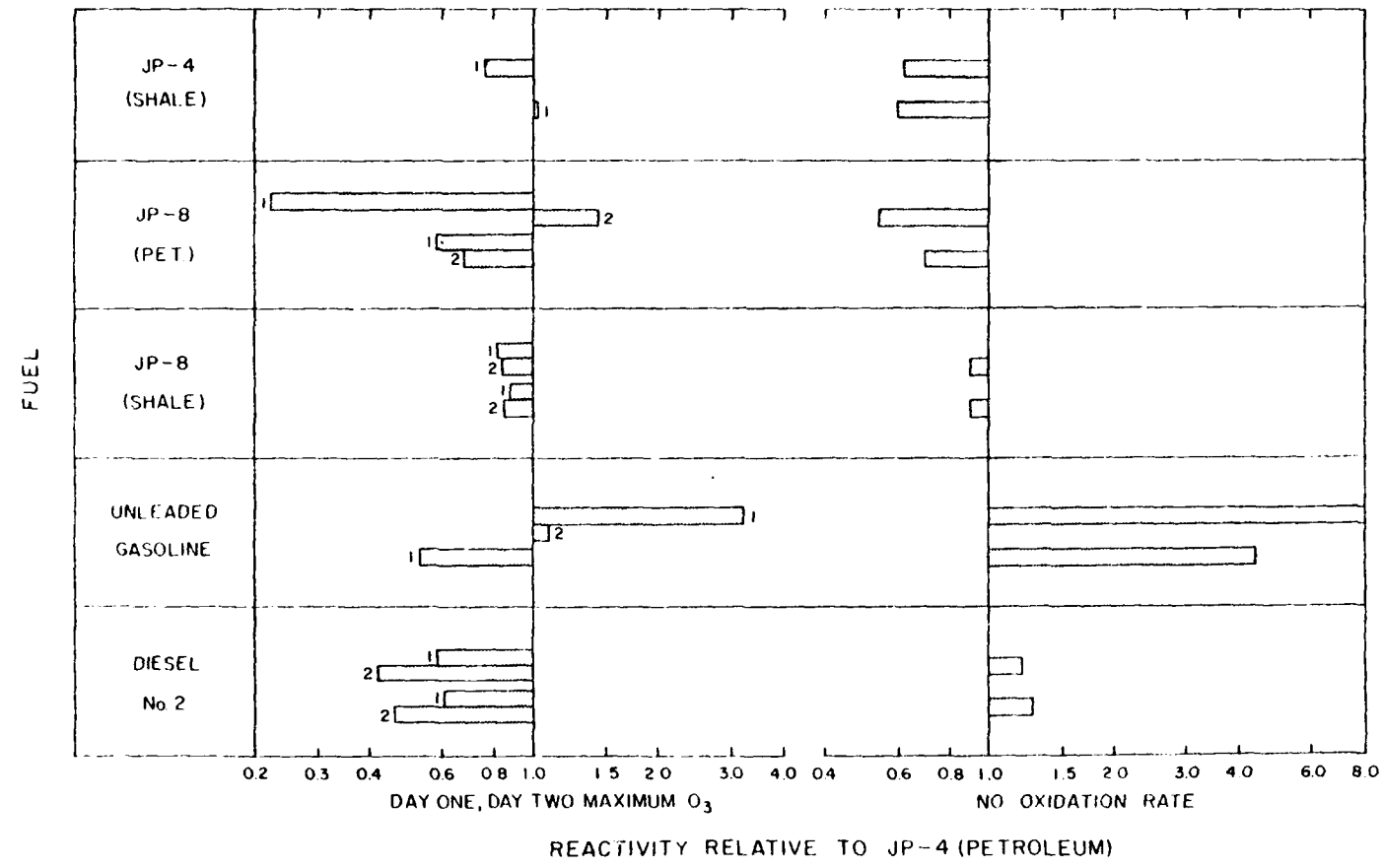

Figure 40. Plots of Ratios of NO Oxidation Rates and Day One and Day Two Maximum Yields Observed in the Fuel-NO_x Sides, Relative to Those Observed in the JP-4(Pet)-NO_x Sides, in the Dual-Chamber Fuel vs JP-4(Pet) Runs.

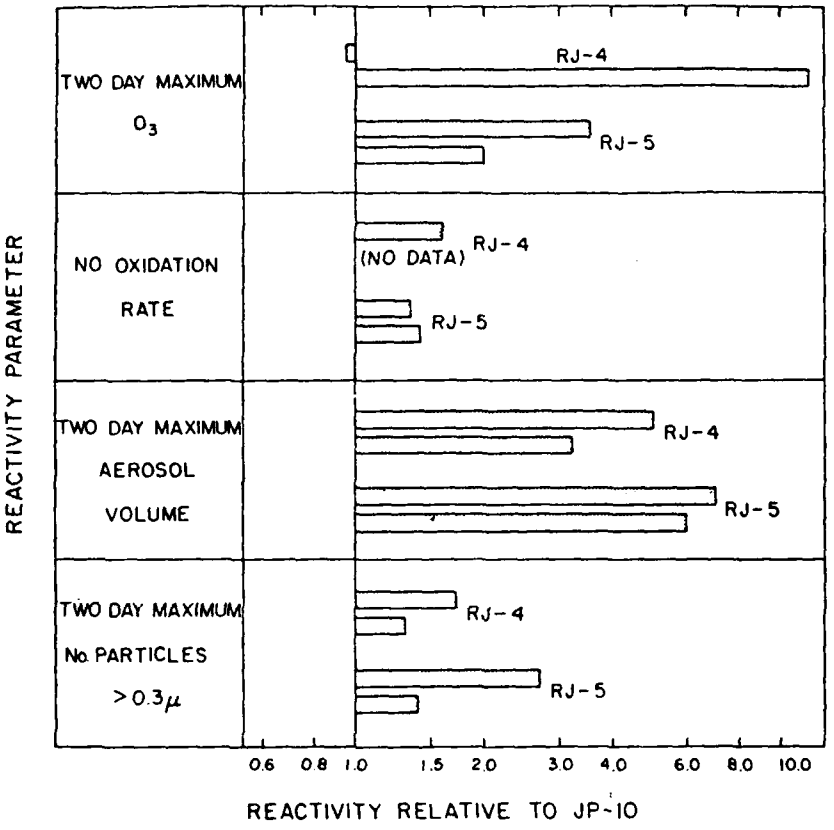

Figure 41. Plots of Ratios of Selected Reactivity Parameters Observed in the Fuel-NO_x Sides, Relative to Those Observed in the JP-10-NO_x Sides, in the Dual-Chamber Fuel vs JP-10 Irradiations.

The ratios of selected aerosol data obtained from the RJ-4 and RJ-5 versus JP-10 runs are shown in Figure 41. These results indicate JP-10 formed less aerosol volume than did RJ-4 or RJ-5, but JP-10 formed relatively large (> 0.3 μ) particles. This is consistent with the results of the replicate standard runs shown in Figure 38 (Section 4.2.3), since the differences between the JP-10 and the other high energy fuels were less when the number of particles > 0.3 μ was measured than when aerosol volume was measured.

Ratios of selected aerosol data from the fuel versus JP-4 (pet) runs are shown in Figure 42. These data are reasonably consistent with the results of the replicate runs shown in Figure 38, when the variability inherent in the aerosol measurements is considered. The data confirm that unleaded gasoline and diesel No. 2 formed measurably more aerosol material than did the other fuels, while JP-4 (pet) and the two JP-8 fuels formed comparable amounts of aerosols. Furthermore, the data in Figure 42 indicate that JP-4 (shale) formed measurably less aerosol than the other fuels from the replicate runs are more ambiguous regarding this point (Figure 38). These data also indicate that JP-4 (pet) formed fewer larger particles as well as particles in the light scattering range than the other fuels, with the possible exception of JP-4 (shale). However, in many cases the inherent variability of the aerosol data from only two runs clearly precludes drawing any firm conclusions about differences in aerosol size distribution.

4.2.5 Effect of Initial Reactant Concentrations

For each of the nine fuels studied in this program, one two-day dual-chamber experiment was performed in which the initial concentration of the fuel was varied, while the NO_x was held constant; another two-day dual-chamber experiment was performed in which the initial NO_x was varied, while the fuel concentration was held constant. In all cases, a standard run (~25 ppmC fuel, 0.5 ppm NO_x) was carried out in one side of the chamber, and the variable-NO_x runs were conducted by injecting half the normal amount of NO_x in the "low NO_x" side. In the variable-fuel runs employing JP-4, unleaded gasoline, and diesel No. 2, the fuel was varied by injecting half the standard amount of fuel on the "low fuel" side. For the other, generally less reactive fuels (JP-8, JP-10, RJ-4, and RJ-5),

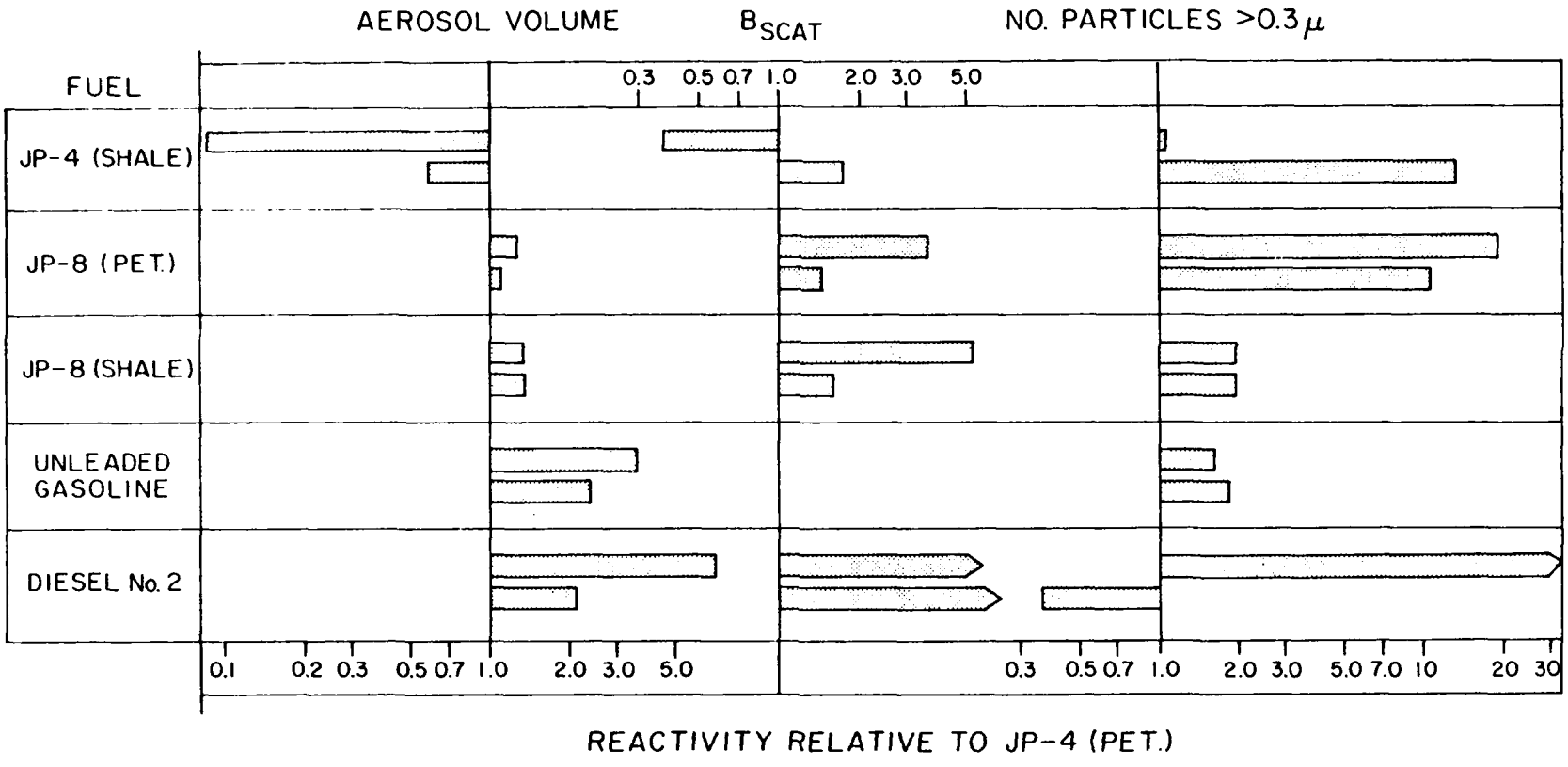

ıre 42. Plots of Ratios of Selected One-Day Maximum Aerosol Values Observed in the Fuel-NO_x Sides, Relative to Those Observed in the JP-4(Pet)-NO_x Sides, in the Dual-Chamber Fuel vs JP-4(Pet) Irradiations.

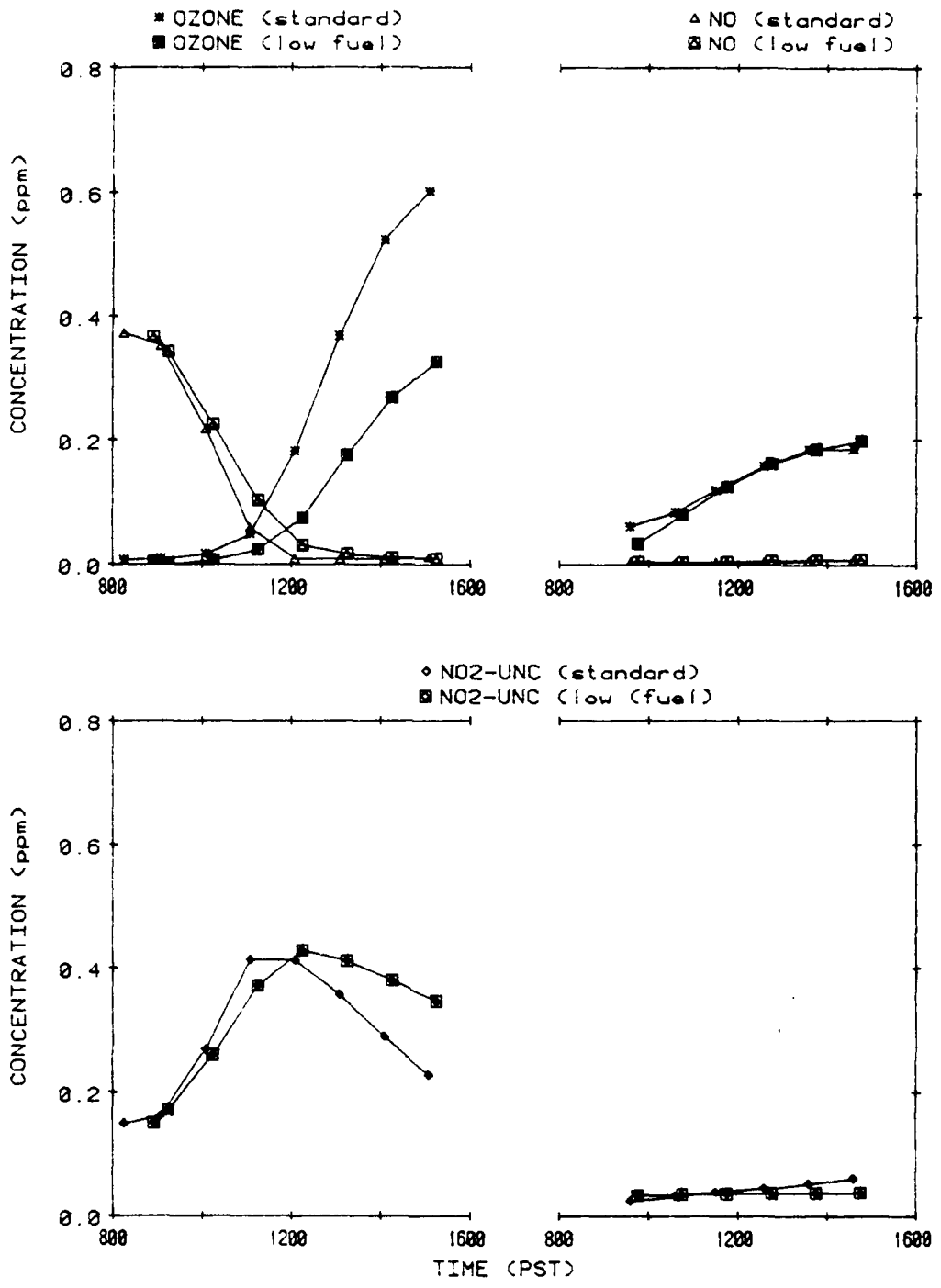

Figure 43. Concentration-Time Profiles for O_3, NO, and NO_2 for the JP-4 (Pet) Variable Initial Fuel Run AFF-34.

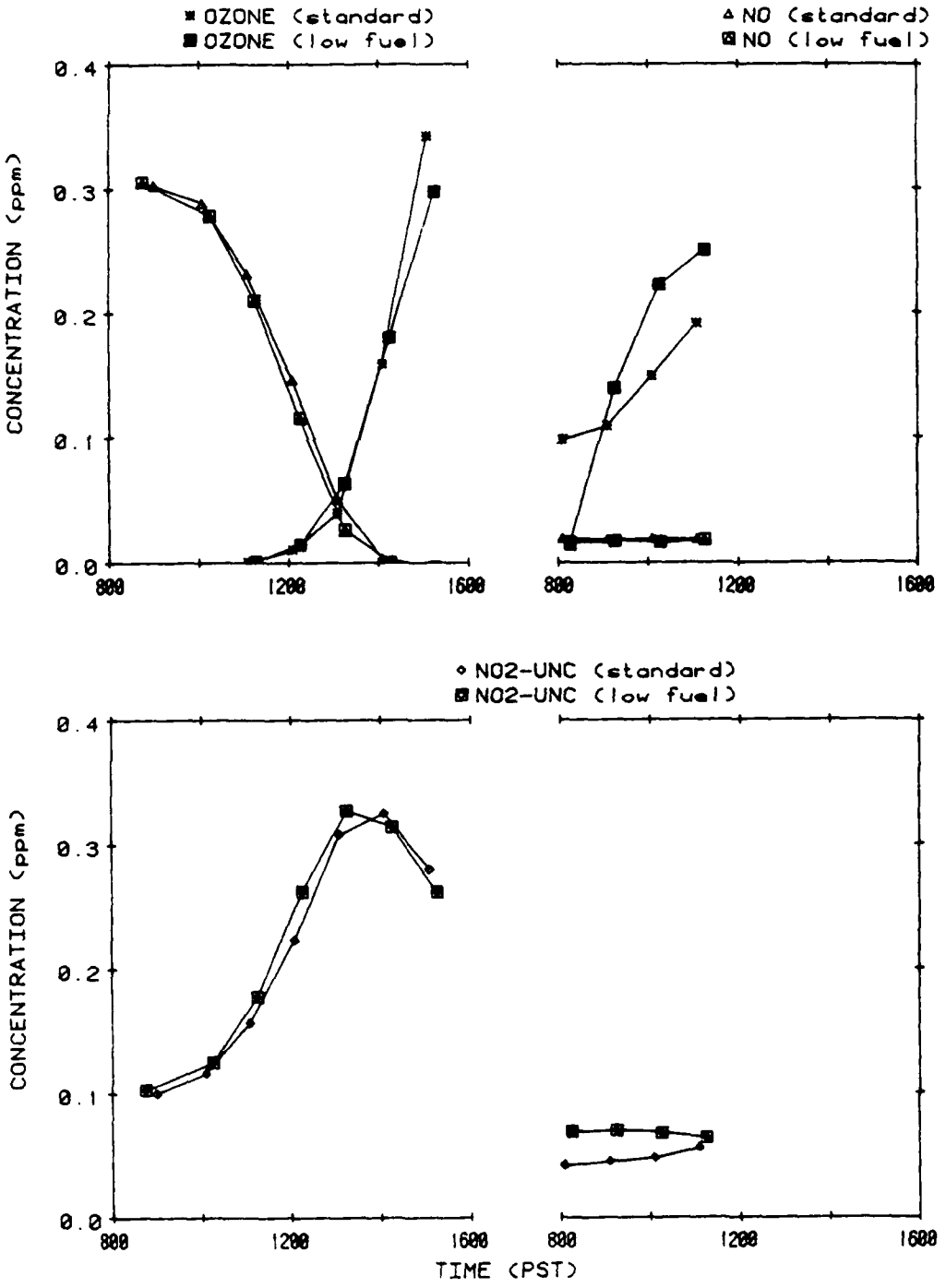

Figure 44. Concentration-Time Profiles for O_3, NO, and NO_2 for the JP-4 (Shale) Variable Initial Fuel Run AFF-9.

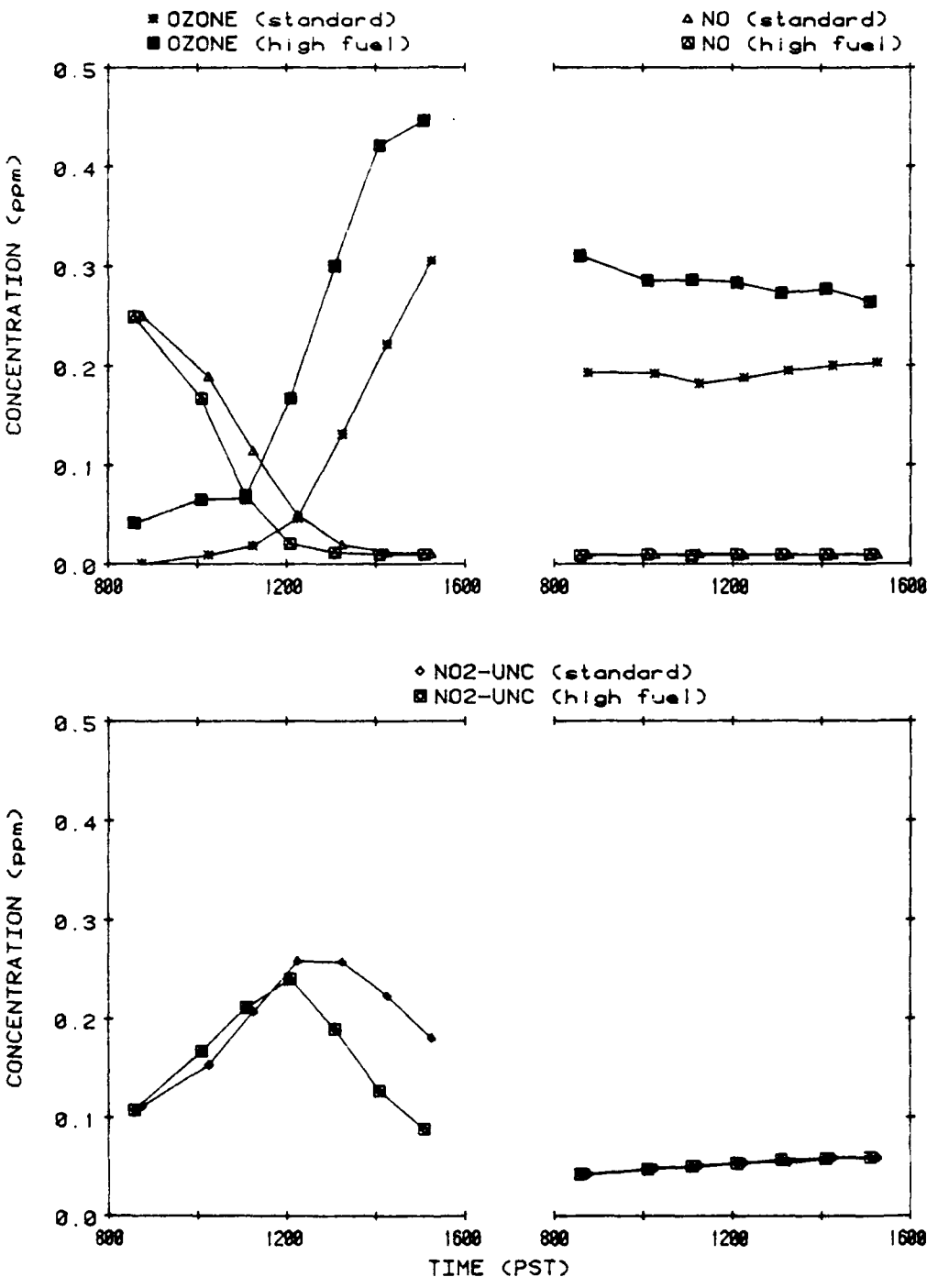

Figure 45. Concentration-Time Profiles for O_3, NO, and NO_2 for the JP-8 (Pet) Variable Initial Fuel Run AFF-71.

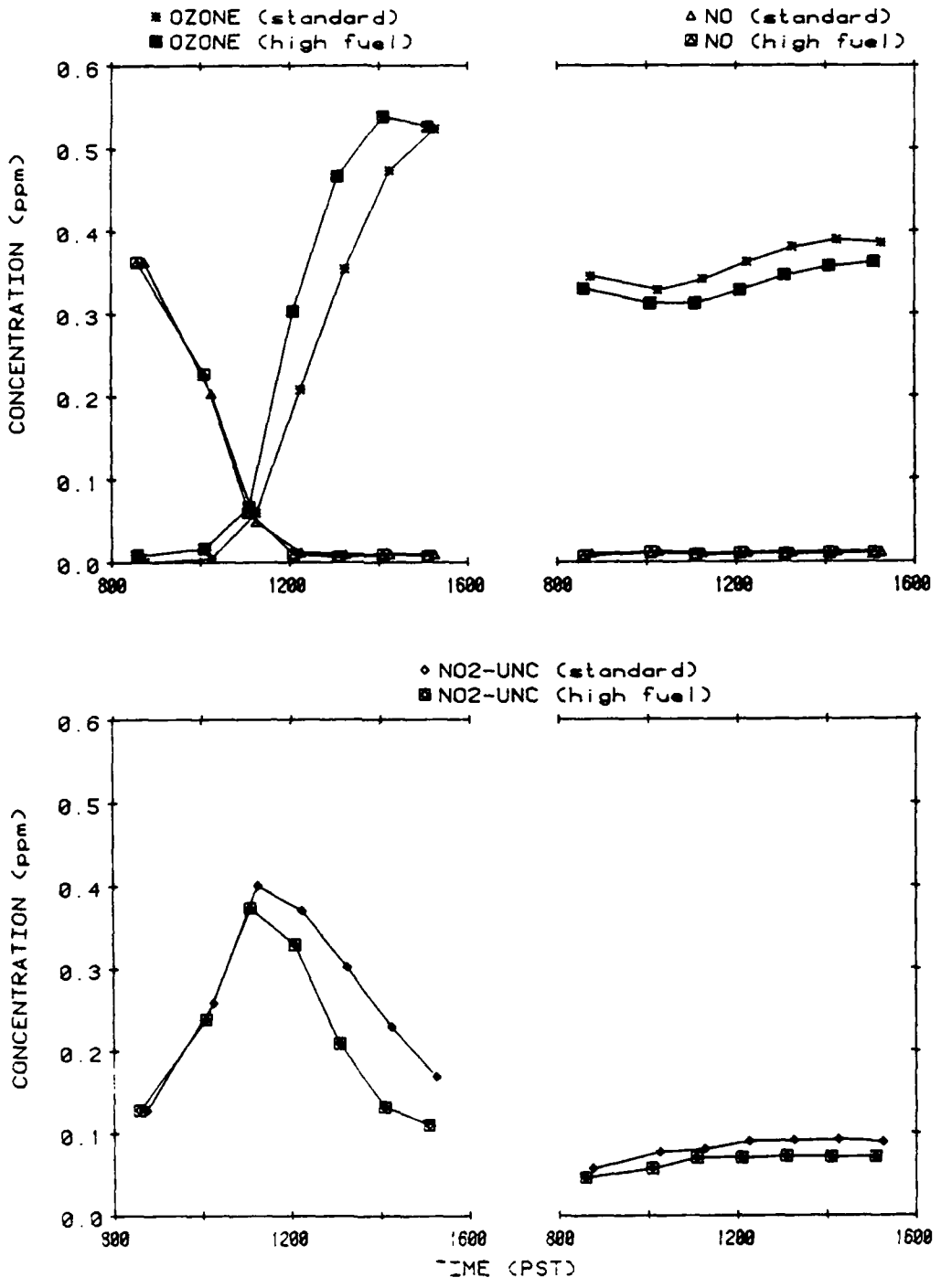

Figure 46. Concentration-Time Profiles for O_3, NO, and NO_2 for the JP-8 (Shale) Variable Initial Fuel Run AFF-81.

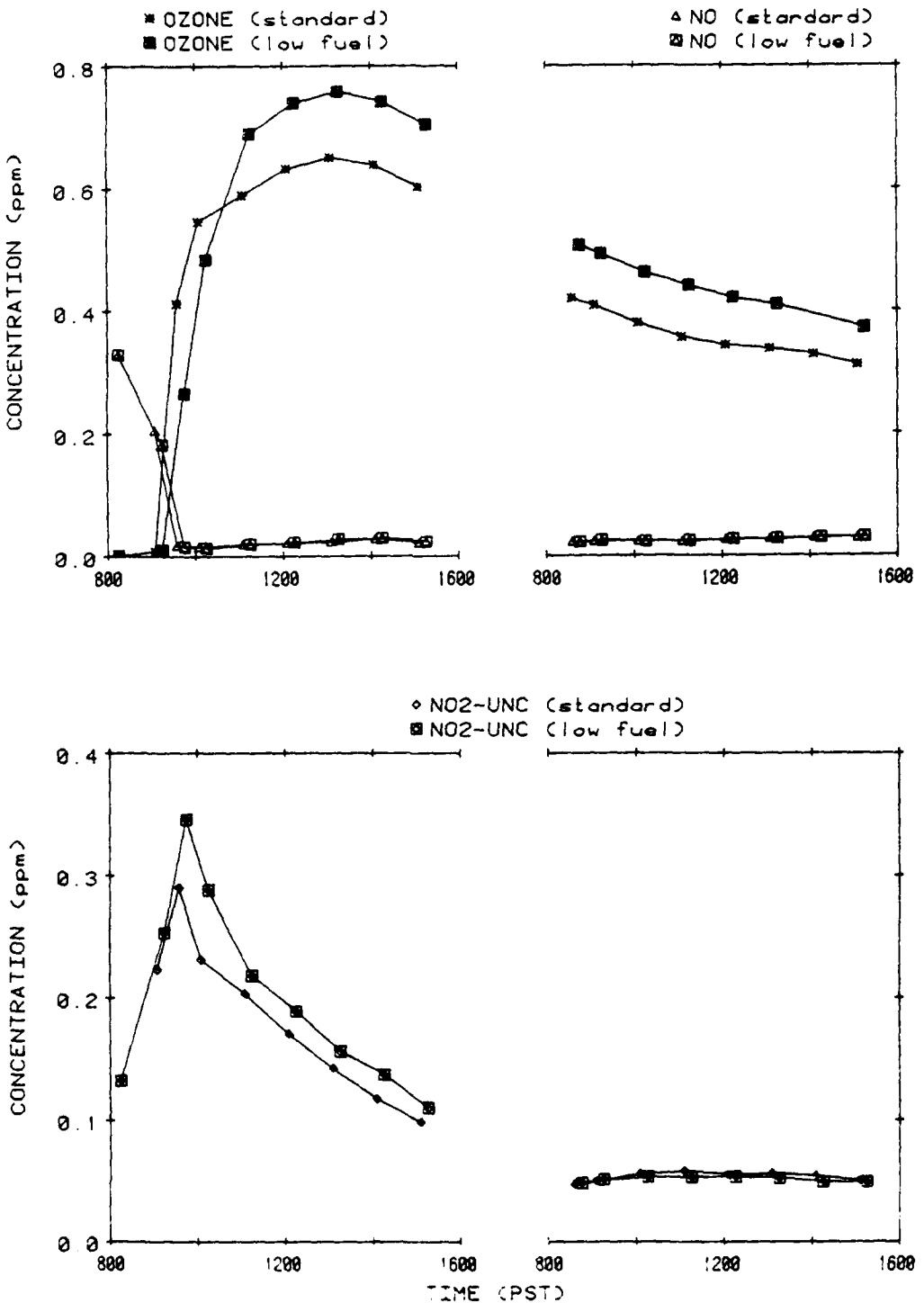

Figure 47. Concentration-Time Profiles for O_3, NO, and NO_2 for the Unleaded Gasoline Variable Initial Fuel Run AFF-42.

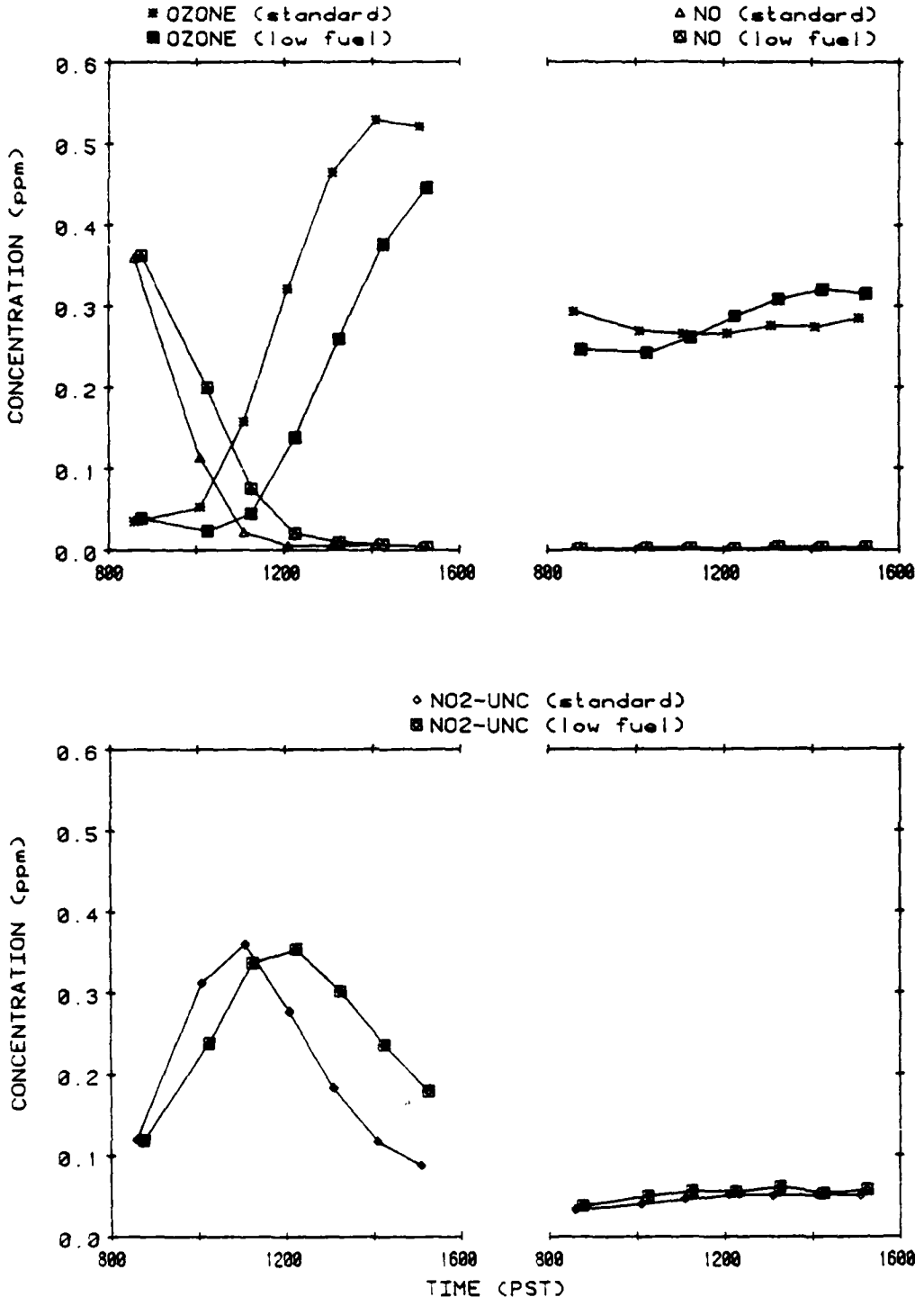

Figure 48. Concentration-Time Profiles for O_3, NO, and NO_2 for the Diesel No. 2 Variable Initial Fuel Run AFF-125.

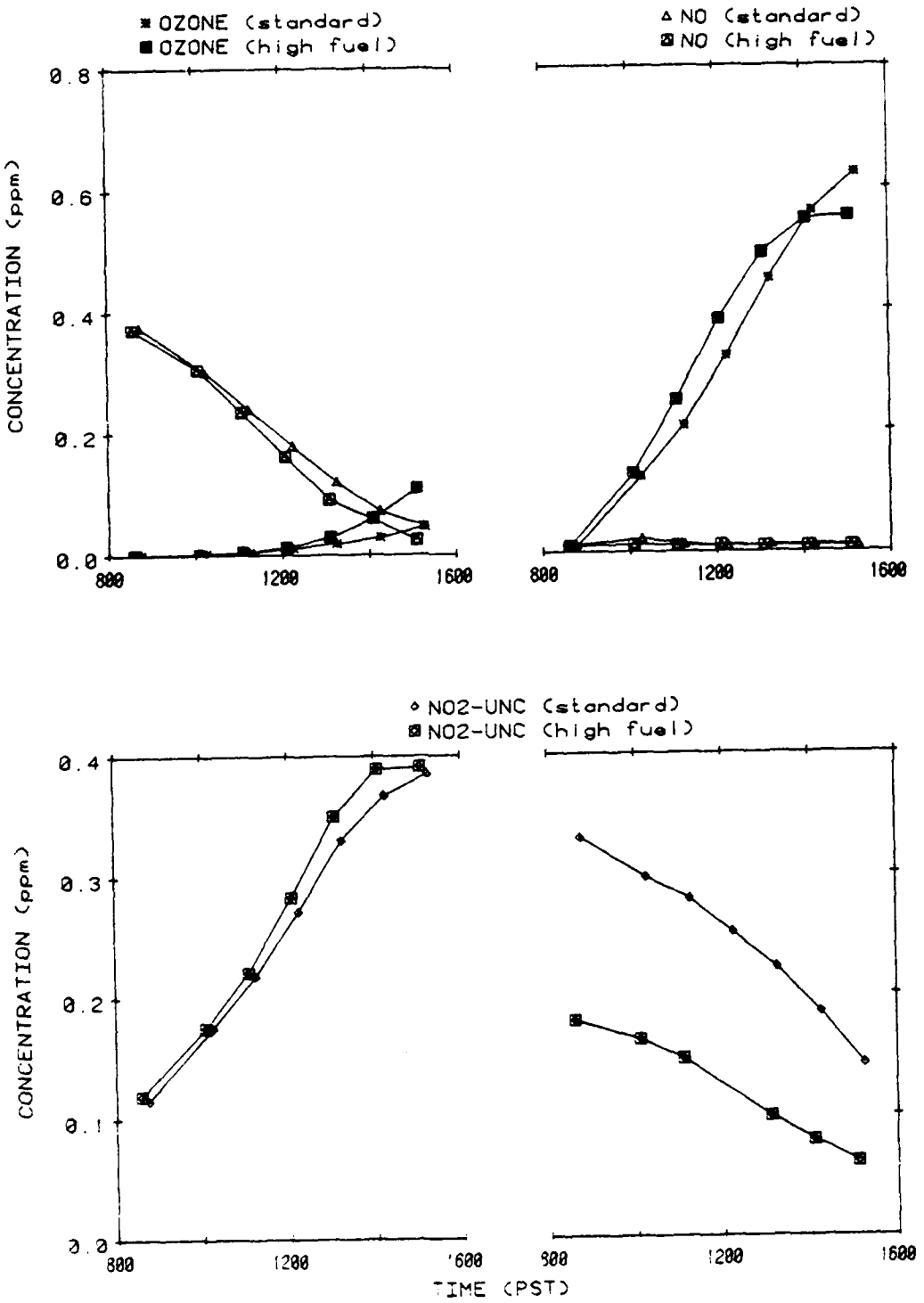

Figure 49. Concentration-Time Profiles for O_3, NO, and NO_2 for the JP-10 Variable Initial Fuel Run AFF 101.

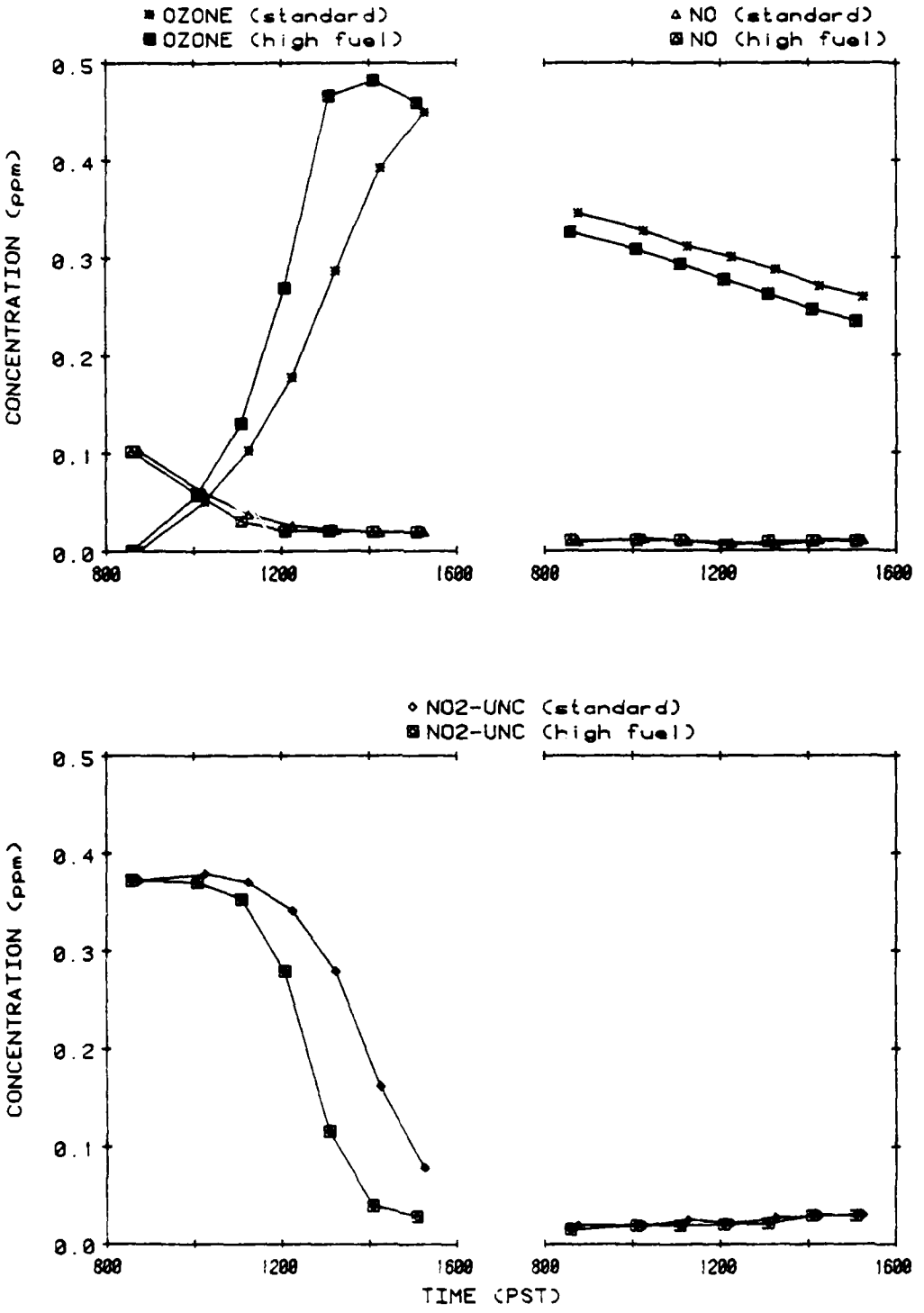

Figure 50. Concentration-Time Profiles for O_3, NO, and NO_2 for the RJ-4 Variable Initial Fuel Run AFF-100.

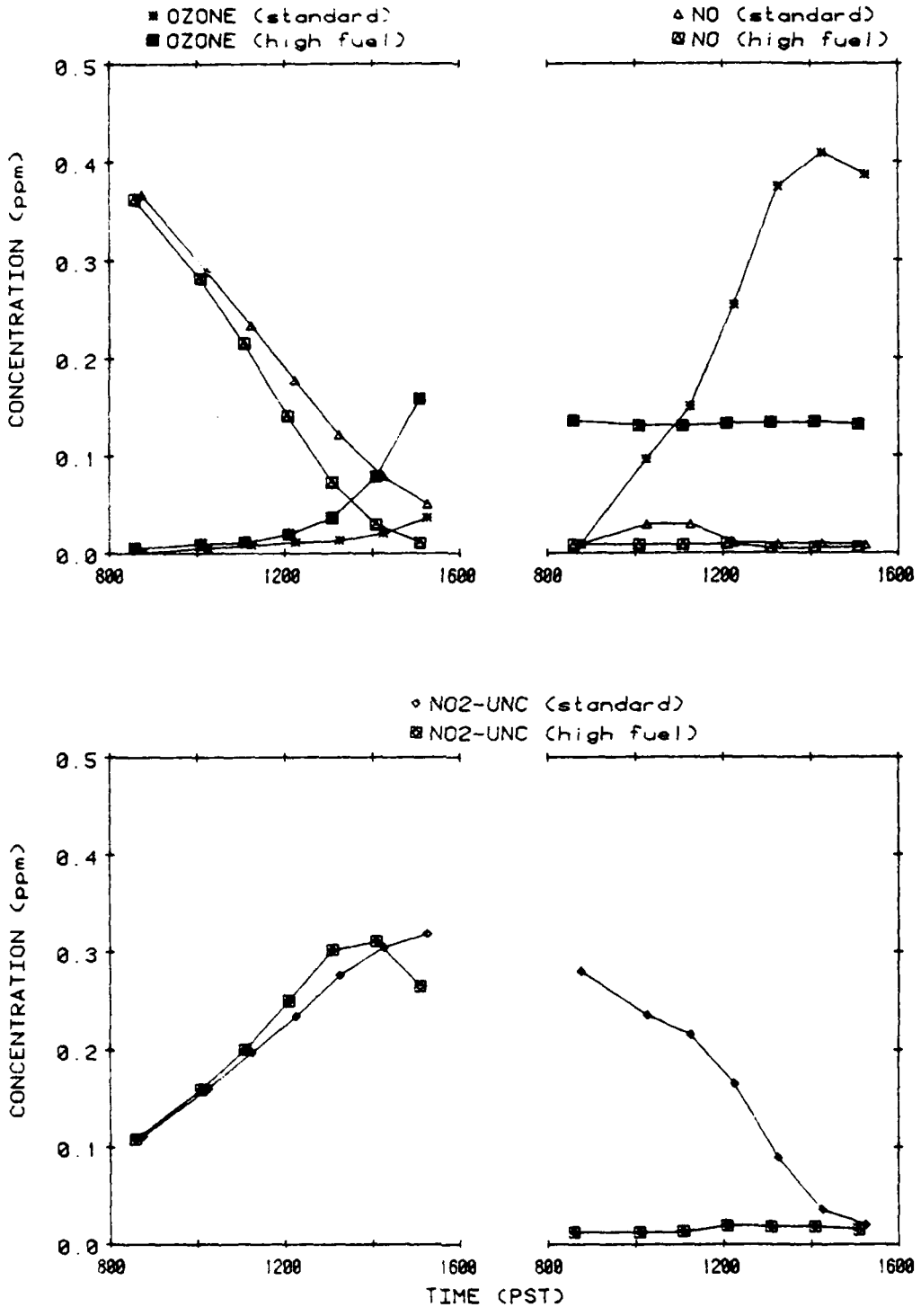

Figure 51. Concentration-Time Profiles for O_3, NO, and NO_2 for the RJ-5 Variable Initial Fuel Run AFF-111.

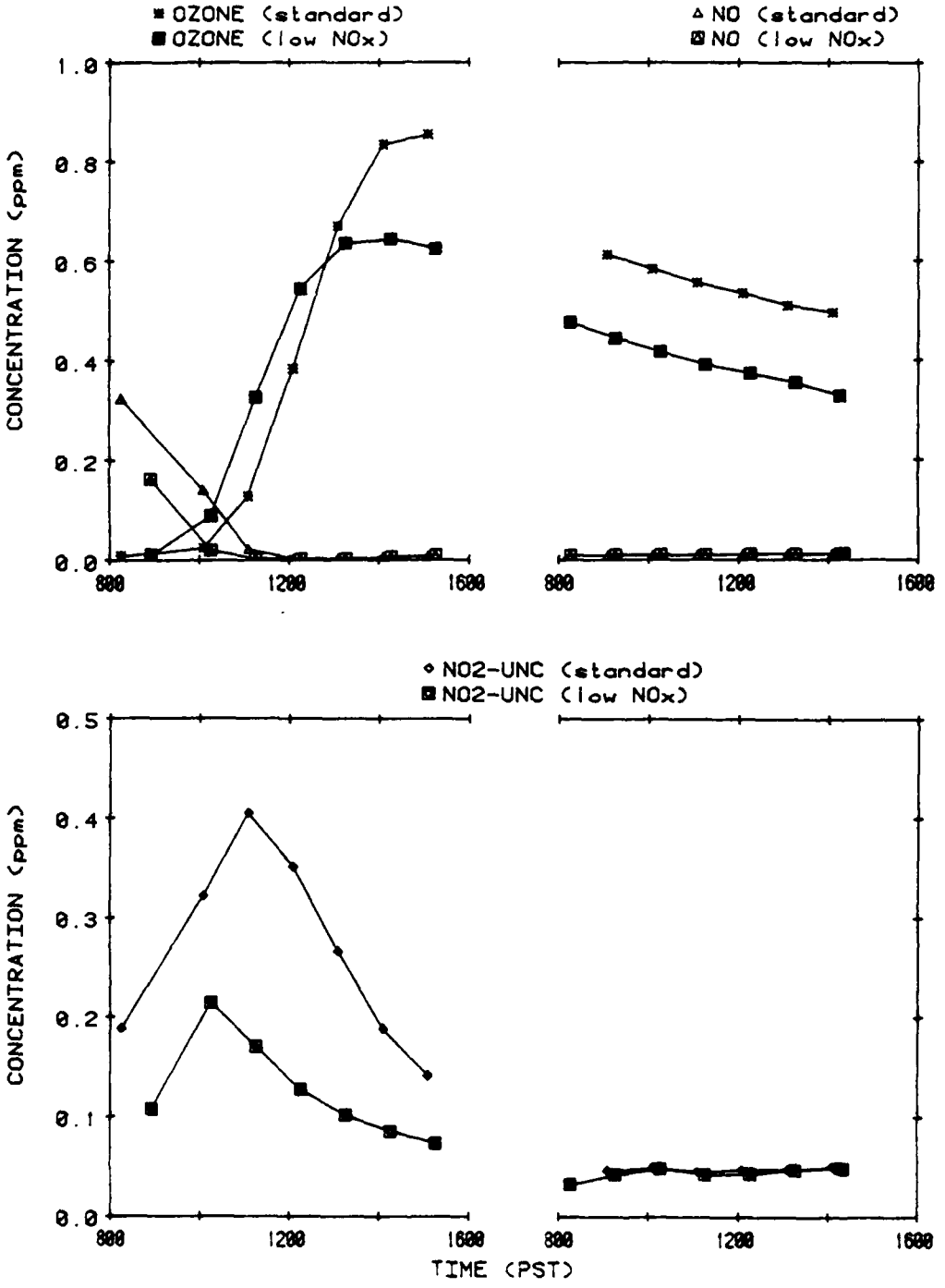

Figure 52. Concentration-Time Profiles for O_3, NO, and NO_2 for the JP-4 (Pet) Variable Initial NO_x Run AFF-32.

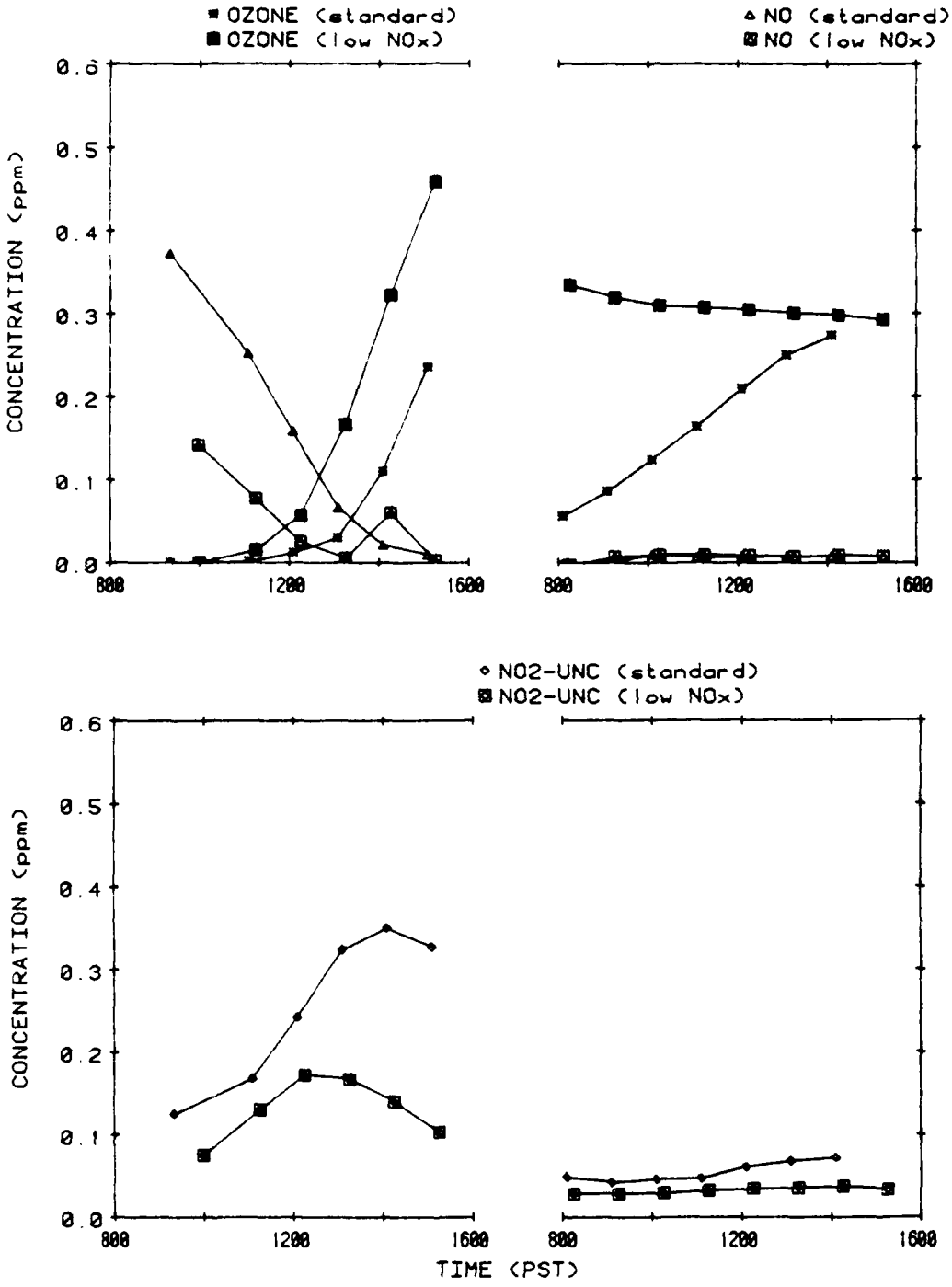

Figure 53. Concentration-Time Profiles for O_3, NO, and NO_2 for the JP-4 (Shale) Variable Initial NO_x Run AFF-10.

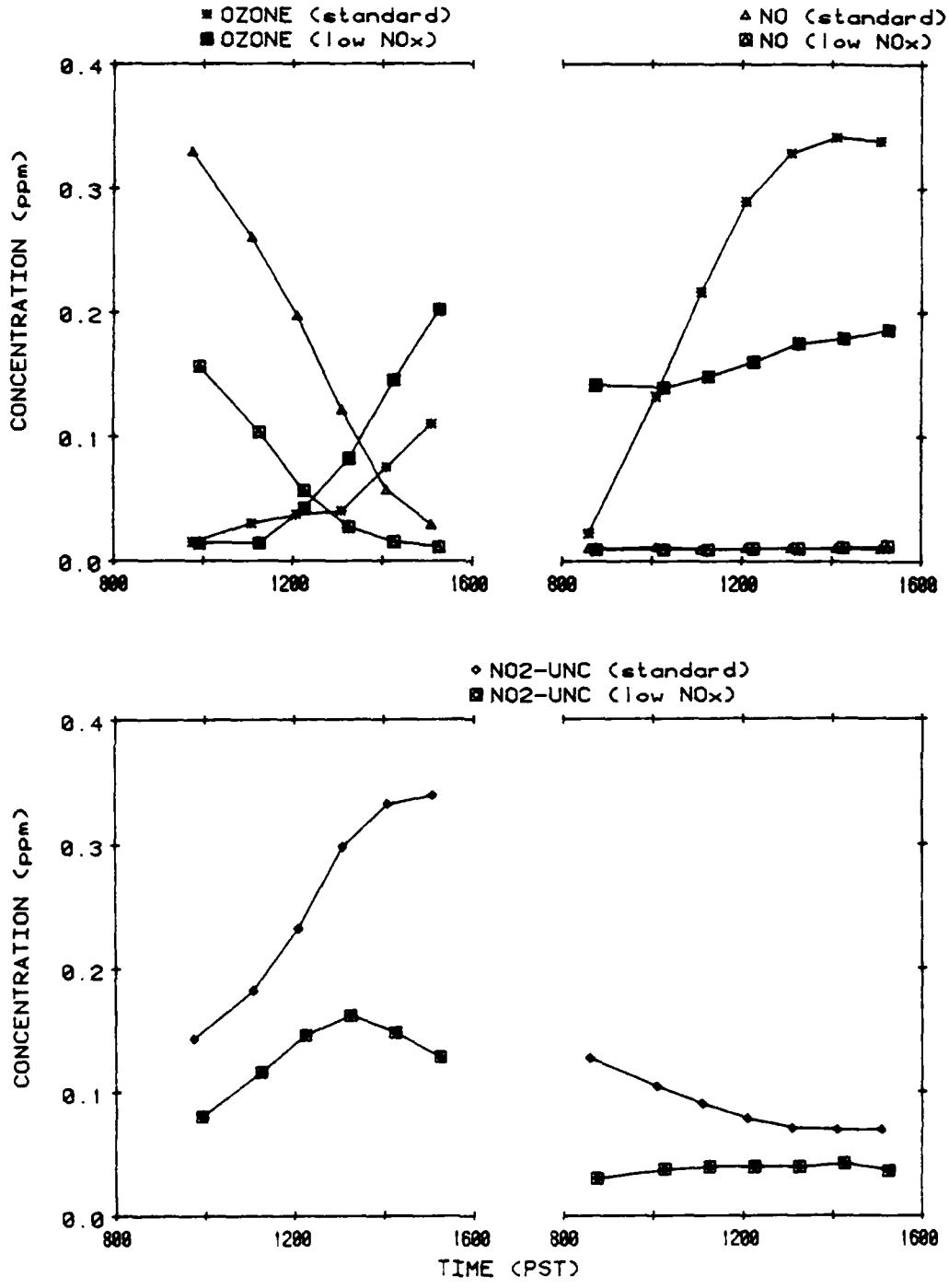

Figure 54. Concentration-Time Profiles for O_3, NO, and NO_2 for the JP-8 (Pet) Variable Initial NO_x Run AFF-70.

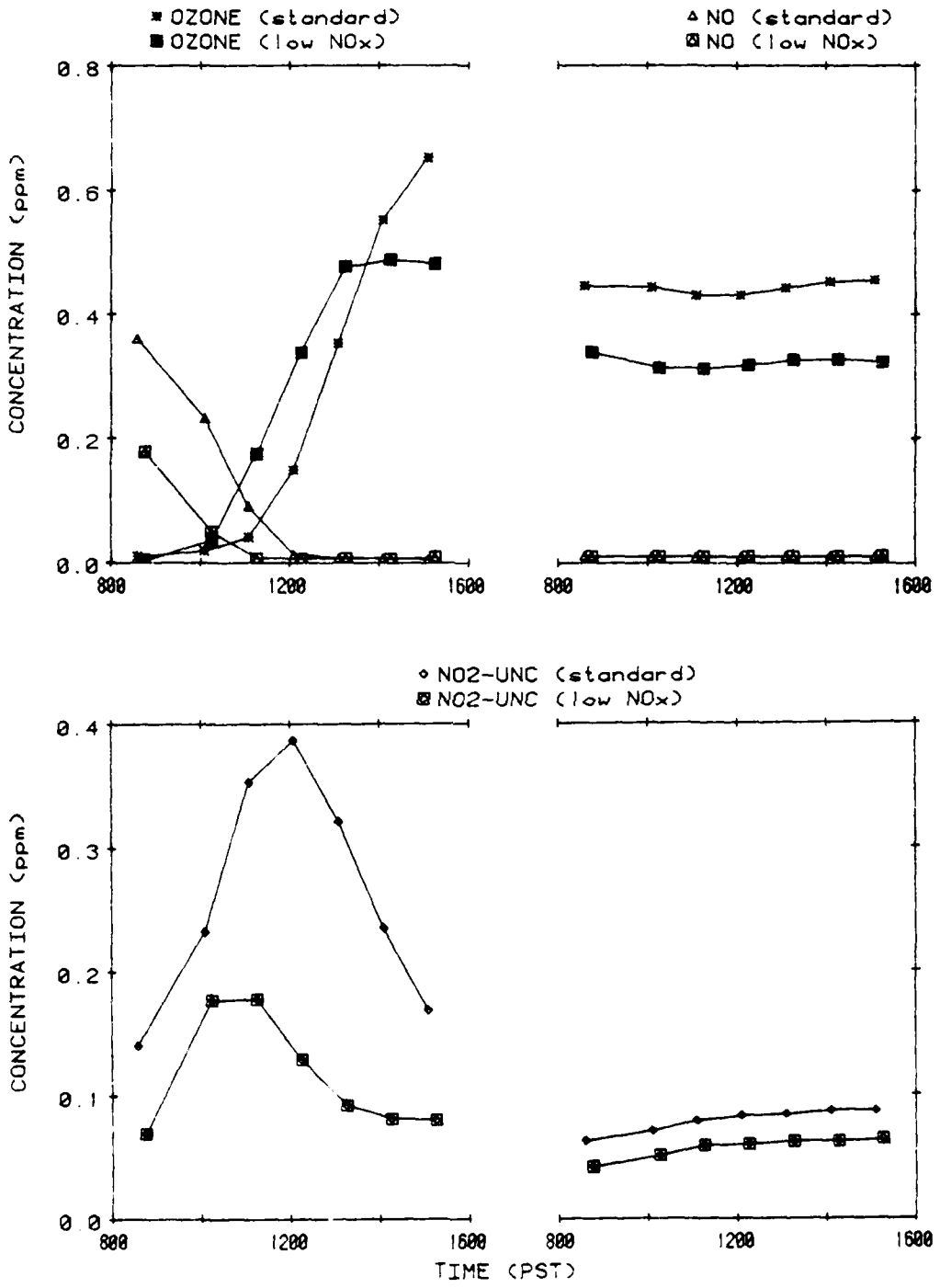

Figure 55. Concentration-Time Profiles for O_3, NO, and NO_2 for the JP-8(Shale) Variable Initial NO_x Run AFF-80.

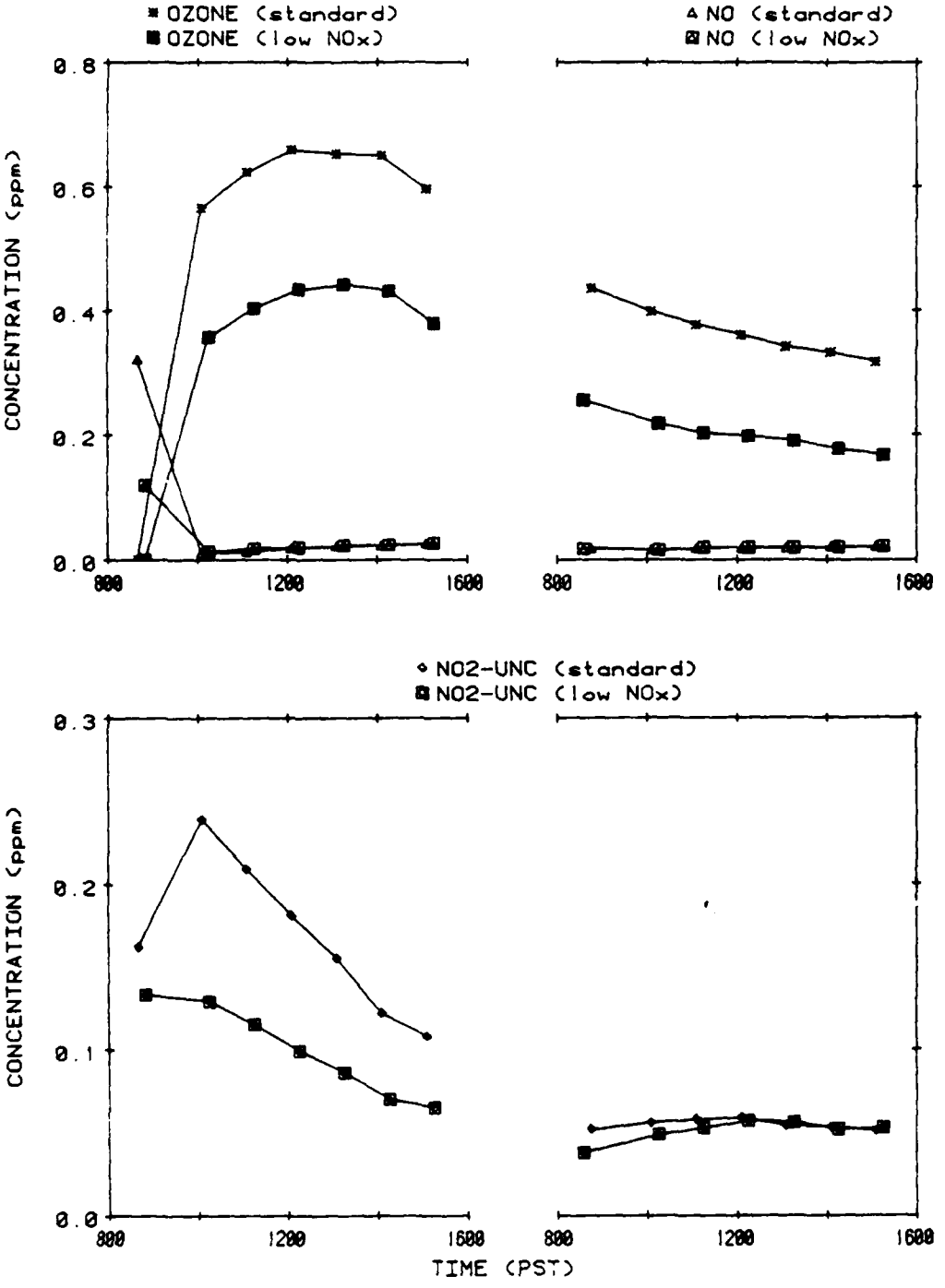

Figure 56. Concentration-Time Profiles for O_3, NO, and NO_2 for the Unleaded Gasoline Variable Initial NO_x Run AFF-40.

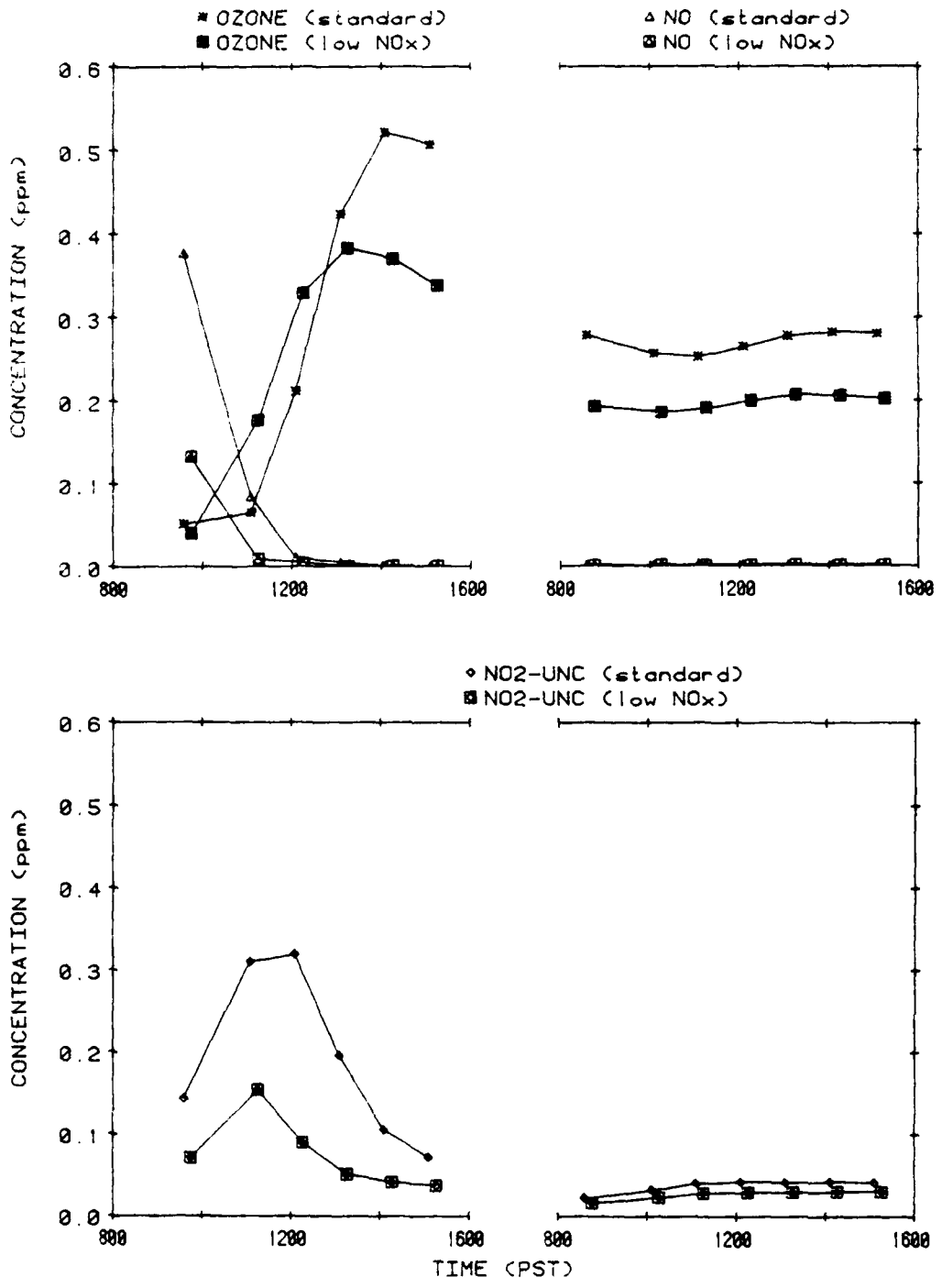

Figure 57. Concentration-Time Profiles for O_3, NO, and NO_2 for the Diesel No. 2 Variable Initial NO_x Run AFF-124.

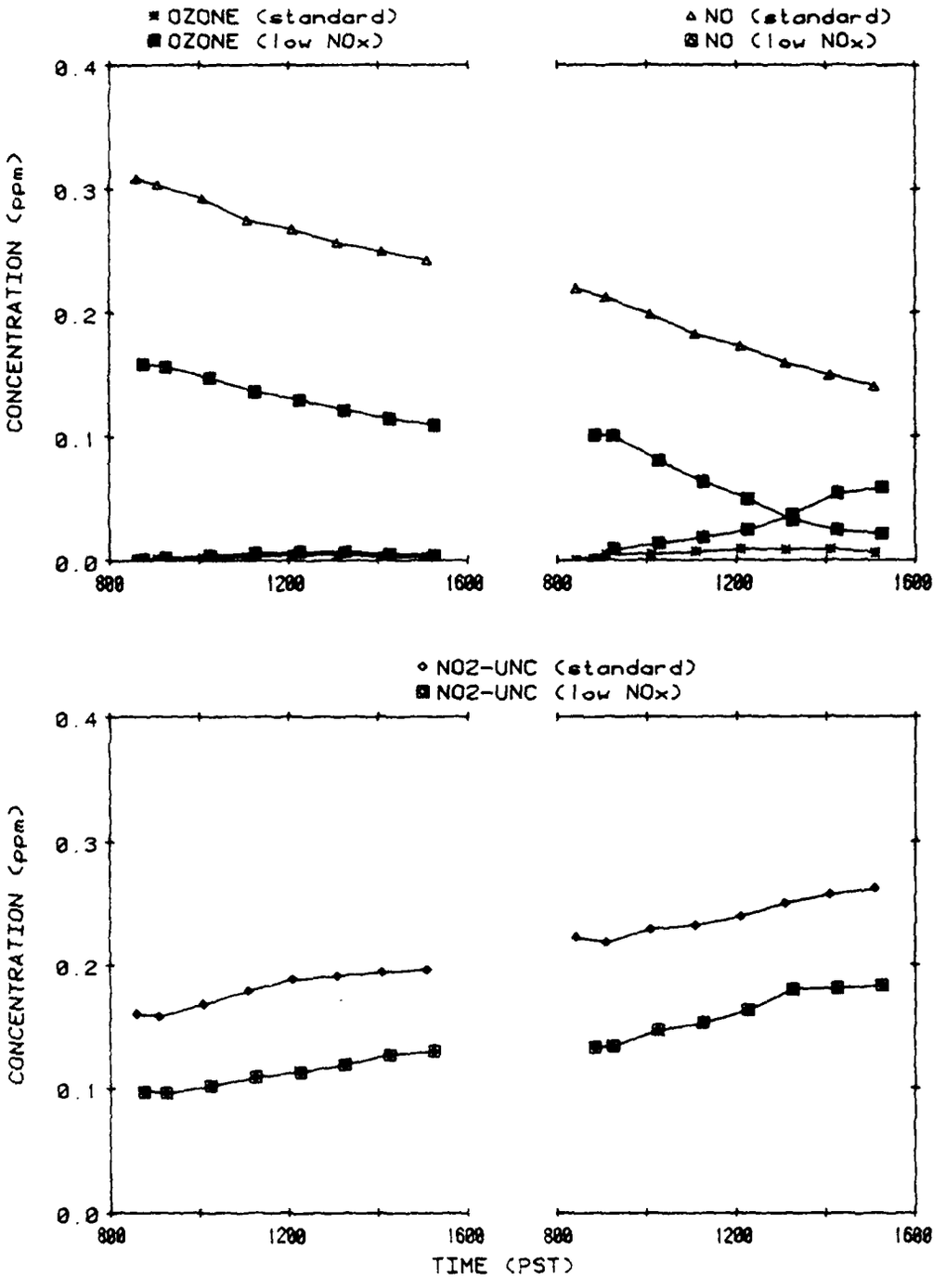

Figure 58. Concentration-Time Profiles for O_3, NO, and NO_2 for the JP-10 Variable Initial NO_x Run AFF-52.

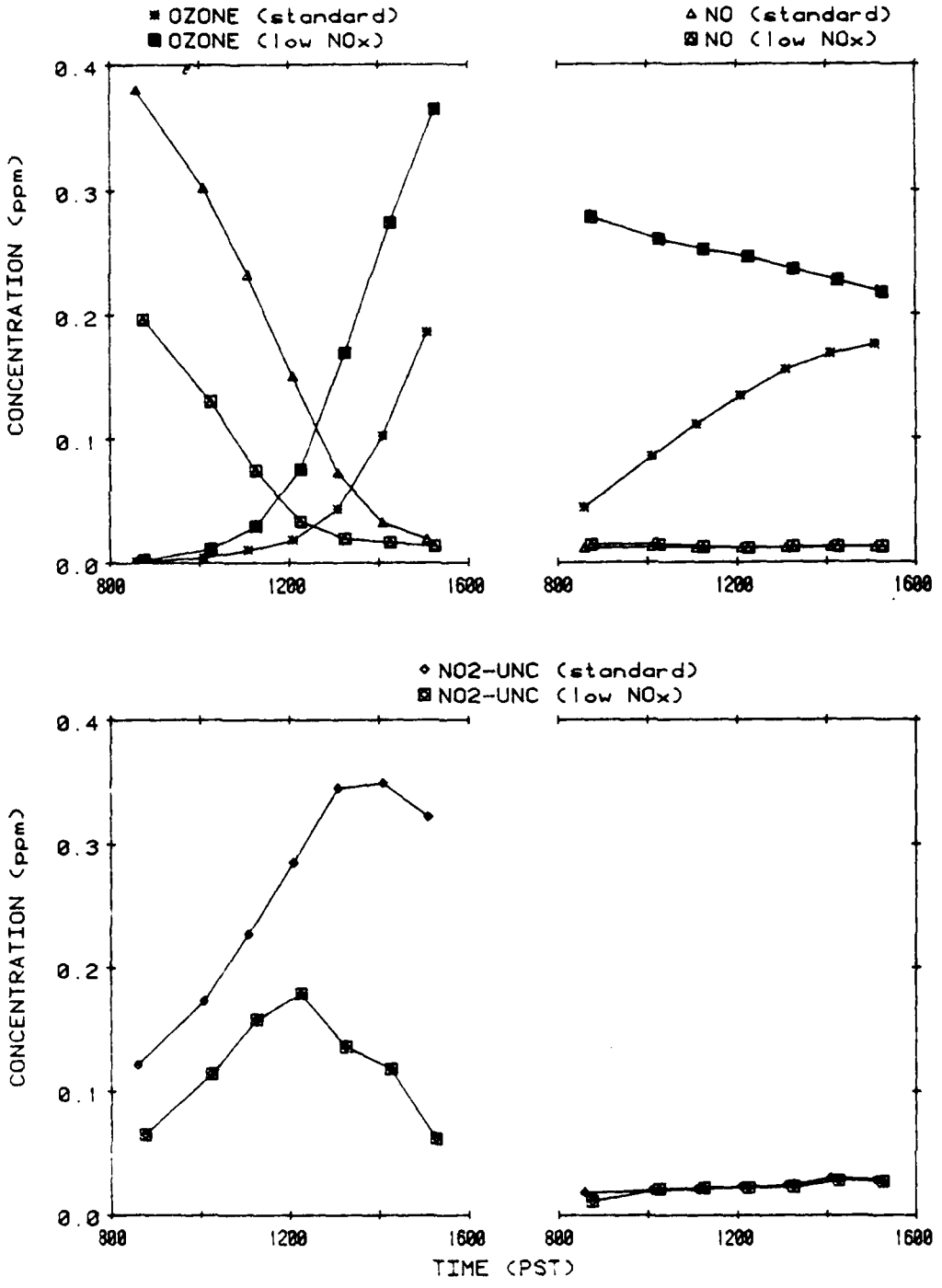

Figure 59. Concentration-Time Profiles for O_3, NO, and NO_2 for the RJ-4 Variable Initial NO_x Run AFF-97.

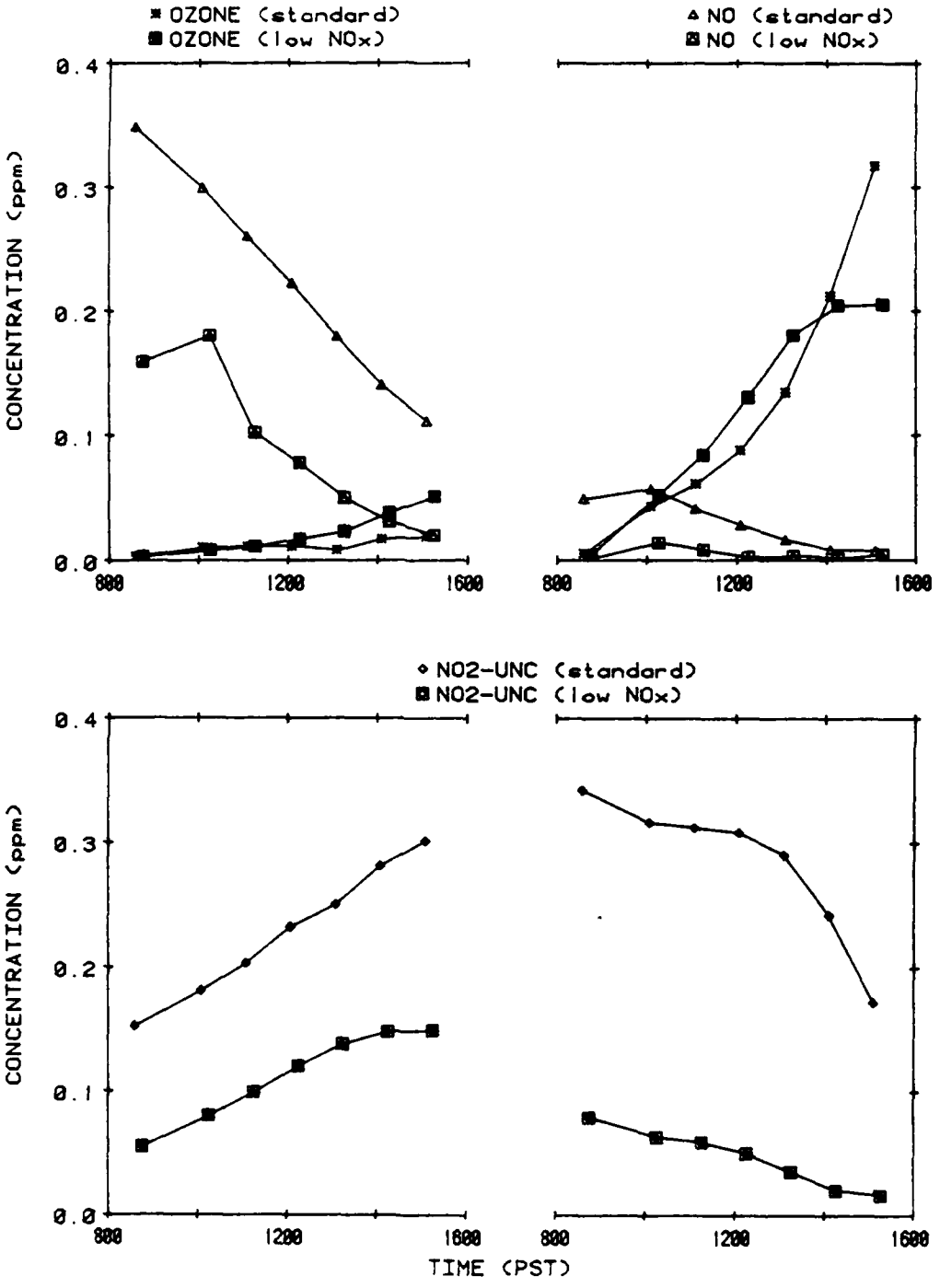

Figure 60. Concentration-Time Profiles for O_3, NO, and NO_2 for the RJ-5 Variable Initial NO_x Run AFF-110.

TABLE 34. RATIOS OF SELECTED REACTIVITY PARAMETERS OBSERVED IN THE VARIABLE INITIAL FUEL AND VARIABLE INITIAL NO_x DUAL-OUTDOOR CHAMBER RUNS.

	Relative Reactivity							
	High Fuel/Low Fuel				High NO_x/Low NO_x			
Fuel	NO Oxid. Rate	O_3 Maximum Day 1	O_3 Maximum Day 2	Aerosol Volume	NO Oxid. Rate	O_3 Maximum Day 1	O_3 Maximum Day 2	Aerosol Volume
JP-4 (pet)	1.4	2.6	0.9	2.6	1.1	1.3	1.3	1.5
JP-4 (shale)	0.9	1.2	0.8	0.2	1.4	1.1	1.0	0.5
JP-8 (pet)	1.3	1.2	1.3	1.8	1.3	0.7	1.9	0.8
JP-8 (shale)	1.0	0.9	0.9	1.5	0.6	1.3	1.3	1.1
Unleaded gasoline	1.6	0.9	0.8	2.0	2.2	1.5	1.7	1.4
Diesel No. 2	1.9	1.2	0.9	1.4	1.4	1.4	1.4	1.5
JP-10	1.0	2.6	0.9	0.6	1.4	a	~0[b]	0.6
RJ-4	1.2	1.1	0.9	1.1	1.1	0.7	0.6	0.9
RJ-5	1.2	6.8	0.3	1.6	1.5	0.3	1.5	1.2

[a]Negligible amounts of ozone formed on both sides.

[b]Negligible amounts of O_3 formed on higher NO_x side; 59 ppb formed on the lower NO_x side.

twice the standard amount of fuel was injected for the "high fuel" side. Plots of the concentration-time profiles for O_3, NO, and NO_2 (uncorrected for interferences from PAN and other nitrogen-containing compounds) are shown in Figures 43-51 for the variable-fuel runs and in Figures 52-60 for the variable-NO_x runs. Summaries of the results of these non-standard runs are given for each fuel in Tables 21-29. Table 34 summarizes the major aspects of these results by giving the ratios of selected reactivity parameters observed in the variable-fuel and the variable-NO_x runs.

Increasing the initial fuel tended to increase the rates of NO_x oxidation and hence caused O_3 formation to occur earlier (Figures 44-51). The magnitude of this effect varied from essentially negligible for JP-4 (shale) (Figure 44) to causing the ozone maximum to occur one full day

earlier for RJ-5 (Figure 51). On the other hand, increasing the NO_x concentration (Figures 52-60) tended to delay O_3 formation. In most cases, it also caused higher ultimate O_3 formation, either on the first day for the more reactive fuels (JP-4 [pet], JP-8 [shale], unleaded gasoline and diesel No. 2) or on the second day (JP-8 [pet] and RJ-5). For the JP-4 (shale) and RJ-4 variable NO_x runs, the ozone on the high NO_x side approached that of the lower NO_x side by the end of the second day. Only in the JP-10 variable-NO_x run was the reactivity so low that O_3 formation on the high NO_x side did not approach or exceed that of the lower NO_x side by the end of two days.

It can be seen from Table 34 that the ratios of the reactivity parameters resulting from changing the initial fuel or the initial NO_x were variable. However, a number of generalizatons can be made. Increasing either the initial fuel or the initial NO_x tended to result in increased NO oxidation rates, though this increase was generally less than the factor of two increase in the concentration of the reactant. Increasing the fuel resulted in higher ozone yields on the first day, though for all runs, except JP-8 (pet) and unleaded gasoline, lower ozone yields on the second day were observed. Decreasing the NO_x resulted in decreased ozone on both days (less than a factor of two), except for RJ-4 and RJ-5, which were less reactive, and JP-8 (pet), whose variable-NO_x run was done under low temperature conditions.

As expected, the aerosol data were the most variable, though they were consistent with the assumption that increasing the fuel concentration will result in increased aerosol levels. Unfortunately, because of the variability characteristic of outdoor chamber runs, more variable-fuel and variable-NO_x runs would have been required to more quantitatively and unambiguously determine the effects of changing the initial reactant concentrations, and to determine if there were any significant differences between the fuels regarding these effects.

V. DISCUSSION AND CONCLUSIONS

When released into the atmosphere, organic compounds such as those contained in hydrocarbon fuels can affect air quality both in the vicinity of their release and, with transport, in downwind regions. Adverse air quality impacts include the formation of ozone and a wide range of other photochemical oxidants, the formation of secondary aerosols, and in certain cases the formation of toxic organic products. In the following sections, the implications of our results with respect to the atmospheric releases of these fuels are presented. Some of the chemical and physical factors which affect the results of smog chamber experiments designed to investigate such air quality impacts are discussed.

5.1 FACTORS AFFECTING ATMOSPHERIC IMPACTS OF FUEL RELEASES

5.1.1 Ozone Formation and NO_x Removal

The primary process forming O_3 in the lower troposphere is the photodecomposition of NO_2 forming $O(^3P)$ atoms. These $O(^3P)$ atoms then combine with molecular O_2 to form O_3 (Reference 5). In the absence of other reactants (i.e., in a NO_x-air system), this is balanced by the rapid reaction of O_3 with NO, so that there is no net buildup of O_3.

$$NO_2 + h\nu\ (\lambda \leq 400\ nm) \rightarrow NO + O(^3P) \quad (1)$$

$$O(^3P) + O_2 + M \rightarrow O_3 + M \quad (2)$$

$$O_3 + NO \rightarrow O_2 + NO_2 \quad (3)$$

The rates of reactions 1-3 are rapid compared to most other atmospheric processes and, to a reasonable approximation, O_3 can be considered in a photostationary state with NO_2. The following relation can then be derived (Reference 28):

$$[O_3] = k_1[NO_2]/k_2[NO]. \quad (I)$$

From this equation it can be seen that any process that converts NO to NO_2 will cause O_3 to increase. Thus, when organics are added to a NO_x-air mixture, ozone formation occurs, because intermediates which convert NO to NO_2 are formed from the oxidation of the organics.

The only types of organic compounds identified as present in the fuels investigated in this program are saturated or aromatic hydrocarbons. The only significant process which consumes such organics is via reaction with hydroxyl radicals (Reference 13). The major features of the large number of individual reactions that follow initial attack by the OH radical (References 4, 5, 13, 23) can be represented as shown below:

$$\text{Hydrocarbon} + OH \xrightarrow{O_2} RO_2 \quad (4)$$

$$RO_2 + NO \xrightarrow{M} RONO_2 \quad (5)$$

$$RO_2 + NO \rightarrow RO + NO_2 \quad (6)$$

$$RO \rightarrow (products) + R'O_2 \quad (7)$$

$$RO + O_2 \rightarrow HO_2 + (products) \quad (8)$$

$$HO_2 + NO \rightarrow OH + NO_2 \quad (9)$$

$$(Products) + OH \rightarrow R''O_2 \quad (10)$$

The peroxy radicals (RO_2 and HO_2) formed in the oxidation mechanisms lead to NO oxidation and thus are responsible for enhanced ozone formation.

In discussing O_3 formation caused by atmospheric releases of a given organic or mixture of organics (such as the fuels studied in this program), the concept of reactivity is frequently useful. However, among the many reactivity parameters employed, at least two must be considered: (1) how rapidly a given fuel causes ozone to be formed and (2) the maximum amount of ozone that can be formed from a fuel, given a sufficient time for reaction. The first of these is the most important in determining the impact of a fuel release in the immediate and neighboring downwind areas on the first day. The second aspect will generally be more important in determining the impact of the fuel release on subsequent days (i.e., multi-day episodes) and in downwind regions. Entirely different chemical

factors affect these two aspects of reactivity and are discussed separately.

NO Oxidation Rate. How rapidly a fuel causes ozone to be formed is directly determined by how rapidly its oxidation causes NO oxidation. From the point of view of ozone formation, reactions 4-10 can be represented the single overall process

$$(\text{Fuel}) + \text{OH} + \alpha\,\text{NO} \rightarrow (\text{products}) + \beta\,\text{NO}_2 \qquad (11)$$

where $\beta \leq \alpha$ for fuels not containing nitrogen, α is the amount of NO oxidized for a given amount of fuel consumed, and k_{11} is an overall rate constant measuring how fast the major fuel components, on average, react with OH radicals. If reactions of ozone, other than its rapid reaction with NO, are ignored and if it is assumed that the only significant reactions of NO are with O_3 (reaction 2) or with the fuel intermediates (reaction 11) (both of which are reasonable assumptions when O_3 levels are relatively low), then the following kinetic differential equations can be derived:

$$\frac{d[O_3]}{dt} \simeq k_1[NO_2] - k_2[O_3][NO] \qquad (II)$$

$$\frac{d[NO]}{dt} \simeq k_1[NO_2] - k_2[O_3][NO] - \alpha k_{11}[\text{Fuel}][OH]. \qquad (III)$$

Subtracting (III) from (II) yields:

$$\frac{d([O_3]-[NO])}{dt} \simeq \alpha k_{11}[\text{Fuel}][OH]. \qquad (IV)$$

Equation IV suggests that the quantity $d([O_3]- NO])/dt$, referred to as the "NO oxidation rate" in discussion of the results of the fuel runs in Section 4.2, can be used as a direct measure of how rapidly the fuel converts NO to NO_2, at least in the initial stages of the irradiation before significant quantities of O_3 are formed. When higher concentrations of O_3 are present, its other reactions (e.g., photolysis, reaction with NO_2, wall decay) become sufficiently important that equations II-IV are no longer

valid. The NO oxidation rates listed or shown in the tables and figures in Section 4.2 were calculated using $\Delta[O_3]-\Delta[NO]$ from the beginning of the irradiation to 1200 PST, or to the time of the last measurement when $[O_3]$ < 0.1 ppm (whichever came first), and is thus a reasonably good approximation of the true NO oxidation rate during the initial stages of the irradiation.

From equation IV it can be seen that how rapidly an organic or mixture of organics causes ozone to be formed depends on three factors: (1) α, the number of molecules of NO oxidized per molecule of organic consumed in the oxidation mechanism; (2) k_{11}, the rate constant (or set of rate constants) for the reaction of OH with the organics; and (3) the OH levels. The latter may be enhanced or suppressed by the addition of the organics relative to those in NO_x-air mixtures, depending on details of the oxidation mechanisms of the organics and the reactions of the secondary products formed.

The number of molecules of NO oxidized per molecule of organic consumed, α, will vary depending on the detailed oxidation mechanism of the organic, but in general the variation is small. Thus, values of α = 2-3 have been determined for many alkanes and aromatics (References 39, 40). For this reason, the other two factors (k_{11} and [OH]) are probably more important in influencing differences in reactivity between different fuels.

Data are available concerning the rate constants for reactions of hydroxyl radicals with the hydrocarbon constituents of the fuels studied in this program (Reference 13). For saturated hydrocarbons, the rate constants are generally proportional to the number of primary, secondary, and tertiary C-H bonds (Section 2.5); for most of straight-chained, branched, and reasonably unstrained cyclic alkanes present in the kerosene type fuels, the rate constant per carbon does not vary greatly and is generally in the range of 0.9 to 1.5 x 10^{-12} cm^3 carbon-atom^{-1} sec^{-1} (References 13, 41, 42). In addition, JP-10, a polycyclic alkane whose OH rate constant was measured as a part of this program (Section 2.5), also has a rate constant per carbon atom, which falls within this range. It is probable that RJ-4 and RJ-5 have rate constants of a similar magnitude.

The range of rate constants per carbon atom for the aromatics is greater, ranging from (in units of 10^{-12} cm^3 carbon-atom^{-1} sec^{-1}): 0.2

for benzene; 0.7-0.9 for monoalkylbenzenes, 1-3 for dialkylbenzenes, and 4-7 for trialkylbenzenes (Reference 13). The OH radical rate constants for the napthalenes are unknown. However, since the major components of all of the fuels studied here are alkanes, except for unleaded gasoline, it appears probable that the fuels investigated in this program have a similar average rate of reaction with the hydroxyl radical.

A third factor affecting the rates of NO oxidation and ozone formation concerns the impact of the fuel oxidation on radical levels. The atmospheric oxidation of a given organic can either enhance or suppress radicals depending on its photo-oxidation mechanism and the reactivity of the products formed. If a compound reacts to form a product or products which undergo rapid photodecomposition to radicals, then the presence of this compound in a fuel would tend to enhance radical levels and, in turn, rates of NO oxidation. If, on the other hand, the photo-oxidation mechanism of a compound includes significant radical termination reactions, then the presence of the compound would tend to suppress rates of NO oxidation. The fact that the fuels studied in this program exhibited wide differences in NO oxidation rates during fuel-NO_x irradiations (Section 4.2) suggests that most of the differences in these rates are primarily due to factors involving radical initiation and/or termination. In view of our knowledge of the composition of these fuels and of photo-oxidation mechanisms of alkanes and aromatics, this is not unexpected.

Recent studies of the NO_x-air photooxidation of aromatic hydrocarbons such as toluene and the xylenes have shown that their reaction mechanisms involve a significant amount of radical initiation (References 23, 43-45). These photooxidation mechanisms involve the formation of α-dicarbonyls such as glyoxal, methylglyoxal, and biacetyl (References 5, 23, 43-45). For example, a series of reactions accounting for the formation of methylglyoxal from toluene (Reference 23) are shown in Figure 61. Through similar mechanisms, methylglyoxal and/or biacetyl are formed from the xylenes, ethylglyoxal from ethylbenzene, etc. (References 5, 23). The formation of significant yields of biacetyl in o-xylene-NO_x-air irradiations has been directly observed (References 43, 44).

The formation of α-dicarbonyls from aromatics is significant, since these compounds absorb strongly in the 340-460 nm wavelength region (Reference 46) where solar radiation is relatively intense. The substituted

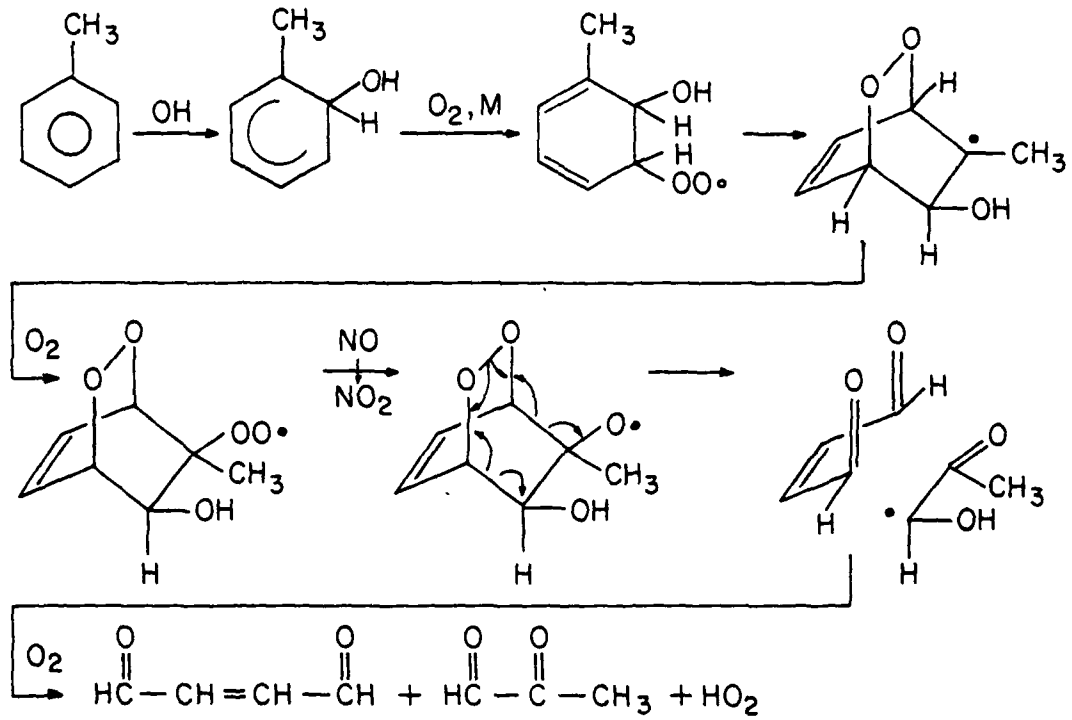

Figure 61. Representative Fragmentation Pathway Forming Methylglyoxal in the Toluene-NO_x-Air Photo-oxidation (from Reference 23).

glyoxals (though not glyoxal) undergo rapid photodecomposition to radicals when photolyzed in this region (References 5, 23):

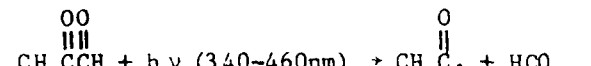

(12)

(13)

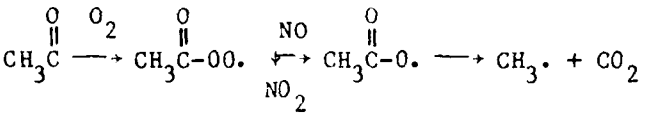

(14)

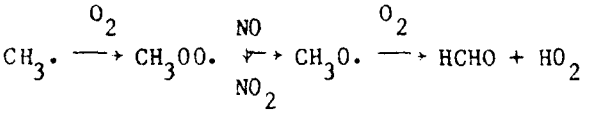

(15)

Computer kinetic models employing such a mechanism have been shown to give good fits to data from toluene-NO_x-air (Reference 23) and m-xylene-NO_x-air (Reference 47) smog chamber experiments.

The results from the present outdoor chamber, fuel-NO_x irradiations are consistent with mechanisms which predict significant radical input from aromatics (especially from alkylbenzenes). First, the NO oxidation rates for the aromatic-containing JP-4, JP-8, and commercial fuels are significantly higher than those for the high-energy fuels (JP-10, RJ-4, RJ-5), which do not contain aromatics. Second, for the fuels containing aromatics, the order of NO oxidation rates (Section 4.2) is: unleaded gasoline >> diesel No. 2 > JP-4 (pet) > JP-8 (shale) > JP-4 (shale) > JP-8 (pet). The alkylbenzene content of these fuels can be obtained from the identified fuel components given in Tables 3-8 of Section 2.2.1 and (for the military fuels) from the volume percent of alkylbenzenes specified in analyses supplied by the Air Force. These alkylbenzene contents are summarized in Table 35, with the fuels listed in the order of their reactivity. Unleaded gasoline is far higher in alkylbenzene content than the other fuels and thus the reason for its high reactivity is evident.

TABLE 35. ALKYLBENZENE CONTENT OF SELECTED FUELS.

	Mole Fraction of Alkylbenzenes Among Identified Components	Volume % Alkylbenzenes from USAF Mass Spectro-Metric Analysis
Unleaded Gasoline	54.8	--
Diesel No. 2	10.0	--
JP-4 (Pet)	17.6	8.2
JP-8 (Shale)	9.9	10.5
JP-4 (Shale)	12.0	7.4
JP-8 (Pet)	9.2	6.7

For the military fuels, the order of reactivity roughly corresponds with the measurements of their alkylbenzene content, though there are some discrepancies.

In contrast with the aromatics, the NO_x-air photo-oxidations of the higher alkanes are expected to suppress radical levels. Thus, the major oxygenated products formed from the large alkanes are expected to be high molecular weight bifunctional compounds which, if they photolyze at all, do so far more slowly than the α-dicarbonyls. Such bifunctional compounds are also expected primarily to condense into the aerosol phase before they can undergo subsequent reaction (Secton 5.1.2). More importantly, it has been shown that radical termination from the reaction

$$RO_2 + NO \xrightarrow{M} RONO_2 \qquad (5)$$

can compete significantly with the normal radical propagation reaction

$$RO_2 + NO \rightarrow RO + NO_2 \qquad (6)$$

if the size of the molecule is sufficiently large (References 4, 5, 25, 48). Current data concerning the ratio $k_5/(k_5+k_6)$ are summarized in Table 36. It can be seen that the ratio generally increases with the size of

TABLE 36. RATE CONSTANT RATIOS $k_5/(k_5 + k_6)$ DERIVED FOR THE REACTION OF RO_2 RADICALS WITH NO.

Alkane	$k_5/(k_5 + k_6)$
propane	0.04[a]
n-butane	$0.08_3 \pm 0.02$[b]; 0.086[a]; 0.05[c]
n-pentane	0.14 ± 0.05[b]; 0.11[c]
n-hexane	0.37 ± 0.08[b]; 0.19[c]

[a]Reference 4

[b]Reference 25

[c]Reference 48

the molecule, being ~0.04 for C_3 radicals and increasing to ~0.2 for the C_6 system. Although the importance of reaction 5 for the larger n-alkanes (i.e., including those found in the high-energy fuels) is presently unknown, it appears probable that this reaction is at least as important as in the case of n-hexane. Even if the ratio is no higher than that for n-hexane, significant inhibition of radicals is expected, since in n-hexane–NO_x-air smog chamber irradiations radical levels are much lower than those in similar experiments using n-butane. Reaction (5) is also required in chemical computer model calculations to fit other alkane–NO_x-air smog chamber data (Reference 48).

The NO oxidation rates observed in our fuel–NO_x irradiations are also reasonably consistent with mechanisms predicting significant inhibition of radicals due to alkyl nitrate formation from larger (C_{6+}) alkanes and cyclo-alkanes. In particular, this reaction can account for the fact that n-butane–NO_x runs have significantly higher NO oxidation rates than those employing JP-10, RJ-4, and RJ-5, despite the fact that n-butane has a lower OH radical rate constant per carbon atom than does JP-10. These high-energy fuels consist exclusively of C_{10}, C_{12}, and C_{14} cycloalkanes, which should have much higher efficiencies for nitrate formation than the 5-9% (Table 36) for n-butane. Inhibition of radicals due to alkyl nitrate formation from larger alkanes can also account in part for the fact that

JP-8 (pet) appears to be only slightly more reactive than n-butane, despite the fact that the former contains aromatics.

Finally, the substantial variability in NO oxidation rates observed in replicate irradiations of the same fuel-NO_x mixture (Section 4.3.3) clearly indicate that these rates are strongly influenced by the conditions under which the irradiations were performed. Except for fuels with extreme differences in reactivity (e.g., unleaded gasoline and JP-10), conditions under which the irradiations were carried out appeared to be the most important factor influencing the NO oxidation rates.

Of the factors involved in equation IV, both the OH radical reaction rate constants, k_{11}, and the number of NO molecules oxidized per organic molecule consumed, α, are not expected to vary significantly with temperature (nor with light intensity) (Reference 5). Hence, the observed variability in the NO oxidation rates are attributed to changes in the radical levels caused by light intensity and/or temperature irradiations.

Both meteorological parameters are known to affect radical levels in environmental chamber irradiations. Changes in light intensity will affect radical levels since, except in aged smog systems containing peroxynitrates or in systems containing O_3 and alkenes, in which radicals are formed almost exclusively from photolytic reactions. Temperature has been observed to significantly affect the photochemical reactivity in NO_x-air irradiations for a number of different types of organics in indoor, constant light intensity, smog chamber experiments (Reference 49). This temperature dependence, at least for the alkane-NO_x-air irradiations, has been subsequently shown to be primarily due to the fact that the unknown chamber radical source increases with temperature (References 34-36). Data from our NO_x-air irradiations (Section 4.1.3) indicates that this radical source is non-negligible even in our large outdoor chamber. However, significant temperature effects have also been observed in toluene-NO_x-air irradiations (Reference 49). Since in these systems radical input from methylglyoxal photolysis makes the chamber radical source somewhat less important, temperature may also affect some aspects of the organic photo-oxidation mechanisms which influence radical levels. Because, in general, the temperature and light intensity both vary (usually together) in outdoor chamber irradiations, the data from this program are not particularly suitable for elucidation of the relative importance of these two

meteorological parameters in determining the rates of NO oxidation and O_3 formation.

Maximum Ozone Formation. Ozone formation in hydrocarbon-NO_x-air systems continues as long as there are reactive organics, NO_x, and sunlight present. However, since NO_x is generally removed from the atmosphere far more rapidly than the organics, it is effectively the NO_x supply and length of the day which determine how long O_3 formation can continue. This is consistent with observations that the major hydrocarbon fuel constituents were present at significant concentrations, even after several days in multi-day irradiations.

The inorganic reactions responsible for the removal of NO_x from NO_x-organic-air systems are (References 4, 5, 23, 37, 38):

$$OH + NO_2 \xrightarrow{M} HNO_3 \quad (16)$$

$$O_3 + NO_2 \rightarrow NO_3 \quad (17)$$

$$NO_3 + NO \rightarrow 2\ NO_2 \quad (18)$$

$$NO_3 + NO_2 \rightarrow N_2O_5 \quad (19)$$

$$N_2O_5 + H_2O \xrightarrow{\text{surface}} 2\ HNO_3 \quad (20)$$

Reaction 16 is an important NO_x sink during the daytime and its rate increases with the overall radical levels in the system. Thus, if a fuel has a high rate of NO oxidation due to enhanced radical levels, it also has an increased rate of NO_x removal due to reaction 16. Consequently, providing that there is sufficient time for the maximum O_3 to be attained and that there are no significant NO_x sinks which are independent of radical levels, higher NO oxidation rates do not necessarily imply higher O_3 yields.

Unlike reaction 16 and most of the NO_x-removal reactions in the organic oxidation mechanisms (see below), reactions 17-20 can occur at night. These reactions account for observations that, if O_3 and NO_x are present at the end of the day, both are observed to decline at night.

Usually only the species present in excess on the previous evening remain to any significant extent on the following morning. If NO_x is absent at the end of the day, the overnight decline in O_3 is relatively modest and can be accounted for by its dark decay. If O_3 is absent at the end of the day, the NO_x levels are largely unaffected. It should be noted that the rate-determining step in this process is reaction 20, which is thought to be heterogeneous and, hence, chamber dependent (Reference 4). If reaction 20 was negligible in the ambient atmosphere, then NO_x would be "stored" as N_2O_5 (in equilibrium with NO_2 and NO_3) and would be regenerated after sunrise by NO_3 photolysis (References 5, 50)

$$NO_3 + h\nu \rightarrow NO + O_2 \qquad (21a)$$

$$\rightarrow NO_2 + O(^3P) \qquad (21b)$$

together with reaction 18. Reaction 18 also converts NO to NO_2, which would cause at least some of the lost O_3 to be re-formed as well. In view of the potential importance of nighttime NO_x removal, the importance of reaction 20 and other possible dark NO_x removal reactions in the ambient atmosphere must be determined.

Such nighttime reactions in the chamber clearly have a significant impact on the next day's maximum O_3-forming potential, since not only is O_3 removed, but NO_x (which otherwise would permit O_3 formation to occur) is also removed. The impact is greatest in the runs where O_3 formation and NO_x consumption occur at moderate rates, such that both O_3 and NO_x are present in significant amounts at the end of the day. For extremely reactive mixtures (where NO_x is essentially completely consumed and the maximum O_3 is already formed by the end of the first day) or for extremely unreactive runs (where essentially no O_3 is formed on the first day to react with the NO_x at night), nighttime NO_x and O_3 removal is less important in affecting the maximum O_3 yields.

This nighttime chemistry, combined with the changes in NO oxidation and O_3 formation rates caused by variations in temperature and light intensity, accounts for the wide variability in O_3 yields observed in the multi-day runs. For the more reactive fuels, maximum O_3 formation occurred on the first day under favorable weather conditions. If meteorological conditions were less favorable, the O_3 formation may have been

insufficient to remove NO_x in one day. If this were the case, then the ultimate O_3 yields would be lower because of the nighttime reactions of the remaining NO_x with O_3. Since unleaded gasoline and diesel No. 2 formed sufficiently high radical levels that maximum O_3 formation usually occurred on the first day, the maximum O_3 yields for these fuels fell in comparatively narrow ranges, relative to the other fuels (Figure 36, 37). For the less reactive fuels, a negative correlation between favorable conditions and ultimate O_3 yields sometimes occurred. If the weather was favorable for rapid O_3 formation, then partial O_3 formation occurred on the first day and it reacted with the remaining NO_x at night so that little additional O_3 was formed on the second day. Conversely, if the weather was less favorable and little O_3 formation occurred on the first day, then much less O_3 and NO_x was consumed on the first night, allowing O_3 formation to occur on the second day. Similar considerations also account for the fact that, in some dual chamber runs involving the less reactive fuels, more O_3 was present at the end of day two on the side with either less fuel or the less reactive fuel (Figure 51).

Although the reactivity with respect to rates of NO oxidation and the meteorological conditions were clearly very important in affecting the maximum O_3 yields, they were not the only factors which must be considered. In particular, if the NO_x-air photo-oxidation mechanism of a particular fuel consitutent includes reactions which remove NO_x from the system, the rate of NO_x removal relative to the rate of O_3 formation is enhanced. This causes the maximum amount of O_3 which can be formed under favorable conditions to be reduced. One important atmospheric NO_x sink in the oxidation of organics arises from the formation of peroxyacetyl nitrate (PAN) and its analogues (reaction 21) (Reference 49).

$$RC(=O)-OO\cdot + NO_2 \rightleftarrows RC(=O)OONO_2 \qquad (21,-21)$$

PAN is formed in the photo-oxidations of both alkanes and aromatics (References 4, 5, 23), and was observed in our outdoor chamber experiments for all fuels except JP-10 and RJ-5. PAN, however, is only a temporary NO_x sink under multi-day conditions, since it undergoes thermal decomposition

back to its precursors (reaction -21) (Reference 5). If NO is introduced into mixtures containing PAN, the PAN is destroyed and NO_x is regenerated, due to reaction -21 followed by reaction 22:

$$CH_3\overset{O}{\overset{\|}{C}}-OO\cdot + NO \rightarrow CH_3\overset{O}{\overset{\|}{C}}-O\cdot + NO_2 \qquad (22)$$

A potentially more important process for removing NO_x from the system is alkyl nitrate formation via the reaction of RO_2 radicals with NO:

$$RO_2 + NO \xrightarrow{M} RONO_2 \qquad (5)$$

This reaction, which is also radical terminating (as are many of the NO_x removal reactions), is important in the NO_x-air photo-oxidations of the larger alkanes (Reference 25). In addition, there is indirect evidence that reaction (5) is important in the NO_x-air oxidations of the aromatics as well (Reference 23). Thus, it was necessary to assume ~25% alkyl nitrate formation in the toluene system in order for model calculations to fit the O_3 yields observed in indoor smog chamber irradiations (Reference 23). Alkyl nitrates are much more stable than PAN or its analogues, and although they do react slowly with OH radicals, kinetic evidence indicates that the probability of OH radical attack occurring near the nitrate group is relatively low (Reference 51). Thus it is likely that little, if any, NO_x is released in the subsequent reactions.

Finally, recent laboratory and smog chamber modeling studies have indicated that there are additional, significant NO_x sinks in the aromatic photo-oxidation mechanism (References 23, 52, 53). Although aromatics exhibit extremely high rates of NO oxidation and O_3 formation in NO_x-air irradiations, their maximum O_3 yields are relatively low, compared to other classes of organics. In a recent study performed in this laboratory, it was observed that the addition of small amounts of toluene to an organic-NO_x-air mixture tended to decrease the maximum O_3 yields. This can be accounted for only in part by assuming that significant alkyl nitrate formation occurs; there must be other NO_x sinks in the mechanism in order for model calculations to fit the data (References 23, 53). Although it is probable that not all of the NO_x sinks in the aromatic

photo-oxidation have been identified, an important process is undoubtedly the rapid reaction of NO_3 with phenolic compounds (Reference 54), which are formed in an ~20% yield from the toluene system.

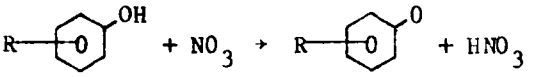

(23)

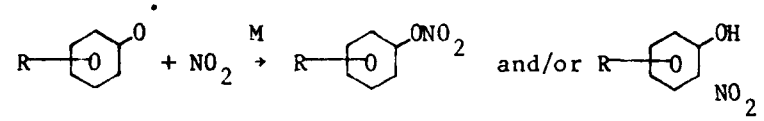

(24)

It can be seen that reaction of one molecule of cresol consumes two molecules of NO_x. In addition, benzaldehyde and its analogues are also formed in aromatic systems (References 5, 23), and their subsequent reactions also cause NO_x consumption:

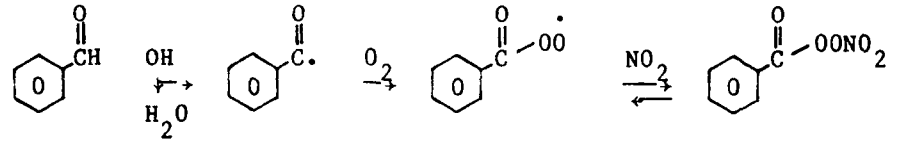

(25)

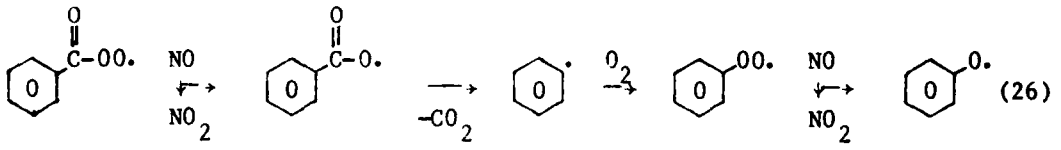

(26)

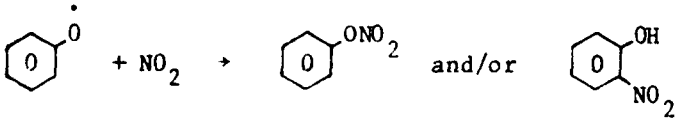

(24)

In general, NO_x consumption processes appear to be more important in the NO_x-air photo-oxidation of aromatics than for other classes of organics. Thus the presence of aromatics in fuels is expected to suppress maximum O_3 yields, despite the fact that they enhance the rates of O_3 formation.

Unfortunately, the variability in the O_3 formation rates and the complications introduced by the nighttime chemistry make outdoor chamber

irradiations not well suited for comparison of maximum O_3 forming potentials, particularly for the less reactive fuels. Only the JP-4 fuels, JP-8 (shale), unleaded gasoline, and diesel No. 2 were sufficiently reactive so that there were runs where the maximum (or near-maximum) ozone yield was attained in one day. Unleaded gasoline has by far the highest aromatic content; the maximum one-day O_3 concentrations observed with that fuel were considerably less than those obtained in the most favorable JP-4 runs (Figure 36). The maximum O_3 yields from JP-8 (shale) were also lower than those for JP-4 and were about the same as those for unleaded gasoline. JP-8 contains larger alkanes than JP-4 and unleaded gasoline and thus may have higher rates of NO_x removal by alkyl nitrate formation. It is possible that the lower O_3 yields from JP-8 (shale) could also be due to less of this heavy fuel being injected into the gas phase, relative to JP-4 or unleaded gasoline (Section 2.3, Table 11). This may be the reason for the low O_3 yields from diesel fuel, since from Table 11 less than one-third of the liquid fuel was introduced into the gas phase.

5.1.2 Reaction Products and Aerosol Formation

Ozone formation, though important, is not the only factor which must be considered in assessing environmental impacts of fuel releases. The atmospheric fate of the fuel components themselves must also be considered. For example, air quality in the vicinity of the fuel release would be adversely affected, if the fuel components oxidized to form toxic products or products which condense into the aerosol phase causing visibility degradation. In addition, the ultimate atmospheric fate of the carbon-containing products, particularly the ultimate partitioning of the oxidized fuel material between the gaseous and aerosol phase, must be considered.

Unfortunately, the product data which were obtained in the smog chamber experiments performed in this program were very limited. However, when examined in terms of what is currently known about the oxidation mechanisms of compounds such as those contained in the fuels, the results of these experiments do yield information as to the nature and ultimate fates of the products formed. This is discussed below.

Products Expected in the Atmospheric Oxidation of Larger Alkanes. Normal, branched, and cyclic alkanes are major constituents of the kerosene-type fuels studied in this program (Section 2.2) while the high-

energy fuels studied consist almost exclusively of various polycyclic alkanes. The oxidation mechanisms of the smaller alkanes are reasonably well understood (References 4, 5); they involve formation of PAN, formaldehyde, and simple aldehydes and ketones. These products eventually react further to give rise to CO and CO_2, with negligible aerosol formation (see, for example, the results of the n-butane-NO_x irradiations performed in this program). However, recent research has indicated that the oxidation mechanisms of the larger (C_{6+}) alkanes are significantly different (References 25, 55).

All alkanes are consumed primarily by reaction with hydroxyl radicals and the resulting peroxy radicals react primarily (though not exclusively) with NO to form alkoxy radicals (reactions 4-6, Section 5.1.1). Unlike the smaller alkanes, where the alkoxy radicals primarily react with O_2 to form simple aldehydes or ketones or undergo fragmentation by β-scission (Reactions 7, 8), the larger alkoxy radicals can undergo rapid isomerization via a six-member ring transition state (Reference 55) to ultimately give rise to bifunctional products. For example, for the 2-hexoxy radical formed in the n-hexane-NO_x oxidations, the following reactions are believed to occur (Reference 5, 55):

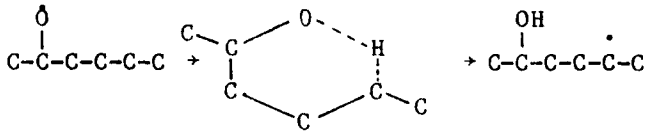

(27)

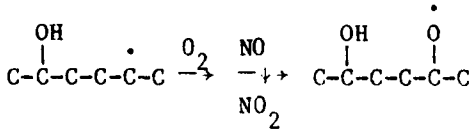

(28)

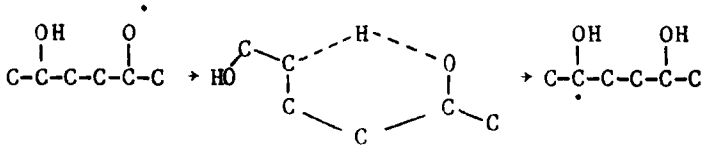

(29)

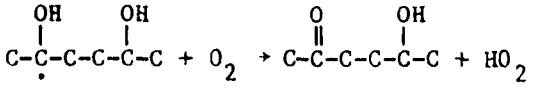

(30)

Until recently there was some uncertainty concerning reaction (30). Reaction (31) appears to be equally reasonable,

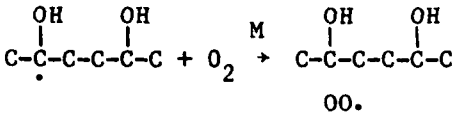

(31)

but recent laboratory studies (References 56, 58) of α-hydroxy-alkoxy radicals have shown that abstraction (e.g., reaction 30) is by far the more important process. Although the occurrence of this isomerization does not significantly affect considerations regarding O_3 formation and radical levels discussed in Section 5.1.1 (since reactions 27-30 still convert NO to NO_2, and do not remove or add radicals), it does affect the type of products formed. In particular, the isomerization competes with fragmentation or the formation of products, which subsequently undergo fragmentation, and has the effect that the integrity of the carbon skeleton tends to be preserved as the alkane is being oxidized. The bifunctional products formed will have much lower vapor pressures than the parent alkane and, for the heaviest alkanes, they will probably condense into the aerosol phase without reacting further. For moderate-sized alkanes, the bifunctional products may remain in the gas phase long enough to undergo reaction. It is probable that many of the subsequent reaction pathways will involve additional isomerizations, resulting in formation of even less volatile polyfunctional compounds with the carbon skeleton still intact.

For the cycloalkanes, particularly the polycyclics such as JP-10 and the RJ-4 and RJ-5 isomers, steric considerations make isomerizaton of the initially-formed alkoxy radicals less likely. However, reactions which cause fragmentation in a polycyclic system will cause ring opening and subsequent formation of bifunctionals in a cyclic system. For example, while β-scission of alkoxy radicals is a common mode of fragmentation in the oxidation mechanisms of smaller acyclic alkanes, in cyclohexane (for example) it gives rise to trifunctional compounds,

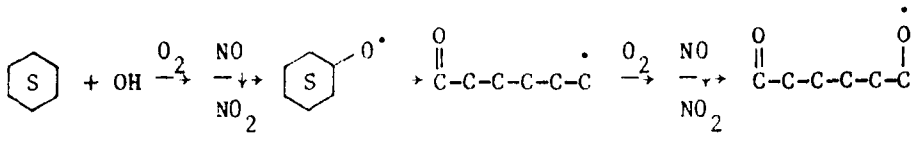

(32)

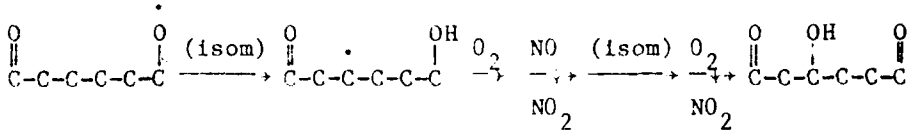

(33)

and in one (of the several) major oxidation pathways of JP-10, it gives rise to a bicyclic dialdehyde.

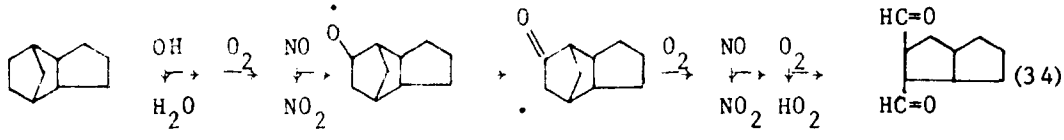

(34)

The trifunctional compound formed in reactions 32 and 33 may condense into the aerosol phase and so may the bifunctional compound formed in reaction 34 or its products.

As discussed previously in conjunction with impacts on O_3 formation and radical levels, alkyl nitrate formation is also an important process in the oxidation of larger alkanes (References 5, 25, 48). For a sufficiently large system, the monofunctional nitrates themselves will probably condense into the aerosol phase without undergoing subsequent reaction. If they do react, the considerations discussed above regarding isomerization (in acyclic systems) or ring opening (in cyclic systems) to form bi- or poly-functionals will probably also be applicable to the alkyl nitrate oxidation mechanism, and thus aerosol formation is expected to be their major fate.

Products Formed in the Atmospheric Oxidation of Aromatics. The atmospheric chemistry of the aromatic hydrocarbons, which are present in the commercial and the kerosene-type military fuels studied in this program, is not completely understood. However, more information is available concerning the products formed in their NO_x-air photo-oxidation than

is the case for the larger alkanes. The most studied aromatic compound to date is toluene and measurements of a number of products have been made. Products observed which retain the aromatic ring include benzaldehyde, cresols, nitrotoluene, and nitrocresols in the gas phase (Reference 23 and references therein) and dihydroxynitrotoluenes in the aerosol phase (Reference 59). Fragmentation of the aromatic ring forming methylglyoxyl (for toluene) and 2-butene-1,4-dial is expected to occur ~60% of the time (References 5, 13). The observation of PAN, HCHO, and CO (References 23, 52) as secondary products from toluene, together with biacetyl as a primary product from o-xylene (References 43, 44), is consistent with this. The mechanism for the formation of some of these products has been discussed briefly in Section 3.1.1, and has been discussed in detail by Atkinson, et al. (Reference 23).

Most of the published product studies report very poor gas phase carbon balances, and it appears that some of the reacting aromatics form aerosol (Reference 59). From a mechanistic point of view, the products retaining the aromatic ring may form the bulk of the aerosol material, since the fragmentation products (Figure 61) are known or expected to be extremely reactive (Reference 23). On the other hand, as discussed in Section 5.1.1, the principal aromatic products are expected primarily to give rise to nitrocresols via reactions 23-26 (Reference 23, 59). As with the phenols and the cresols (Reference 54), the nitrocresols are expected to react rapidly with NO_3 to give rise to further substituted aromatics through reactions analogous to 23 and 24, in the aerosol phase.

Gas Phase Products Observed in the Fuel-NO_x Irradiations. Although attempts were made, using GC-FID, to look for product formation in the NO_x-air photooxidations of all the fuels studied, the major result was negative. No products were detected except formaldehyde, PAN, and several GC peaks on the GC-FID instrument used to monitor PAN, the latter being attributed to alkyl nitrates. The SAPRC technique for analyzing oxygenated products (the C-600 GC system, Section 3.2.8) was not useful for this purpose, because of interference by the fuel components. However, if significant formation of gas phase oxygenated products (other than formaldehyde) occurred, additional growing peaks should have been observed on the capillary GC system. Despite a careful search, no peaks were observed.

The only gas phase products for which concentration-time data were obtained were PAN and formaldehyde, though measurements for the former are somewhat uncertain because of possible interferences by 2-butyl nitrate; the reported data must be considered upper limits to the true yields. The averages of the maximum one-day yields of these products are summarized in Table 32. As with the ozone, NO_x, and aerosol data, the results were quite variable; but, it can be seen that the kerosene-type and commercial fuels give significantly more of these products than the high-energy fuels.

The formaldehyde and PAN yields from RJ-4 were higher than from the other high-energy fuels. This can be explained by the fact that RJ-4 contains methyl groups, while JP-10 and RJ-5 do not (Figure 1). Any methyl radicals produced from fragmentation reactions will be oxidized primarily to formaldehyde. In addition, the lack of PAN formation from JP-10 and RJ-5 can be attributed to the fact that PAN contains a methyl group; there are no known mechanisms for forming new C-H bonds in atmospheric oxidation systems in the concentration range employed in this study.

The fact that other gas phase products were not observed may be in part due to deficiencies in analytical techniques used, but is probably due primarily to such products being removed from the gas phase by condensation on the walls or into the aerosol phase. The maximum total aerosol volume (measured by the electrical aerosol size analyzer) formed in a typical fuel run was approximately 1% of the total volume of fuel injected. This estimate of ~1% is a lower limit to the gas-to-particle conversion efficiency, since only a fraction of the total fuel reacts each day. Aerosol materials formed in environmental chambers are known from previous unpublished work at SAPRC to be rapidly deposited on the walls. Additional evidence for a rapid loss of aerosol material to the walls was shown by the near loss of aerosol materials during the night in multi-day runs. Thus, ~1% conversion to aerosol is in fact a relatively large amount. Clearly, aerosol formation is important for these fuels at the precursor concentrations employed.

Aerosol Formation. As discussed above, aerosol formation was important for all of the fuels studied in this program. In particular, the aerosol volume, light scattering, and numbers of larger particles measured

by various techniques in these experiments were frequently higher than observed on the worst days in polluted urban atmospheres. For example, based on our measurements in the California South Coast Air Basin (CSCAB), light scattering on the worst days ranges from (5-10) x 10^{-4} m^{-1} (Reference 60) and aerosol volume rarely exceeds ~50 μm^3 cm^{-3}. For comparison (Figure 38), light scattering frequently exceeded 10 x 10^{-4} m^{-1} and aerosol volume frequently exceeded 100 μm^3 cm^{-3}.

It should be noted that the hydrocarbon concentrations used in these runs is considerably higher than is typical of urban atmospheres and much less aerosol material may be formed if lower concentrations are employed. On the other hand, it should also be noted that no measurable aerosol is formed in "surrogate" hydrocarbon-NO_x-air irradiations in SAPRC chambers, where the surrogate hydrocarbon mixture consists of 14 lighter alkanes, alkenes, aromatics, and oxygenates, designed to represent hydrocarbon emissions into the CSCAB from all sources (Reference 61). In addition, much of the aerosol formed in the CSCAB is believed to be inorganic (e.g., H_2SO_4, NH_4NO_3, NH_4SO_4) (Reference 60); in our experiments it is probable that the aerosol formed in the present experiments was primarily organic (see above). Thus, release of these fuels even into already polluted atmospheres may result in a degradation of air quality due to increases in levels of organic aerosol.

5.2 SUMMARY AND CONCLUSIONS

Results with considerations concerning the known and expected atmospheric chemistry of the fuel components allow a number of conclusions to be drawn. These concern the atmospheric reactivities of the fuels which have been studied, the methodologies for determining such reactivities, and the utility of multi-day outdoor chamber organic-NO_x-air irradiations in general. Conclusions are summarized briefly below:

- Results obtained in outdoor chamber irradiations exhibit significant variability. Much of this variability can be attributed to day-to-day and season-to-season variations in temperature and light intensity, both of which are known to affect rates of transformations in organic-NO_x-air irradiations. For example, NO oxidation rates and ozone yields were found to correlate moderately well with temperature and light intensity

(Figures 32-37). On the other hand, some measurements of aerosol formation did not correlate with these factors. In a number of cases, differences in NO oxidation rates and O_3 yields were observed which could not be accounted for by known differences in meteorological parameters. In general, for fuels not greatly different in reactivity (e.g., JP-4 and JP-8), the variability of results from run-to-run for a given fuel was comparable to, or greater than, the differences between runs employing different fuels. This presents a severe methodological difficulty in using such experiments for fuel intercomparison purposes.

- Because of the inherent variability of the results of outdoor chamber irradiations, it is concluded that the only way to reliably use such irradiations for fuel reactivity comparisons is to perform a large number of irradiations under a wide variety of meteorological conditions. If the dependence of results on meteorological parameters can be determined, then corrections for variations in these parameters could be made. Despite the large number of runs performed in this program, it is probable that only for petroleum-derived JP-4 and, to a lesser extent, JP-10 were an adequate number of experiments done for this purpose.

- There is evidence that nighttime removal of NO_x and O_3, when both are present together, can be important in outdoor chamber irradiations. This is believed to be due to N_2O_5 formation from the reaction of NO_2 with O_3, followed by heterogeneous hydrolysis of N_2O_5 to HNO_3. Because of the heterogeneous nature of N_2O_5 hydrolysis, it is not clear whether this process is as important in ambient air as it is in chambers. If the hydrolysis is slow in the ambient system, N_2O_5 may remain to react the following morning to regenerate NO_x and at least some of the reacted O_3.

This nighttime removal of NO_x and O_3 has interesting implications concerning maximum O_3 yields in multi-day irradiations. In particular, these reactions will significantly reduce O_3 yields in moderately reactive situations (e.g., a reactive fuel together with unfavorable weather, or a less reactive fuel with favorable weather) where both O_3 and NO_2 are present at the end of the first day. On the other hand, these reactions will not be important in high reactivity situations where all of the NO_x is removed and the maximum O_3 is formed on the first day, or in low reactivity situations where substantial O_3 formation does not begin until the second day. This can result in a negative correlation between reactivity

and O_3 yields as observed in a number of instances. One implication of this is that fuel A may form more O_3 in good weather than fuel B, while fuel B may form more O_3 in poor weather. This is another reason for conducting outdoor chamber irradiations under a variety of weather conditions.

- For JP-4 (pet), JP-10, and n-butane, adequate data were obtained to determine the dependence of their reactivities on meteorological conditions. In general, the rates of NO oxidation and O_3 formation increased monotonically with temperature and UV intensity, with the differences between the fuels decreasing as the temperature and/or UV intensity increased. The effects of temperature and UV intensity could not be separated, since they generally varied together. However, for all temperatures in the 20°C-40°C range, the order of reactivity with respect to NO oxidation rates was JP-4 (pet) > n-butane > JP-10.

The first day ozone yields also had strong temperature dependencies. The data indicate that when the standard 25 ppmC fuel, 0.5 ppm NO_x mixture is irradiated, no significant O_3 formation will occur on the first day at temperatures below ~10°C for JP-4 (pet), below ~30°C for n-butane, and below ~45°C for JP-10. For JP-4 (pet) and n-butane, the O_3 yields increased monotonically with temperature above these temperatures, at least up to ~40°C. However, since these data were obtained in Teflon® bags which are known to exhibit significant temperature dependent chamber effects (Reference 49), extrapolation of these conclusions to the ambient atmosphere may not be valid.

- The high-energy fuels, JP-10, RJ-4, and RJ-5 (which consist almost entirely of various polycyclic C_{10} to C_{14} isomers) are much less reactive with respect to NO oxidation rates than is n-butane (which in turn is less reactive than the kerosene-derived fuels). The low reactivity of these polycyclic alkanes is attributed to the fact that they do not form many photoreactive products. Furthermore, there is probably more radical inhibition resulting from alkyl nitrate formation in these systems than for n-butane. Among these fuels, RJ-4 appears to be significantly more reactive than the others, with JP-10 being possibly slightly less reactive than RJ-5. The relatively high reactivity of RJ-4 may be due to photolysis of formaldehyde formed from the methyl groups present in that fuel.

It can be concluded that pure alkane fuels such as these will, in general, lead to only slow formation of O_3 in NO_x-air mixtures.

- For the other fuels studied which were complex mixtures containing primarily alkanes and aromatics, the rates of NO oxidation appeared to correlate with the aromatic content. Unleaded gasoline had the highest aromatic content of any of the fuels studied and formed O_3 at the fastest rate. Diesel No. 2 was also more reactive than any of the military fuels, even though it was too heavy for all of it to be injected into the gas phase. This suggests that, although its actual aromatic content relative to the other fuels was uncertain, the fraction of diesel No. 2 fuel successfully injected was also relatively high in aromatics. For the kerosene-based military fuels, the order of reactivity appears to be: JP-4 (pet) > JP-8 (shale) > JP-4 (shale) > JP-8 (pet), which agrees with the order of alkylbenzene content measured by several techniques. Therefore, it is concluded that, as the aromatic content of a fuel increases, its reactivity with respect to O_3 formation in NO_x-air mixtures will also increase.

- Despite wide differences between how rapidly the fuels studied formed O_3, the results of this study suggest that the total amount of O_3 that can be formed from each of these fuels under optimum conditions may not be greatly different. However, the conditions under which optimum O_3 formation will occur will vary from fuel to fuel, because of the effect of nighttime NO_x and O_3 removal (see above). Unfortunately, outdoor chamber irradiations are not particularly well-suited for determining maximum O_3 yields since for many fuels, particularly those which form O_3 more slowly, optimum conditions do not occur very frequently. The runs giving the highest O_3 yields were those for petroleum-derived JP-4. This is probably because more runs were done using that fuel than any of the others; thus the probability of optimum conditions occurring was higher. For some of the other fuels, no runs were done under optimum conditions; even for a highly unreactive fuel such as JP-10, high O_3 yields comparable to those obtained from the most reactive fuels were occasionally observed on the second day.

Diesel No. 2 is the only fuel which our data clearly indicates forms less O_3 under favorable conditions. This is probably because less of it can be injected into the gas phase. It is probable that unleaded gasoline

may also form somewhat less O_3 than the other fuels. Thus, it formed O_3 so rapidly that maximum O_3 concentrations were reached in essentially every experiment; yet there were runs employing other fuels which formed considerably more O_3 than did those using unleaded gasoline. Lower O_3 yields from high-aromatic fuels (such as unleaded gasoline) are expected, because the aromatic components should cause more rapid rates of NO_x removal than other fuel components. This tends to decrease the maximum amount of O_3 which can be formed.

- A major result of this study is that all of the hydrocarbon fuels examined formed significant amounts of aerosol material, regardless of their reactivity with respect to O_3 formation. This is an important factor which must be considered when assessing the impacts of fuel releases upon air quality. This is not an unexpected result in view of the expected oxidation mechanisms of the components of these fuels, since they are expected to form primarily very non-volatile polyfunctional products.

Significant differences were observed in the size distributions of the particles formed from the different fuels. Diesel No. 2 formed more large particles and unleaded gasoline formed more small particles than the military fuels. The variation from fuel to fuel in the amount (volume) of aerosol materials formed was comparable or less than the variation from run to run. The possible exception was JP-10, which generally formed less aerosol material than the other fuels (this may be because less of it reacts). With this exception, there was no great difference in aerosol results between runs employing the high energy fuels and the other military fuels, despite significant differences in fuel composition and reactivity.

- There appears to be no obvious relation between reactivity of the kerosene-type fuels, as measured by any of the indices considered, and whether the fuel was petroleum- or shale oil-derived. For example, petroleum-derived JP-4 formed O_3 more rapidly than shale-derived JP-4, but shale-derived JP-8 was more reactive in this regard than petroleum-derived JP-8. Furthermore, all of the kerosene-type military fuels appear to be approximately the same in their maximum O_3-forming potential and in the amount and general size distribution of the aerosol material formed, at

least to within the measurement precision afforded by these outdoor chamber experiments. The differences in NO oxidation rate and O_3 formation which were observed between the shale- and petroleum-derived fuels are probably determined primarily by the aromatic content of the fuel, which may be more a function of how the fuel was refined than how it was derived.

5.3 RECOMMENDATIONS FOR FUTURE WORK

Although a large body of experimental data was obtained in this program, it is clear that additional research is required to completely elucidate both the atmospheric impacts of releases of hydrocarbon fuels and the changes in those impacts caused by changes in fuel composition, derivation, or type. Although nine fuels were studied (ten if n-butane is counted), a sufficient data base could only be obtained for unleaded gasoline and perhaps petroleum-derived JP-4 due to limitations in the scope of the program and the variability of the results of outdoor chamber irradiations and their dependence on weather. These and other uncontrolled factors mean that a large number of runs have to be carried out for each fuel in order to obtain statistically significant data. Thus, using the methodology employed in this study, a program of a much greater magnitude would be required to adequately study the fuels in question.

Considering possible refinery-to-refinery and lot-to-lot variations of fuels of the same type and derivation, a more cost-effective methodology for comparing the atmospheric impacts of releases of the fuels is required. In order to circumvent the problems and variability associated with outdoor chamber experiments, future studies are recommended, particularly those concerned with fuel intercomparisons and effects of changes in fuel composition, based primarily on indoor chamber experiments. Outdoor chamber experiments should be restricted to further studies of one or two representative fuels (e.g., the JP-4 (pet), JP-10, and n-butane samples studied in this program), which are used as bases for comparison with similar fuels. Indoor chamber studies recommended fall into three general categories:

(1) Since the kerosene-derived fuels are comprised mainly of alkanes and aromatics, the atmospheric chemistry of selected components (e.g., n-alkanes, branched alkanes, cycloalkanes, aromatics) should be studied in detail in single hydrocarbon-NO_x-air irradiations. A body of experimental

data obtained for carefully selected single components, together with detailed analysis of the fuels, will enable the effects of changing fuel composition on photochemical reactivity to be assessed from complementary chemical-kinetic, computer-modeling studies.

(2) Indoor chamber experiments should be performed with several representative fuels which can be used as bases of comparison with other fuels. For example, JP-4 (pet) (taken from the same lot as the sample used in this study) seems a logical choice to be used as a standard against which to compare kerosene-derived fuels. Much relevant data was obtained not only from outdoor chamber experiments in this program, but from indoor chamber runs carried out on another, ongoing study being conducted (USAF Contract No. F08635-80-C-0359). Likewise, JP-10 is a logical choice to represent the high energy fuels. The whole fuel should be studied under a variety of conditions with temperature, light intensity, and initial reactant concentrations varied. These conditions should include, but not be restricted to, those favoring complete NO_x consumption so that maximum O_3-forming potentials can be unambiguously determined.

(3) The data obtained in the multi-day irradiations in this program are of great interest from not only a fundamental point of view, but also as a basis for assessing the effects of multi-day air pollution episodes. Thus, further studies involving multi-day irradiations should be conducted, but under more controlled conditions than are possible with outdoor chamber irradiations. Indoor chambers, using pseudo-diurnal light intensities (Reference 62), should be used for this purpose. Compounds studied should include not only the representative fuels, but representative individual fuel components as well.

In addition to these chamber studies, there are areas where fundamental laboratory and/or atmospheric studies are required to elucidate a number of uncertainties important to our ability to quantitatively predict impacts of fuel releases. Several major areas where basic studies are required are indicated below.

(1) With regard to multi-day episodes, studies aimed at elucidating the nighttime chemistry are essential. Of particular concern is whether the nighttime removal of NO_x and O_3, when both are present together, occurs in the ambient atmosphere as was observed to be the case in our outdoor chambers experiments. In addition, there is evidence for slow

formation of HONO in the open atmosphere at night (Reference 63); this can significantly affect reactivity on the following morning (Reference 63). In general, dark reactions of nitrogeneous species which occur in the atmosphere (e.g., NO_2, NO_3, N_2O_5, HNO_3, HONO) must be better understood.

(2) Further work must be done in order to understand the nature and magnitude of unknown, chamber radical sources; for low reactivity organics, these can cause large perturbations in the reactivities observed in chamber simulations. Of particular concern is whether this chamber radical source is also important in the ambient atmosphere. Such an understanding is essential if we are to extrapolate results of chamber experiments, even outdoor chamber experiments, to ambient air.

(3) Basic laboratory studies are required to elucidate a number of areas in the photo-oxidation mechanisms of the various fuel components. For example, reactions forming alkyl nitrates in the photo-oxidation of larger alkanes (and perhaps aromatics) have major impacts on predicted fuel reactivities. These reactions are poorly understood and there is no universal agreement among atmospheric scientists concerning their validity. In addition, relatively little is known about the oxidation mechanism of the polycyclic alkanes; for example, it is not known whether they form alkyl nitrates as effectively as the n-alkanes. The exact identity of the major gas- and aerosol-phase organic products formed from the atmospheric oxidations of larger alkanes, whether straight chain, branched, cyclic, or polycyclic, has yet to be determined experimentally. Many significant gaps remain in understanding the atmospheric chemistry of the aromatics, particularly the naphthalenes (about which essentially nothing is known).

The ultimate goal of these studies would be to develop and validate photochemical kinetic computer models which can be used by the Air Force and the control agencies to predict, a priori, impacts of fuel releases. Such an approach would be much more cost effective than having to perform separate experiments, particularly outdoor chamber experiments, for both present and future fuels. The studies suggested above are necessary for the development and validation of such models. Basic laboratory studies and single-component chamber studies are required to assure that the detailed chemistry is valid, while the whole fuel studies are required to test the chemical model in its entirety.

REFERENCES

1. Burdette, G. W., H. R. Lander and J. R. McCoy, "High-Energy Fuels for Cruise Missiles," J. Energy, 2, 289 (1978).

2. Clewell, H. J. III., "Fuel Jettisoning by U. S. Air Force Aircraft," Volume 1: Summary and Analysis. Report No. ESL-TR-80-17, March 1980.

3. Bouble, R. W. and J. A. Martone, "USAF Aircraft Engine Emission Goals: A Critical Review," Report No. ESL-TR-79-30, September 1979.

4. Carter, W. P. L., A. C. Lloyd, J. L. Sprung and J. N. Pitts, Jr., "Computer Modeling of Smog Chamber Data: Progress in Validation of a Detailed Mechanism for the Photooxidation of Propene and n-Butane in Photochemical Smog," Int. J. Chem. Kinet., 11, 45 (1979).

5. Atkinson, R. and A. C. Lloyd, "Evaluation of Kinetic and Mechanistic Data for Modeling of Photochemical Smog," Final Report to EPA Contract No. 68-02-3280, ERT Document No. P-A040, Environmental Research and Technology, Inc., Westlake Village, California.

6. Pitts, J. N. Jr., A. M. Winer, W. P. L. Carter, G. J. Doyle, R. A. Graham and E. C. Tuazon, "Chemical Consequences of Air Quality Standards and Control Implementation Programs," Final Report to California Air Resources Board Contract No. A7-175-30, June 1980.

7. EPA/NIH Mass Spectral Data Base, S. R. Heller and G. W. A. Milne. National Standard Reference Data System, U. S. Supt. of Docs. No.: C1348:63.

8. Ashland Oil, Inc. "Development of a Process for Producing the High Energy Missile Fuel Tetra-Hydro-Norbornadiene Dimer," Air Force Report No. AFAPL-TR-75-42, May 1975.

9. Handbook of Chemistry and Physics, 56th ed. C.R.C. Press, Cleveland, Ohio (1975).

10. Pitts, J. N. Jr., A. M. Winer, K. R. Darnall, G. J. Doyle, R. A. Graham and E. C. Tuazon, "Chemical Consequences of Air Quality Standards and of Control Implementation Programs: Roles of Hydrocarbons, Oxides of Nitrogen, Oxides of Sulfur and Aged Smog in the Production of Photochemical Oxidant and Aerosol," Final Report to California Air Resources Board Contrct No. A6-172-30, June 1979.

11. Zafonte L., P. L. Rieger and J. R. Holmes, "Nitrogen Dioxide Photolysis in the Los Angeles Atmosphere," Environ. Sci. Technol. 11, 483 (1977).

12. Doyle, G. J., P. J. Bekowies, A. M. Winer and J. N. Pitts, Jr., "Charcoal-Adsorption Air Purification System for Chamber Studies Investigating Atmospheric Photochemistry," Environ. Sci. Technol., 11, 45 (1977).

13. Atkinson, R., K. R. Darnall, A. C. Lloyd, A. M. Winer and J. N. Pitts, Jr., "Kinetics and Mechanisms of the Reaction of the Hydroxyl Radical with Organics in the Gas Phase," Adv. Photochem, 11, 375 (1979).

14. Atkinson R., K. R. Darnall and J. N. Pitts, Jr., "Rate Constants for the Reactions of OH Radicals and Ozone with Cresols at 300 ± 1 K," J. Phys. Chem., 82, 2759 (1978).

15. Hansen, D. A., R. Atkinson and J. N. Pitts, Jr., "Rate Constants for the Reaction of OH Radicals with a Series of Aromatic Hydrocarbons," J. Phys. Chem., 79, 1763 (1975).

16. Perry, R. A., R. Atkinson and J. N. Pitts, Jr., "Kinetics and Mechanism of the Gas Phase Reaction of OH Radicals with Aromatic Hydrocarbons over the Temperature Range 296-473 K," J. Phys. Chem., 81, 296 (1977).

17. Nicovich, J. M., R. L. Thompson and A. R. Ravishankara, "Kinetics of the Reactions of OH with Xylenes," J. Phys. Chem., 85, 2193 (1981).

18. Ravishankara, A. R., S. Wagner, S. Fischer, G. Smith, R. Schiff, R. T. Watson, G. Tesi and D. D. Davis, "A Kinetics Study of the Reactions of OH with Several Aromatic and Olefinic Compounds," Int. J. Chem. Kinet., 10, 783 (1978).

19. Darnall, K. R., R. Atkinson and J. N. Pitts, Jr., "Rate Constants for the Reaction of the OH Radical with Selected Alkanes at 300 K," J. Phys. Chem., 82, 1581 (1978).

20. Davis, D. D., W. Bollinger and S. Fischer, "A Kinetics Study of the Reactions of the OH Free Radical with Aromatic Compounds. 1. Absolute Rate Constants for Reaction with Benzene and Toluene at 300°K," J. Phys. Chem., 79, 293 (1975).

21. Tully, F. P., A. R. Ravishankara, R. L. Thompson, J. M. Nicovich, R. C. Shah, N. M. Kreutter and P. H. Wine, "Kinetics of the Reactions of Hydroxyl Radical with Benzene and Toluene," J. Phys. Chem., 85, 2262 (1981).

22. Wilson, W. E. Jr., E. L. Merryman, A. Levy, and H. R. Taliaferro "Aerosol Formation in Photochemical Smog. 1. Effect of Stirring," J. Air Pollut. Centr. Assoc., 21, 128 (1971).

23. Atkinson, R., W. P. L. Carter, K. R. Darnall, A. M. Winer and J. N. Pitts, Jr., "A Smog Chamber and Modeling Study of the Gas Phase NO_x-Air Photooxidation of Toluene and the Cresols," Int. J. Chem. Kinet., 12, 779 (1980).

24. Winer, A. M., J. W. Peters, J. P. Smith and J. N. Pitts, Jr., "Response of Commercial Chemiluminescent NO-NO_2 Analysers to other Nitrogen Containing Compounds," Environ. Sci. Technol., 8, 1118 (1974).

25. Darnall, K. R., W. P. L. Carter, A. M. Winer, A. C. Lloyd and J. N. Pitts, Jr., "Importance of RO_2 + NO in Alkyl Nitrate Formation from C_4-C_6 Alkane Photooxidations under Simulated Atmospheric Conditions," J. Phys. Chem., 80, 1948 (1976).

26. Joseph, D. W. and C. W. Spicer, "Chemiluminescence Method for Atmospheric Monitoring of Nitric Acid and Nitrogen Oxides," Anal. Chem., 50, 1400 (1978).

27. Peterson, J. T., "Calculated Actinic Fluxes (290-700 nm) for Air Pollution Photochemistry Applications," EPA-600/4-76-025, June 1976).

28. Leighton, P. A., "Photochemistry of Air Pollution," Academic Press, New York, 1961.

29. Whitby, K. T. and W. E. Clark, "Electric Aerosol Particle Counting and Size Distribution Measuring System for the 0.015 to 1μ Size Range," Tellus, 18 573 (1966).

30. Pitts, J. N. Jr., K. Darnall, W. P. L. Carter, A. M. Winer and R. Atkinson, "Mechanisms of Photochemical Reactions in Urban Air," Final Report, EPA-600/3-79-110, November 1979.

31. Darley, E. F., K. A. Kettner and E. R. Stephens, "Analysis of Peroxyacetyl Nitrates by Gas Chromatography with Electron Captive Detection," Anal. Chem., 35, 589 (1963).

32. Stephens, E. R. and M. A. Price, "Analysis of an Important Air Pollutant: Peroxyacetyl Nitrate," J. Chem. Educ., 50, 351 (1973).

33. Smith, R. G. R. J. Bryan, M. Feldstein, B. Levadie, F. A. Miller, E. R. Stephens and N. E. White, "Tentative Method of Analysis for Formaldehyde Content of the Atmosphere (Colorimetric Method, H.L.S., 7, (1) Supplement, 87, (1970).

34. Pitts, J. N. Jr., A. M. Winer, W. P. L. Carter, R. Atkinson and E. C. Tuazon, "Chemical Consequences of Air Quality Standards and Control Implementation Programs," Final Report to California Air Resources Board Contract No. A8-145-31, March 1981.

35. Carter, W. P. L., R. Atkinson, A. M. Winer and J. N. Pitts, Jr., "Evidence for Chamber-Dependent Radical Sources: Impact on Kinetic Computer Models for Air Pollution," Int. J. Chem. Kinet., 13, 735 (1981).

36. Carter, W. P. L., R. Atkinson, A. M. Winer and J. N. Pitts, Jr., "An Experimental Investigation of Chamber-Dependent Radical Sources," Int. J. Chem. Kinet., submitted for publication.

37. Hampson, R. F., Jr., and D. Garvin, "Reaction Rate and Photochemical Data for Atmospheric Chemistry - 1977," National Bureau of Standards Special Publication 513, May 1978.

38. Baulch, D. L., R. A. Cox, R. F. Hampson, Jr., J. A. Kerr, J. Troe and R. T. Watson, "Evaluated Kinetic and Photochemical Data for Atmospheric Chemistry," J. Phys. Chem. Ref. Data, 9, 295 (1980).

39. Washida, N. G., Inoue, H. Akimoto and M. Okuda, "Potential of Hydrocarbons for Photochemical Conversion of NO to NO_2," Bull. Chem. Soc. Japan, 51, 2215 (1978).

40. Cox, R. A., R. G. Derwent and M. R. Williams, "Atmospheric Photooxidation Reactions. Rates, Reactivity, and Mechanism for Reaction of Organic Compounds with Hydroxyl Radicals," Environ. Sci. Technol., 14, 57 (1980).

41. Atkinson R., S. M. Aschmann, W. P. L. Carter, A. M. Winer and J. N. Pitts, Jr., "Kinetics of the Reactions of OH Radicals with n-Alkanes at 299 ± 2K," Int. J. Chem. Kinet, submitted for publication (1981).

42. Atkinson, R., S. M. Aschmann, W. P. L. Carter and J. N. Pitts, Jr., "Rate Constants for the Gas Phase Reactions of OH Radicals with a Series of Bi-and Tri-Cycloalkanes at 299 ± 2K," manuscript in preparation (1981).

43. Darnall, K. R., R. Atkinson and J. N. Pitts, Jr., "Observation of Biacetyl from the Reaction of OH Radicals with o-Xylene. Evidence for Ring Cleavage," J. Phys. Chem. 83, 1943 (1979).

44. Takagi, H., N. Washida, H. Akimoto, K. Nagasawa, Y. Usui and M. Okuda, "Photooxidation of o-Xylene in the NO-H_2O-Air System," J. Phys. Chem., 84, 478 (1980).

45. Hendry, D. G., A. C. Baldwin, J. R. Barker and D. M. Golden, "Computer Modeling of Simulated Photochemical Smog," EPA-600/3-78-059, June 1978.

46. Calvert, J. G., and J. N. Pitts, Jr., "Photochemistry," Wiley, New York, N.Y., 1966.

47. Atkinson R., A. C. Lloyd and L. Winges, "An Updated Chemical Mechanism for Hydrocarbon/NO_x/SO_2 Photooxidations Suitable for Inclusion in Atmospheric Simulation Models," Atmos. Environ., in press (1981).

48. Carter, W. P. L., R. Atkinson, A. M. Winer and J. N. Pitts, Jr., "Photooxidation Mechanisms of Higher Alkanes in Polluted Atmospheres," paper presented at the 28th Congress International Union of Pure and Applied Chemistry, Vancouver, BC, 16-21 August 1981.

49. Carter, W. P. L., A. M. Winer, K. R. Darnall and J. N. Pitts, Jr., "Smog Chamber Studies of Temperature Effects in Photochemical Smog," Environ. Sci. Technol., 13, 1094 (1979).

50. Magnotta, F., and H. S. Johnston, "Photodissociations Quantum Yields for the NO_3 Free Radical," Geophys. Res. Lett., 7, 769 (1980).

51. Atkinson, R., S. M. Aschmann, W. P. L. Carter and J. N. Pitts, Jr., "Rate Constants for the Gas Phase Reaction of OH Radicals with a Series of Alkylnitrates at 299 ± 2K," manuscript in preparation.

52. O'Brien, R. J., private communication (1980).

53. Whitten, G. Z., J. P. Killus and H. Hogo, "Modeling of Simulated Photochemical Smog with Kinetic Mechanisms," Volume 1, Final Report. EPA-600/3-80-028a, February 1980.

54. Carter, W. P. L., A. M. Winer and J. N. Pitts, Jr., "Major Atmospheric Sink for Phenol and the Cresols. Reaction with the Nitrate Radical," Environ. Sci. Technol., 15, 829 (1981).

55. Carter, W. P. L., K. R. Darnall, A. C. Lloyd, A. M. Winer and J. N. Pitts, Jr., "Evidence for Alkoxy Radical Isomerization in Photooxidations of C_4-C_6 Alkanes under Simulated Atmospheric Conditions," Chem. Phys. Lett., 42, 22 (1976).

56. Niki, H., P. D. Maker, C. M. Savage and L. P. Breitenbach, "Mechanism for Hydroxyl Radical Initiated Oxidation of Olefin-Nitric Oxide Mixtures in Parts Per Million Concentrations," J. Phys. Chem., 82, 135 (1978).

57. Carter, W. P. L., K. R. Darnall, R. A. Graham, A. M. Winer and J. N. Pitts, Jr., "Reactions of C_2 and C_4 α-Hydroxy Radicals with Oxygen," J. Phys. Chem., 83, 2305 (1979).

58. Radford, H. E., "The Fast Reaction of CH_2OH with O_2," Chem. Phys. Lett., 71, 195 (1980).

59. Grosjean, D., K. Van Cauwenberghe, D. R. Fitz and J. N. Pitts, Jr., "Photooxidation Products of Toluene-NO_x Mixtures under Simulated Atmospheric Conditions," presented at the 175th National ACS Meeting, Anaheim, 12-17 March 1978.

60. Pitts, J. N., Jr., D. Grosjean, G. J. Doyle, D. R. Fitz, P. L. Johnson S. L. Midland, T. M. Mischke, K. J. Pettus, M. P. Poe and J. P. Smith, "Detailed Characterization of Gaseous and Size-Resolved Particulate Pollutants at a South Coast Air Basin Smog Receptor Site: Levels and Modes of Formation of Sulfate, Nitrate and Organic Particulates and Their Implications for Control Strategies," Final Report to California Air Resources Board Contracts Nos. ARB-5-384 and A6-171-30, December 1978.

61. Pitts, J. N., Jr., A. M. Winer, W. P. L. Carter, G. J. Doyle, R.A. Graham and E. C. Tuazon, "Chemical Consequences of Air Quality Standards and Control Implementation Programs," Final Report to ARB Contract No. A7-175-30, June 1980.

62. Darnall, K. R., R. Atkinson, A. M. Winer and J. N. Pitts, Jr., "Effects of Constant versus Diurnally-Varying Light Intensity on Ozone Formation," J. Air Pollut. Control Assoc., 31, 262 (1981).